AD-A193 122 CONAN: CHEMISTRY OF NITROGEN-A NASCENCE(U) PHYSICAL 1/2
SCIENCES INC ANDOVER MA L G PIPER ET AL JAN 88
PSI-076/TR-593 AFWL-TR-86-95 F29601-84-C-0076

UNCLASSIFIED F/G 7/2 NL

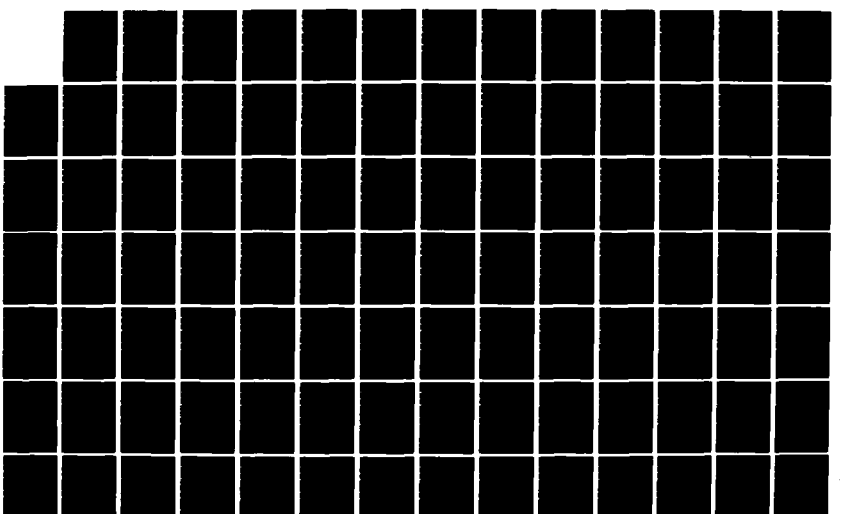


1·0
1·1
1·25
1·4
1·6
2·0
1·8

AFWL-TR-86-95

AFWL-TR-86-95

CONAN: CHEMISTRY OF NITROGEN-A NASCENCE

L. G. Piper, et al

Physical Sciences Inc.
Research Park
Andover, MA 01810

January 1988

Final Report

AIR FORCE WEAPONS LABORATORY
Air Force Systems Command
Kirtland Air Force Base, NM 87117-6008

This final report was prepared by Physical Sciences, Inc, Andover, Massachusetts under Contract F29601-84-C-0076, Job Order 33261W14 with the Air Force Weapons Laboratory, Kirtland Air Force Base, New Mexico. Captain Brian D. McFeeters (ARBI) was the Laboratory Project Officer-in-Charge.

This report has been reviewed by the Public Affairs Office and is releasable to the National Technical Information Service (NTIS). At NTIS, it will be available to the general public, including foreign nations.

If your address has changed, if you wish to be removed from our mailing list, or if your organization no longer employs the addressee, please notify AFWL/ARBI, Kirtland AFB, NM 87117-6008 to help us maintain a current mailing list.

This technical report has been reviewed and is approved for publication.

Brian D McFeeters

BRIAN D. McFEETERS
Captain, USAF
Project Officer

FOR THE COMMANDER

Gerald A Hasen

GERALD A. HASEN
Major, USAF
Chief, Advanced Chemical Laser Branch

HARRO ACKERMANN
Lt Col, USAF
Chief, Laser Science and Technology Office

DO NOT RETURN COPIES OF THIS REPORT UNLESS CONTRACTUAL OBLIGATIONS OR NOTICE ON A SPECIFIC DOCUMENT REQUIRES THAT IT BE RETURNED.

REPORT DOCUMENTATION PAGE

1a. REPORT SECURITY CLASSIFICATION UNCLASSIFIED	1b. RESTRICTIVE MARKINGS
2a. SECURITY CLASSIFICATION AUTHORITY	3. DISTRIBUTION / AVAILABILITY OF REPORT Approved for public release; distribution unlimited.
2b. DECLASSIFICATION / DOWNGRADING SCHEDULE	
4. PERFORMING ORGANIZATION REPORT NUMBER(S) PSI-076/TR-593	5. MONITORING ORGANIZATION REPORT NUMBER(S) AFWL-TR-86-95
6a. NAME OF PERFORMING ORGANIZATION Physical Sciences, Inc 6b. OFFICE SYMBOL (If applicable)	7a. NAME OF MONITORING ORGANIZATION Air Force Weapons Laboratory
6c. ADDRESS (City, State, and ZIP Code) P.O. Box 3100, Research Park Andover, MA 01810	7b. ADDRESS (City, State, and ZIP Code) Kirtland Air Force Base, NM 87117-6008
8a. NAME OF FUNDING / SPONSORING ORGANIZATION 8b. OFFICE SYMBOL (If applicable)	9. PROCUREMENT INSTRUMENT IDENTIFICATION NUMBER F29601-84-C-0076
8c. ADDRESS (City, State, and ZIP Code)	10. SOURCE OF FUNDING NUMBERS PROGRAM ELEMENT NO. 62601F; PROJECT NO. 3326; TASK NO. 1W; WORK UNIT ACCESSION NO 14

11. TITLE (Include Security Classification)

CONAN: CHEMISTRY OF NITROGEN-A NASCENCE

12. PERSONAL AUTHOR(S) Piper, L.G.; Davis, S.J.; Murphy, H.C.; Cummings, W.C.; Walkauskas, L.P.; DeFaccio, M.A.; Cowles, L.M.; Rawlins, W.T.; Marinelli, W.J.; and Green, B.D.

13a. TYPE OF REPORT	13b. TIME COVERED	14. DATE OF REPORT (Year, Month, Day)	15. PAGE COUNT
Final	FROM 4Sep84 TO 4Jun86	1988 January	192

16. SUPPLEMENTARY NOTATION

17 COSATI CODES		
FIELD	GROUP	SUB-GROUP

18 SUBJECT TERMS (Continue on reverse if necessary and identify by block number)
Active nitrogen, Energy transfer, N2(A) NF(a)
Nitrogen metastables, Quenching rates, N2(B) NF(b)
Energy pooling, Excitation rates, NF2 (over)

19. ABSTRACT (Continue on reverse if necessary and identify by block number)

Rate coefficients for production of excited nitrogen have been measured, and energy-transfer reactions utilizing the excited nitrogen have been studied. Three reactions were involved in chemical production of excited nitrogen (N_2*) when H and NF_2 were mixed:

$$H + NF_2 \rightarrow HF + NF\ (a^1\Delta) \quad (1)$$

$$H + NF\ (a^1\Delta) \rightarrow HF + N\ (^2D) \quad (2)$$

$$H\ (^2D) + NF\ (a^1\Delta) \rightarrow N_2^* + F \quad (3)$$

Reaction (2) is slow, $k_2 = (3.1 \pm 0.6) * 10^{-13}$ $cm^3 molecule^{-1} sec^{-1}$. Reaction (3) is essentially gas kinetic, $k_3 = (1.6 \pm 0.7) * 10^{-10} cm^3 molecule^{-1} sec^{-1}$, and produces mostly $N_2(B^3\Pi_g)$. The $N_2(A^3\Sigma_u^+)$ which is observed is probably produced from radiative cascade (over)

20 DISTRIBUTION / AVAILABILITY OF ABSTRACT	21 ABSTRACT SECURITY CLASSIFICATION
☒ UNCLASSIFIED/UNLIMITED ☐ SAME AS RPT ☐ DTIC USERS	UNCLASSIFIED
22a NAME OF RESPONSIBLE INDIVIDUAL Brian D. McFeeters, Captain, USAF	22b TELEPHONE (Include Area Code) (505) 844-0661
	22c OFFICE SYMBOL ARBI

DD FORM 1473, 84 MAR 83 APR edition may be used until exhausted
All other editions are obsolete

18. SUBJECT TERMS (Continued)

Nitrogen atoms
Hydrogen atoms
Iodine monofluoride

19. ABSTRACT (Continued)

from $N_2(B)$. The major impediment to production of large number densities of $N_2(A,B)$ using this system is the rapid quenching of $N_2(A)$ by atomic hydrogen.

Energy transfer reactions from $N_2(A)$ to potential laser species revealed that NO quenches $N_2(A)$ with a rate coefficient of approximately $7 * 10^{-11}$ $cm^3 molecule^{-1} sec^{-1}$, efficiently producing $NO(A^2\pi, v'=0,1)$. When IF is added to a flow of active nitrogen three different band systems are excited, one of which is IF ($B\ ^3\pi_0^+$). The other two IF systems remain to be identified. The excitation rate of these systems, if $N_2(B)$ is the exciting species, is an order of magnitude faster than gas kinetic. Therefore, $N_2(B)$ is thought to be only a tracer of the actual species exciting IF; the most likely source is excited ground state nitrogen. The quenching of $N_2(B)$ by molecular nitrogen is quite rapid, with a rate of approximately $2 * 10^{-11} cm^3 molecule^{-1} sec^{-1}$. Argon does not quench $N_2(B)$ electronically, but strongly redistributes vibrational energy to lower vibrational levels.

Energy pooling of two $N_2(A)$ molecules proceeds with a rate coefficient of approximately $3 * 10^{-10} cm^3 molecules^{-1} sec^{-1}$, when both molecules are in $v'=0$, and about 50 percent faster when one molecule is in $v'=1$. In both cases, the products are $N_2(B)$, $N_2(C^3\pi_u)$ and bands of the Herman infrared system.

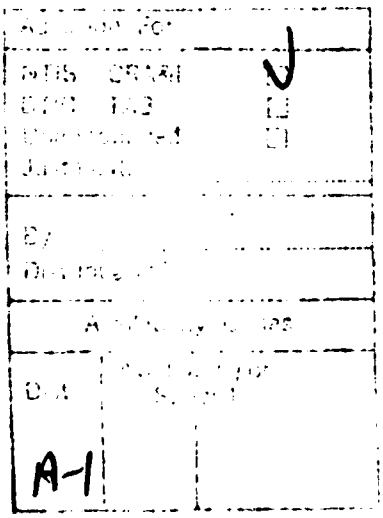

SUMMARY

This report summarizes work aimed toward understanding chemical pathways for producing excited nitrogen molecules, and energy transfer reactions of the excited nitrogen molecules which might prove important in potential laser devices. The main thrust of the effort on chemical production of excited nitrogen involved detailed studies of several important reactions in the following reaction sequence:

$$H + NF_2 \rightarrow HF + NF(a^1\Delta) \quad (1)$$

$$H + NF(a^1\Delta) \rightarrow HF + N(^2D) \quad (2)$$

$$N(^2D) + NF(a^1\Delta) \rightarrow N_2^* + F \quad (3)$$

All observations lend support to this mechanism as being the route to making N_2^* when H and NF_2 are mixed together. Measurements show that the rate coefficient for reaction 2 is relatively slow, $k_2 = (3.1 \pm 0.6) \times 10^{-13}$ cm^3 molecule^{-1} s^{-1}. In contrast, the rate coefficient for the third reaction is essentially gas kinetic, $k_3 = (1.6 \pm 0.7) \times 10^{-10}$ cm^3 molecule^{-1} s^{-1}. The quoted rate coefficient for this reaction is actually the rate cofficient for producing $N_2(B^3\Pi_g)$, v' = 1-12) rather than the total reaction rate coefficient. Observations of other products, e.g., $N_2(a^1\Pi_g)$, indicate that the channel which produces $N_2(B)$ is far and away the largest one. Some $N_2(A^3\Sigma_u^+)$ from the reaction is observed, as demonstrated by observing Vegard-Kaplan emission in the ultraviolet, but these observations indicate that the $N_2(A)$ most likely is produced by radiative cascade from $N_2(B)$. This point remains to be clarified.

The species $NF(b^1\Sigma^+)$ and $N(^4S)$ were not significant precursors to $N_2(B)$ formation. The population of NF(b) was too small to affect any observations, while $N(^4S)$ was formed subsequent to $N_2(B)$ formation.

Reaction 3 appears to be a rapid and efficient source of $N_2(B)$, and one might indeed be able to generate large number densities of $N_2(A,B)$, if one can produce large number densities of NF(a) and $N(^2D)$. The major impediment we foresee in using this scheme to produce large number densities of $N_2(A,B)$ is that atomic hydrogen appeared to quench $N_2(A)$ rather efficiently. Thus one would have to adjust conditions to minimize the existence of free hydrogen atoms.

Observations on N_2^* energy transfer reactions focussed upon the transfer of electronic energy between $N_2(A^3\Sigma_u^+)$ and NO, upon the products of $N_2(A)$ energy pooling, upon the excitation of IF by active nitrogen, and the characterization of vibrationally excited $N_2(X,v)$ in active nitrogen. We demonstrated that $N_2(A)$ excites NO(A) very efficiently ($k = 7 \times 10^{-11}$ cm^3 molecule^{-1} s^{-1}). The efficiency of the reaction, furthermore, does not degrade as the pressure in the reactor increases. Spectroscopic observations of NO(A) emission indicate a significant variation in the transition moment of the $NO(A^2\Sigma^+ - X^2\Pi)$ transition with r-centroid. The effect is such as to increase the relative importance of transitions with larger Δv, implying that

laser gain for the red shifted transitions 0,2-0,5 will be somewhat larger than anticipated. This increases the probability of adequate gain on these transitions for a laser device. Finally, it has been determined that the radiative lifetime of $N_2(A)$ is about 30 percent longer than previously thought.

Studies on $N_2(A)$ energy pooling determined the production rates of various vibrational levels of $N_2(C^3\Pi_u)$, $N_2(B^3\Pi_g)$, and the Herman infrared system as a function of vibrational level of the $N_2(A)$ molecules involved in the pooling process. Results indicate a total rate coefficient for the energy pooling process of about 4.0×10^{-10} cm^3 molecule^{-1} s^{-1} when we use the $N_2(A)$ Einstein coefficients of Shemansky. If the hypothesis is correct that these Einstein coefficients are about 30 percent too large, then the actual value of the energy pooling rate coefficient will be roughly 2.5×10^{-10} cm^3 molecule^{-1} s^{-1}. Clearly, the issue of the $N_2(A)$ lifetime must be resolved to clear up this point.

Observations both in the $N_2(B)$ formation from reaction 3 as well as that from energy pooling shows fairly dramatic changes in the vibrational level distribution of the $N_2(B)$ as a function of argon pressure, even for pressures below 3 torr. Molecular nitrogen, on the other hand, appears to quench the electronic energy in the $N_2(B)$ quite efficiently, $k \sim 2 \times 10^{-11}$ cm^3 molecule^{-1} s^{-1}, but does not change the vibrational level distribution strongly. These issues of $N_2(B)$ quenching and vibrational redistribution are vital to modeling potential laser operation. Clearly, if the end result of $N_2(B)$ quenching is formation of $N_2(B, v' = 0,1)$--levels we could observe either poorly or not at all--or $N_2(A)$, then apparent quenching of the higher vibrational levels of $N_2(B)$ probably will not affect efficiencies as the system is scaled to higher pressures of argon or nitrogen. Similarly energy-pooling losses will be reduced in that energy-pooling reactions which produce $N_2(C)$ or $N_2(B)$ ultimately regenerate $N_2(A)$. Thus the effective loss is only one molecule per pooling event rather than two. If, however, $N_2(B)$ quenching produces ground-state nitrogen, then at higher pressures, effective N_2^* formation from reaction 3 would be reduced and the pooling losses would double.

A diagnostic was developed for $N_2(X,v)$ in active nitrogen which is based upon the Penning ionization reaction between metastable helium atoms and molecular nitrogen. This reaction produces $N_2^+(B^2\Sigma^+)$ state in Franck-Condon transitions from the ground state. The resultant vibrational distribution of the $N_2^+(B^2\Sigma_u^+ \text{--} X^2\Sigma_g^+)$ emission, therefore, mirrors the vibrational distribution of the $N_2(X,v)$. We have also demonstrated the production of $N_2^+(C^2\Sigma_u^+)$ in Penning ionization of metastable helium with $N_2(X,v)$. This indicates the presence of vibrational excitation in excess of 3.8 eV in the ground-state nitrogen.

It has been shown that three different band systems of IF are excited when IF is added to a flow of active nitrogen. One of these systems is the well-known $IF(B^3\Pi_{0^+} \text{--} X^1\Sigma^+)$ system, while we have been unable to identify the other two systems as yet. The excitation rates of all three systems

varies in proportion to the number density of $N_2(B)$ in the reactor. The effective excitation rate coefficient implied by the data however, is an order of magnitude greater than gas kinetic. Thus the $N_2(B)$ is only a tracer of the actual species responsible for the IF excitation. We have, so far, been unable to identify the IF excitation source, but think that the most likely hypothesis is $N_2(X,v)$.

ACKNOWLEDGEMENT

Partial funding for this work has also been received from the Air Force Geophysics Laboratories under Contract No. F19628-82-C-0050 and from SDIO/IST and Los Alamos National Laboratories. This extra support allowed a more detailed and complete study.

CONTENTS

CONTENTS (Continued)

FIGURES

FIGURES (Continued)

FIGURES (Continued)

FIGURES (Continued)

FIGURES (Continued)

FIGURES (Continued)

TABLES

1. INTRODUCTION

The lowest-lying metastable state of N_2, $A^3\Sigma_u^+$, is a well-known energy reservoir (~6 eV) which has potential as an energy-storage candidate for use in short-wavelength laser systems. As such, knowing the means to generate this species efficiently and understanding its energy-transfer kinetics in the lasing medium are essential requirements for laser-device design. This program was designed to quantify the fundamental kinetics and mechanisms of several key aspects of $N_2(A)$ generation and utilization. These investigations provide a fundamental data base which is a necessary first step in developing an $N_2(A)$ transfer laser.

Several laboratory investigations have identified methods for forming $N_2(A)$ chemically. Two methods, in particular (Refs. 1 through 5), may be capable of producing $N_2(A)$ in sufficient quantities to drive a transfer laser. The first method consists of a set of reactions initiated by the reaction of atomic hydrogen with NF_2, and appears to involve the metastables $NF(a^1\Delta)$ and $N(^2D)$ as key intermediate species (Refs. 1 through 3). An intriguing second method is the bimolecular disproportionation of the highly energetic azide radical, N_3 (Refs. 4,5). The former method has a potentially high efficiency per unit mass, but requires the handling of the hazardous species N_2F_4 (the thermal source of NF_2), and may present serious kinetic complications upon scale-up from laboratory experiments. The latter method, which uses ionic metal azides such as NaN_3 as thermal sources of N_3 radicals, is also potentially efficient per unit mass.

Additional aspects which govern the efficiency of potential chemical laser devices are the efficiency of transferring energy from $N_2(A)$ into the lasing medium and the efficiency with which energy is drained from the $N_2(A)$, both by other species in the medium as well as by itself. Several candidate energy-transfer schemes have been identified whose kinetics and efficiencies need to be quantified in the laboratory. Under previous sponsorship (Refs. 6,7), PSI studied the energy transfer from $N_2(A)$ to IF in detail. Measurements shown here demonstrated a rapid, efficient transfer which results in

fluorescence from the $B^3\Pi_{0^+} \rightarrow X^1\Sigma^+$ transition of IF between 500 and 800 nm. (Additional measurements using discharged nitrogen showed that other excited forms of nitrogen, perhaps vibrationally excited N_2, also contribute to IF excitation. It is conceivable that the $N_2(A)$ generation schemes will also produce such excited N_2 species.) During the course of this work, another excitation process was studied which appears to have potential in a laser device: the excitation of $NO(A^2\Sigma^+)$ by $N_2(A)$. In addition the kinetics of $N_2(A)$ energy pooling was studied in great detail. The efficiency of the energy pooling reactions govern the maximum N_2 excited-state number densities available in the laser medium. Finally, the preliminary measurements on the excitation of IF by active nitrogen were extended.

All experimental measurements were carried out on discharge-flow reactors, one of which was developed specially for this program. Introducing selected chemical reagents and excited species into the main reactor isolated individual elementary reactions for unambiguous kinetic measurements. A variety of well-characterized ultraviolet, visible, and infrared spectroscopic techniques identified the species present, determined their number densities, and allowed their kinetic behavior to be quantified. All diagnostics were calibrated using well-established, but not always well understood, methods.

Section 2 details the kinetics of the $H + NF_2$, $H + NF(a^1\Delta)$, and $N(^2D) + NF(a^1\Delta)$ reactions. Extensive measurements on metastable nitrogen energy-transfer kinetics comprise Section 3. This section includes studies on the $N_2(A) + NO$ reaction, the $N_2(A)$ energy-pooling reactions, and the active nitrogen plus IF reaction in addition to the development and implementation of a diagnostic for $N_2(X,v)$ in active nitrogen. Section 4 summarizes findings. This report does not have a separate experimental section. Rather, the apparatus and techniques germane to each set of experimental measurements is described along with the measurements.

2. H + NF_2 REACTION SEQUENCE STUDIES

2.1 INTRODUCTION

This Task was concerned with excited molecular nitrogen production from the H + NF_2 reaction sequence. This reaction has been the subject of several previous studies and its history in the literature is intriguing. The first report was by Clyne and White in 1970 (Ref. 8). They observed that the reaction of H + NF_2 produced NF($a^1\Delta$), NF($b^1\Sigma$), and $N_2(B^3\Pi_g)$, and proposed that recombination of N(^4S) atoms was the source of $N_2(B)$.

In 1973 Herbelin and Cohen (Ref. 9) performed a similar chemiluminescence study and suggested the following mechanism

$$H + NF_2 \rightarrow NF(a) + HF \quad (1)$$

$$H + NF(a) \rightarrow N(^2D) + HF \quad (2)$$

$$N(^2D) + NF(a) \rightarrow N_2(B) + F \quad (3)$$

Although they could not prove this model they presented indirect evidence for its validity and argued that spin and angular momentum conservation would be major constraints in reaction product channel availability. In particular they emphasized that the reaction of H + NF(a) would produce N(^2D) exclusively if these correlation rules rigorously held. In spite of these early observations the reaction mechanism for this potentially important source of N_2^* has remained unclear.

In the early 1980's Clyne and coworkers embarked on a series of detailed experiments designed to clarify this interesting reaction sequence (Refs. 1,2,3). Using sensitive diagnostic techniques, they observed that N(^2D) was indeed the primary product of reaction (2) and concluded that Herbelin and Cohen's proposed mechanism was probably correct. In addition they made preliminary estimates for the rate coefficients of reactions (2) and (3).

$$k_2 = 2.5 \times 10^{-13} \text{ cm}^3\text{-molecule}^{-1}\ \text{s}^{-1}$$

$$k_3 = 7 \times 10^{-11} \text{ cm}^3\text{-molecule}^{-1}\ \text{s}^{-1}$$

The purpose of this Task was to measure rate coefficients for reactions 2 and 3 and to study the efficiency of N_2^* production from the sequence. By determining these rate coefficients systematically we had hoped to be able to provide further evidence concerning the validity of Herbelin and Cohen's model.

The remainder of this section is presented in several subsections. First the initial studies of the chemiluminescence produced by the H + NF_2 reaction sequence are studied. Next the rate coefficient determination results for reactions 2 and 3 are presented. Some modeling results are also described. Finally, we attempt to relate these results to possible development of this scheme as a chemical source of N_2^*.

2.2 H + NF_2 CHEMILUMINESCENCE STUDIES

2.2.1 Flow Tube Description--The new fast flow reactor (CONAN) was completed and tested specifically for these experiments. The flow tube is constructed from 5 cm id Pyrex, and the observation region is a 5 cm id stainless steel chamber coated with Teflon (Dupont Poly TFE #852-201). Prior to Teflon coating the entire observation chamber was painted with a flat black primer. The black primer/Teflon combination serves two functions. The primer reduces scattered light which facilitates all spectroscopic observations. The Teflon also reduces wall reactions and recombinations. The entire CONAN flow tube is shown in Fig. 1, and a detailed section of the observation chamber is presented in Fig. 2.

As indicated in Fig. 1, the flow tube is modular and configuration changes are conveniently made. All gas flows are monitored by electronic mass flowmeters. The flowmeters were calibrated by measuring the change in pressure versus time of gas flows into a standard volume (6.5 l or 12.0 l flasks). The pressure change was measured using a Validyne pressure transducer that had been calibrated against a mercury or oil manometer.

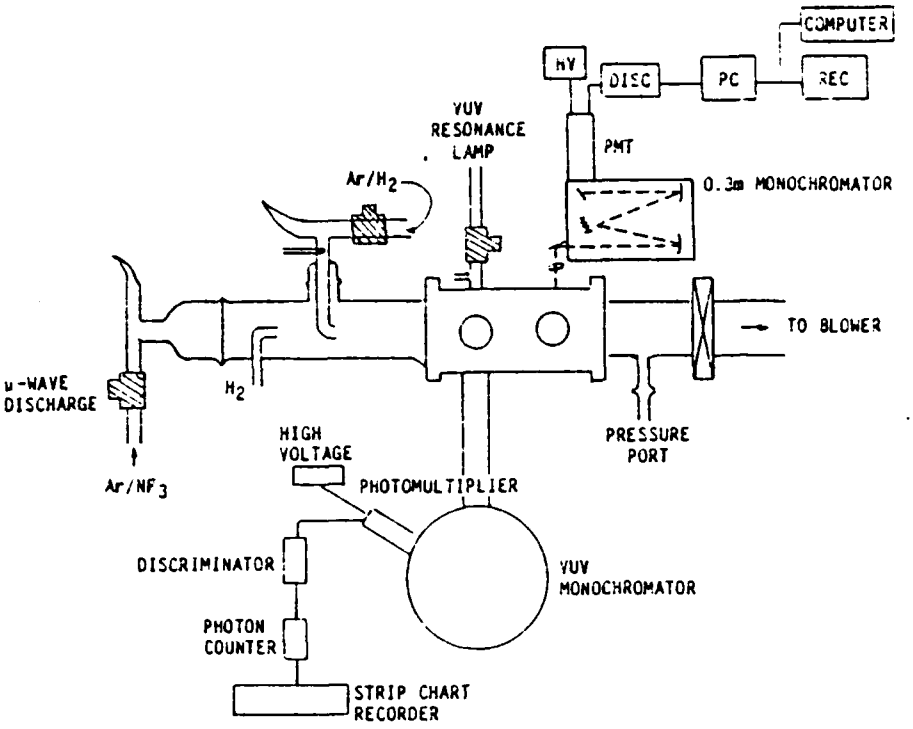

Figure 1. Block diagram of the CONAN flow tube.

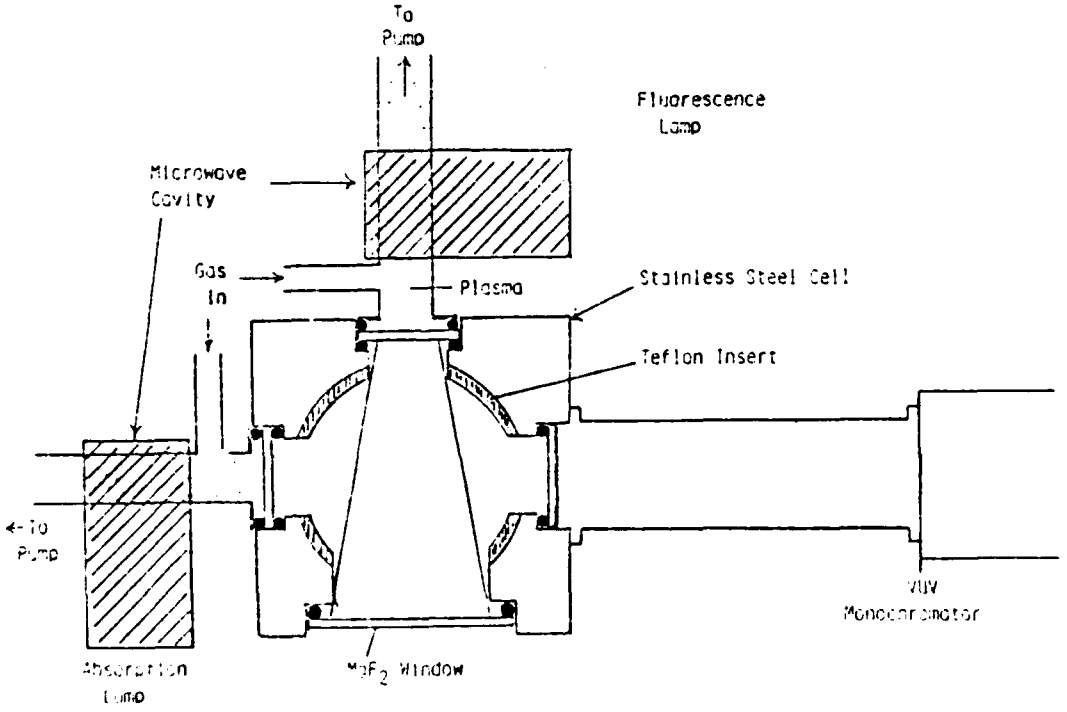

Figure 2. Detailed view of observation chamber.

The pressure in the flow tube is measured using a Baratron 0 to 100 torr* capacitance manometer. Typical flow tube pressures ranged from 0.13 to 2.5 torr. Flow velocities could be varied from 500 to 5300 cm/s. The flow velocity was determined using the

$$v = \frac{1}{AN_{tot}} (f)$$

where

$f \equiv$ gas flow rate in number of molecules/s

$N_{tot} \equiv$ total number density in the flow tube

$A \equiv$ flow tube area

$v \equiv$ bulk gas velocity.

The term f is measured with the mass flowmeter and N_{tot} is calculated as the sum of the component densities found from the capacitance manometer pressure reading.

If the total pressure in the flow tube is P_T(torr) at temperature T(K), then the number density of reactant i is given by:

$$N_i = \frac{f_i}{\Sigma_i f_i} \left(\frac{P_T N_o}{RT} \right)$$

where f_i = flow rate of reactant i, Σf_i total flow rate of all reactants in flow tube, N_o is Avogadro's number, and R is the gas constant.

Four of the eight viewing ports in the observation chamber are indicated in Fig. 2. In the present configuration, three ports are used for optical detection. Ultraviolet, visible, and near infrared chemiluminescence are monitored using a 0.3 m McPherson monochromator and a Hammamatsu GaAs PMT. A second port is used to monitor NO emission used in calibrating H atom number densities (described later), and a third port is used to observe resonance fluorescence for N atom detection.

---

*1 torr = 133.3 Pascals.

2.2.2 Visible and Near Infrared Studies--To study the chemical production of excited states from the reaction of H + NF_2, we utilized the reaction of hydrogen with the products of a microwave discharge of NF_3 dilute in Ar. Initial runs showed that the emitting species produced by the NF_3 discharge consisted almost exclusively of NF(b→X) and NF(a→X) emissions at 528 and 843 nm, respectively. Weak N_2(B→A) first-positive emission was also observed, but since the radiative lifetime for N_2(B) is orders of magnitude shorter than those for NF(a) and NF(b), the N_2(B) is a minor product.

Upon the addition of hydrogen to the effluents of the NF_3 discharge, the NF(a and b) emissions became approximately an order of magnitude more intense. In addition N_2(B→A) emission became more intense. The NF and N_2 emission intensities also varied as a function of H_2 flow. A spectrum covering the range 520 to 880 nm is shown in Fig. 3.

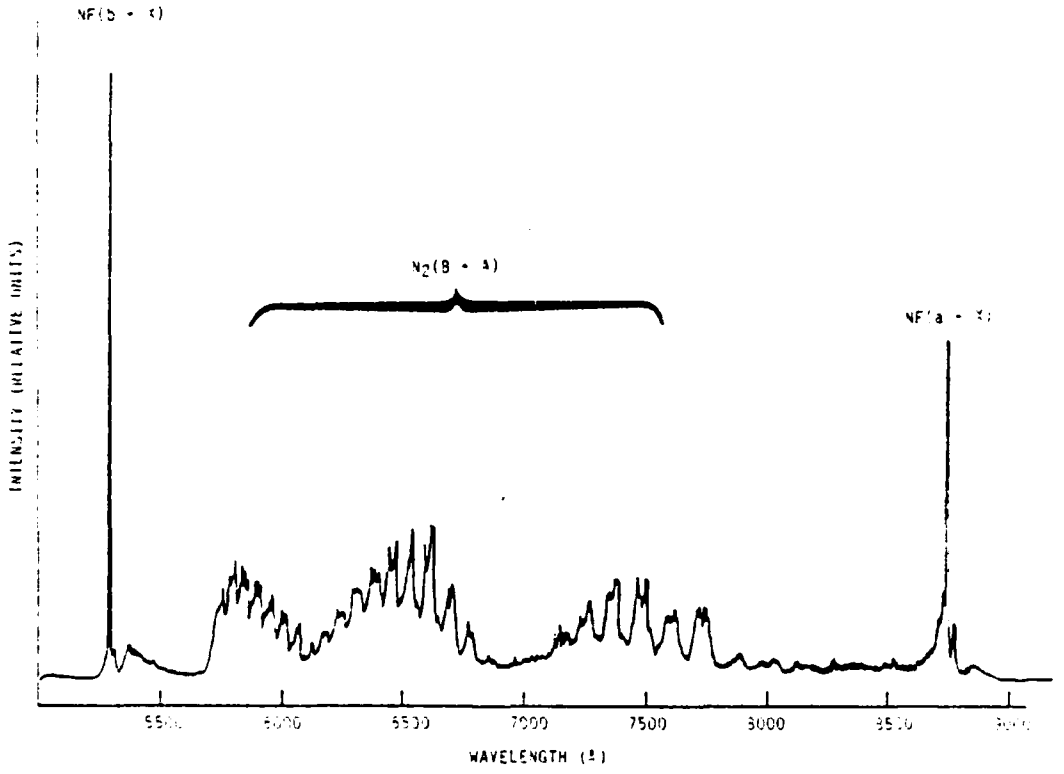

Figure 3. Chemiluminescence in the 500 to 900 nm region produced by the reaction of H_2 with discharged NF_3. Total pressure was 0.16 torr.

The observation of enhanced NF(a) emission when H_2 was added to the discharge effluents is evidence that in addition to NF(a,b) both NF_2 and F are products of the NF_3/Ar microwave discharge. Rapid reaction of F with added H_2 produces atomic hydrogen which can react via the abstraction reaction:

$$H + NF_2 \rightarrow NF(a) + HF$$

These observations are also in accord with those reported by Herbelin and coworkers (Ref. 9). The dependence of the NF(a→X) emission upon the H_2 flow rate is shown in Fig. 4. Note that as H_2 is added, the [NF(a)] increases, goes through a peak, then appears to reach an asymptotic limit at high H_2 flows. The fact that the NF(a) concentration appears to be essentially independent of $[H_2]$ at high H_2 flows is utilized in the measurement of the quenching rate of NF(a) by H atom as described later.

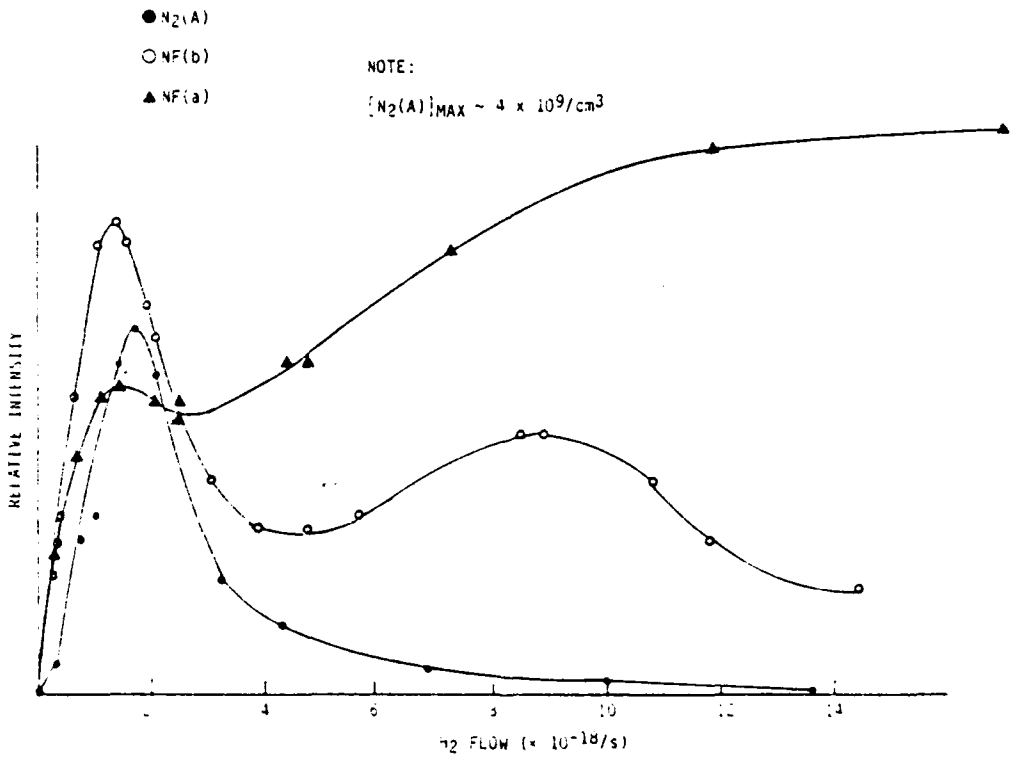

Figure 4. Dependence of NF(a→X), NF(b→X), and $N_2(A)$ emissions as a function of H_2 flow.

2.2.3 Ultraviolet Emission Studies--The spectral region 220 to 330 nm was scanned to study any production of $N_2(A)$ from:

$$H + NF_2 \rightarrow NF(a) + NF$$

$$NF(a) + H \rightarrow N(^2D) + HF$$

$$NF(a) + N(^2D) \rightarrow N_2(A) + F \qquad (4)$$

It is important to note that Clyne et al. (Refs. 8,9,10) proposed that the final step was:

$$N(^2D) + NF(a) \rightarrow N_2(B,a) + F$$

Direct A state production was presumably discarded because of orbital angular momentum correlations. However, spin correlation which is typically more rigorously obeyed in these types of reactions would allow N_2 singlet and triplet formation. Since orbital angular momentum correlations are often violated especially for nonlinear collision complexes, it seems reasonable to expect that direct $N_2(A)$ production should be possible from reaction 4.

Typical scans are presented in Figs. 5 and 6. Figure 5 shows intense NH emission originating from two band systems $NH(c^1\Pi \rightarrow a^1\Delta)$ and $NH(A^3\Pi \rightarrow X^3\Sigma^-)$. Clyne (Ref. 1,2,3) observed the identical systems in the $H + NF_2$ system further supporting the contention that under our experimental conditions, the $H + NF_2$ system was effectively imitated by using discharged NF_3. Upon removal of H_2, the NH spectrum vanished. The most likely production source of NH^* is by the reaction:

$$N(^2D) + H_2 \rightarrow NH(X) + H \qquad (5)$$

followed by:

$$NH(X) + N_2(A) \rightarrow NH(c,A) + N_2(X) \qquad (6)$$

This had been previously argued as indirect evidence for the presence of $N_2(A)$ in the flow of products resulting from the reaction of $N + NF_2$.

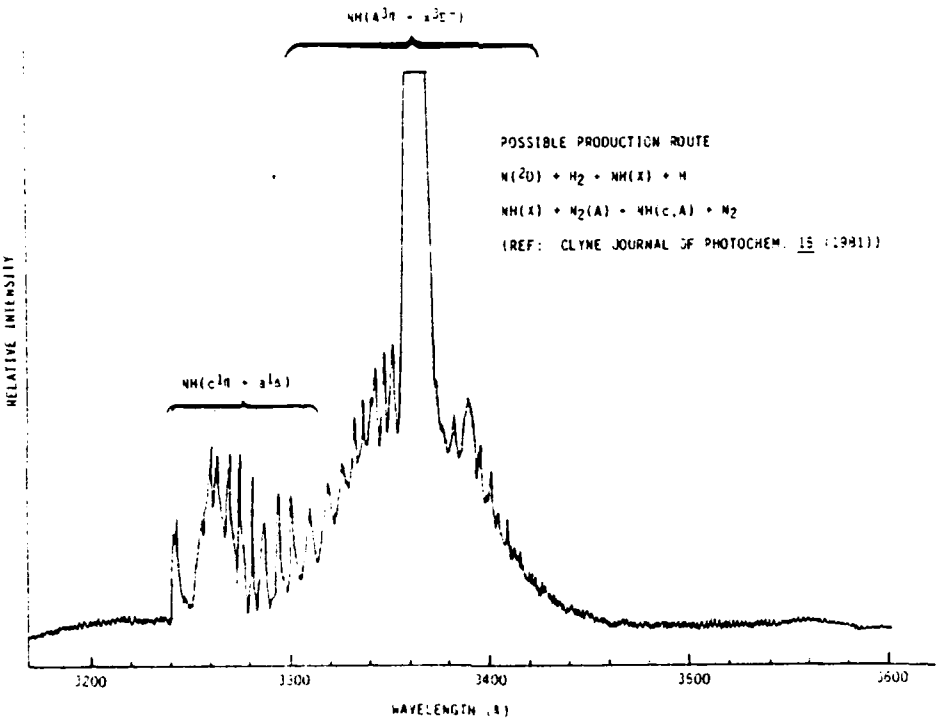

Figure 5. NH (c→a) and (A→X) systems produced in the H_2+ discharged NF_3 reaction.

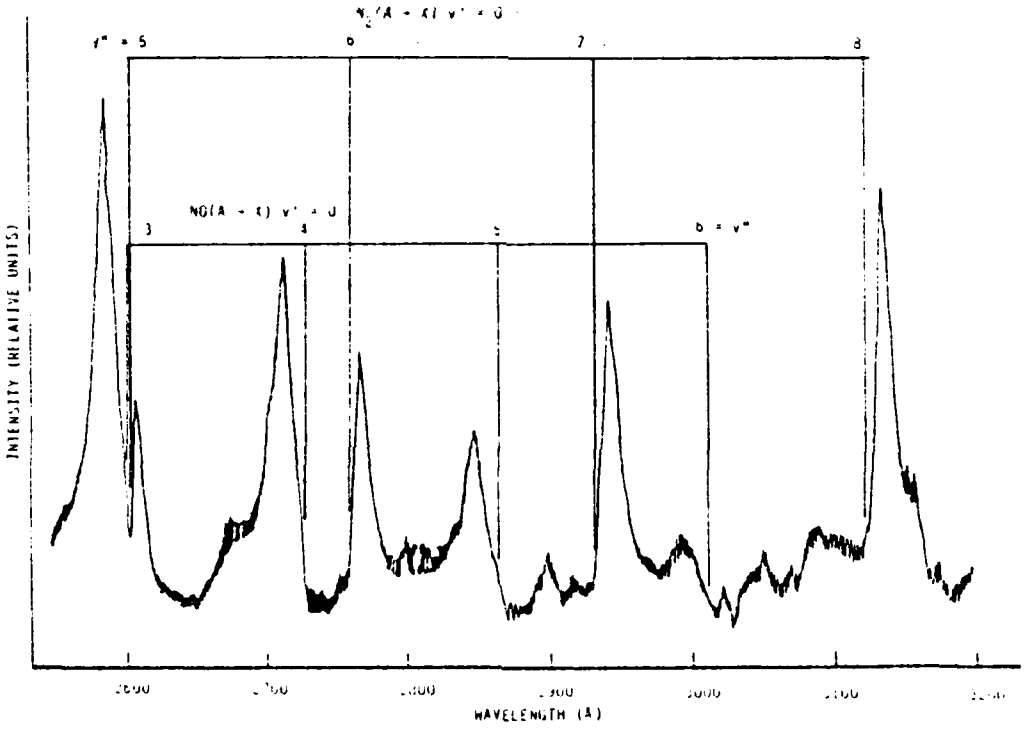

Figure 6. NO(A→X) and N_2(A→X) system produced by reacting H_2 + discharged NF_3.

During the course of the initial experiments on the CONAN flow tube the chemical production of $N_2(A)$ was observed by detecting the Vegard Kaplan (V-K) system near 280 nm. A typical spectrum is shown in Fig. 6. The strong NO(γ) bands are probably due to slight contamination by NO produced in the NF_3/Ar discharge. The distinct red degraded $N_2(A \rightarrow X)$ system is clearly evident and vanishes upon extinction of the H_2 flow. Thus, it is not a discharge product. To our knowledge, this is the first direct observation of $N_2(A)$ chemical production and graphically demonstrates that at least some branching of the reaction energy into this highly metastable state. Some measurements were made of the number densities of $N_2(A)$ produced, and these results and the source of the $N_2(A)$ is discussed later in Subsections 2.4.3.5 and 2.4.3.6.

The $N_2(a-X)$ LBH system near 150 nm as shown in Fig. 7 was also observed. This emission also vanished when H_2 was removed. The production of $N_2(a)$ provides a graphic demonstration of the extreme exothermicity of the $H + NF_2$ reaction sequence since $N_2(a)$ lies 8.5 eV above $N_2(X)$.

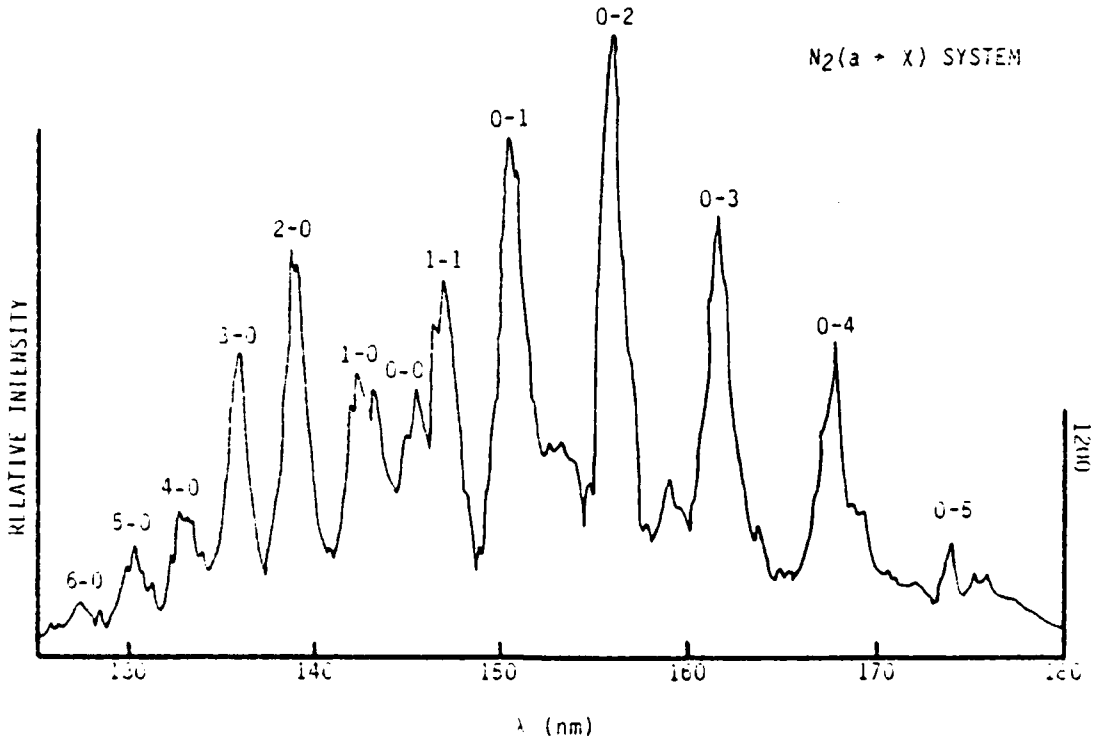

Figure 7. Emission spectrum of the N_2 $a^1\Pi_g \rightarrow X^1\Sigma_g^+$ system.

2.2.4 Phenomenological Kinetic Investigations--It was believed that to interpret the planned kinetic rate measurements, it would be advantageous to examine some of the dependencies of the various excited species upon reactant concentrations. Relevant to $N_2(A)$ production are the data presented in Fig. 4 which show relative $[N_2(A)]$ as a function of H_2 flow at a constant NF_3/Ar flow. The $N_2(A)$ concentration rises rapidly then turns over at $[\dot{H}_2] \sim 2 \times 10^{18}$ s^{-1}.

The data in Fig. 4 were obtained at a distance of 36 cm from the H_2 injector. This represents a reaction time of ~7 ms. To obtain a temporal profile of the $N_2(A)$ produced in the reaction, the fixed H_2 injector was replaced with a movable injector. By holding all flows constant, the $N_2(A)$ concentration profile was obtained by moving the H_2 injector in the flow direction. The results of this scan are shown in Fig. 8. Also shown are

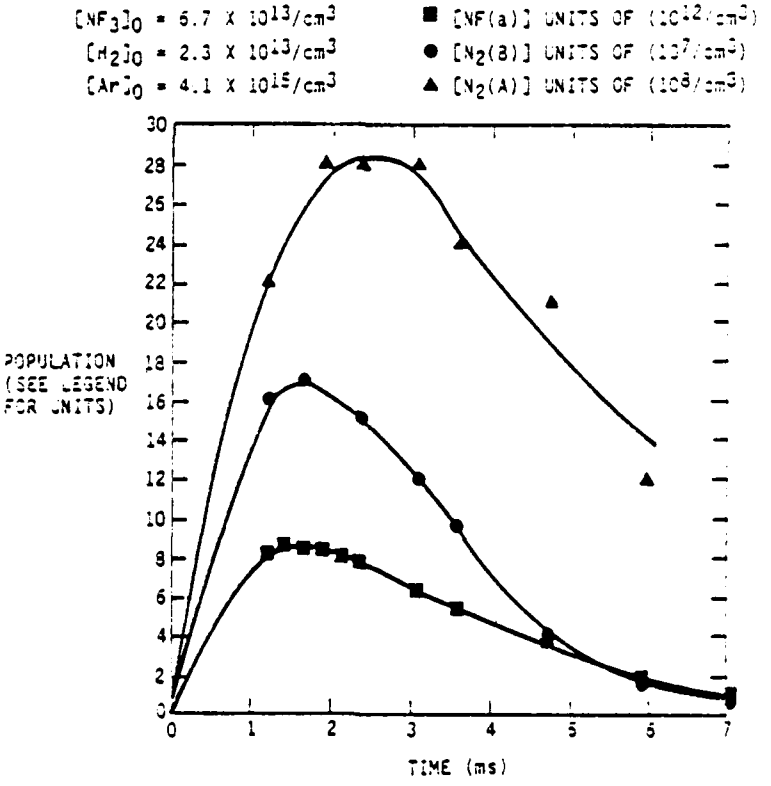

Figure 8. Temporal profiles of NF(a), $N_2(A)$, and $N_2(B)$.

nearly the same time suggesting that they are kinetically related. Since the radiative lifetime of NF(a) is 6s, its decay is not due to radiative loss. Rather, observations support the hypothesis that at least some NF(a) reacts eventually to form $N_2(A)$. The rapid decay of $N_2(A)$ is also nonradiative and is probably due to a combination of wall loss and reactive loss. Some $N_2(A)$ may be consumed in pumping NH(X) to the A and c states. Time constraints have precluded a detailed study of these processes, and these data are preliminary observations. Systematic studies of the production of NF(a), $N_2(B)$ and $N_2(A)$ are presented in Subsection 2.4.

2.3 KINETIC RATE COEFFICIENT DETERMINATIONS

2.3.1 Apparatus--Several changes were incorporated into the apparatus for the kinetic studies. The output of the photon counter was connected to a COMPAQ microcomputer to collect chemiluminescence spectra on floppy disk. The data were later analyzed on PSI's DEC MICROVAX computer system using the spectral fitting routine. Resonance fluorescence and absorption lamps were incorporated into the flow tube to measure $N(^2D)$ atom concentrations. Finally, the 0.3 m monochromator was moved to a different viewing port which permitted monitoring of $N(^2D)$, NF(a), NF(b), $N_2(A)$, $N_2(B)$ and $N_2(a)$ at the same spatial position in the flow tube.

2.3.2 Rate Constant for H + NF(a)--The rate equation for NF(a) in the flow tube is given by:

$$\frac{d[NF(a)]}{dt} = -(k[H] + \kappa_w)\,[NF(a)] \qquad (7)$$

where quenching of [NF(a)] by ground state NF and undissociated NF_3 was neglected. Experimentally we keep the initial NF_3 concentration low ($< 10^{13}$/cc). In addition the NF_3 flow rate is constant for each run. Even if some quenching were present, it should be a constant term independent of changes in H. If we neglect wall collisions, the integrated rate equation becomes:

$$[NF(a)]/[NF(a)]_o = e^{-k[H](z/\bar{v})} \qquad (8)$$

where z is the distance from H injection to the observation port, and $\bar{v}$ is the bulk gas velocity in the flow tube. If the concentration of [H] is much greater than that of NF(a), plots of ln(NF(a) chemiluminescence intensity) as a function of $[H](z/\bar{v})$ yield k, the desired rate coefficient. A diagram of the flow tube used for these studies is shown in Figure 9.

Although the form of Eq. (8) is simple, there were several demanding experimental requirements that had to be met. The first was to ascertain that a detectable flow of NF(a) could be established. The initial studies demonstrated that this could be obtained. We next had to investigate whether H_2 was a quencher of NF(a). The data presented in Fig. 10 indicate that conditions can be established where NF(a) is essentially independent of H_2 flow.

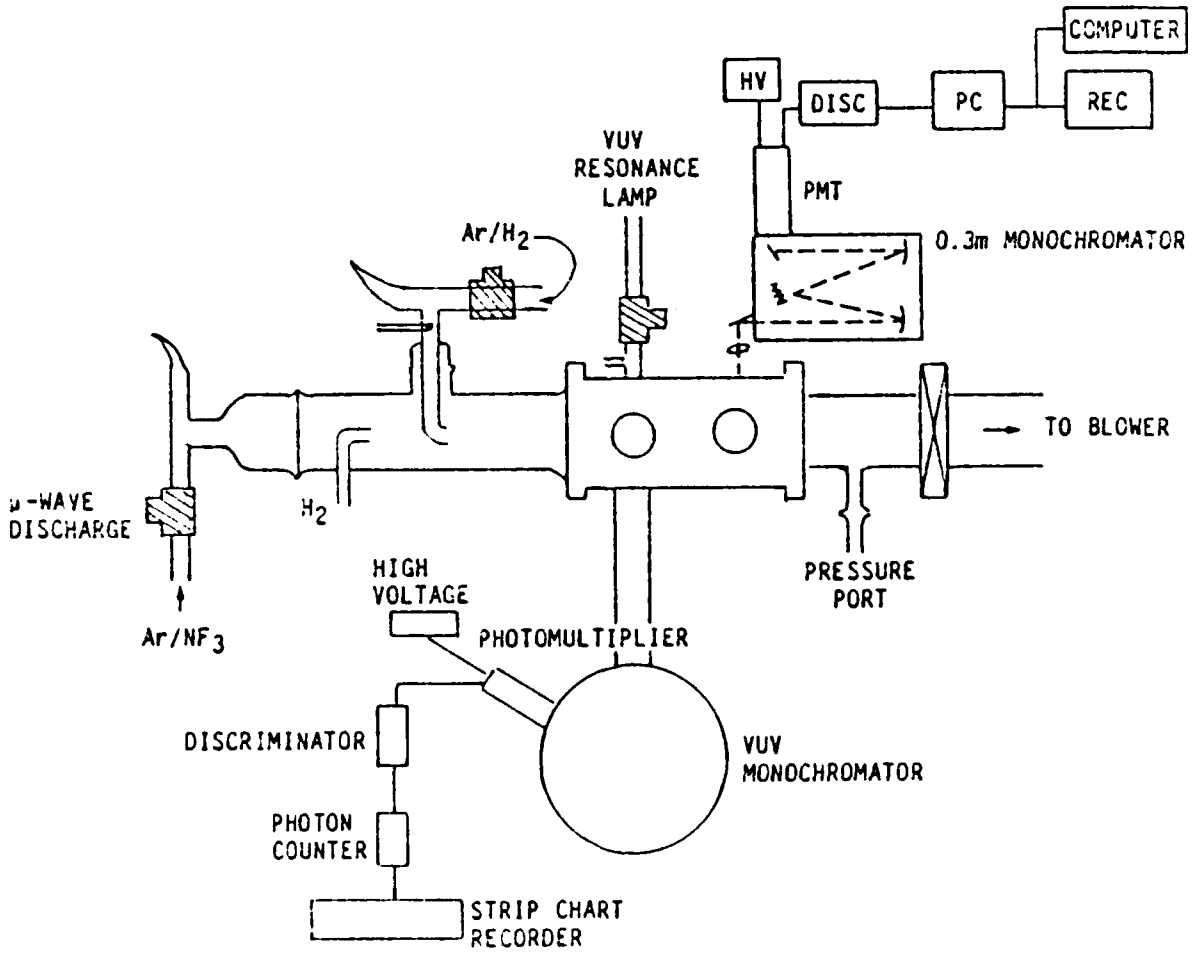

Figure 9. Block diagram of CONAN flow tube.

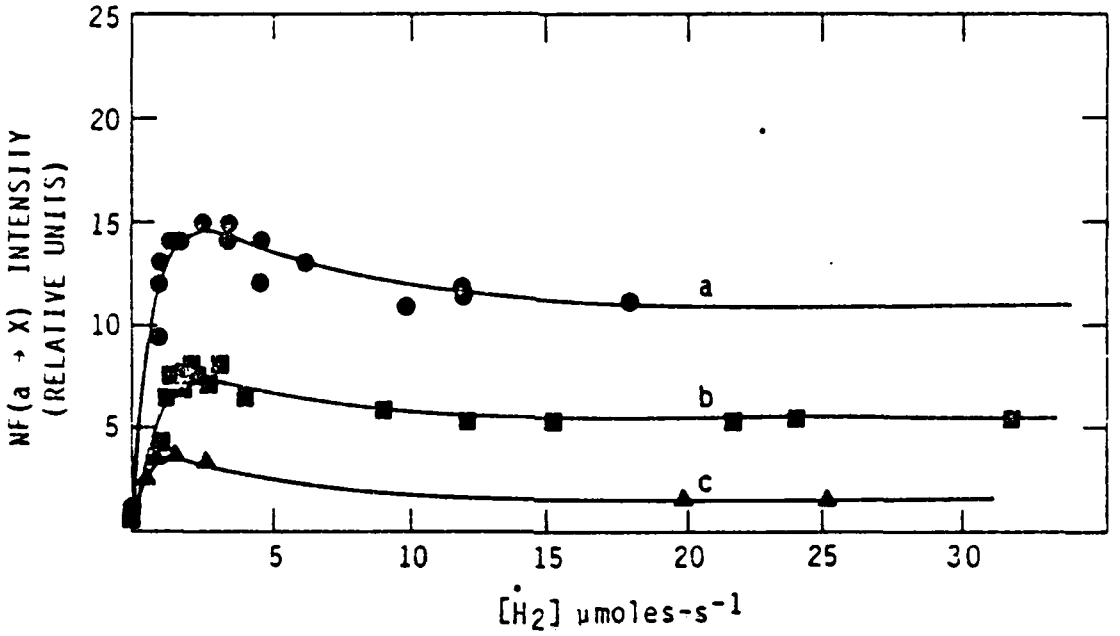

Figure 10. Relative concentration of NF(a) as a function of H_2 Flow for three different NF_3 flows: a) [$\dot{N}F_3$] = 6 μmoles-s^{-1}; b) [$\dot{N}F_3$] = 2.7 μmoles-s^{-1}; c) [$\dot{N}F_3$] = 1.25 μmoles-s^{-1}.

The motivation for adding a large excess of H_2 with respect to NF_3 was to react away any free F and NF_2 produced in the discharge. In addition, by injecting a large excess of H_2 in the formation region of NF(a), subsequent addition of smaller amounts of undissociated H_2 further downstream would have minimal effect on the NF(a) concentration. All removal then could be attributed to H atoms.

The H atom quenching experiments are thus run as follows. A small flow of NF_3 (typically 0.2 μmoles s^{-1}) in a flow of Ar (2 mmoles s^{-1}) are discharged in an Evenson cavity using ~6W of microwave power. Approximately 0.2 mmoles s^{-1} of H_2 was added 20 cm downstream from the NF_3/Ar injection region. A mixture of H_2/Ar was discharged in a second cavity (50W) and injected 15 cm downstream from the first H_2 injector. For clarity this H_2 flow is referred to as the secondary H_2. The Ar flow carrying the secondary H_2 was kept constant (typically 0.4 mmole s^{-1}). To assure that NF(a) decay

due to H atoms could indeed be observed, some preliminary runs were made. Figure 11 shows two scans of NF(a→X) emission under identical conditions except that in Fig. 11b the secondary H_2 discharge is on. The diminution of NF(a) due to H atoms is clear. The [NF(a)] was monitored as a function of added discharged H_2. These experiments were performed by holding all flows constant except for the secondary H_2. No detectable change in [NF(a)] was observed for any secondary H_2 flow without the discharge. Large changes (~ an order of magnitude) could be observed when the secondary H_2 discharge was initiated. Although we had not yet calibrated the detection system to measure absolute H atom concentrations, it was felt that it was prudent to monitor relative [NF(a)] as a function of secondary H_2. At relatively low secondary H_2 flows (< 4 μmoles s^{-1}), ln (NF(a) chemiluminescence intensity) varied linearly with the secondary H_2 flow. At these low flows one would expect that the dissociation fraction of H_2 is essentially constant. Thus, the H atom concentration would be a constant fraction of the secondary H_2. At higher flows of secondary dary H_2 the plots displayed a curved behavior indicative of a diminishing dissociation efficiency. Only a few such runs were made to become convinced that NF(a) decays could be detected in the presence of H atoms. The next step was to calibrate the detection system, outlined as follows.

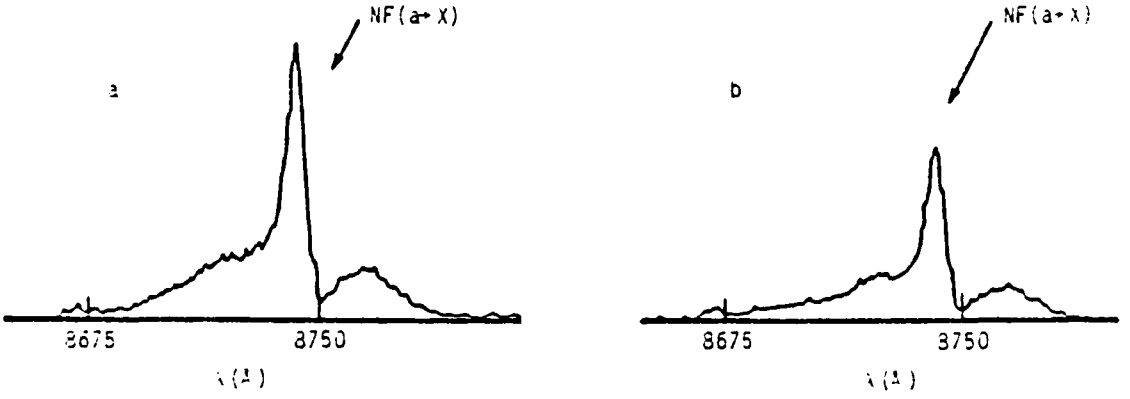

Figure 11. Scans of NF(a→X) emission showing removal by hydrogen atoms: a) H_2 discharge off; b) H_2 discharge on. Conditions as follows: pressure = 1.24 torr; secondary H_2 flow = 860 μmoles-s^{-1}.

The titration of NO was used with H to measure H atom concentrations. The recombination reaction of H + NO produces HNO emission. The intensity is proportional to [H][NO] and is pressure independent (Refs. 10,11). The proportionality constant is determined by the following titration.

2.3.2.1 H atom calibration procedure--Having established that we could indeed detect removal of NF(a) by H atoms, the next step was to develop a calibration standard for H atom number density. These calibration experiments are described as follows.

The titration of H + NOCl first described by Clyne and Stedman (Ref. 10) was chosen. The reaction sequence is

$$H + NOCl \rightarrow HCl + NO \qquad (9)$$

$$H + NO + M \rightarrow HNO^* + M \qquad (10)$$

followed by radiative emission from HNO^*. When [H] > [NOCl], unreacted H combines with NO to produce the $HNO^* \rightarrow HNO + h\nu$ red afterglow (Ref. 11). When [NOCl] > [H] the glow is extinguished. To use this titration one adds a metered flow of NOCl to an unknown flow of H while monitoring the HNO* emission. This chemiluminescence has four characteristic features at 627.2, 692.5, 762.5, and 796.5 nm (Ref. 11). We used a 9 nm bandpass filter centered at 690.5 nm to monitor the 692.2 nm peak with a Hamamatsu R955 PMT.

Earlier work by Clyne and Thrush (Ref. 11) had shown that the HNO* emission intensity resulting from the three body recombination H + NO + M → HNO* + M is described by

$$I_{HNO} = K[H][NO]$$

and is independent of total pressure over the range of 1 to 2.5 torr. We note that I_{HNO} is proportional to [H] for a given [NO]. To utilize this titration as a calibration standard, the proportionality constant K must be determined. Since I/[NO] is proportional to [H] it is also true that $I/[NOCl]_{added}$ is

proportional to [H]. Note that $[H] = [H]_0 - [NOCl]$ where $[H]_0$ is the atomic hydrogen concentration in the absence of NOCl.

Therefore

$$I = K([H]_0 - [NOCl])[NOCl]$$

A plot of I/[NOCl] versus [NOCl] will be linear with a slope of K and an abscissa intercept of $[H]_0$. With K determined by this method, the H atom concentration can readily be measured by adding a known concentration of NO to the unknown H flow.

Although straightforward in principle the NOCl calibration proved to be tedious with several subtle problems. The initial calibration produced non-linear behavior and irreproducible results when plots of I/[NOCl] versus [NOCl] were constructed. The probable cause of this problem was traced to a wall reaction. A detailed study of Clyne and Stedman's[10] paper revealed that they had observed a similar behavior on bare pyrex walls. The postulated reaction sequence including wall effects is

$$H + NOCl \rightarrow HCl + NO$$

$$H + NO + M \rightarrow HNO^* + M$$

$$H + HCl \rightarrow H_2 + Cl \qquad (11)$$

$$Cl + Cl \xrightarrow[Wall]{} Cl_2 \qquad (12)$$

$$H + Cl_2 \rightarrow HCl + Cl \qquad (13)$$

The catalytic recombination of Cl on the wall forms Cl_2 which then consume H via the rapid Cl_2 + H reaction. By treating their flow tube walls with phosphoric acid which inhibits wall recombination of Cl, Clyne and Stedman's results became much more reproducible.

A section of the flow tube was uncoated Pyrex. This design permitted visual examination of chemiluminescence in the flow tube. Subsequently this reaction cell was coated with Teflon in an effort to solve this problem. The calibration plots of I/[NOCl] versus [NOCl] did become much more reproducible and the linearity improved. Although the NOCl titration technique proved to be more difficult to use than anticipated, the titrations performed in the Teflon coated flow tube gave satisfactory results.

A typical plot of I/[NOCl] as a function of added [NOCl] using the fully coated reactor is shown in Fig. 12. An average of five calibration runs at various conditions yielded a proportionality constant K = 0.46 x 10^{-7} A/(mtorr) with a standard deviation of 15 percent. With a known K one can add a known concentration of NO to the flow and determine [H] from $I_{HNO}/K[NO] = [H]$.

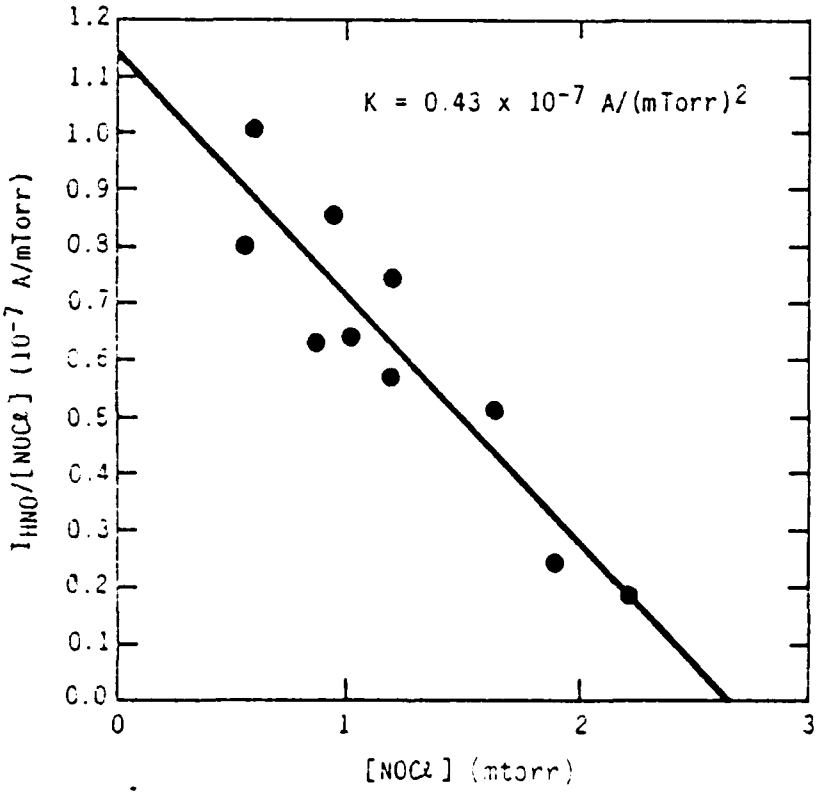

Figure 12. Typical data for H + NOCl titration. Shown is a plot of $I_{HNO}/[NOCl]_{added}$ versus $[NOCl]_{added}$. The slope of the plot is used to determine the proportionality constant $K = I_{HNO}/[H][NO]$

The H atom production at a given microwave power and at a constant Ar/H_2 flow rate was not constant with respect to time. The data in Fig. 13 graphically demonstrate this behavior. These data were obtained by keeping the H_2/Ar and NO flow rates constant while varying the microwave power. The numbers attached to the data points indicate the order in which the data were recorded. Note the reduction in the intensity of the HNO* emission for a constant microwave power (points 4 and 5) and the apparent hysteresis-like behavior when the power was reduced from 90 to 40 W. The cause of this problem was heating of the microwave cavity. Even though a flow of compressed air was forced through the cavity, it provided insufficient cooling for uniform H atom production. The difficulty was resolved by flowing the cooling air through an ice bath prior to introduction into the microwave cavity. This allowed constant H atom production for at least a minute at any microwave power. Since it required only a few seconds to measure both the NF(a→X) and HNO* emission intensities, this was a satisfactory remedy. A further improvement might be realized using a different design such as that of Ding et al. (Ref. 10) who used a fluid as a coolant.

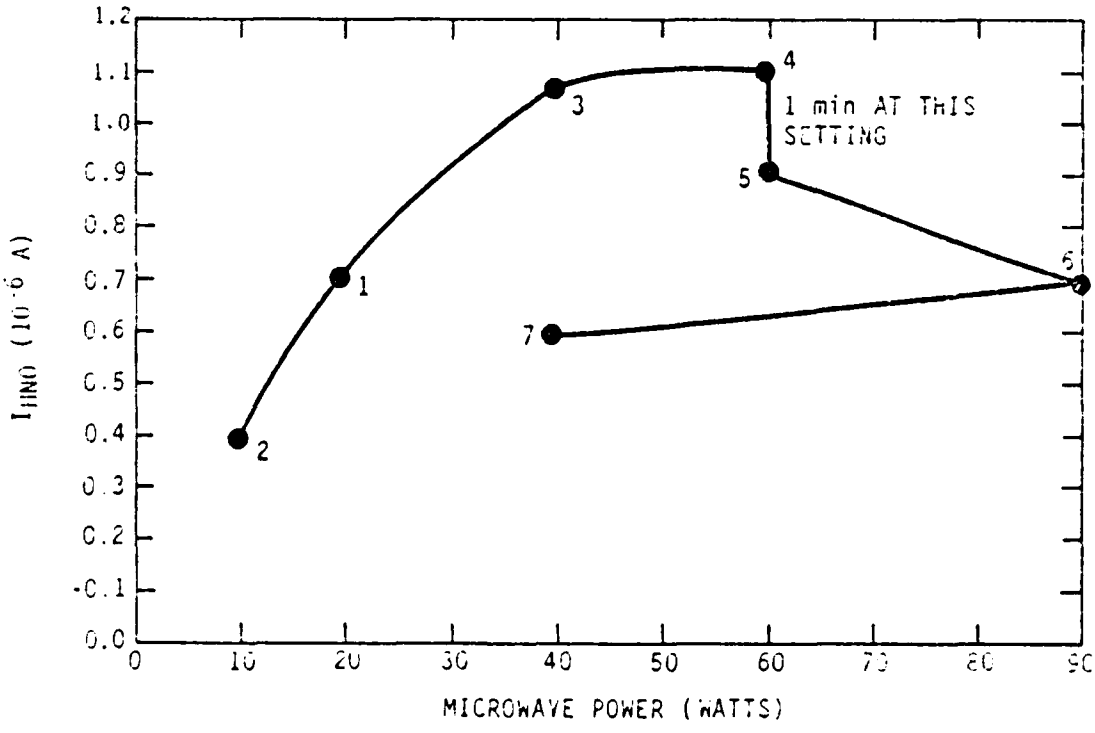

Figure 13. Plot of I_{HNO} (proportional to H) as a function of microwave power. Note that the production efficiency for H atom production is strongly dependent upon the microwave discharge power. (Numbers refer to the temporal order in which data was obtained.)

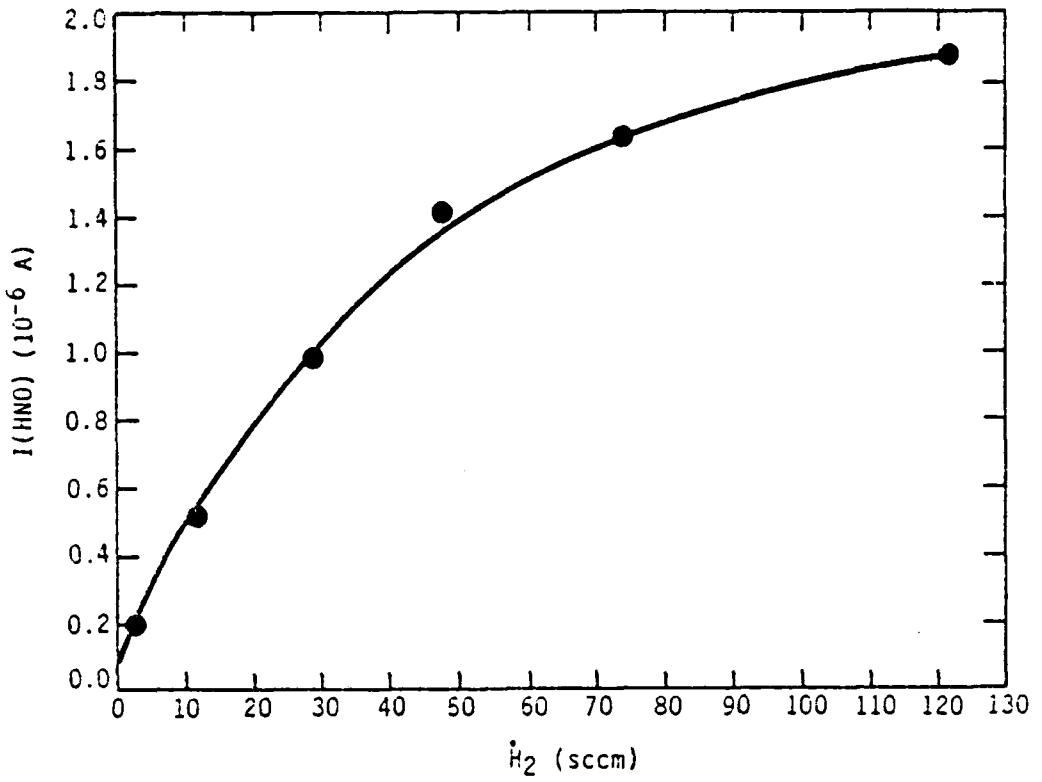

Figure 14. I_{HNO} as a function of $[H_2]_{added}$ for constant [NO] and constant microwave discharge power.

In practice the microwave power was held fixed and [H] variations were obtained by changing the H_2 flow rate. A typical plot of $I_{(HNO)}$ versus H_2 flow rate at constant [NO] is shown in Fig. 14. Note that as $[H_2]$ is increased, the dissociation efficiency is reduced. This observation coupled with the dependence of H atom production on the temperature of the microwave cavity clearly indicate that [H] must be measured for each H_2 flow. One cannot rely upon comparable conditions to give the same [H].

Next the response of I_{HNO} at constant [H] was checked while changing the NO flow. Figure 15 clearly shows that I_{HNO} is indeed proportional to added NO. With these checks and the previously described calibration completed we were in a position to measure the desired H + NF(a) → Products rate constant. It was noted also that typical [H] was $\gtrsim 10^{14}$ atoms cm^{-3} while $[NF_3]$ (which represents the maximum possible [NF(a)]) was $\sim 10^{13}$ molecules cm^{-3}. (Later experiments showed that the maximum [NF(a)] was no greater than 2×10^{12} molecules cm^{-3}. Thus, the pseudo first order condition with H in excess was satisfied.

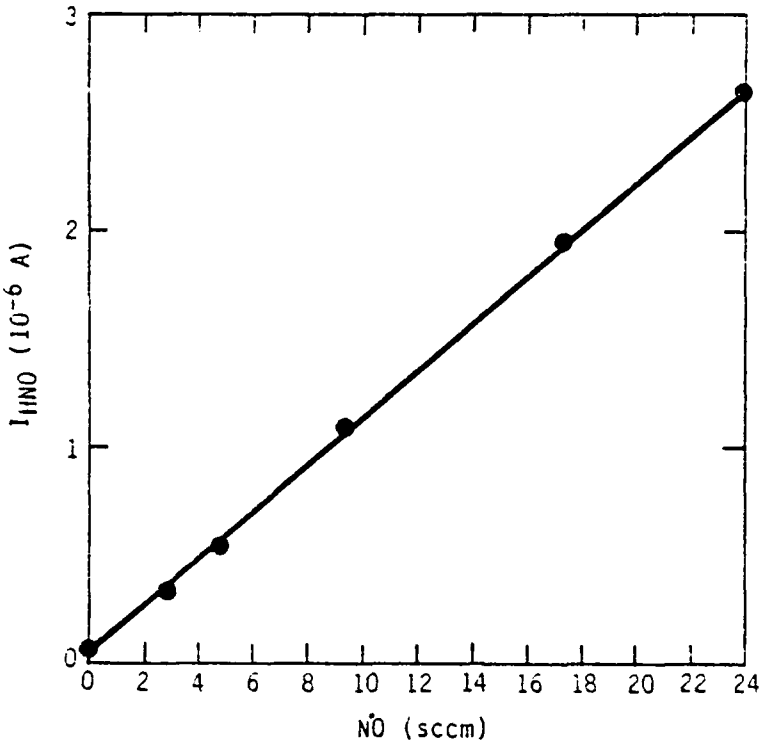

Figure 15. I_{LNO} versus $[NO]_{added}$ for constant [H].

Typical scans of the NF(a→X) emission with and without H atoms was previously presented in Fig. 11. In practice the peak NF(a→X) signal was monitored at 374.2 nm but periodically scanned the entire band to check for any possible spectral interferences from $N_2(3\rightarrow A)$ and HF(v). At the high H_2 flows used in these studies no interferences were detected.

A sample plot of ln[NF(a)] as a function of [H] is shown in Fig. 16. These data yielded a rate coefficient of 2.9×10^{-13} cm^3 molecule^{-1} s^{-1}. The rate coefficient was measured under several different sets of conditions. Table 1 summarizes the results.

The average of all runs is

$$k = (3.1 \pm 0.6) \times 10^{-13} \text{ cm}^3 \text{ molecule}^{-1} \text{ s}^{-1}$$

The error represents the best estimate of the systematic uncertainties in the measurements. These arise from the H atom calibration which is the dominant source of error. This value is in excellent agreement with the value of

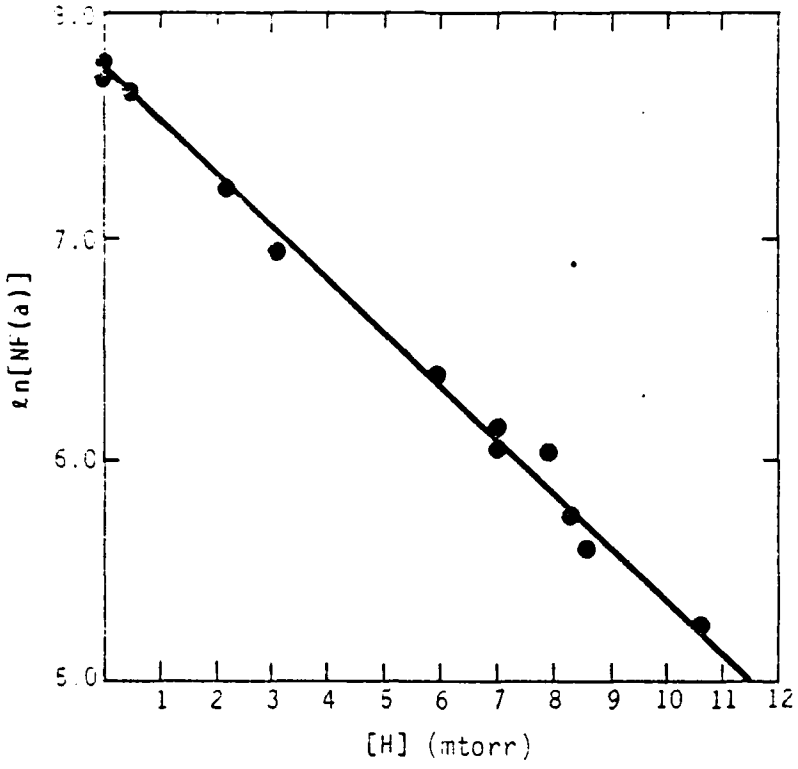

Figure 16. Plot of ℓn[NF(a)] as a function of added [H]. Total pressure for this run using Ar carrier gas was 1.79 torr

TABLE 1. Compilation of Conditions for Measurement of H + NF(a) → Products Rate Coefficient.

Pressure (Torr)	Flow Velocity (cm s^{-1})	Effective Reaction Time (10^{-3}s)	Rate Coefficient (cm^3 $molecule^{-1}$ s^{-1})
1.49	2048	21.9	2.81×10^{-13}
1.79	1641	26.6	2.85×10^{-13}
0.91	3191	14.1	3.33×10^{-13}
1.61	1804	42.9	3.38×10^{-13}

NOTE: Buffer gas in all cases was Ar. Distance from H atom injector to observation port was 45 cm.

2.5×10^{-13} cm^3 $molecule^{-1}$ s^{-1} estimated by Clyne et al. (Ref. 2,3). It is apparent that the first step in the proposed excitation scheme of N_2^* is relatively slow.

Throughout these studies it was observed that [NF(a)] was essentially independent of [H_2] added. No decrease in [NF(a)] could be seen even though sensitivity was more than adequate to see a 10 percent degradation. From these observations, an upper limit for H_2 quenching of NF(a) was estimated to be 1×10^{-14} cm^3 $molecule^{-1}$ s^{-1}. This can be compared to an earlier measurement of D_2 quenching of NF(a) by Kwok et al. (Ref. 13) who reported a value of $k < 7 \times 10^{-14}$ cm^3 $molecule^{-1}$ s^{-1}.

2.4 PRODUCTION RATE FOR $N_2(B)$ EXCITATION

2.4.1 Background--Determination of the production rate of excited N_2 from the H + NF_2 reaction scheme is of critical importance to the possible utilization and development of this system into a chemical laser pump source. Since $N_2(B)$ is relatively easy to monitor and is the likely source of $N_2(A)$ produced in this scheme via $N_2(B \rightarrow A)$ emission, we chose to test the mechanism previously postulated in the Refs. 3,9,10. The salient model is described by two steps

$$NF(a) + H \rightarrow N(^2D) + NF$$

$$NF(a) + N(^2D) \rightarrow N_2(B) + F$$

The initial approach was to add $N(^2D)$ atoms produced by a microwave discharge to a flow of microwave discharged NF_3 dilute in Ar (which produces NF(a)). The difficulty of strong $N_2(B \rightarrow A)$ emission from three body recombination of $N(^4S)$ atoms (produced from our discharge source of $N(^2D)$ atoms) was encountered. This would have been the preferred approach since interferences caused by H atom chemistry would have been eliminated. The strong recombination N_2 first positive emission, however, made data from this approach difficult to interpret.

An alternate approach involved the entire H + NF_2 reaction sequence. Although more complex than the first method attempted, it does offer the advantage of permitting a detailed study of the actual chemical production of N_2^* in an environment similar (but not identical) to what one would expect in a laser device.

The model described by Eqs. (2) and (3) leads to predictions of the $N_2(B)$ production that can be tested experimentally. If reactions (2) and (3) are an accurate description, then the rate of change of $[N_2(B)]$ with time is given by

$$\frac{d[N_2(B)]}{dt} = k_3[NF(a)][N(^2D)] - [N_2(B)]\left(A_{B\rightarrow A} + K_Q\right) \qquad (14)$$

where $A_{B\rightarrow A}$ is the radiative rate for N_2 first positive emission and K_Q is the first order quenching rate of $N_2(B)$ by species in the flow.

The $N_2(B)$ emits radiatively essentially instantaneously with respect to the spatial volume in which it is formed in the flow tube. Thus, $N_2(B)$ is in steady state with NF(a) and $N(^2D)$. Hence, from Eq. (14)

$$k_3[NF(a)][N(^2D)] = [N_2(B)]\left(A_{B\rightarrow A} + K_Q\right) \qquad (15)$$

Note that a plot of $[N_2(B)]$ versus the product of [NF(a)] x $[N(^2D)]$ should be linear with a slope of $k_3/(A_{B\rightarrow A} + K_Q)$. To extract an excitation rate from such an analysis one must simultaneously measure absolute concentrations of NF(a), $N_2(B)$, and $N(^2D)$. Careful and systematic calibrations are required and are described as follows.

The $[N_2(B)]$ and [NF(a)] were determined by measuring the intensities of the N_2 first-positive and NF(a→X) systems. The relative response function of the monochromator and detection system was determined using spectral standard deuterium and quartz-halogen lamps. The next section describes how the relative response curve was placed on an absolute basis.

2.4.2 Absolute photon emission rate measurements

2.4.2.1 General procedure--The observed signal is related to the true volume emission rate through

$$I_{obs} = I_{true} \frac{\Omega}{4\pi} \eta_\lambda T_\lambda V \qquad (16)$$

where $\Omega/4\pi$ is the effective solid angle subtended by the detection system, η_λ is the quantum efficiency of the photomultiplier at the wavelength of interest, T_λ is the transmission of the optical system (e.g., mirror reflectivities and grating efficiency) and V is the observed volume of luminous gas in the reactor. The wavelength dependence of the product $\Omega/4\pi\ \eta_\lambda T_\lambda V$ is given by the relative monochromator response function R_λ. Absolute values of that product are obtained in a calibration experiment using the O/NO air afterglow at one or several specific wavelengths. Absolute values at wavelengths other than those chosen for calibration experiments are obtained by scaling with R_λ.

As stated earlier, the relative spectral response of the monochromator was calibrated between 200 and 900 nm using standard quartz-halogen and D_2 continuum lamps.* Additional confirmation of the calibration between 500 and 800 nm is obtained by scanning the air afterglow spectrum and comparing observed relative signal levels with the relative intensities given by Fontijn et al. (Ref. 14). The absolute spectral response of the detection system is measured at 580 nm using the O/NO air afterglow as described in the following paragraph.

When atomic oxygen and nitric oxide are mixed, a continuum emission extending from 375 nm to beyond 3000 nm is observed (Refs. 14-22). The intensity of this emission is directly proportional to the product of the number densities of atomic oxygen and nitric oxide, and independent of pressure of bath gas, at least at pressures above about 0.2 torr. Thus, the volume-emission rate of the air afterglow is given by

$$I_{true} = k_\lambda [O][NO]\ \Delta\lambda \qquad (17)$$

where k_λ is the air afterglow rate coefficient in units of cm^3 $molecule^{-1}$ s^{-1} nm^{-1} and $\Delta\lambda$ is the monochromator bandwidth. Literature values for this rate coefficient span a range of more than a factor of two (Refs. 14-20) but recent

*Optronic Laboratories Inc., Silver Spring, Maryland.

studies (Ref. 19) indicate that the original work of Fontijn et al. (Ref. 14) is probably correct at wavelengths shorter than ≈ 800 nm. We use a value of 1.25×10^{-19} cm^3 molecule^{-1} s^{-1} nm^{-1} at λ = 580 nm. Combining Eqs. (16) and (17) gives the observed air afterglow intensity:

$$I_\lambda^{O/NO} = k_\lambda [O][NO] \Delta\lambda \frac{\Omega}{4\pi} \eta_\lambda T_\lambda V \tag{18}$$

Air afterglow calibration experiments give a calibration factor,

$$<_\lambda = \frac{I_\lambda^{O/NO}}{[O][NO]} = k_\lambda \Delta\lambda \frac{\Omega}{4\pi} \eta_\lambda T_\lambda V \tag{19}$$

the determination of which will be described in the next paragraph.

Absolute number densities of emitters are obtained by dividing absolute volume emission rates by known transition probabilities. The air afterglow calibration factor, $<_\lambda$, and the moderately well established value of the air afterglow rate constant, k_λ, are used to convert observed emission intensities to volume emission rates:

$$I_{true} = \frac{I_{obs} k_{\lambda_c} \Delta\lambda_c R_{\lambda_c}}{<_{\lambda_c} R_{\lambda_{obs}}} \tag{20}$$

where λ_c represents the wavelength of the calibration experiments and λ_{obs} is the wavelength of the transition of interest. The I_{obs} must be the total integrated band intensity. In this work the measured emission intensities were measured in terms of peak intensities. A calibration factor consisting of the ratio of the integrated band intensity to the product of the spectrometer bandwidth and the peak intensity was determined for cases in which total intensities were needed. In calibration experiments, the band areas were integrated numerically using spectral scans which were greatly expanded along the wavelength axis.

A series of calibration experiments taken over a period of time established the calibration factor, $<_{580}$, to ±15 percent. An additional uncertainty of ±25 percent exists in the absolute value of the air afterglow rate coefficient k_{580}. Further uncertainties in the determination of the absolute photon-emission rate for $N_2(B)$ come in through the relative monochromator response function. There were also some errors introduced in determining absolute NF(a→x) emission rates because the a→X emission band intensities were needed. In calibration experiments, the band areas were integrated numerically using spectral scans which were greatly expanded along the wavelength axis.

2.4.2.2 Air afterglow calibration procedure--In air afterglow calibration experiments, the intensity at the calibration wavelength is measured when known quantities of both atomic oxygen and nitric oxide are added to the reactor. Known quantities of atomic oxygen are prepared by titration of nitrogen atoms with excess nitric oxide:

$$N + NO \rightarrow N_2 + O \qquad (21)$$

($k_{21} = 3.5 \times 10^{-11}$ cm^3 molecule^{-1} s^{-1}) (Refs. 23-25)

In the absence of added nitric oxide, N atom recombination produces chemiluminescence from the nitrogen first-positive bands, the intensity of which is proportional to the square of the N atom number density. The kinetic processes are described as follows.

$$N + N + M \rightarrow N_2(B^3\Pi_g) \qquad (22)$$

$$N_2(B^3\Pi_g) \rightarrow N_2(A^3\Sigma_u^+) + h\nu \quad \text{(first-positive bands)} \qquad (23)$$

Upon addition of NO the first-positive emission intensity decreases until the quantity of NO added balances the amount of N atoms initially in the flow. At this point, the end point of the NO titration, all N initially in the reactor has been quantitatively converted to O, and no emission is observed in the

reactor. As NO is further added to the reactor, the air afterglow emission begins to be observed, and the intensity of the emission varies linearly with the amount of NO added. Such a titration plot is shown in Fig. 17. The equation describing the change in the air afterglow intensity as a function of added NO for NO additions beyond the titration end point is

$$I_{O/NO} = \kappa[O][NO] = \kappa[N]_o([NO]_o - [N]_o) \qquad (24)$$

where κ is the constant of proportionality relating the air afterglow intensity to the product [O][NO], $[N]_o$ is the number density of N atoms initially in the reactor prior to NO addition, and $[NO]_o$ refers to the NO number density which would be obtained in the absence of reaction (21). The factor κ then is determined to be the ratio of the square of the slope to the intercept of the line describing the change in air afterglow intensity with [NO].

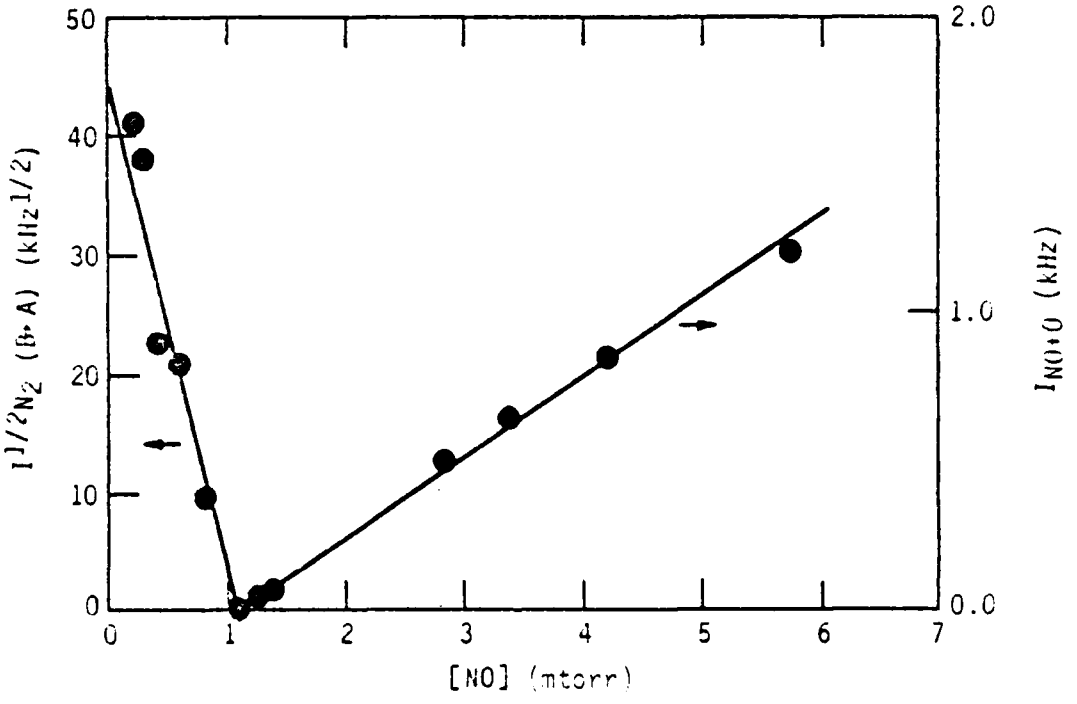

Figure 17. Plot showing O + NO titration procedure.

Two major complications can lead to problems in using the technique in Eq. (24) to calibrate the apparatus for absolute photon-emission rates or for [O] measurements. If the initial N-atom number density is greater than about 10^{14} atoms cm^{-3}, some O_2 spectral features from O-atom recombination will begin to be observable above the air afterglow continuum, and can lead to incorrect air-afterglow intensity determinations (Refs. 26,27). A more serious problem, however, lies in the slow removal of O-atoms in a three-body recombination with NO. The important reactions are:

$$O + NO + M \rightarrow NO_2 + M \qquad (25)$$

($k_{25} = 7 \times 10^{-32}$ cm^6 molecule^{-2} s^{-1} for M = Ar) (Ref. 28)

and

$$O + NO_2 \rightarrow NO + O_2 \qquad (26)$$

($k_{26} = 9.5 \times 10^{-12}$ cm^3 molecule^{-1} s^{-1}) (Ref. 28)

Reaction (26) is fast, and essentially acts to maintain a constant NO number density and to double the effective rate at which O is removed in reaction (25). This effect becomes a problem at higher pressures (> 1.5 torr), longer mixing times (> 30 ms) and large NO concentrations (> 10^{14} molecules cm^{-3}).

It is just these adverse conditions which give the best signal-to-noise in the calibration experiments. The calibrations for the experiments described in this report were corrected when necessary for the effects of removal of O in reactions (25) and (26).

2.4.3 $N(^2D)$ resonance lamp calibration

2.4.3.1 Background--As mentioned earlier resonance fluorescence was used to detect $N(^2D)$ atoms. The lamp is of a special design and is shown in Fig. 18. Two crucial features are: (a) the gas inlet to the lamp is near the lamp output and the gas flow is out the back; and (b) the microwave cavity

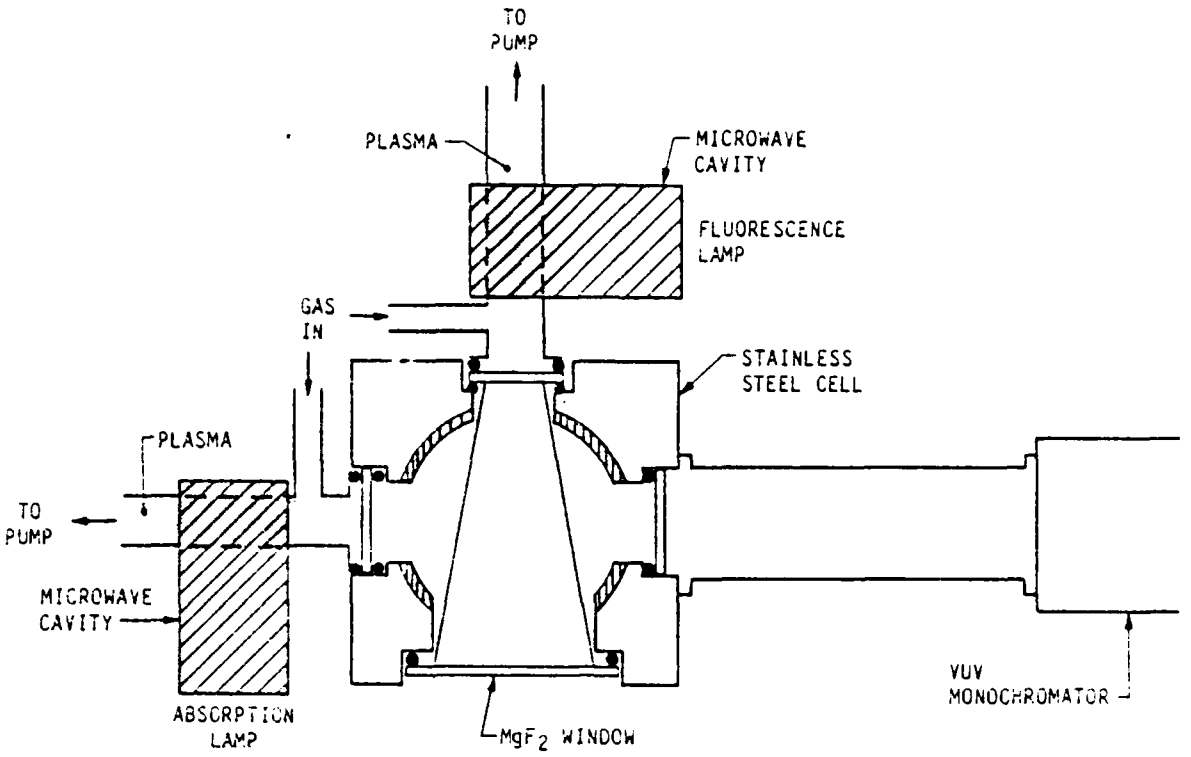

Figure 16. Details of the resonance fluorescence/absorption lamps used for $N(^2D)$ concentration measurement.

is situated so that the discharge plasma extends to the lamp output window. This minimizes the degree of lamp self-reversal.

For the present studies the lamp was run at 1.5 mtorr of He with a trace of N_2 introduced through a Granville Phillips calibrated leak valve. This procedure ensures reproducible lamp operation. The microwave power to the lamp was kept at the moderate value of 20 W. These operating points were chosen to utilize the results of previous studies (Ref. 29) that reported gas temperatures of ~600 K in the lamp under these conditions. As is well known in resonance fluorescence or absorption measurements, the temperatures of the lamp and the absorbing medium both influence the observed signal strength.

The calibration procedure for the $N(^2D)$ resonance fluorescence lamp involved relating the $N(^2D)$ fluorescence intensity I_F to $N(^2D)$ concentrations measured by resonance absorption. Two identical lamps were used. The absorption lamp was attached to the flow tube opposite the VUV monochromator while

the fluorescence lamp was normal to both the monochromator and the absorption lamp. The calibration is complicated by the energy level structure of N atoms as shown in Fig. 19. Since the $2s^2 2p^3(^2P^\circ)$ and $2s^2 2p^3(^2D^\circ)$ levels are both radiatively connected to the $2s^2 2p^2 3s(^2P)$ level, fluorescence at 149.3 nm can contain contributions from both $^2P^\circ$ and $^2D^\circ$. The degree of contamination, of course, depends upon the ratio of the resonance lamp intensity at 174.3 nm to that at 149.3 nm. In these experiments a dielectric coated filter (MgF substrate) was used at the lamp output. The filter rejected 174.3 nm while passing 149.3 nm. With the filter in place the lamp output was measured at both wavelengths and it was found that the ratio of the intensity at 174.3 nm to that at 149.3 nm was approximately 1 percent.

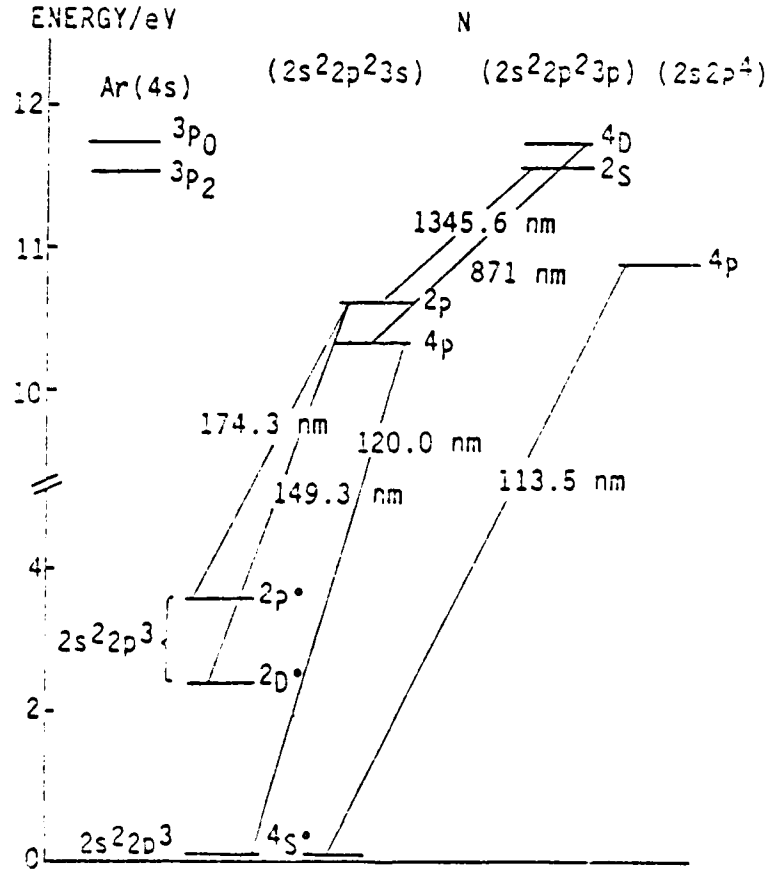

Figure 19. Energy level structure of N. Relevant transitions are indicated.

As an additional check selective quenching studies were performed on $N(^2D)$ and $N(^2P)$. These experiments were done by adding CO_2 to a flow of $N(^2D)$ and $N(^2P)$. The $N(^2D)$ and $N(^2P)$ atoms were produced in a microwave discharge of N_2 dilute in Ar. The relative concentration of $N(^2D)$ was measured using resonance fluorescence and $N(^2P)$ was monitored using $(^2P \rightarrow {}^4S)$ emission at 347 nm. Since the quenching rate of N^2D by CO_2 is greater than that for N^2P, the N^2D is selectively quenched. If part of the observed 149 nm fluorescence originates from the resonance lamp exciting $N(^2P)$ atoms, then plots of $\ln\left(I_F(149\text{ nm})\right)$ versus $[CO_2]$ and $\ln\left(I(347\text{ nm})\right)$ versus $[CO_2]$ should become parallel when the N^2D is totally quenched. However, it was observed that the 149 nm fluorescence signal was still decaying faster than the 347 nm signal even at the highest flow rates of CO_2. It was concluded from the study that the upper limit of $N(^2P)$ contribution to the $N(^2D)$ fluorescence signal was less than 8 percent.

Following these systematic checks, the resonance lamp calibrations were performed. These measurements were accomplished by constructing a curve of growth for $N(^2D)$. A flow of N_2 dilute in Ar was discharged in a microwave cavity to produce an unknown concentration of $N(^2D)$. Resonance absorption on the 149.3 nm line was used to measure the concentration of $N(^2D)$. Since resonance fluorescence and absorption display some subtleties in atomic N these phenomena will be described as follows.

2.4.3.2 Review of resonance fluorescence and absorption--The general techniques of resonance absorption and fluorescence have been described in detail in Ref. 30. Only the salient features are outlined as follows.

For an isolated line Beer's law is usually written

$$I_{Trans}(\nu) = I_0(\nu)\, e^{-N\sigma(\nu)\ell} = I_0(\nu)\, e^{-\kappa(\nu)\ell} \qquad (27)$$

where

I_0 = incident intensity at frequency ν

I_{Trans} = transmitted intensity after transversing the absorbing medium a distance ℓ

N = number density of absorbers

$\sigma(\nu)$ = absorption cross-section at frequency ν

$k(\nu)$ = absorption coefficient at frequency ν

For small absorptions ($N\sigma(\nu)\ell \ll 0.1$)

$$I_{Trans}(\nu) \sim I_0(\nu)(1 - N\sigma(\nu)\ell) \tag{28}$$

or

$$\ell n(I_0/I_{Trans}) = \ell n\left(\frac{1}{1-A}\right) = N\sigma(\nu)\ell = k(\nu)\ell \tag{29}$$

where

$$A \equiv \frac{I_0 - I_{Trans}}{I_0} \tag{30}$$

Thus, for absorption at a single frequency the measured fractional absorption can be used to determine N. In practice, however, one cannot measure the fractional absorption at an isolated frequency. Rather, the fractional absorption covering a frequency range that typically encompasses the entire absorption line is measured. This integrated fractional absorption is the quantity that is relevant to the present discussion.

In this case the fractional absorption A is related to the absorption coefficient k_ν through

$$A = \frac{I_0 - I_{Trans}}{I_0} = \frac{\int_{-\infty}^{\infty} I(\nu)\left(1 - e^{-k\nu\ell}\right) d\nu}{\int_{-\infty}^{\infty} I(\nu)\, d\nu} \tag{31}$$

When the line is predominantly Doppler broadened the absorption coefficient can be approximated by

$$k_\nu = k_0 e^{-\omega^2} \tag{32}$$

where k_0 = the absorption coefficient at line center, and

$$\omega = \frac{2(\nu - \nu_0)}{\Delta\nu_D} \sqrt{\ln 2} \tag{33}$$

In Eq. (33) $\Delta\nu_D(cm^{-1}) = (2.287 \times 10^{-3})\ \bar{\nu}_0 \sqrt{\frac{T}{M}}$ is the Doppler width at frequency $\bar{\nu}_0$.

It can also be shown that in general the absorption coefficient integrated over all frequencies is given by

$$\int_{-\infty}^{\infty} k_\nu d\nu = \frac{\pi e^2}{mc} Nf \tag{34}$$

where f is the oscillator strength of the transition, m is the electron mass, e is the electron charge, and c is the speed of light. If the approximation $k_\nu = k_0 e^{-\omega^2}$ in Eq. (34) is used, we find that

$$k_0 = \frac{2}{\Delta\nu_D} \sqrt{\frac{\ln 2}{\pi}} \frac{\pi e^2}{mc} Nf \tag{35}$$

In many situationsm including the present one, the source of resonance radiation (lamp) and the absorbers (N^2D in flow tube) are at different temperatures. This is usually treated using the empirical expression

$$I_\nu = I_0 e^{-(\omega/x)^2} \tag{36}$$

for the intensity of the lamp as a function of frequency.

where $x \equiv \dfrac{\text{Emission line breadth}}{\text{Absorption line breadth}}$

Thus, we arrive at an expression for the integrated absorption for the case of the lamp and absorber at different temperatures both being Doppler broadened.

$$A = \frac{I_0 - I_{Trans}}{I_0} = \frac{\int_{-\infty}^{\infty} \left(1 - e^{-k_0 \ell e^{-\omega^2}}\right) e^{-(\omega/\alpha)^2} \, d\omega}{\int_{-\infty}^{\infty} e^{-(\omega/\alpha)^2} \, d\omega} \qquad (37)$$

The actual emission line shape may differ from the Gaussian form of Eq. (37) due to self-absorption (which preferentially affects the center of the line) or monoenergetic excitation processes (e.g., energy transfer from metastable Ar). Mathematical treatments of these effects have been given by Kaufman and coworkers (Refs. 31,32) and by Clyne and coworkers (Refs. 33-35). The self-absorption model of Rawlins and Kaufman[31] gives an excellent match to O(I) absorption data over a wide range of lamp optical thickness. However, the inclusion in some applications of self-absorption (Ref. 36) can be vitally important. It will not be considered here since it is not a factor in the experiments. Monoenergetic effects are often collisionally moderated in steady-state line sources. In any case, since only the integral over the line is observed, Eq. (37) is often an adequate description.

Equation (37) can be integrated in a straightforward manner by the method of Gaussian quadrature. However, for the purpose of the present discussion, the following analytic expression for A is useful:

$$A = \sum_{n=1}^{\infty} (-1)^{n-1} \frac{(k_0 \ell)^{1/2}}{n!(1 + n\alpha^2)^{1/2}} \qquad (38)$$

The expressions hold only in the case of a single line. However, the 149 and 174 nm transitions consist of multiplets which are difficult to resolve fully. For the case of unresolved multiplets (line separation << instrument resolution), an expression similar to Eq. (37) holds:

$$A = \frac{\sum_i C_i \int_{-\infty}^{\infty} \left(1 - e^{-k_{0i} \ell e^{-\omega_i^2}}\right) e^{-(\omega/\alpha)^2} d\omega}{\sum_i C_i \int_{-\infty}^{\infty} e^{-(\omega_i/\alpha)^2} d\omega} \tag{39}$$

where the C_i represent the relative intensities of the components of the multiplet. The spectroscopic properties of the $N(^2D)$ and $N(^2P)$ resonance multiplets are given in Table 2.

A weighted average of the oscillator strengths for the three unresolved components near 149.3 nm combined with Eq. (35) gives

$$\langle k_0 \ell \rangle = 2.18 \times 10^{-13} N\ell \tag{40}$$

TABLE 2. Resonance Lines for Metastable Nitrogen Atoms

Atom	Wavelength nm	Upper State	Lower State	g_ℓ	Relative Intensity	$f_{\ell u}$ [a]
$N(^2D)$	149.2615	$^2P_{3/2}$	$^2D^\circ_{5/2}$	6	9	0.078
	149.2812	$^2P_{3/2}$	$^2D^\circ_{3/2}$	4	1	0.013
	149.4668	$^2P_{1/2}$	$^2D^\circ_{3/2}$	4	5	0.065
$N(^2P)$	174.2717	$^2P_{3/2}$	$^2P^\circ_{3/2}$	2	1	0.021
	174.2725	$^2P_{3/2}$	$^2P^\circ_{3/2}$	4	5	0.053
	174.5246	$^2P_{1/2}$	$^2P^\circ_{1/3}$	2	2	0.043
	174.5255	$^2P_{1/2}$	$^2P^\circ_{3/2}$	4	1	0.011

a. Lawrence, G.M. and Savage, B.D., "Radiative Lifetimes of UV Multiplets in Boron, Carbon and Nitrogen," Phys. Rev. 141, 67 (1966).

Finally, since ℓ = 5.0 cm

$$N = 9.14 \times 10^{11} \langle k_0 \ell \rangle \tag{41}$$

A determination of $\langle k_0 \ell \rangle$, thus, allows us to calculate N via Eq. (38). A Gaussian-quadrature numerical method was used to calculate $k_0 \ell$ from the observed fractional absorption using Eq. (37). A typical calibration plot of I_F versus $\ell n(1/1-A)$ for $N(^2D)$ is shown in Fig. 20. Using this calibration curve allowed us to determine $[N(^2D)]$ from a measurement of the fluorescence intensity I_F.

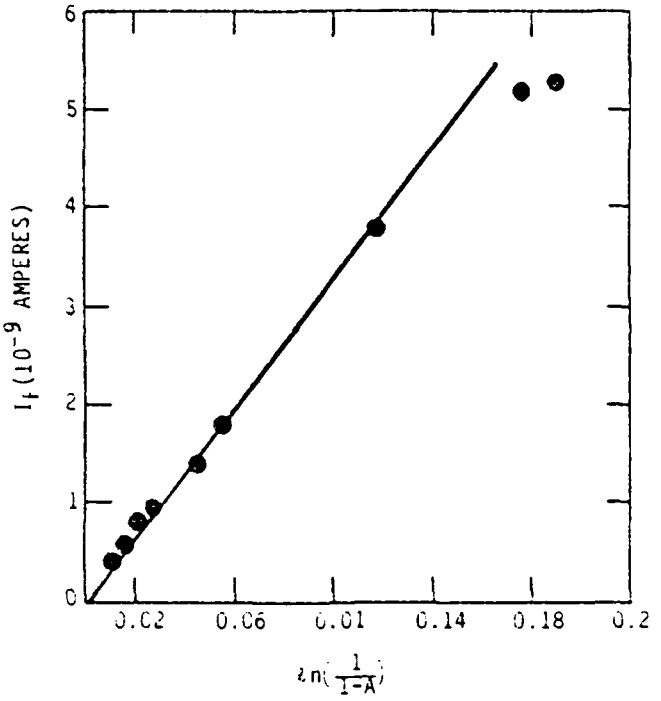

Figure 20. Plot of $N(^2D)$ resonance fluorescence signal I_F versus $\ell n(1/1-A)$.

2.4.3.3 Measurement Technique for $N_2(B)$ Excitation Rate--The actual data collection for measurement of the excitation rate coefficient, k_3, consisted of scans of the chemiluminescence due to $N_2(B \rightarrow A)$ and $NF(a \rightarrow X)$. In addition the $[N(^2D)]$ was determined each time $N_2(B \rightarrow A)$ and $NF(a \rightarrow X)$ were measured. Detection of all three species were done at one spatial position as

noted earlier. A run consisted of the measurements just described each at a constant H_2 flow. This was repeated for several H_2 flows with all other conditions held constant. Most runs were done using a fixed H_2 injector, but one set utilized a sliding H_2 injector. The bath gas pressure (0.7→3.2 Torr), bath gas species (Ar and He), and flow velocity (1.1×10^3 cm/s to 5.5×10^3 cm/s) were varied in completing a series of runs. The spectral scans were recorded on a COMPAQ microcomputer and stored on floppy disk for later analysis using the spectral fitting code. A sample scan and corresponding fit are shown in Fig. 21.

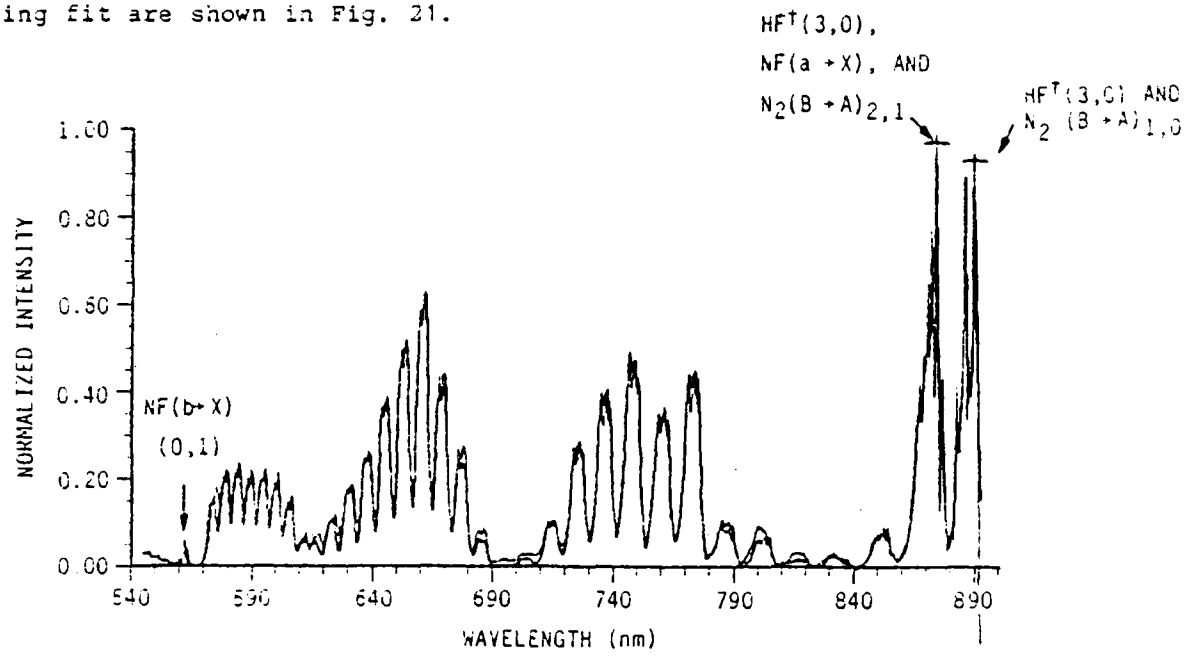

Figure 21. Chemiluminescence spectrum (thin line) showing NF(b→X), N_2(B→A), NF(a→X), and $HF^{\dagger}$(3→0) systems. The thick line trace is a computer fit to the data derived from the spectral fitting code.

Figure 21 points out the prominent emission features originating from the excited states NF(a), NF(b), N_2(B), and $HF^{\dagger}$. During the scans, due to the NF(b→X) (0,0) band, a large off-scale feature was observed at 528 nm. This system is not shown in Fig. 21 since it was used in the computer fits. To record, on scale, a spectral feature several times more intense than all other features would decrease the sensitivity for detection of the weaker features. Rather the (0,1) band at 560 nm was used to monitor [NF(b)]. This

approach was used so that a complete spectral scan could be recorded using a single sensitivity setting for an entire scan. The intensity of the NF(b→X) (0,1) band was related to that of the (0,0) band by making careful scans over the range 525-570 nm. It was found that the (0,1) band was 33 ± 2 times weaker than the (0,0) band.

It is important to note that the NF(b→X) (0,0) band appeared to be much stronger than the NF(a→X) (0,0) band. This is due almost entirely to the ratio of the Einstein A coefficients for the two states (Ref. 37):

$$A_{NF(b)}/A_{NF(a)} = \frac{43\ s^{-1}}{0.178\ s^{-1}} = 241$$

In actuality it was found that [NF(a)]/[NF(b)] was greater than 100 for these conditions.

The spectral fitting routine utilized the absolute spectral response calibration data, consequently it calculated absolute number densities for the species $N_2(B)$, NF(a) and NF(b). Since v' = 0 in $N_2(B)$ could not be detected the results are for $N_2(B;\ v=1-12)$. The $N(^2D)$ concentrations were determined separately. A sample of the results for a run is presented in Table 3.

To obtain an $N_2(B)$ excitation rate, plots of $[N_2(B;v)]$ versus [NF(a)] x $[N(^2D)]$ were constructed. A typical plot is shown in Fig. 22. Note that the $[NF(a)][N(^2D)]$ product was varied by nearly two orders of magnitude. Recalling Eq. (15) it is noted that the slope of this plot should equal $k_3/(A_{B\rightarrow A} + K_Q)$. To accurately determine k_3 one must determine the production rates into the individual vibrational levels of $N_2(B)$. This stems from $A_{B\rightarrow A}$ being dependent upon v (Ref. 38). The total rate coefficient, k_3, is then calculated from

TABLE 3. Sample Data Showing $[N_2(B)]$, [NF(a)] and $[N(^2D)]$ as a Function of $[H_2]$ Added.

$[H_2]$	[NF(a)]	$[N(^2D)]$	$[N_2(B)]$	[NF(a)]x$[N(^2D)]$	$[N_2(B)]/[N(^2D)]$
1.37×10^{13}	7.13×10^{11}	3.24×10^{10}	2.22×10^{7}	2.3×10^{22}	6.8×10^{-4}
3.48×10^{13}	7.11×10^{11}	2.84×10^{10}	2.81×10^{7}	2.0×10^{22}	9.9×10^{-4}
7.95×10^{13}	6.72×10^{11}	2.4×10^{10}	1.56×10^{7}	1.6×10^{22}	6.5×10^{-4}
2.09×10^{14}	7.23×10^{11}	1.35×10^{10}	8.91×10^{6}	9.7×10^{21}	6.6×10^{-4}
4.04×10^{14}	7.23×10^{11}	7.87×10^{9}	4.7×10^{6}	5.7×10^{21}	6.0×10^{-4}
2.48×10^{12}	1.41×10^{11}	2.92×10^{9}	4.4×10^{5}	4.1×10^{20}	1.5×10^{-4}

NOTE: All entries are in molecule cm^{-3}. The bath gas was Ar, and the total pressure was 3.06 torr.

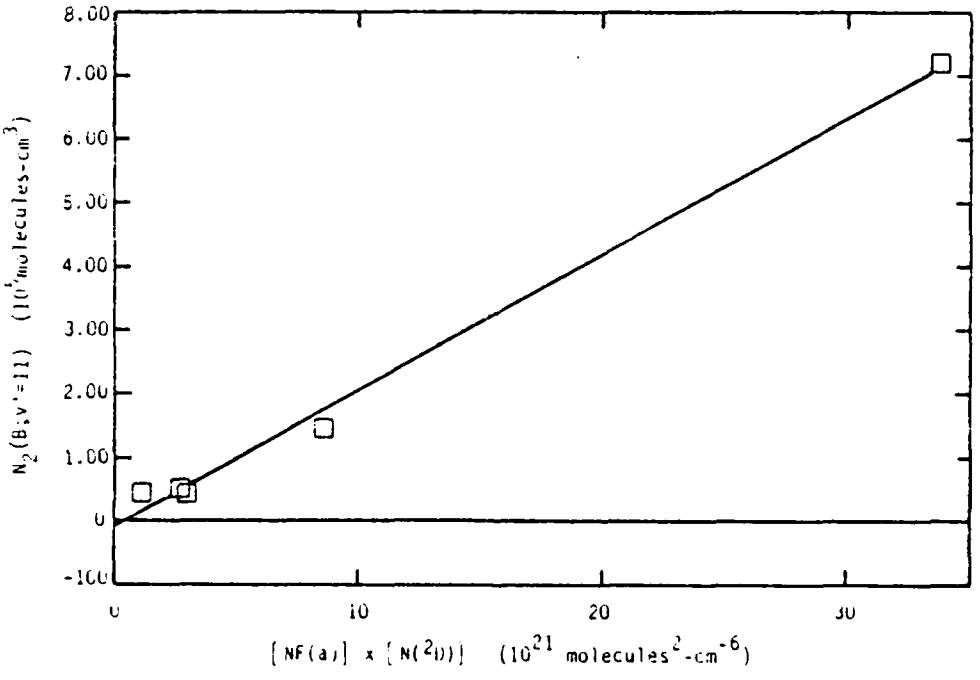

Figure 22. Plot showing linear dependence of $[N_2(B)]$ with respect to the product [NF(a)]x$[N(^2D)]$. Run conditions: pressure = 3.06 torr Ar bath gas.

$$k_3 = \sum_{i=0}^{12} k_3^{v_i} \qquad (42)$$

Using plots similar to that shown in Fig. 22, the total excitation rate coefficient was computed from Eq. (42). Note that we could not monitor v' = 0 so the k_3 is only for levels v' = 1 to 12.

The detailed $k_3(v_i)$ are presented in Table 4. Also shown are the sums, k_3. The total excitation rate coefficients for the six runs are tabulated in Table 5.

In Fig. 23 a plot is presented of $[N_2(B)]$ versus $[NF(a)] \times [N(^2D)]$ all the data collected. The spread in the data is typical of absolute photometric measurements and considering that these runs were made under differing conditions and over a period of three weeks, the reproducibility is satisfactory.

Although the data in Fig. 24 do not indicate a discernable dependence of $[N_2(B)]$ upon bath gas pressure or species, the data for the individual runs, summarized in Table 5, perhaps show a slight quenching of $N_2(B)$ by Ar and He. At the highest pressure (~3 torr) the excitation rate coefficients (proportional to $[N_2(B)]$) are ~15 percent reduced from the values at the lowest pressures (~0.7 torr). In addition Ar may be a slightly more efficient quencher of $N_2(B)$.

Not shown in Table 5 are populations for [NF(b)]. As stated earlier [NF(b)] was typically two orders of magnitude smaller than [NF(a)]. In light of k_3 being nearly gas kinetic, $NF(b) + N(^2D)$ reactions can be discarded as a significant source of $N_2(B)$ excitation.

It is to be noted that the spectral region of 874 nm contains contributions from NF(a-X) and the (2,1) band of the $N_2(B-A)$ system. The HF(3,0) overtone emission was in some data observed. Although the spectral fitting routine can treat this situation, problems can arise if the $N_2(B-A)$ or HF

TABLE 4. Measured k_3 for v' = 1-12 at Various Bath Gas Pressures. Conditions are Indicated.

Buffer Gas	Pressure (torr)	v'	Excitation Rate Coefficient, $k_{v'}$ (cm^3-molecule^{-1}-s^{-1})
Ar	0.7	1	1.273×10^{-11}
		2	2.335×10^{-11}
		3	1.447×10^{-11}
		4	1.912×10^{-11}
		5	1.612×10^{-11}
		6	1.628×10^{-11}
		7	1.546×10^{-11}
		8	1.412×10^{-11}
		9	1.140×10^{-11}
		10	8.473×10^{-12}
		11	5.882×10^{-12}
		12	2.644×10^{-12}
			Sum=1.600×10^{-10}
Ar	1.36	1	1.220×10^{-11}
		2	2.231×10^{-11}
		3	1.528×10^{-11}
		4	1.804×10^{-11}
		5	1.186×10^{-11}
		6	1.226×10^{-11}
		7	1.262×10^{-11}
		8	1.353×10^{-11}
		9	9.102×10^{-12}
		10	5.534×10^{-12}
		11	3.533×10^{-12}
		12	7.047×10^{-13}
			Sum=1.379×10^{-10}
Ar	3.06	1	1.116×10^{-11}
		2	2.313×10^{-11}
		3	1.545×10^{-11}
		4	1.726×10^{-11}
		5	9.785×10^{-12}
		6	1.128×10^{-11}
		7	1.363×10^{-11}
		8	1.534×10^{-11}
		9	8.865×10^{-12}
		10	4.086×10^{-12}
		11	2.448×10^{-12}
		12	9.771×10^{-13}
			Sum=1.422×10^{-10}

TABLE 4. (Concluded).

Buffer Gas	Pressure (torr)	V'	Excitation Rate Coefficient, $k_{v'}$ (cm^3-molecule^{-1}-s^{-1})
He	0.79	1	2.215×10^{-11}
		2	2.948×10^{-11}
		3	1.482×10^{-11}
		4	2.208×10^{-11}
		5	2.583×10^{-11}
		6	2.914×10^{-11}
		7	2.163×10^{-11}
		8	1.560×10^{-11}
		9	1.196×10^{-11}
		10	1.035×10^{-11}
		11	8.394×10^{-12}
		12	5.071×10^{-12}
			Sum=2.165×10^{-10}
He	2.18	1	1.762×10^{-11}
		2	2.165×10^{-11}
		3	1.058×10^{-11}
		4	1.599×10^{-11}
		5	2.047×10^{-11}
		6	2.536×10^{-11}
		7	1.959×10^{-11}
		8	1.399×10^{-11}
		9	1.015×10^{-11}
		10	8.426×10^{-12}
		11	6.742×10^{-12}
		12	3.944×10^{-12}
			Sum=1.745×10^{-10}
He	3.30	1	2.047×10^{-11}
		2	1.958×10^{-11}
		3	9.322×10^{-12}
		4	1.576×10^{-11}
		5	1.559×10^{-11}
		6	1.984×10^{-11}
		7	1.642×10^{-11}
		8	1.215×10^{-11}
		9	7.626×10^{-12}
		10	5.666×10^{-12}
		11	4.152×10^{-12}
		12	2.336×10^{-12}
			Sum=1.489×10^{-10}

TABLE 5. Summary of Conditions for Measurements of $N_2(B)$ Excitation Rate Coefficient.

Buffer Gas	Pressure (torr)	Flow Velocity (V) (cm/s)	Distance (D) H_2 Injector to Observation Port (cm)	Time from H_2 Injector to Observation Port (D/V) (10^{-3} s)	Excitation Rate (cm^3-$molecule^{-1}$-s^{-1})
Ar	1.36	2985	30	10.0	1.38×10^{-10}
Ar	0.70	3047	30	9.8	1.60×10^{-10}
Ar	3.06	1155	20	17.3	1.42×10^{-10}
He	0.79	5480	30	5.5	2.16×10^{-10}
He	3.30	1333	20	15.0	1.49×10^{-10}
He	2.18	1961	Variable (Sliding Injector)	2.0→10	1.74×10^{-10}
				$\langle k_3 \rangle = 1.63 \times 10^{-10}$	

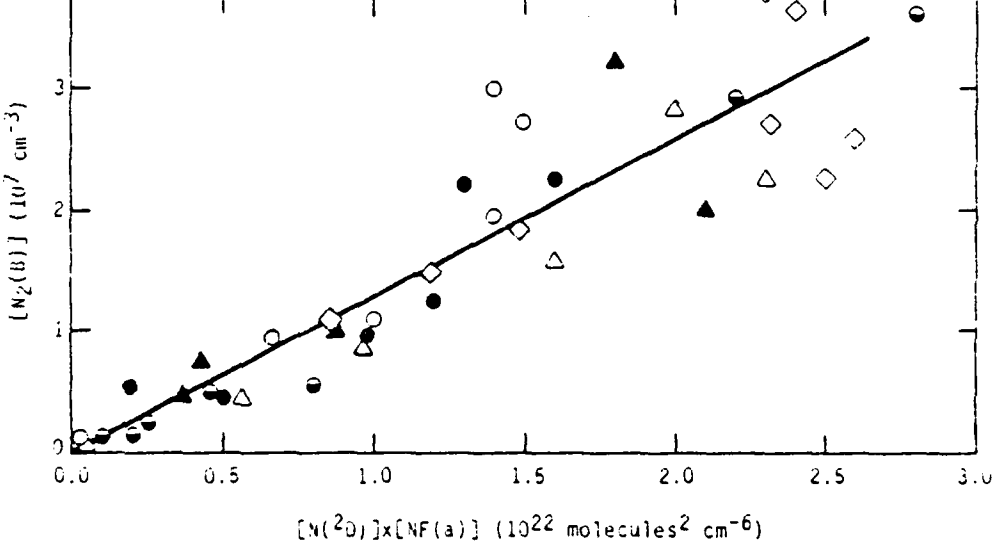

Figure 23. Composite plot of $[N_2(B)]$ as a function of the product $[NF(a)] \times [N(^2D)]$ for all data collected; ▲: Ar buffer gas (0.70 torr), ●: Ar buffer gas (1.37 torr), △: Ar buffer gas (3.06 torr), ○: He buffer gas (0.79 torr), ◒: He buffer gas (3.30 torr), ◇: He buffer gas (2.18 torr)

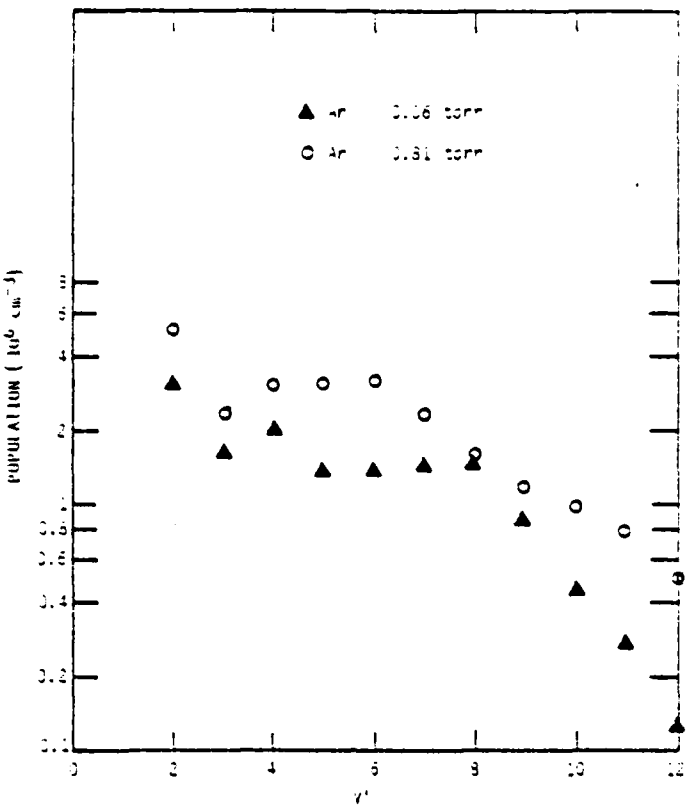

Figure 24. Populations of $N_2(B;v')$ as a function of v' for two Ar pressures.

overtone emissions are stronger than the NF(a→X). In that case the [NF(a)] is underrepresented; the $N_2(B)$ and $HF^\dagger$ are too heavily weighted. It is a problem that we are attempting to alleviate. For the present this was circumvented by working at conditions where NF(a→X) was at least as strong as either the HF(3,0) or $N_2(B\rightarrow A)$ in the region of NF(a→X) near 674 nm. The problem was especially prominent when the sliding injector was used. Data recorded from 0 to 2.5 ms downstream of the H_2 injector were heavily contaminated with HF(3,0) emission. Consequently only those NF(a) data for t > 2.5 ms were used. It is significant, however, that when clean NF(a→X) spectra in the region of 2.5 → 10 ms were utilized the data gave an excitation rate for $N_2(B)$ in good agreement with all fixed H_2 injector data. (These movable injector data are included in Fig. 14 and in Tables 4 and 5.)

The initial result is quoted for the excitation rate coefficient, k_3, for $N_2(B\rightarrow A)$ formation in vibrational levels v' = 1→12 as

$$k_3 = (1.6 \pm 0.7) \times 10^{-10} \text{ cm}^3\text{-molecule}^{-1}\text{-s}^{-1}$$

where the error is the best estimate of the systematic uncertainties inherent in the measurement. These include the calibrations for the $[N(^2D)]$, $[NF(a)]$, and $[N_2(B)]$ diagnostics. The NO/O calibration procedure introduces a 29 percent error: (25 percent for the O + NO rate coefficient and 15 percent reproducibility in the measurements of the NO/O titration). The estimated error in the $N(^2D)$ calibration is ~15 percent. The reported value of the NF(a) lifetime probably carries an additional 25 percent error. Combining this with the results presented in Table 5 gives ~42 percent. The apparently large error is due to the errors quoted in the literature for results that we have used to reduce data.

2.4.3.4 Vibrational relaxation in $N_2(B)$--Since these studies were performed at several pressures from 0.7 to 3.0 torr some vibrational redistribution was observed in the $N_2(B)$ manifold. Examples of this are shown in Fig. 24 where the populations ($N_{v'}$) in $N_2(B;v)$ are plotted as a function of v' for two Ar pressures. At 3 torr the effects of vibrational relaxation are seen, especially for v' > 8. (The bottlenecking in v' = 8 has also been observed in the $N_2(A)$ energy pooling work.) A much flatter v' distribution is observed at 0.7 torr.

It is clear that the distribution at 3.0 torr is not nascent. While we cannot state with certainty that the data at 0.7 torr represent a nascent distribution it is certainly much closer to the initial distribution produced by the NF(a) + $N(^2D)$ reaction. Clearly one must exercise caution when interpreting populations in $N_2(B)$ from chemiluminescence intensity measurements.

It is of interest to examine the individual rate coefficients ($k_{v'}$) for $N_2(B;v)$ production as a function of v'. Figure 25 presents plots of $k_{v'}$ versus v' at two Ar both gas pressures (3.06 and 0.80 torr). Also seen are the effects of vibrational relaxation in the vibrational manifold of $N_2(B)$. The differences between the respective $k_{v'}$ at the two different pressures are apparently due to vibrational relaxation prior to $N_2(B \rightarrow A)$ emission.

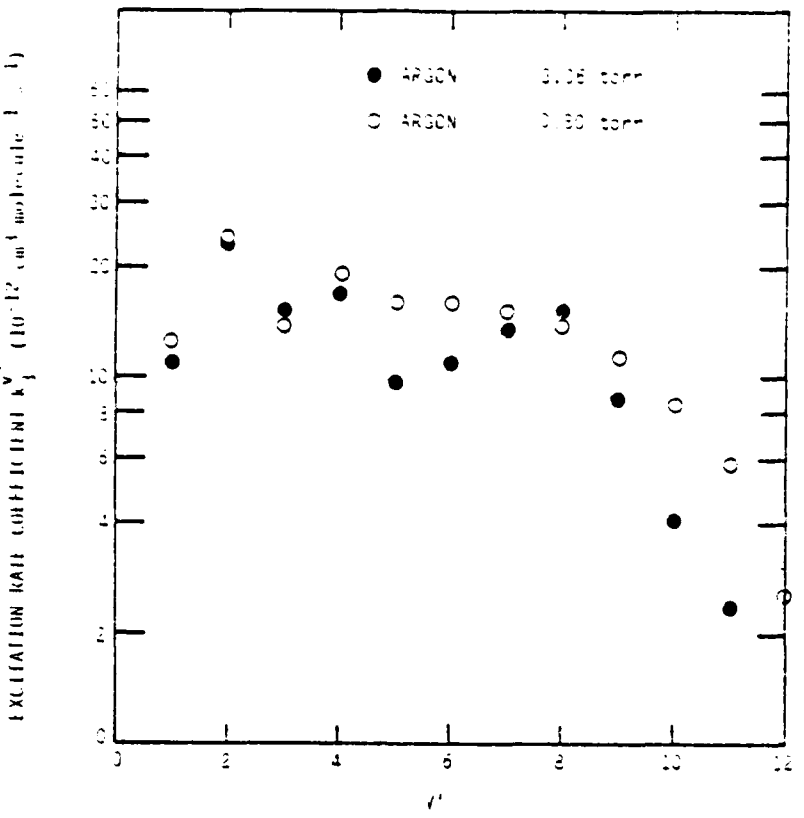

Figure 25. Dependence of measured excitation rate coefficient, k_3, as a function of v' for two Ar pressures.

2.4.3.5 Other observations--The data presented in Table 3 show an interesting relationship between the excited species produced and the amount of H_2 added. In Fig. 26 we plot [NF(a)], [N_2(B)], and [$N(^2D)$] all as a function of [H_2] added using the data from Table 3. The [NF(a)] seems to reach a steady value as previously observed. In contrast [$N(^2D)$] first increases reasonably consistent with the previously measured quenching of $N(^2D)$ by H_2 (Ref. 39). The [N_2(B)] follows the same pattern.

Since N_2(B) is in steady state with $N(^2D)$ it is expected that at constant [NF(a)] the ratio of [N_2(B)]/[$N(^2D)$] will be constant. In the last column of Table 3 it is seen that for the first five entries $\langle$[NF(a)]$\rangle$ = (7.1 ± 0.2) x 10^{11} cm^{-3} and $\langle$[N_2(B)]/[$N(^2D)$]$\rangle$ = (7.2 ± 1.4) x 10^{-4}. Similar behavior was observed for all runs. As expected, the value of [N_2(B)]/[$N^2(D)$] depended upon [NF(a)], e.g., for one set of runs [NF(a)] = (1.0 ± 0.1) x 10^{12} cm^{-3} and [N_2(B)]/[$N(^2D)$] = (1.3 ± 0.2) x 10^{-3}. However, for any set of runs with constant [NF(a)], [N_2(B)]/[$N^2(D)$] was constant to within ±20 percent.

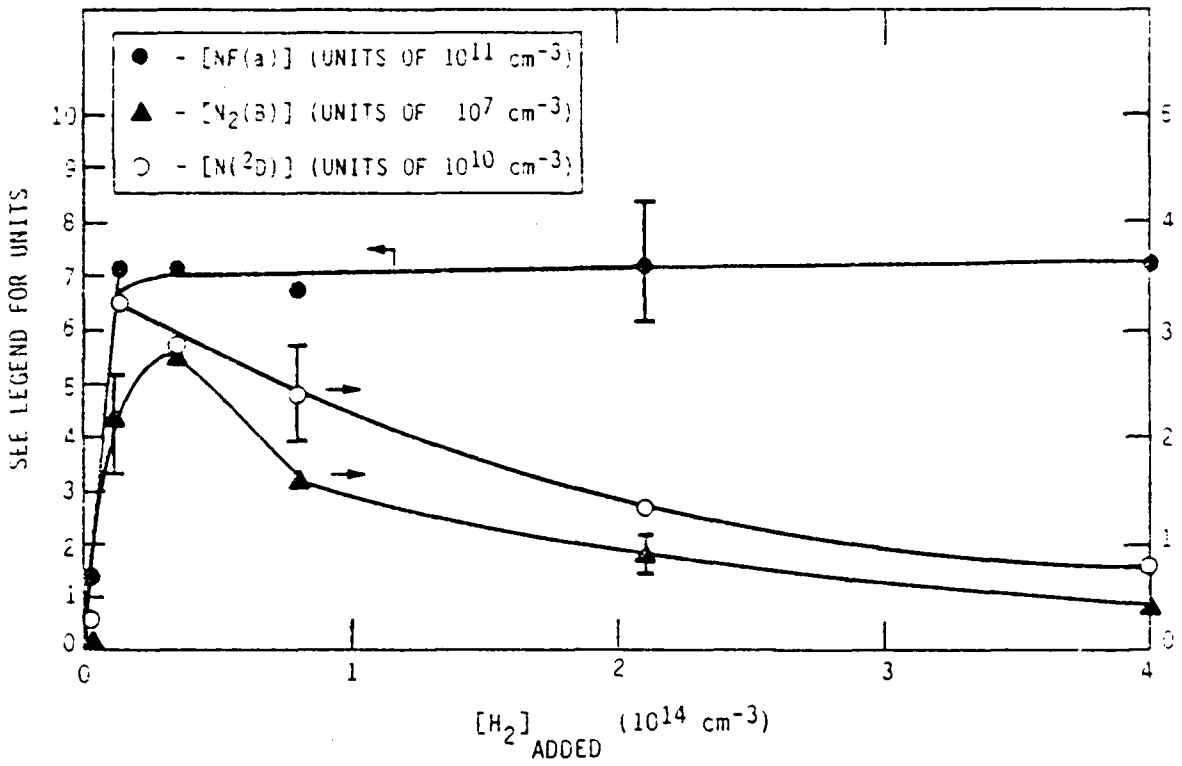

Figure 26. Plot of [NF(a)], [N_2(B)] and [N(^{2}D)] as functions of [H_2] added. a) Total pressure = 3.06 torr (Ar); effective reaction time = 17.3 ms.

In the third quarterly report it was pointed out that the N_2(A) production showed a strong dependence upon the amount of H_2 added to the microwave discharged NF_3. The current results demonstrate a similar dependence for N_2(B) and N(^{2}D) as indicated in Fig. 27. (Also included in Fig. 27 are data for N_2(a) obtained by monitoring the N_2(a→X) system at 149.5 nm.) Note that if H_2 were quenching N_2(B) directly a quenching rate coefficient of ~10^{-9} cm^3 $molecule^{-1}$ s^{-1} would be required to explain its observed decay. Rather, as stated above H_2 quenching of N(^{2}D), the probable precursor to N_2(B), is a much more likely explanation.

The data presented in Fig. 27 combined with the previous observation on N_2(A) support the reaction between NF(a) and N(^{2}D) as being the key excitation step for all N_2^*.

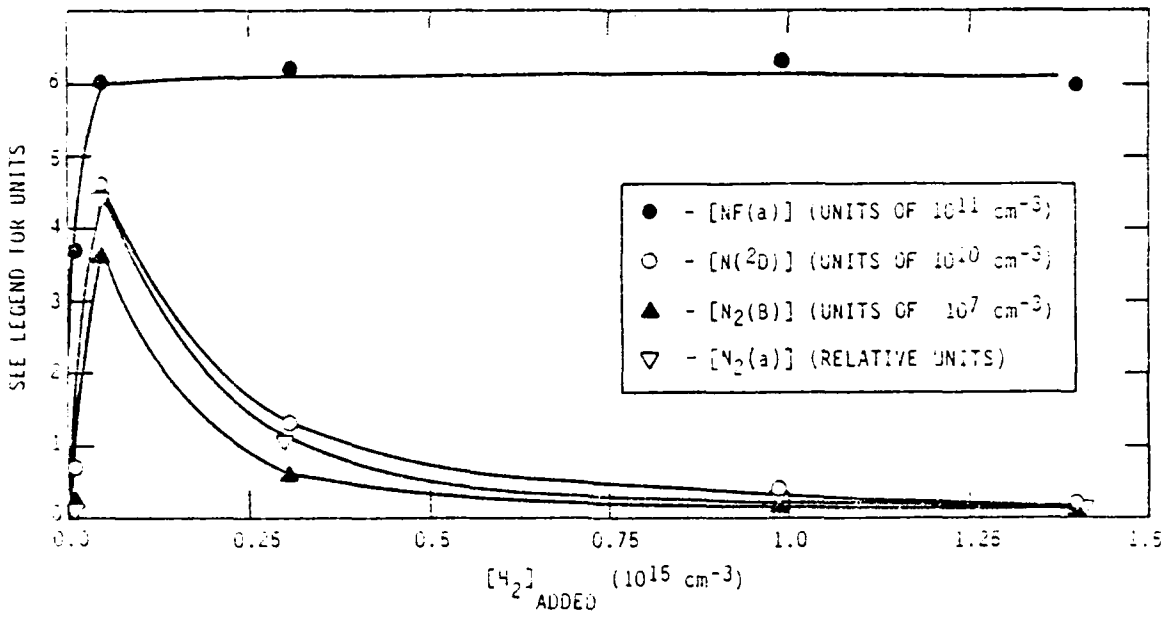

Figure 27. Plot of [NF(a)], [N_2(B)], [N(^{2}D)] and relative [N_2(a)] as functions of [H_2] added. Total pressure = 3.3 Torr; reaction time = 15 ms.

During the course of this program other observations have been made that are relevant to the potential of the H + NF_2 reaction sequence as a source of N_2(A). There is not an estimate for [N_2(a)]. We observed N_2(a;v'=6) and N_2(B;v'=12) which are both at the predissociation limit of 10 eV. The only two relevant reactions energetic enough to produce the excitation are

$$N(^2D) + NF(a) \rightarrow N_2 + F \qquad \Delta E = 10.05 \text{ eV}$$

and

$$N(^2D) + NF(b) \rightarrow N_2 + F \qquad \Delta E = 10.97 \text{ eV}$$

As pointed out above the [NF(b)] is probably too small to contribute significantly. Thus, the conclusion is that all N_2^* may be produced by reaction 3. Since reaction 3 is exothermic enough to produce excitation up to the predissociation limit, and since production of N_2^* is indeed observed all the way to predissociation there may be an inherent inefficiency in the system with respect to partitioning into specific N_2^* states.

Also relevant is an observation made while performing some early survey work on $N_2(A)$ production. The $N_2(A)$ was produced using the H_2 + (Ar/NF_3)discharge reaction, and the $N_2(A \rightarrow X)$ Vegard-Kaplan bands were monitored. In the hope of producing a higher $[N_2(A)]$ a microwave discharge was initiated in the H_2 flow. The $[N_2(A)]$ was degraded by a factor of 2. Although only a qualitative observation, it appears that H atom quenching of $N_2(A)$ or a precursor could be a serious problem. The quenching reaction to form NH + H is slightly endothermic. However one quantum of vibrational energy in $N_2(A)$ would make this process exothermic. Perhaps the opening of a reactive channel may explain why the rate appears to be so fast.

2.4.3.6 Modeling results--A major goal of Task 2 was to determine several key rate coefficients that could be incorporated into the comprehensive computer code, ALFA.* This code has been recently tailored to describe chemical excitation of excited N_2. To aid in the data interpretation some computer modeling of the H + NF_2 system has been performed. While not intended to be a comprehensive study, the modeling results described in the following paragraphs were helpful in data interpretation.

A kinetic model was used that integrated a system of first order differential equations given an initial set of conditions which consisted of number densities of all relevant species. The model also assumed that all species were premixed. The reactions considered and the corresponding rate package are presented in Table 6. The comprehensive rate package of Ref. 40 was used in the present analysis.

Since data interpretation was a major goal of the modeling investigation, our efforts were concentrated on comparisons of model predictions with experimental data. The most relevant comparisons were temporal profiles of the species of interest. The majority of the experimental work monitored $N_2(B)$, $NF(b)$, and $NF(a)$ and it is the set of species that is now consider.

---

*Exists at the Air Force Weapons Laboratory, Kirtland AFB, New Mexico.

TABLE 6. Rate Package Used in Modeling Study

			Reference
(1)	$F + H_2 \rightarrow HF(1) + H$	RC = 7.30E-12 cm^3 $molecule^{-1}$ s^{-1}	Ref. 40
(2)	$F + H_2 \rightarrow HF(2) + H$	RC = 2.40E-11 cm^3 $molecule^{-1}$ s^{-1}	Ref. 40
(3)	$F + H_2 \rightarrow HF(3) + H$	RC = 1.20E-11 cm^3 $molecule^{-1}$ s^{-1}	Ref. 40
(4)	$H + NF_2 \rightarrow HF(0) + NF(a)$	RC = 8.00E-12 cm^3 $molecule^{-1}$ s^{-1}	Ref. 40
(5)	$H + NF_2 \rightarrow HF(1) + NF(a)$	RC = 3.00E-12 cm^3 $molecule^{-1}$ s^{-1}	Ref. 40
(6)	$H + NF_2 \rightarrow HF(2) + NF(a)$	RC = 7.70E-13 cm^3 $molecule^{-1}$ s^{-1}	Ref. 40
(7)	$H + NF_2 \rightarrow HF(3) + NF(a)$	RC = 1.20E-13 cm^3 $molecule^{-1}$ s^{-1}	Ref. 40
(8)	$H + NF_2 \rightarrow HF(0) + NF(b)$	RC = 2.60E-13 cm^3 $molecule^{-1}$ s^{-1}	Ref. 40
(9)	$H + NF_2 \rightarrow HF(0) + NF(X)$	RC = 9.10E-13 cm^3 $molecule^{-1}$ s^{-1}	Ref. 40
(10)	$H + NF(a) \rightarrow HF(0) + N(^2D)$	RC = 3.10E-13 cm^3 $molecule^{-1}$ s^{-1}	This work
(11)	$H + NF(b) \rightarrow H + NF(a)$	RC = 5.00E-12 cm^3 $molecule^{-1}$ s^{-1}	Ref. 40
(12)	$HF(2) + NF(a) \rightarrow NF(b) + HF(0)$	RC = 8.30E-12 cm^3 $molecule^{-1}$ s^{-1}	Ref. 40
(13)	$HF(3) + NF(a) \rightarrow NF(b) + HF(1)$	RC = 7.50E-11 cm^3 $molecule^{-1}$ s^{-1}	Ref. 40
(14)	$HF(4) + NF(a) \rightarrow NF(b) + HF(2)$	RC = 3.30E-12 cm^3 $molecule^{-1}$ s^{-1}	Ref. 40
(15)	$N(^2D) + NF(a) \rightarrow N_2(B) + F$	RC = 1.90E-10 cm^3 $molecule^{-1}$ s^{-1}	This work
(16)	$HF(1) + HF(1) \rightarrow HF(0) + HF(2)$	RC = 1.70E-11 cm^3 $molecule^{-1}$ s^{-1}	Ref. 40
(17)	$HF(1) + HF(2) \rightarrow HF(0) + HF(3)$	RC = 2.00E-11 cm^3 $molecule^{-1}$ s^{-1}	Ref. 40
(18)	$HF(1) + HF(3) \rightarrow HF(0) + HF(4)$	RC = 2.20E-11 cm^3 $molecule^{-1}$ s^{-1}	Ref. 40
(19)	$HF(4) + HF(0) \rightarrow HF(3) + HF(0)$	RC = 4.30E-11 cm^3 $molecule^{-1}$ s^{-1}	Ref. 40
(20)	$HF(3) + HF(0) \rightarrow HF(2) + HF(0)$	RC = 2.00E-11 cm^3 $molecule^{-1}$ s^{-1}	Ref. 40
(21)	$HF(2) + HF(0) \rightarrow HF(1) + HF(0)$	RC = 7.20E-12 cm^3 $molecule^{-1}$ s^{-1}	Ref. 40
(22)	$HF(1) + HF(0) \rightarrow HF(0) + HF(0)$	RC = 1.20E-12 cm^3 $molecule^{-1}$ s^{-1}	Ref. 40
(23)	$HF(4) + H_2 \rightarrow HF(3) + H_2$	RC = 8.50E-13 cm^3 $molecule^{-1}$ s^{-1}	Ref. 40
(24)	$HF(3) + H_2 \rightarrow HF(2) + H_2$	RC = 3.90E-13 cm^3 $molecule^{-1}$ s^{-1}	Ref. 40
(25)	$HF(2) + H_2 \rightarrow HF(1) + H_2$	RC = 1.30E-13 cm^3 $molecule^{-1}$ s^{-1}	Ref. 40
(26)	$HF(1) + H_2 \rightarrow HF(0) + H_2$	RC = 2.00E-14 cm^3 $molecule^{-1}$ s^{-1}	Ref. 40
(27)	$HF(1) + NF_2 \rightarrow HF(0) + NF_2$	RC = 1.40E-14 cm^3 $molecule^{-1}$ s^{-1}	Ref. 40
(28)	$HF(2) + NF_2 \rightarrow HF(1) + NF_2$	RC = 9.70E-14 cm^3 $molecule^{-1}$ s^{-1}	Ref. 40
(29)	$HF(3) + NF_2 \rightarrow HF(2) + NF_2$	RC = 2.50E-13 cm^3 $molecule^{-1}$ s^{-1}	Ref. 40
(30)	$HF(4) + NF_2 \rightarrow HF(3) + NF_2$	RC = 5.30E-13 cm^3 $molecule^{-1}$ s^{-1}	Ref. 40
(31)	$NF(b) \rightarrow NF(X) + h\nu$	RC = 4.50E+01 s^{-1}	Ref. 40
(32)	$F + NF_2 + M \rightarrow NF_3 + M$	RC = 1.00E-30 cm^6 $molecule^{-2}$ s^{-1}	Ref. 40
(33)	$NF(a) + NF_2 \rightarrow NF(X) + NF_2$	RC = 2.70E-16 cm^3 $molecule^{-1}$ s^{-1}	Ref. 40
(34)	$N_2(B) \rightarrow N_2(A) + h\nu$	RC = 1.50E+05 s^{-1}	Ref. 36
(35)	$N_2(A) + WALL \rightarrow N_2(X) +$	RC = 2.18E+02 s^{-1}	Calculated
(36)	$N(^2D) + WALL \rightarrow N(^4S) +$	RC = 2.34E+02 s^{-1}	Calculated
(37)	$N(^2D) + H_2 \rightarrow N(^4S) + H_2$	RC = 2.30E-12 cm3 molecule-1 s-1	Ref. 39
(38)	$N(^2D) + NF_3 \rightarrow N(^4S) + NF_3$	RC = 3.00E-13 cm^3 $molecule^{-1}$ s^{-1}	This work*
(39)	$N(^4S) + NF_2 \rightarrow NF(X) + NF(X)$	RC = 3.00E-12 cm^3 $molecule^{-1}$ s^{-1}	Ref. 1
(40)	$N_2(A) + N_2(A) \rightarrow N_2(B) + N_2(X)$	RC = 7.70E-11 cm^3 $molecule^{-1}$ s^{-1}	This work
(41)	$N_2(A) + N_2(A) \rightarrow N_2(C) + N_2(X)$	RC = 14.6E-11 cm^3 $molecule^{-1}$ s^{-1}	This work
(42)	$NF(a) + WALL \rightarrow NF(X)$	RC = 100 s^{-1}	Model parameter

*Preliminary measurement.

The model was run by specifying an initial set of conditions for all species concentrations. The rate equations were then integrated and the species concentrations were predicted from 0 to 10 ms at 1 ms intervals. (This range was identical to that of the experimental runs when the sliding injector was used.)

Initial conditions in the model were chosen to be identical to those of the actual experiments. The $[Ar]_0$ and $[H_2]_0$ were measured directly from the mass flowmeter readings. The largest uncertainty in initial condition determination occurred for $[NF_2]_0$ and $[F]_0$; since we had a diagnostic for neither of these their concentrations were estimated. The upper limit of the $[NF_2]_0$ was $[NF_3]_0$ while $[F]_0$ is required to be less than $3[NF_3]$. Because molecular hydrogen was introduced into the flow tube, atomic hydrogen is produced by the reaction of $F + H_2$.

As pointed out previously, when H_2 is added to the products of the NF_3 discharge, [NF(a)] rises then reaches a plateau which is independent of further H_2 increases. This titration end point is interpreted to occur when all F has been consumed, i.e., $[H_2]_0 \sim [F]_0$. Examination of the data in this manner indicates that approximately four F atoms must be produced by the discharge for every five NF_3 molecules that are introduced into the cavity.

The estimate for $[NF_2]_0$ is less certain. Since this model best fits the data when $[NF_2]_0/[F]_0 \sim 1/2$, it appears that the microwave discharge produces about a 50 percent yield of NF_2 from the NF_3. Note that the discharge is always run at a relatively low power, ~10 W. When the discharge was increased to 30 W the NF(a) and $N_2(B)$ concentrations were drastically reduced indicating that at high microwave fluxes NF_2 is dissociated. In addition as the microwave power increased, $N(^4S)$ (detected at 120 nm by resonance fluorescence) also was enhanced.

In Fig. 28 a comparison of predicted and measured profiles for is shown NF(a), $N(^2D)$, and $N_2(B)$ using the rates determined for reactions 2 and 3. Given that the estimated uncertainties for these two rate coefficients are ~20 and 30 percent, respectively, the agreement is quite good.

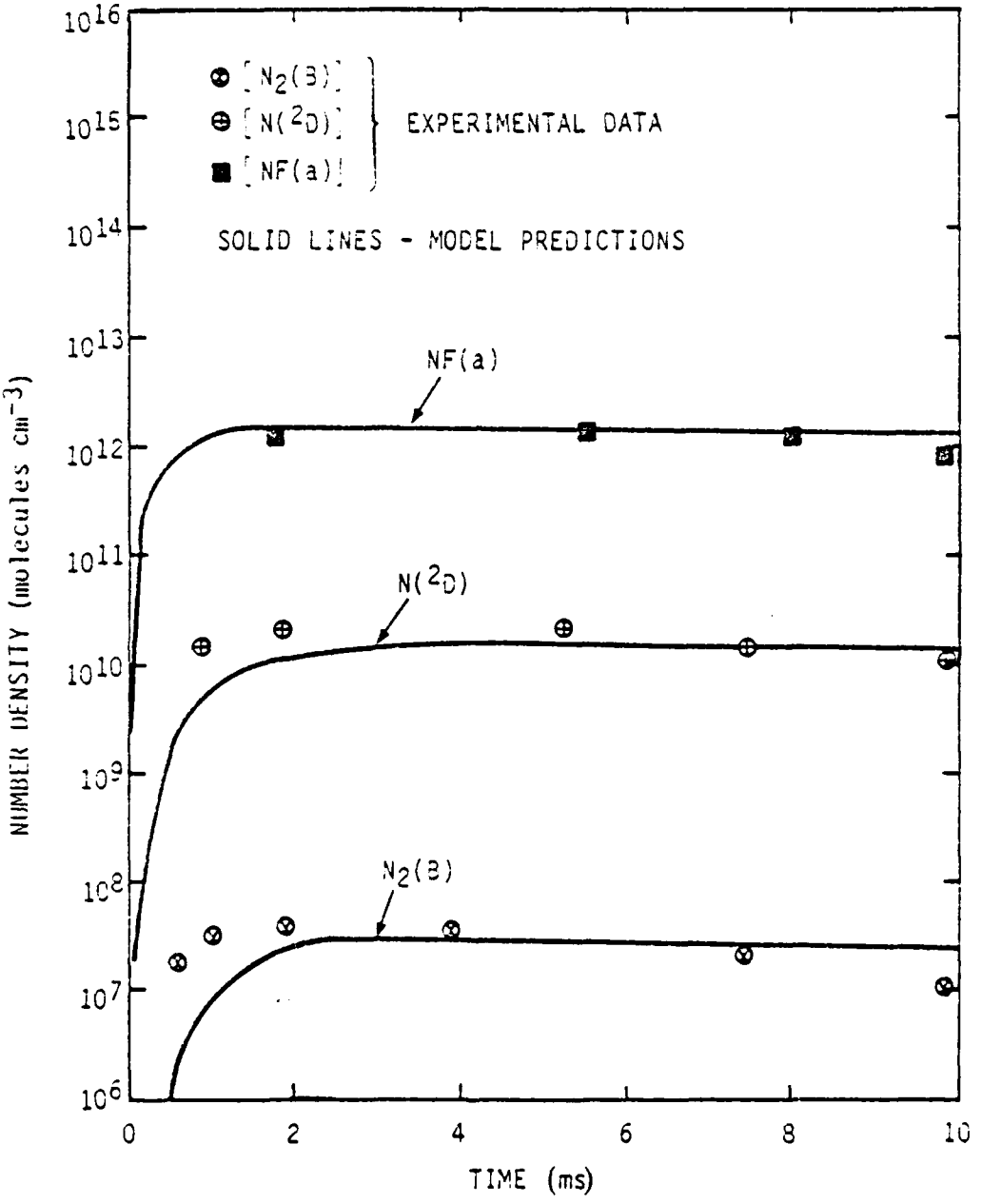

Figure 38. Comparison of predicted and measured population profiles for NF(a), N(^{2}D), and N_2(B). Total bath gas pressure was 2.2 torr (He).

It is important to note that to obtain the predicted profiles an empirical removal rate for NF(a) has to be included. The actual source of this removal is not presently understood, but wall reactions seem to be an unlikely explanation (Ref. 3). This removal of NF(a) is an open question and the possibility of a bimolecular reaction must be considered. More work on this problem is indicated.

As indicated, the modeling study was completed to aid in data interpretation. The model supports two important features of the proposed H - NF_2 mechanism. First it is consistent with a two-step production of $N_2(B)$ via reactions 2 and 3 with $k_2 << k_3$. Secondly, it supports the hypothesis that $N(^2D)$ is the primary product of reaction 2.

For completeness we also experimentally monitored by resonance fluorescence at 120 nm $N(^4S)$ production from reaction 2. Although not an absolutely calibrated diagnostic the relative $N(^4S)$ could be easily observed. In Figure 29 we show relative concentration profiles for $N(^4S)$ and $N_2(B)$ (which as shown previously closely follows $[N^2(D)]$). It is clear that $N(^4S)$ is not a primary reaction product and is only formed at relatively late reaction times. Its role in N_2^* production can therefore be only minimal.

In an effort to shed some further insight into the mechanism for N_2^* production from the H + NF_2 sequence we made some computerized data acquisition runs recording both $N_2(A \rightarrow X)$ and $N_2(B \rightarrow A)$ chemiluminescence. A sample spectral fit of the $N_2(B \rightarrow A)$ spectrum has been previously presented in Figure 21. In Figure 30 we present a similar spectral fit for the $N_2(A \rightarrow X)$ region. In addition to the $N_2(A \rightarrow X)$ emission strong NO(γ) bands are also observed; these were almost certainly from $N_2(A)$ to NO(A) E-E transfer. The $[N_2(A)]$ number densities we measured ranged from 2 x 10^9 cm^{-3} to 8 x 10^9 cm^{-3} for a variety of conditions. The highest concentrations were obtained at relatively high pressures (~1 Torr) where wall losses would be minimized. Typically $[N_2(A)]$ exceeded $[N_2(B)]$ by about two orders of magnitude. This is in qualitative agreement with our modeling predictions which has $N_2(B \rightarrow A)$ emission as the only source of $N_2(A)$. While not wishing to extrapolate the results of these studies beyond their range of validity, they do support the supposition that the dominant production of $N_2(A)$ is by $N_2(B \rightarrow A)$ radiation.

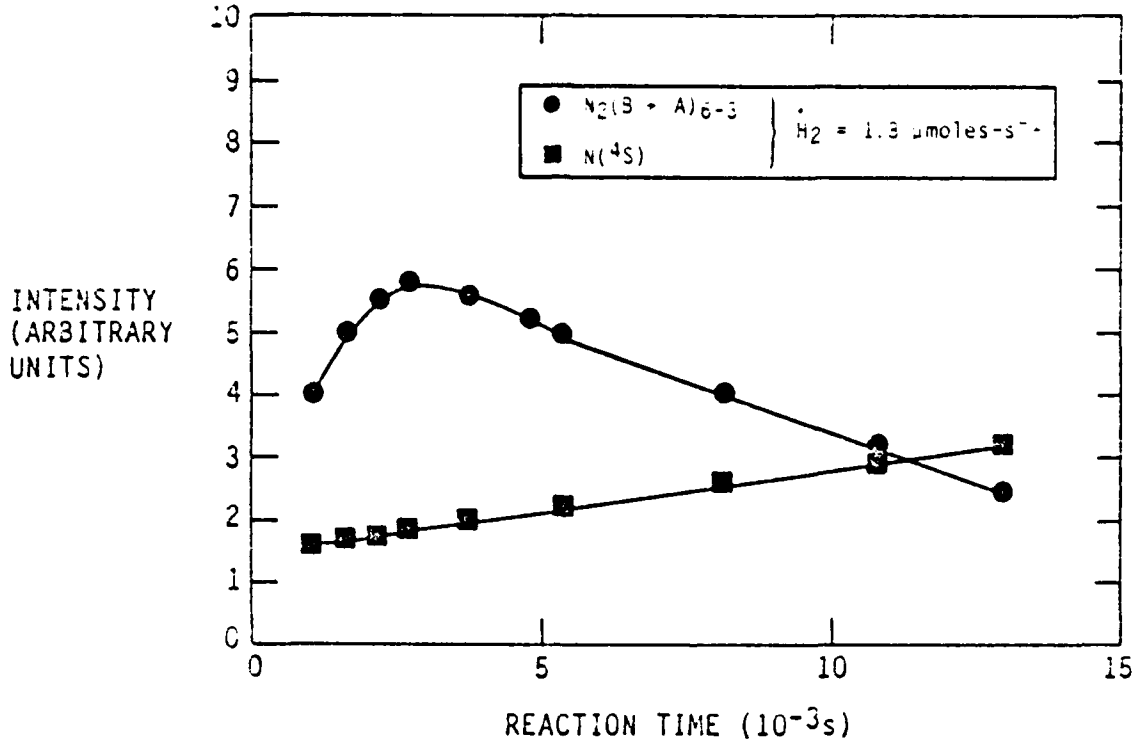

Figure 29. Temporal profiles of $N_2(B)$ and $N(^4S)$ produced in the H + NF_2 reaction sequence.

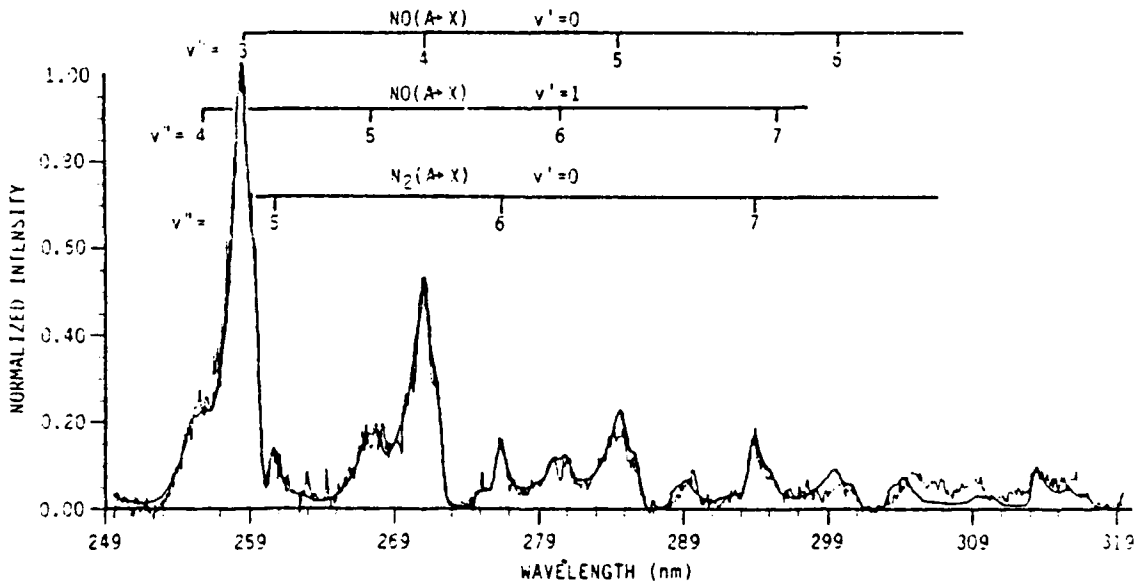

Figure 30. Chemiluminescence spectrum (dark line) and spectral fit (light line) produced from the H + NF_2 reaction sequence. Prominent features are indicated.

3. N_2 ENERGY-TRANSFER STUDIES

This section discusses work on understanding some energy-transfer reactions of electronically excited nitrogen. After Burrows (Ref. 41) demonstrated optically pumped lasing of the NO γ-bands, $NO(A^2\Sigma^+ -- X^2\Pi)$, the idea of using $N_2(A)$ to pump the γ-bands chemically in an energy-transfer reaction followed. The studies on the $N_2(A)$ plus NO energy-transfer reaction have two different aspects. First, determination of variation in the electronic transition moment with r-centroid for the $NO(A^2\Sigma^+ -- X^2\Pi)$ transition had to be made. It was found that proper interpretation of the energy-transfer results required this information. Secondly, both the total quenching of $N_2(A)$ by NO and the excitation of $NO(A^2\Sigma^+)$ and $NO(B^2\Pi)$ by $N_2(A^3\Sigma_u^+)$ were studied. The excitation-rate coefficients have been made state-to-state so that we can specify the efficiency for exciting each of the NO(A) vibrational levels by each of the different $N_2(A)$ vibrational levels present in our reactor. Paragraph 3.1.2 details the experimental facility used in all three sets of measurements under this task. Additional experimental details appear where needed in Paragraphs 3.2.2 and 3.3.2.2.

A major concern in developing a chemical laser based upon energy transfer from a storage state of one molecule or atom into a lasing state of another molecule or atom is how large a number density of the excited reservoir molecules can be generated. The reservoir molecules can be destroyed either in quenching reactions with other species in the laser medium, or in self-quenching, or energy-pooling reactions. It has been found that energy pooling of $N_2(A)$ molecules produces nitrogen in the $C^3\Pi_u$ and $B^3\Pi_g$ states as well as generating emission from the Herman Infrared system, the upper state of which has yet to be characterized. Paragraph 3.2 describes state-to-state kinetic measurements of the rate coefficients for producing various vibrational levels of each of the products from the various vibrational levels of the pooling $N_2(A)$ molecules.

It has been shown previously that active nitrogen excited $IF(B^3\Pi_{0^+})$ efficiently (Ref. 6). Although the precursor of the IF(B) emission unequivocally could not be identified, these data indicated that $N_2(A^3\Sigma_u)$, $N_2(B^3\Pi_g)$,

$N_2(a^1\Pi_g)$, $N_2(a'^1\Sigma_u^-)$, and $N(^2D)$ probably were not the precursor states. Rather, our evidence pointed to $N_2(X,v)$ as being the likely precursor state with high vibrational levels of the ground-electronic state of nitrogen above v" = 10 exciting the IF in a vibrational-to-electronic, V-E, transfer. Paragraph 3.3 describes some additional studies on the nature of active nitrogen and its subsequent transfer of energy to IF. A diagnostic has been developed for vibrationally excited, ground-state nitrogen, and have further characterized the energy transfer reactions between components in the active nitrogen and IF.

3.1 STATE-TO-STATE ENERGY TRANSFER FROM $N_2(A^3\Sigma_u^+, v' = 0,1,2)$ TO $NO(A^2\Sigma^+, v' = 0,1,2)$

3.1.1 Introduction--The excitation of the NO γ-bands in the energy-transfer reaction between $N_2(A)$ and NO is now well established (Refs. 43,44,45,49). What is not well established is the fraction of total $N_2(A)$ quenching which results in NO(A) excitation. The published values of the rate coefficient for excitation of NO(A) by $N_2(A)$ (Refs. 43,44) are both a factor of 2 greater than most of the measurements of the rate coefficient for the destruction of $N_2(A)$ by NO (Refs. 42,43,45,46,47). The magnitude of this discrepancy demands further investigation. In addition, the state-to-state partitioning between vibrational levels of the $N_2(A)$ pumping reagent and the NO(A) is uncertain. Callear and Wood (Ref. 45) claim a strong difference in the ratio of NO(A) v' = 0 to v' = 1 excited by $N_2(A, v' = 0)$ (9.8:1) compared to that excited by $N_2(A, v' = 1)$ (1.9:1). Some preliminary results from a study* a number of years ago aimed at using NO γ-bands as a monitor of system purity (Ref. 49) indicate a much smaller difference (7:1 and 4:1, respectively). It is also not clear if there is a strong difference in the quenching rate coefficients for the different $N_2(A)$ vibrational levels. Dreyer et al. (Ref. 47) found NO quenched $N_2(v' = 1)$ almost 70 percent faster than $N_2(A, v' = 0)$ while Clark and Setser (Ref. 43) and Young and St. John (Ref. 44) say both $N_2(A)$ levels are quenched by NO with equal efficiency. Consequently, a careful investigation was undertaken which is reported here.

---

*Physical Sciences Inc., Research Park, P.O. Box 3100, Andover, MA 01810.

3.1.2 Experimental--The apparatus is a 2-in flow tube pumped by a Leybold-Heraeus Roots blower/forepump combination capable of producing linear velocities up to 5×10^3 cm s^{-1} at pressures of 1 torr. The flow-tube design is modular (Fig. 31), with separate source, reaction, and detection sections which clamp together with O-ring joints. It has been described in its various configurations a number of times (Refs. 49-54). The detection region is a rectangular stainless-steel block bored out internally to a 2-in circular cross section and coated with Teflon® (Dupont Poly TFE #852-201) to retard surface recombination of atoms (Refs. 55-59). Use of a black primer prior to the Teflon® coating reduces scattered light inside the block dramatically. The block has two sets of viewing positions consisting of four circular ports each on the four faces of the block. These circular ports accommodate vacuum-ultraviolet (VUV) resonance lamps and visible monochromator interfaces, laser delivery side-arms and a spatially filtered photomultiplier/interference filter combination.

In these experiments a suprasil lens collected light from the center of the flow tube and focussed it on the entrance slit of a 0.5 m Minuteman monochromator which is outfitted with a 1200 groove mm^{-1} grating blazed at 250 nm.

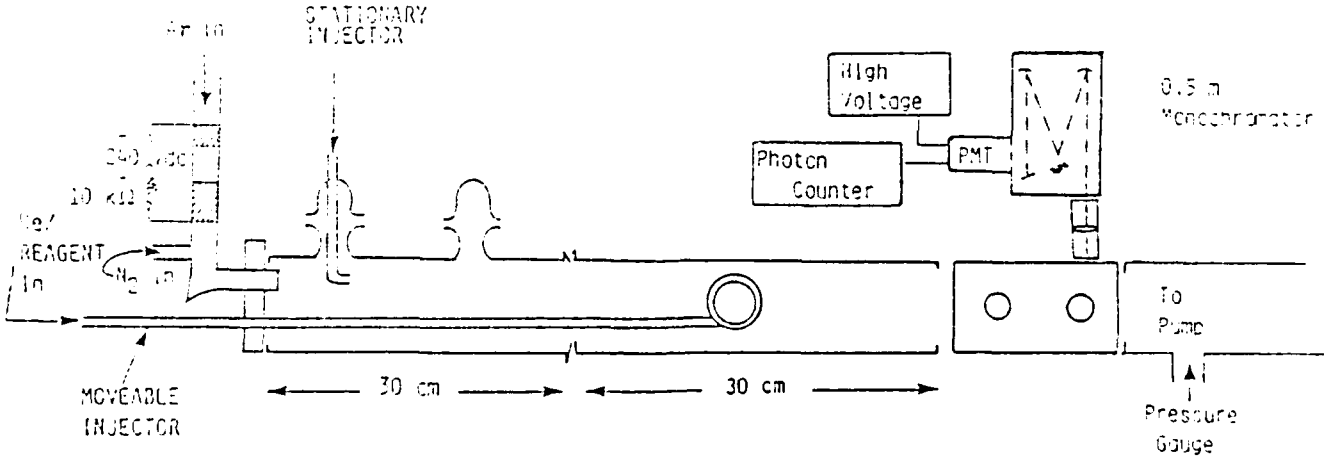

Figure 31. Flow tube apparatus configured for $N_2(A)$ decay kinetics measurements.

A thermoelectrically-cooled photomultiplier (HTV/R943-02) detected photons with the aid of an SSR 1105 photon-counting rate meter. A laboratory computer system digitized the analog output from the rate meter and stored the information on floppy disks for further processing. The computer system comprises an IBM PC with 512 K of RAM, two 360 K diskette drives, a monochrome monitor, and a 160 cps dot-matrix printer with graphics capability. Data Translation* manufactures the I/O system (DT2801A), which features 16 channels of A/D inputs, two channels of D/A output, two 8-bit digital I/O ports, software programmable gain, single-ended or differential input, and data acquisition rates as fast as 14 kHz. Laboratory Technologies Inc** software package "Real-time Laboratory Notebook," interfaces the computer to the D/A board and organizes data in a form compatible for analysis using the Lotus 123 business spreadsheet software or for sending to the PRIME 400 computer in PSI's computer center for analysis on that machine. Much of the analysis revolves around least-squares fitting of spectra. This code (Ref. 60) generates basis functions consisting of a synthetic electronic spectrum for a unit population in each vibrational level of each electronic state appearing in the spectral region of interest. A least-squares routine then finds the populations of each vibronic band which when multiplied by the appropriate basis function gives a composite spectrum most nearly matching the experimental spectrum.

Standard quartz-halogen and D_2 lamps were used to calibrate the spectral system for relative response as a function of wavelength. Excellent agreement between observed and calculated intensities of a number of bands of the $N_2(A^3\Sigma_u^+ - X^1\Sigma_g^+)$ system between 220 and 400 nm confirmed the reliability of the ultraviolet calibration.

The reaction between metastable $Ar(^3P_{0,2})$ and molecular nitrogen produces the metastable nitrogen molecules, $N_2(A^3\Sigma_u^+)$ (Refs. 61,62). This transfer excites $N_2(C^3\Pi_u)^{63}$ which quickly cascades radiatively to the metastable $A^3\Sigma_u^+$ state via the $B(^3\Pi_g)$ state. A hollow-cathode discharge source operating at 240 Vdc and 3mA produces the argon metastables. The argon and nitrogen are purified by flowing them through traps filled with 5 A molecular sieve. Since the experiments involve metastable nitrogen, it is not necessary to remove the nitrogen impurity from the Ar carrier.

---

* Data Translation, Inc, Marlborough, MA.

** Laboratory Technologies Inc, Santa Clara, CA.

Observations of strong Vegard-Kaplan, $N_2(A^3\Sigma_u^- - X^1\Sigma_g^+)$, emission downstream of the Ar/N_2 mixing zone confirms the production of the nitrogen metastables (Fig. 32). Codischarging the N_2 with the Ar increases the $N_2(A)$ yield by a factor of about 6 (Ref. 64) but it has been found that this procedure also produces some atomic N_2, vibrationally excited N_2 and metastable $N_2(a'^1\Sigma_u^-)$ (Ref. 65). Unequivocal measurements on $N_2(A^3\Sigma_u^+)$ reactions therefore, demand that the N_2 be added downstream of the discharge.

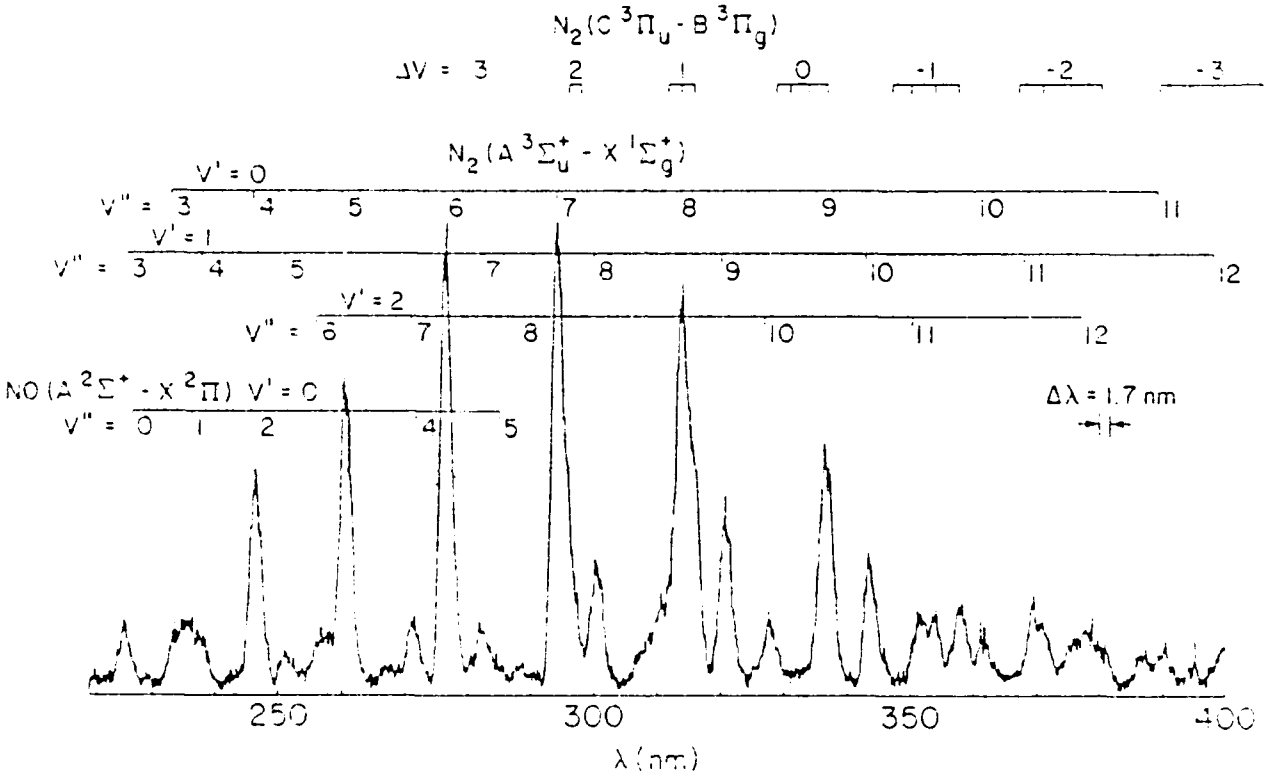

Figure 32. Vegard-Kaplan emission in flow reactor 9 ms downstream from the discharge.

Nitric oxide enters the flow tube through a 1-in-dia loop injector seated on the end of a 1/4-in-dia tube which slides along the bottom of the flow tube and parallel to its axis. This allows a variety of reaction distances for accurate kinetic studies. Adding CH_4, CF_3H, or CF_4 to the gas stream through a fixed, hook-shape injector, just downstream from where the N_2A entered the flow reactor relaxed N_2A vibrational excitation without significant electronic quenching (Refs. 66,67).

Mass-flow meters or rotameters monitor gas flow rates. All flowmeters were calibrated by measuring rates of increase of pressure with time into 6.5 or 12 ℓ flasks, using appropriate differential pressure transducers (Validyne DP-15) which themselves have been calibrated with silicon oil or mercury manometers. Typical flow rates for Ar, N_2, and He through the injector are 2000-5000, 100-500 and 50 μmol s^{-1}, while the NO flow rate ranges between 0 or 1 and 0 and 0.01 μmol s^{-1} for decay or excitation rate measurements, respectively. Total pressures, as measured by a Baratron® capacitance manometer, range from 0.3 to 10 torr, and flow velocities vary from 500 to 5000 cm s^{-1}.

The number density of reactant i is given by

$$N_i = \frac{f_i p_{tot}}{\sum_i f_i} \times \frac{N_o}{RT}$$

where the f_i represent reagent flow rates, p_{tot} is the total flow tube pressure in torr, N_o Avogadro's number, R the gas constant (6.236×10^{-2} torr cm^3 μmol^{-1} K^{-1}), and T the absolute temperature.

Nitric oxide is purfied by slowly flowing it at atmospheric pressure through an Ascarite® trap and then through a cold finger surrounded by a methanol/LN_2 slush bath (-100°C). The NO is then diluted in Ar and the mixtures stored in 5-ℓ Pyrex® flasks. Mixtures of 5-8% NO sufficed for decay rate measurements while the excitation-rate determinations required NO mole fractions $\lesssim 10^{-3}$.

3.1.3 <u>The Electronic Transition Moment for the NO($A^2\Sigma^+ - X^2\Pi$) Transition</u>--The issue of whether or not there is a significant variation in the electronic transition moment with r-centroid for the NO($A^2\Sigma^+ - X^2\Pi$) transition has been the subject of a number of papers over the last several decades (Refs. 67-78). While a number of papers have shown evidence of a significant transition-moment moment variation (Refs. 67-72), several groups have disputed this contention (Refs. 73-78). References 72 and 76 review most of the relevant literature. The general consensus in the scientific community seems to be that no significant transition moment variation occurs for the NO

γ-bands. Recently, while studying the electronic energy transfer between $N_2(A\ ^3\Sigma_u^+)$ and NO, inconsistencies were found in $NO(A\ ^2\Sigma^+)$ excitation rates measured using different bands originating from v' = 0 if a constant transition moment was invoked. The excitation of the NO γ-bands by N_2 $(A\ ^3\Sigma_u^+)$ energy transfer to NO $(X\ ^2\Pi)$ provides a source of γ-band emission which is free from other significant overlapping band systems in the spectral region. It was found that the observed branching ratios for transitions from a common vibrational level in the upper state cannot be explained by variations in the Franck-Condon factors. Observations show variation in the electronic transition moment of more than 40% over the r-centroid range 1.13-0.97 Å. This contention is supported in the following paragraphs.

Correct transition probabilities for the NO A-X system bear directly upon atmospheric science through such processes as the measurement of NO column densities in the mesosphere (Ref. 79) or the interpretation of emissions in a strong aurora. In addition, proper NO A-X transition probabilities are needed to calculate the gain for various transitions in the optically pumped NO A-X laser. However, proper NO(A-X) transition probabilities affect a wider range of studies. ever. Because they are easy to excite, the NO γ-bands are often used to establish the relative spectral response of monochromators in the ultraviolet (Refs, 73,75). Using incorrect branching ratios for the A-X transition will, of course, result in an incorrect response function, and will thereby invalidate all other measurements which depend upon the spectral response determined from the γ-band branching ratio measurements. The technique of laser-induced fluorescence on NO A-X transitions has become an increasingly important tool for probing the vibrational distributions of ground electronic state NO produced in chemical or photolytic reactions (Refs. 80,81). Incorrect values for the NO A-X transition probabilities invalidates the results of these measurements, and the validity of dynamical interpretations of the results become doubtful.

The intensity of emission from a given band is the product of the number density in the upper state and the Einstein coefficient for spontaneous radiation. The Einstein coefficient can be integrated into a product of the

Franck-Condon factor, the cube of the transition frequency, and the square of the electronic transition moment. Thus

$$I_{v'v''} = N_{v'}A_{v'v''} = \text{const} \times N_{v'} q^{3}_{v'v''} \nu_{v'v''} \bar{|R_e(r^{2}_{v'v''})|} \qquad (43)$$

The transition-momentless population in the upper state is then determined from the ratio of the integrated band intensity to the product of the Franck-Condon factor and the cube of the transition frequency:

$$N^{*}_{v'v''} = \frac{I_{v'v''}}{q_{v'v''} \nu^{3}_{v'v''}} = N_{v'} \bar{|R_e(r_{v'v''})|}^{2} \qquad (44)$$

The ratios of these transition-momentless populations to each other should be constant unless the transition moment varies with r-centroid. The relative variation in the transition moment with r-centroid results from the ratio of the various momentless populations to one reference population. Scaling the relative transition moments to experimentally determined lifetime or oscillator-strength data is then a relatively simple process. The spectral response function of the monochromator/detector system was accurately calibrated and verified by fitting the N_2 (A-X) Vegard-Kaplan transition features which occurs in the same spectral region.

It was determined that transition-momentless populations of the bands emanating from v'=0 and 1 using pectral fitting routine for each Δv sequence from Δv = 1 to Δv = -6. The fitting routine corrected for spectral overlap between the transitions for v' = 0 and 1. The fit included different effective rotational temperatures for the two vibrational levels. Each of these populations was ratioed to the ones determined for the Δv = -3 sequence. This sequence is in the middle of the wavelength range for the band system and, thus, should minimize any systematic errors in the relative monochromator response function. The Franck-Condon factors of both Nicholl's (Ref. 82) and Albritton et al. (Ref. 83) gave similar results. The final results incorporate the latter set.

Figure 33 shows the electronic transition moment relative to its value for the $\Delta v = -3$ sequence plotted against r-centroid. The variation is small, but consistent, up through the $\Delta v = -3$ sequence, but rises much more sharply for the $\Delta v = -5$ sequences. The diamonds in Fig. 33 show our reanalysis of the branching-ratio measurements of McGee et al (Ref. 77). They excited NO(A, $v' = 0$) with a laser and reported relative band emission intensities. Their results agree with ours. Finally, the transition moment variation was completed. This variation was given by Brzozowski et al. (Ref. 71) who observed band emission in electron-beam excited NO during studies on NO predissociation.

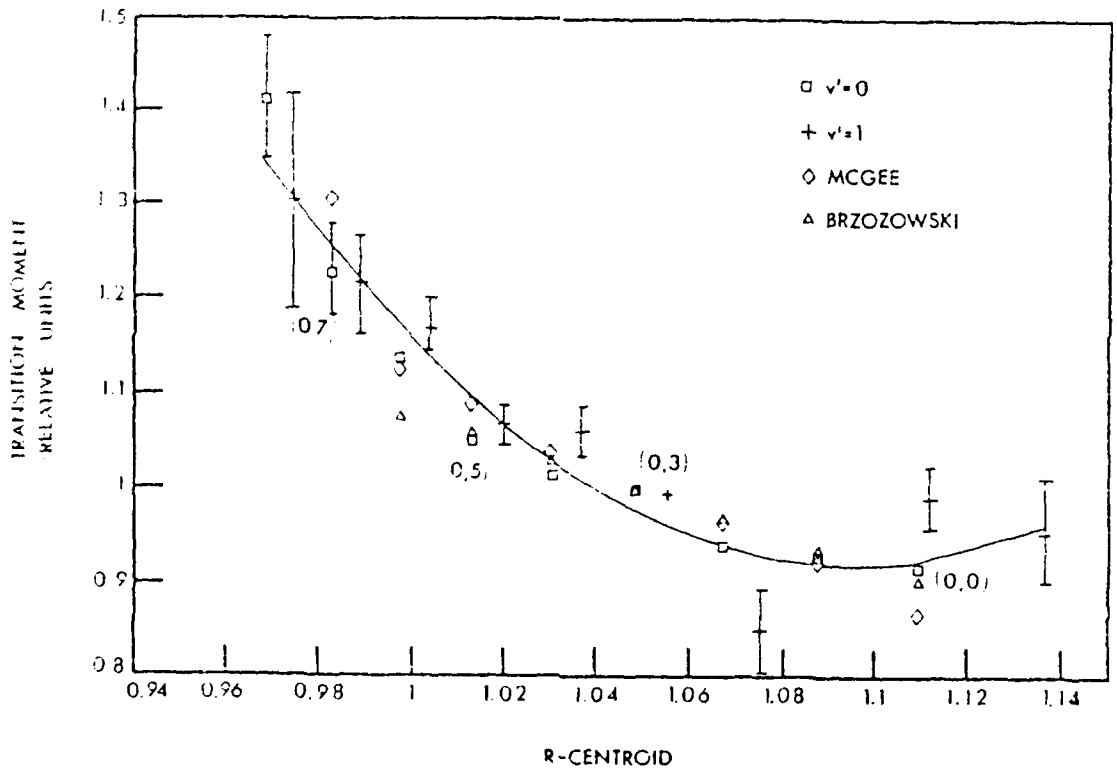

Figure 33. Variation in electronic transition moment with r-centroid for the NO($A^2\Sigma^+ - X^2\Pi$) transition.

We fit the results of the three experiments to a quadratic function of r-centroid:

$$|R_e(\bar{r}_{v'v''})|_{rel} = 33.08 - 58.77\ \bar{r}_{v'v''} + 26.85\ \bar{r}_{v'v''}^2 \qquad (45)$$

Using this functional form for the relative transition moment, we determined a smoothed set of branching ratios for emission from a given upper state as being

$$BR_{v'v''} = \frac{q_{v'v''}\ \nu^3_{v'v''}\left|R_e(\bar{r}_{v'v''})\right|^2_{rel}}{\sum_{v''} q_{v'v''}\ \nu^3_{v'v''}\left|R_e(\bar{r}_{v'v''})\right|^2_{rel}} \qquad (46)$$

The Einstein coefficient for spontaneous radiation from each band is the product of the branching ratio for the given band to the total radiative decay rate of the upper state vibrational level. The average of nine apparently reliable determinations of the fluorescence lifetime of NO(A, v' = 0) gives a value of (202 ± 14) ns (Refs. 74,76,84-90). Eight different determinations for the v' = 1 level give a value of (192 ± 14) ns (Refs. 76,84,85,88,89,91-93). In both cases the error bars represent one standard deviation. Table 7 lists the Einstein coefficients for each band.

Equation (47) relates the Einstein coefficient for a given v'v" transition to the absorption oscillator strength:

$$f^{abs}_{v'v''} = \frac{m_e\ c\ \lambda_o^2}{8\pi^2\ e^2}\ \frac{d_u}{d_l}\ A_{v'v''} \qquad (47)$$

where m_e is the electron mass, e its charge in esu, c the speed of light, λ_o the transition wavelength, and d_u and d_l are the electronic degeneracies of the upper and lower states, respectively. These last quantities are 1 and 2 for $A^2\Sigma^+$ and $X^2\Pi$, respectively. Applying the Einstein coefficients to Eq. (47) gives absorption oscillator strengths for the 0,0 and 1,0 bands of (3.9 ± 0.3) x 10^{-4} and (8.2 ± 0.6) x 10^{-4}, respectively. These values agree quite well with literature measurements of (4.03 ± 0.22) x 10^{-4} for the 0,0 transition (five different experiments) (Refs. 94-98) and (8.26 ± 0.48) x 10^{-4} for the 1,0 transition (three different measurements) (Refs. 95,97,98). Thus, the transition moment function satisfies the important criterion that the lifetime and absorption measurements be consistent.

TABLE 7. Einstein Coefficients for $NO(A^2\Sigma^+ - X^2\Pi_r)$.

v' = 0	v"	Wavelength (nm)	$q_{v'v"}$	$\bar{r}_{(v'v")}$ (Å)	$R_e(\bar{r})$	Branching Ratio	$A_{v'v"}$ (s^{-1})
	0	226.548	0.15697	1.1091	0.921429	0.202462	1.002E+06
	1	236.604	0.26345	1.0873	0.917005	0.277740	1.378E+06
	2	247.421	0.22646	1.067	0.935830	0.227041	1.124E+06
	3	259.087	0.15962	1.0481	0.973248	0.144264	7.147E+05
	4	271.700	0.090505	1.0303	1.026027	0.078883	3.905E+05
	5	285.377	0.045696	1.0135	1.091448	0.038894	1.926E+05
	6	300.252	0.021285	0.9977	1.166803	0.017777	8.801E+04
	7	316.482	0.009363	0.9827	1.250746	0.007673	3.799E+04
	8	334.256	0.003954	0.9684	1.342021	0.003166	1.568E+04
	9	353.794	0.001622	0.9548	1.439015	0.001259	6.235E+03
	10	375.362	0.000652	0.9419	1.540195	0.000485	2.405E+03
	11	399.263	0.000259	0.9295	1.645876	0.000183	9.061E+02
	12	425.947	0.000102	0.9177	1.754110	0.000067	3.339E+02

v' = 1	v"	Wavelength (nm)	$q_{v'v"}$	$\bar{r}_{(v'v")}$ (Å)	$R_e(\bar{r})$	Branching Ratio	$A_{v'v"}$ (s^{-1})
	0	215.134	0.23353	1.1364	0.962957	0.451795	2.353E+06
	1	224.182	0.10295	1.1108	0.922847	0.113188	5.895E+05
	2	233.870	0.00097	1.0920	0.915801	0.000925	4.818E+03
	3	244.266	0.07231	1.0754	0.925357	0.061794	3.219E+05
	4	255.446	0.10381	1.0551	0.957153	0.106972	5.572E+05
	5	267.499	0.10257	1.0368	1.004782	0.101704	5.297E+05
	6	280.526	0.097792	1.0198	1.065139	0.073099	3.807E+05
	7	294.644	0.060554	1.0039	1.135635	0.044406	2.313E+05
	8	309.990	0.033426	0.9888	1.215151	0.024100	1.255E+05
	9	326.723	0.017042	0.9745	1.301742	0.012043	6.273E+04
	10	345.032	0.008212	0.9609	1.394282	0.005653	2.944E+04
	11	365.139	0.003800	0.9480	1.491236	0.002524	1.315E+04
	12	387.212	0.00171	0.9357	1.592003	0.001084	5.651E+03
	13	411.871	0.000753	0.9238	1.697225	0.000451	2.352E+03
	14	439.206	0.000327	0.9126	1.803203	0.000182	9.507E+02
	15	469.796	0.000141	0.9017	1.912810	0.000072	3.769E+02

v' = 2	v"	Wavelength (nm)	$q_{v'v"}$	$\bar{r}_{(v'v")}$ (Å)	$R_e(\bar{r})$	Branching Ratio	$A_{v'v"}$ (s^{-1})
	0	204.952	0.29246	1.1654	1.050907	0.468229	2.577E+06
	1	213.747	0.017314	1.1516	1.003423	0.022467	1.234E+05
	2	221.886	0.15606	1.1194	0.932396	0.154996	8.516E+05
	3	231.223	0.07289	1.0947	0.915646	0.061695	3.390E+05
	4	241.217	0.00038	1.0770	0.923791	0.000268	1.564E+03
	5	251.936	0.034722	1.0644	0.939840	0.023936	1.315E+05
	6	263.459	0.08771	1.0440	0.983897	0.057946	3.184E+05
	7	275.873	0.10421	1.0265	1.039499	0.066934	3.678E+05
	8	289.281	0.088733	1.0103	1.105627	0.055919	3.072E+05
	9	303.801	0.062245	0.9951	1.180487	0.038608	2.121E+05
	10	319.569	0.038476	0.9807	1.262851	0.023464	1.289E+05
	11	336.744	0.021789	0.9671	1.350863	0.012995	7.140E+04
	12	355.514	0.011589	0.9542	1.443523	0.006707	3.685E+04
	13	376.099	0.005891	0.9419	1.540195	0.003278	1.801E+04
	14	398.761	0.002897	0.9301	1.640572	0.001534	8.432E+03
	15	423.818	0.001392	0.9189	1.742761	0.000693	3.808E+03
	16	451.643	0.000688	0.9081	1.847680	0.000304	1.672E+03

Einstein coefficients have been calculated for v' = 2 assuming the transition moment variation of Eq. (45) and a radiative-decay lifetime for v' = 2 of (182 ± 10) ns (Refs. 76,84,85,88,89). Because transition moment variation was extrapolated to regions outside the fit, the transition probabilities from v' = 2 are less reliable. This may be reflected in the modest disagreement between the absorption oscillator strength of the 2,0 band calculated from the transition probabilities given in Table 7 of (8.1 ± 0.4) x 10^{-4} and the experimental value of (6.8 ± 0.2) x 10^{-4} (Refs. 77,79,80).

Figures 34 and 35 show a comparison between the observed and the synthetic best fit spectra for the case of no assumed transition moment variation, and the transition moment variation determined in this work. Clearly including the transition moment variation makes a significant difference in the quality of the fit. A poor fit could also be the result of having an incorrect relative monochromator response function. In that case analysis for the transition moment function would also be invalid. This does not appear to be a significant problem in this work, however, because of the accurate fit of the Vegard-Kaplan bands of nitrogen over the same wavelength region. In addition, the good agreement between our own results and those of the two other groups alluded to previously (Refs. 71,77) confirms that the wavelength response function is accurate.

3.1.4 The Kinetics of the $N_2(A)$ Plus NO Reaction--Complete characterization of the energy-transfer reaction between $N_2(A)$ and NO,

$$N_2(A^3\Sigma_u^+) + NO(X^2\Pi) \rightarrow NO(A^2\Sigma) + N_2(X) \quad (48a)$$

$$\rightarrow \text{other channels} \quad (48b)$$

$$NO(A^2\Sigma^+) \rightarrow NO(X^2\Pi) + h\nu \quad (49)$$

involves measuring both the rate coefficient for removal of $N_2(A)$ by NO and the rate coefficient for the excitation of the NO γ-bands in the energy

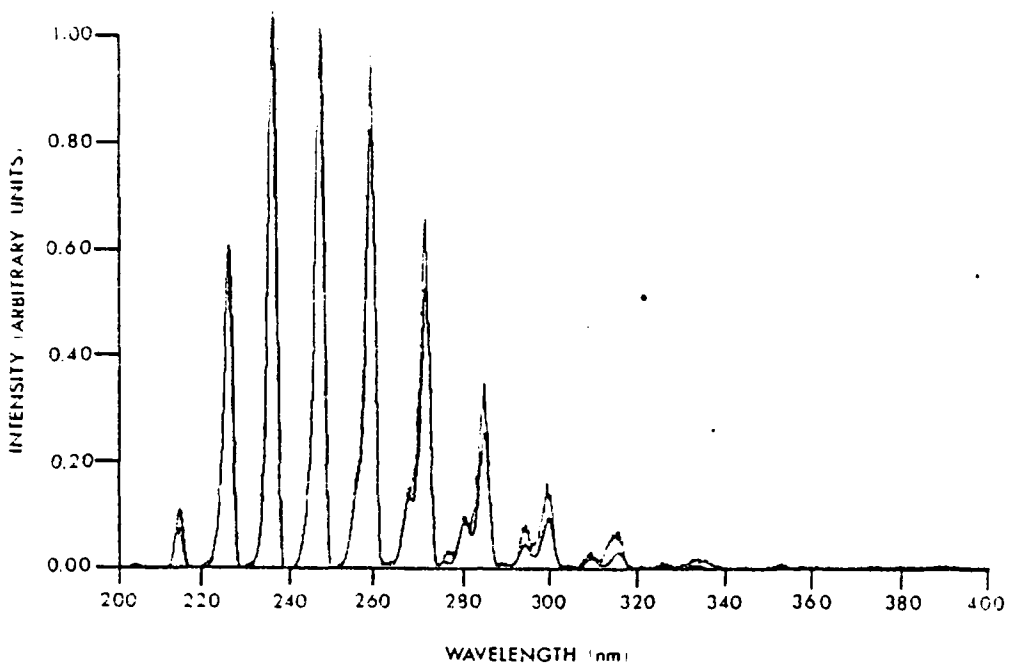

Figure 34. Experimental (light line) and synthetic (heavy line) spectrum for the NO γ-bands assuming a constant electronic transition moment.

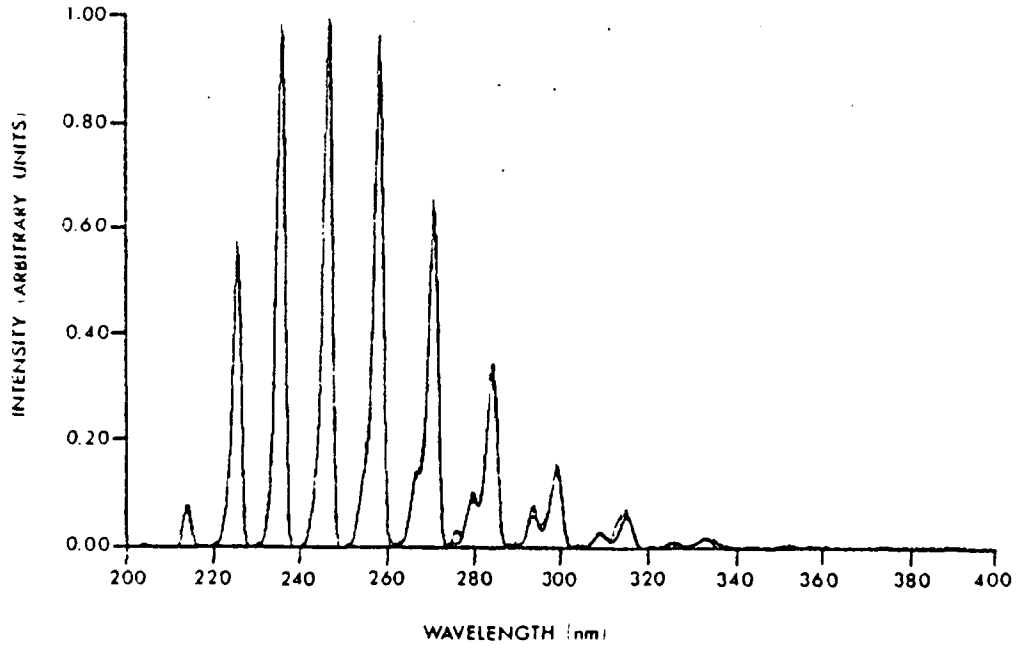

Figure 35. Experimental (light line) and synthetic (heavy line) spectrum of the NO γ-bands using the electronic transition-moment function determined in this work. The major remaining areas of discrepancy between the two spectra at 260, 276, 294, and 313 nm result primarily from small additions to the experimental spectrum from the 0,5 through 0,8 bands of the N_2 Vegard-Kaplan system which were not included in the synthetic fit.

transfer reaction. The rapid vibrational relaxation of $N_2(A)$ by molecules such as CF_4, CF_3H, and CH_4, with no accompanying electronic quenching (Refs. 7,66) allows us to alter the vibrational distribution of the $N_2(A)$. This makes state-to-state measurements possible.

3.1.4.1 The Quenching of N_2 ($A\ ^3\Sigma_u^+$, $v' = 0$) by NO--Measurements of the rate of removal of $N_2(A)$ by NO are not so easy as corresponding measurements of $N_2(A)$ quenching by other molecules. Ordinarily, one follows $N_2(A)$ number density decays by monitoring the Vegard-Kaplan emission (Refs. 7,50,51). The extremely bright NO γ-band emission in the same region of the spectrum however, masks the Vegard-Kaplan bands. The γ-band emission is a sensitive tracer of the $N_2(A)$ number density.

The differential equation describing the rate of change in the $NO(A^2\Sigma^+)$ number density with time is

$$\frac{d[NO(A)]}{dt} = k_{48}[N_2(A)][NO(X)] - k_{49}[NO(A)] \qquad (50)$$

The NO(A) is in steady state in the observation volume because the lifetime of NO(A) is short compared to the time a molecule resides within the field of view of the detector. Thus the intensity of the γ-band emission is

$$I_{NO^*} = k_{49}[NO^*] = k_{48}[N_2(A)][NO] \qquad (51)$$

Upon rearranging this equation, we relate the number density of $N_2(A)$ in the observation volume to the ratio of the γ-band emission intensity and the NO number density:

$$[N_2(A)] = \frac{I_{NO^*}}{k_{48}[NO]} \qquad (52)$$

The differential equation describing the decay of $N_2(A)$ in the reactor is

$$\frac{d[N_2(A)]}{dt} = -(k_{48}[NO] + k_{wall})\ [N_2(A)] \qquad (53)$$

where k_{wall} is the first-order (pressure dependent) rate coefficient for $N_2(A)$ quenching in wall collisions. Because the NO number density is typically several orders of magnitude greater than the $N_2(A)$ number density, it can be assumed that the NO number density is a constant (the pseudo first-order approximation). This approximation leads to an analytical solution to Eq. (53), viz,

$$\ln \frac{[N_2(A)]}{[N_2(A)]^o} = -(k_{48}[NO] + k_{wall})\ z/\bar{v} \qquad (54)$$

where we have replaced the reaction time by the ratio of the distance from flow tube injector to observation volume, z, to the bulk flow velocity, in the reactor, $\bar{v}$. Inserting Eq. (52) into Eq. (54) gives

$$\ln \frac{I_{NO^*}/[NO]}{I^o_{NO^*}/[NO]^o} = -\left(k_{48}[NO] + k_{wall}\right)\ z/\bar{v} \qquad (55)$$

Equation (53) shows that measurements of the logarithm of the ratio of γ-band intensity to NO number density as a function of NO number density but with fixed reaction time will give a linear relationship with a slope of $-k_{48}\ z/\bar{v}$. Such measurements at several different reaction distances, under otherwise constant conditions of pressure, temperature, total flow rate, etc., will correct for noninstantaneous mixing at the injector. The results must further be corrected by a factor of $(0.62)^{-1}$ to correct for the coupling of a radial density gradient in $N_2(A)$ number density with a parabolic velocity profile (Refs. 99-106).

As shown previously (Ref. 50) rate coefficients measured using a tracer can be seriously in error if the tracer is sensitive to several different $N_2(A)$ vibrational levels, each of which quenches at significantly different rates, the $N_2(A)$ vibrational distribution has been relaxed to only $v' = 0$. CF_3H, CF_4, and CH_4 all were used to relax $N_2(A)$ to $v' = 0$. As expected, the results were invariant with relaxation partner.

Figure 36 shows a plot of the ratio of the natural log of the γ-band intensity to the NO number density as a function of the NO number density for several different distances between the injector and observation volume. The linearity of these plots is quite good, extending over more than two orders of magnitude. Figure 37 shows a plot of the slopes of the lines in Fig. 36 and two other sets of data not shown plotted as a function of the reaction time. The slope of this plot, when divided by the radial-profile correction factor, 0.62, gives the rate coefficient for quenching $N_2(A)$ by NO. Note the nonzero intercept, indicative of the finite time required for complete reagent mixing.

A number of experiments spanning a range in total gas pressures from 0.7 to 3.7 torr and reaction times from 11 to 124 ms, and using several different NO/Ar gas mixtures all gave consistent results for the rate coefficient for $N_2(A, v' = 0)$ quenching by NO of $(6.6 \pm 0.8) \times 10^{-11}$ cm^3 molecule^{-1} s^{-1}. The quoted error estimate is one standard deviation in the averaging process. The total experimental uncertainty, including estimates in the uncertainties in the calibrations of the flowmeters, pressure gauges, etc. is about 15 percent. A few decay measurements in which the $N_2(A)$ was not vibrationally relaxed gave decays only slightly larger ($\lesssim$5 percent) than those measured for the relaxed $N_2(A)$. It is inferred that NO quenches vibrationally excited $N_2(A)$ at a rate similar to that for quenching $v' = 0$.

The result disagrees markedly with Dreyer and Perner's reported value of 2.8×10^{-11} cm^3 molecule^{-1} s^{-1} also for v'=0 (Ref. 47). We agree with the recent result of Shibuya et al. (Ref. 107), $(6.9 \pm 0.7) \times 10^{-11}$ cm^3 molecule^{-1} s^{-1}, and also quite well with early measurements by Callear and Wood (Ref. 45), 8.0×10^{-11}, Young and St. John (Ref. 44), 7.0×10^{-11}, Hill et al. (Ref. 42), 7.5×10^{-11} and Piper (Ref. 43) at 196 K, $(9 \pm 2) \times 10^{-11}$. Mandel and Ewing's (Ref. 46), rate coefficient, 4.3×10^{-11} appears to be discordant with the rest of the literature. All the rate coefficients are in units of cm^3 molecule^{-1} s^{-1}. All measurements excepting Dreyer and Perner's used tracer techniques, and were not state specific. As has been pointed out, however, our measurements indicate that the quenching of $N_2(A)$ by NO does not

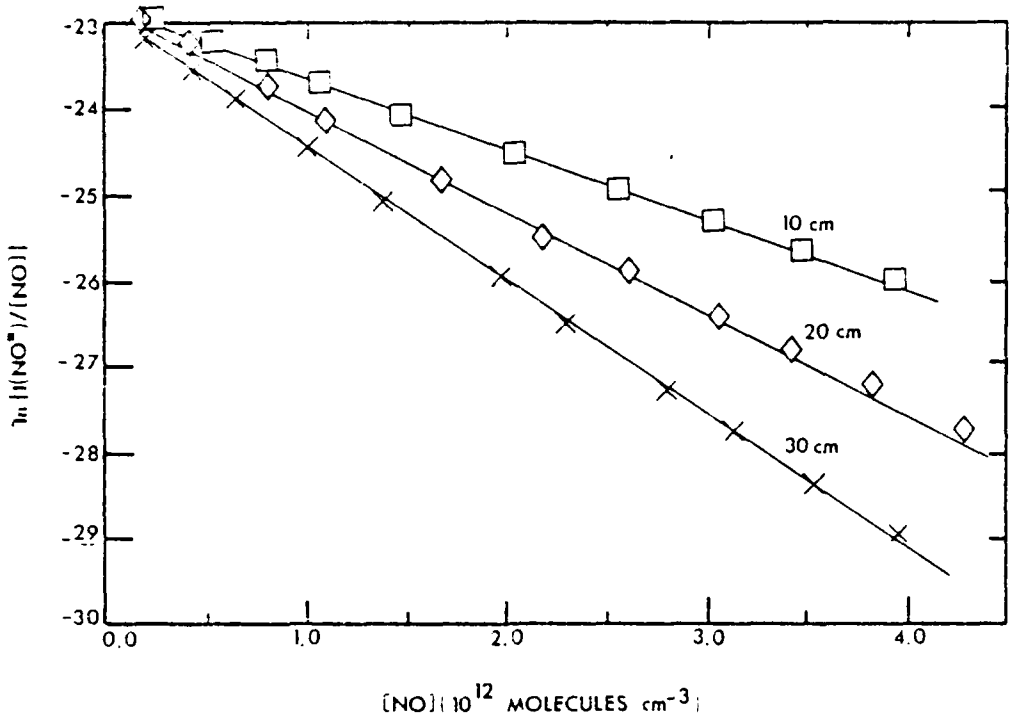

Figure 36. Decay in the natural log of the $N_2(A, v' = 0)$ number density as a function of NO number density at three different reagent mixing distances.

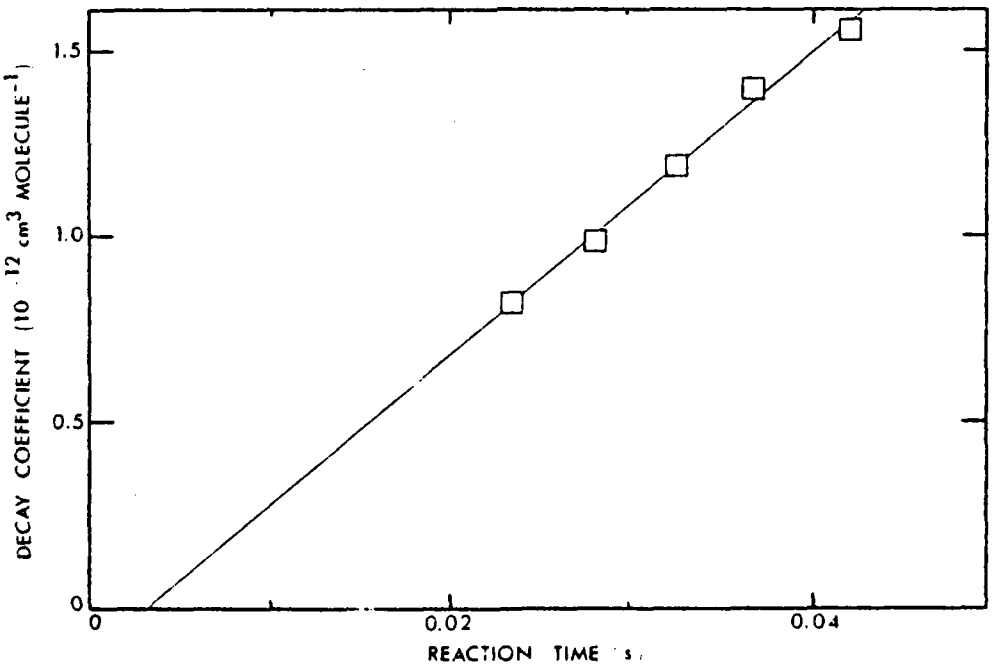

Figure 37. $N_2(A, v' = 0)$ decay constants in NO as a function of reaction time.

appear to show a strong dependence on the $N_2(A)$ vibrational level. Callear and Wood (Ref. 45) also reached this conclusion when they attempted to relax $N_2(A)$ vibration with large additions of helium to their flash photolysis system.

3.1.4.2 The Excitation of $NO(A^2\Sigma^+, v' = 0)$ by $N_2(A^3\Sigma_u^+, v' = 0)$--We have determined the rate coefficient for excitation of $NO(A^2\Sigma^+, v' = 0)$ by measuring the increase in the intensity of several bands originating from $NO(A, v' = 0)$ as a function of added NO number density but for constant $N_2(A)$ number density. If we note that the $N_2(A)$ number density is the intensity of the Vegard-Kaplan bands divided by the Einstein coefficient (Ref. 108) for spontaneous radiation, we can rearrange Eq. (51) to give the working equation for the analysis.

$$I_{NO^*} = k_{48a} \frac{I_{VK}}{A_{VK}} [NO] \tag{56}$$

One convenient feature of this analysis is that the absolute calibrations for photon-emission rate measurements of the two intensities cancel, and only the relative spectral response is important. Thus, the intensity measurements do not introduce significant potential sources of systematic error. In practice, total Vegard-Kaplan intensity was determined from a spectral fit to the whole band system. We then measured the change in the peak intensity of one of the bands of NO(A) as a function of added NO number density, being careful to keep added NO number densities below the range giving significant $N_2(A)$ quenching. Multiplying the peak intensity by a correction factor gave the total integrated intensity under that specific band. Dividing the integrated intensity by the appropriate branching ratio (Paragraph 3.1.3) determined the total emission from NO(A). Observations were made on the 0,1, 0,4 and 0,5 γ-bands. Under the experimental resolution, the 1,5 and 1,6 bands overlap the 0,4 and 0,5 γ-bands and, thus, contribute to the observed emission intensity. This small contribution was subtracted from our data. All three of the observed γ-bands gave excitation rate coefficients which were identical within experimental error.

Figure 38 shows that the intensity of the 0,1 band increases linearly with added NO number density in accord with Eq. (56). A number of such experiments yielded a rate coefficient for exciting NO(A, v' = 0) by N_2(A, v' = 0) of (9.0±2.7) x 10^{-11} cm^3 $molecule^{-1}$ s^{-1}, where the error bars represent the total estimated statistical and systematic error. The major contribution to the uncertainty is in the 20 percent uncertainty quoted for the N_2(A) Einstein coefficient (Ref. 108). Variations of greater than a factor of 5 in pressure, and of more than an order of magnitude in N_2(A) number density gave consistent results. The distance was varied between the NO injector and the observation region to insure that the NO was fully mixed. In addition using Xe* + N_2 as the N_2(A) source, and using several different NO/Ar gas mixtures did not change the results.

Relatively high resolution scans over the 0,6 and 1,7 bands as a function of pressure between 0.4 and 10 torr showed that the ratio of NO(A, v' = 1) to NO(A, v' = 0) excitation by N_2(A, v' = 0) was 0.94 ± 0.06, Fig. 39. Spectral scans between 200 and 400 nm indicated that excitation of NO(A, v' = 2) and NO(B, v' = 0) were both $\gtrsim$ 0.003 as compared to NO(A, v' = 0). Thus, the total rate coefficient for NO excitation by N2(A, v' = 0) is (10 ± 3) x 10^{-11} cm^3 $molecule^{-1}$ s^{-1}.

3.1.4.3 State-to-State Excitation of NO(A, v' = 0,1,2) by N_2(A, v' = 0,1,2)--A number of spectra of the NO γ-bands and N_2 Vegard-Kaplan bands were scanned with fixed NO number density, but with varying CF_4 number density and, thus, varying N_2(A) vibrational distribution (Figs. 40 and 41). The total N_2(A) number density changed little over the series of experiments, but the vibrational distribution changed from one in which more than half of the N_2(A) was vibrationally excited to one in whch well over 80 percent of the N_2(A) was in v' = 0. These measurements therefore tracked how the NO(A) vibrational distribution changed with changes in N_2(A) vibrational distribution. The observed intensity of a given NO(A) vibrational level can be expressed by

$$I_{NO^*_v} = k_{0v} [N_2A]_0 + k_{1v} [N_2A]_1 + k_{2v} [N_2A]_2 [NO] \qquad (57)$$

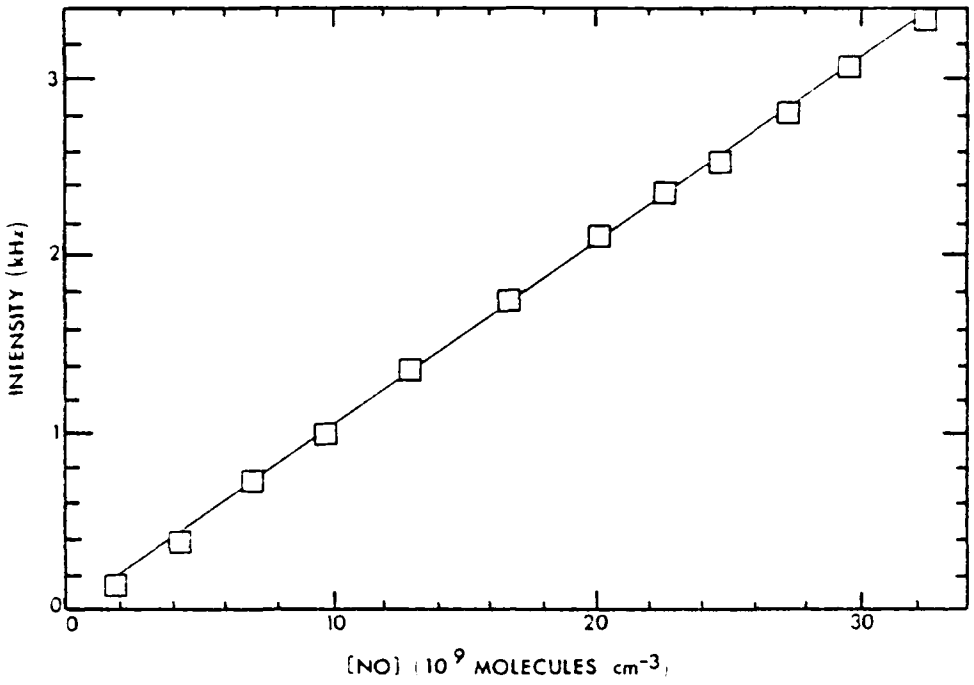

Figure 38. Variation in the peak intensity of the NO(A-X, 0,1) band as a function of added NO number density.

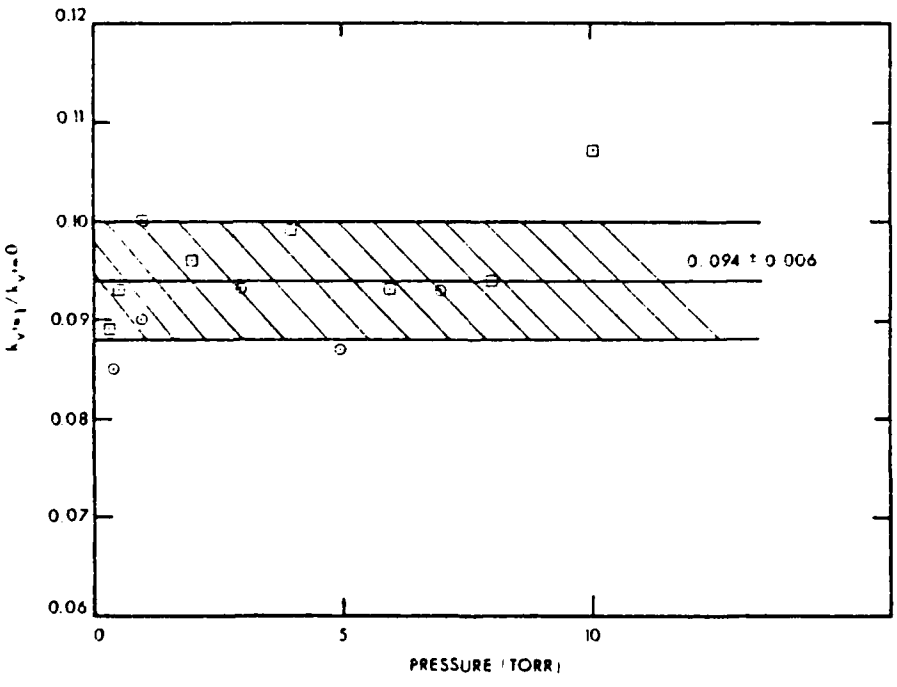

Figure 39. Ratio in the rate coefficients for exciting NO(A, v' = 1) to NO(A, v' = 0) by N_2(A, v' = 0) as a function of argon pressure.

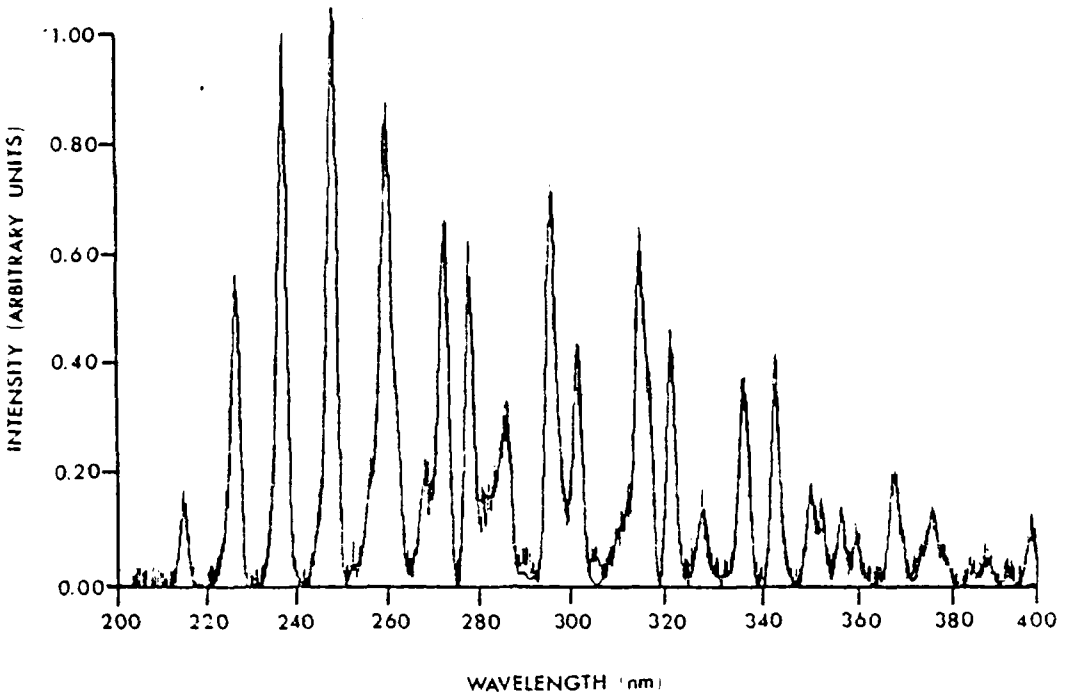

Figure 40. Spectrum of NO(A-X) and N_2(A-X) in the absence of CF_4. The light line shows the experimental data, while the heavy line shows the synthetic best fit to the data.

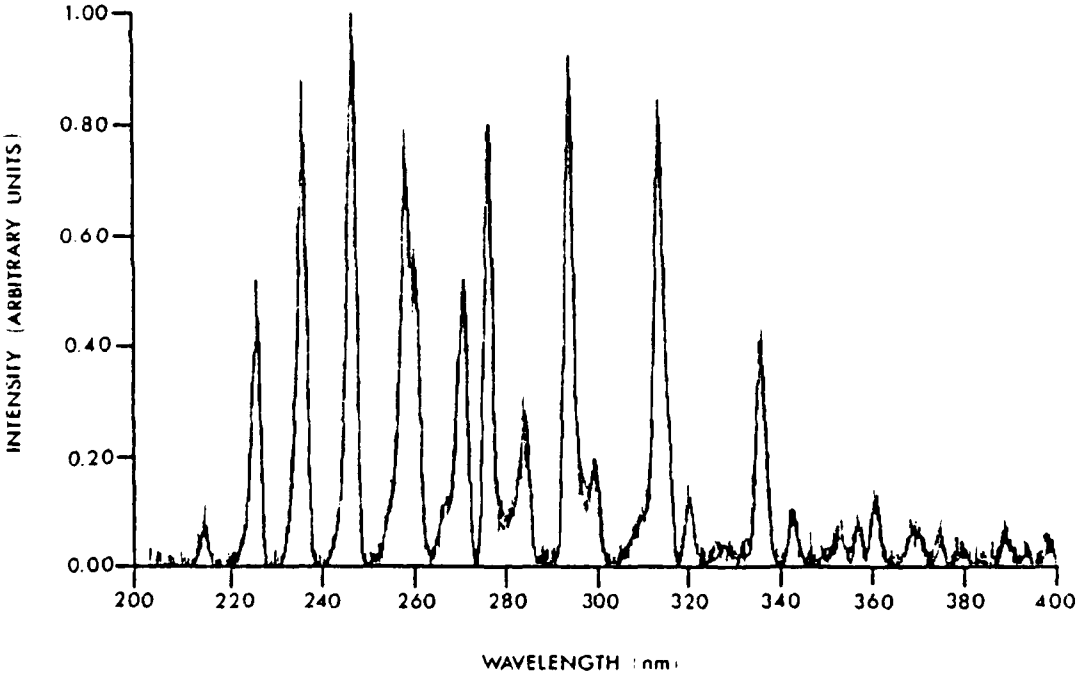

Figure 41. Spectrum of NO(A-X) and N_2(A-X) in presence of CF_4 which relaxes most of the N_2(A) vibrational energy. The light line is the experimental data while the heavy line shows the synthetic best fit.

where the subscripts on the k's represent the vibrational level of the $N_2(A)$ and NO(A), respectively. CF_4 vibrationally relaxes $N_2(A)$ in $\Delta v=1$ transitions, and relaxes $v' > 2$ much more efficiently than it does $v' = 1$ (Ref. 64). Thus, for small CF_4 additions, the $v' = 1$ number density stays relatively constant, and primarily $v' > 2$ is quenched. For moderate to high amounts of vibrational relaxation, therefore, only $N_2(A)$ $v' = 0$ and 1 remain in the reactor and further relaxation beyond that point changes only the ratio of $v' = 1/v' = 0$; thus Eq. (57) can be simplified and rearranged to give,

$$\frac{I_{NO^*_v}}{[N_2A]_0} = k_{0v} + k_{1v} \frac{[N_2A]_1}{[N_2A]_0} [NO] \tag{58}$$

The ratio of the slope to intercept of the linear plot implied by Eq. (58) will give the ratio of the rate coefficients k_{1v}/k_{0v}. Figures 42 and 43 show that this linear relationship does indeed obtain. Using the results for $v' = 1$ excitation derived from the moderate-to-high relaxation data, we can subtract out the contribution to observed excitation from $v' = 1$ for the data showing little relaxation and thereby probe contributions from $v' > 2$. The working equation then becomes

$$\frac{I_{NO^*_v}}{[N_2A]_0} - k_{1v} \frac{[N_2A]_1}{[N_2A]_0} [NO] = k_{0v} + k_{2v} \frac{[N_2A]_2}{[N_2A]_0} [NO] \tag{59}$$

Figures 44 and 45 show the linear relationship implied by this equation, and the ratio of the slope to intercept from these plots gives the ratio k_{2v}/k_{0v}. Because excitation of NO(A, $v' = 2$) and NO(B, $v' = 0$) were such minor channels, only their contributions to the total excitation were estimated by measuring the integrated intensity under the 2,0 gamma band and the 0,7 beta band in several spectra in which the $N_2(A)$ was vibrationally excited and several [illegible] in which it was relaxed. Thus, only an excitation rate coefficient [illegible] for excited and unexcited $N_2(A)$ for these two states. Table [illegible] relative excitation rate coefficients for the state-to-state [illegible] NO(A, $v' = 0,1,2$) and NO(B, $v' = 0$) by $N_2(A, v' = 0,1,$ [illegible]

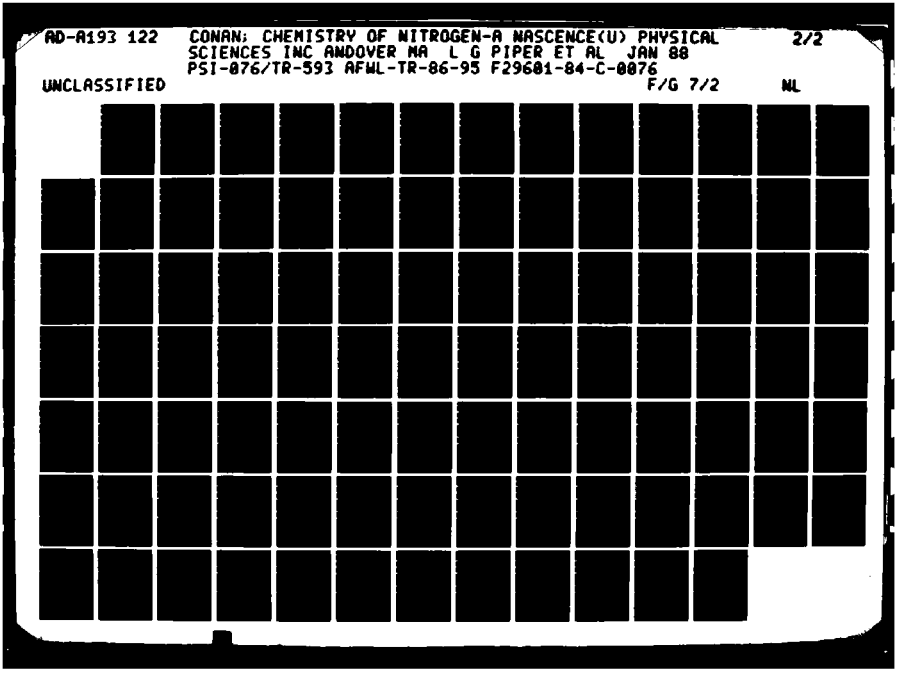
AD-A193 122 CONAN; CHEMISTRY OF NITROGEN-A NASCENCE(U) PHYSICAL 2/2
SCIENCES INC ANDOVER MA L G PIPER ET AL JAN 88
PSI-076/TR-593 AFWL-TR-86-95 F29601-84-C-0076
UNCLASSIFIED F/G 7/2 NL


1·0
1·1
1·25
2·8
3·15
3·5
4·0
4·5
2·0
1·8
1·4
1·6

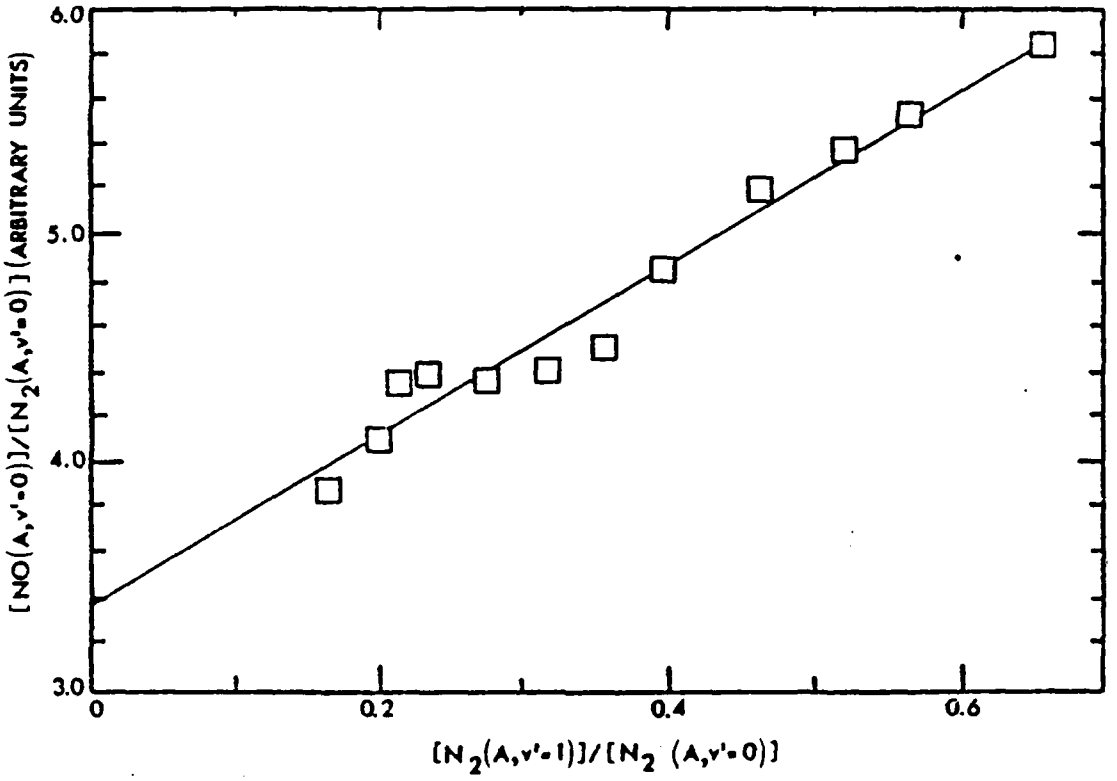

Figure 42. Excitation of NO(A, v' = 0) as a function of the ratio of N_2(A, v' = 1) to N_2(A, v' = 0).

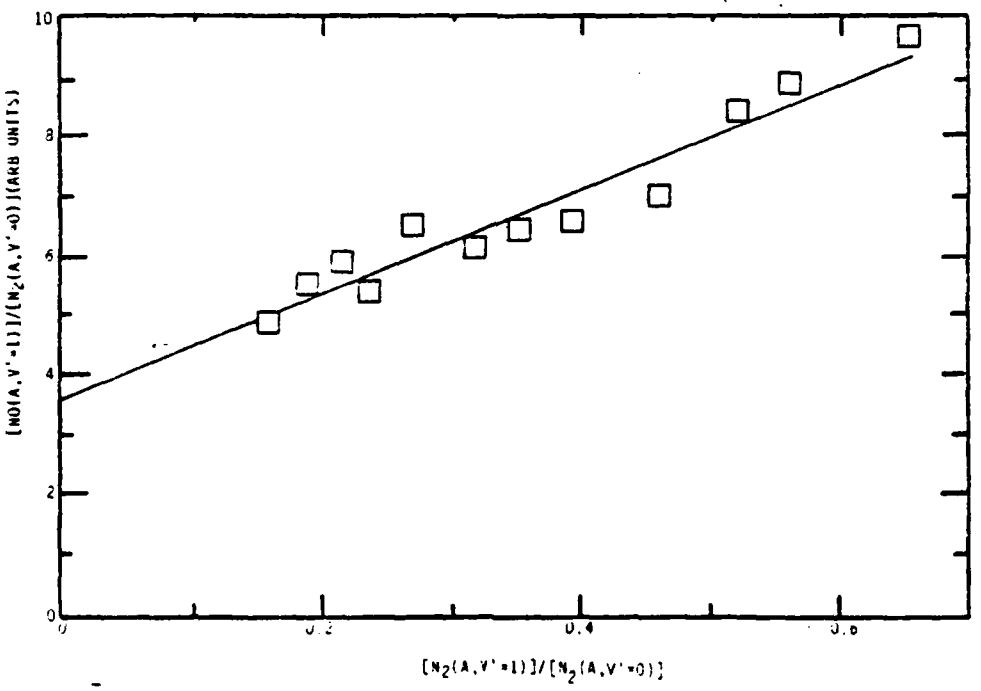

Figure 43. Excitation of NO(A, v' = 1) as a function of the ratio of N_2(A, v' = 1) to N_2(A, v' = 0).

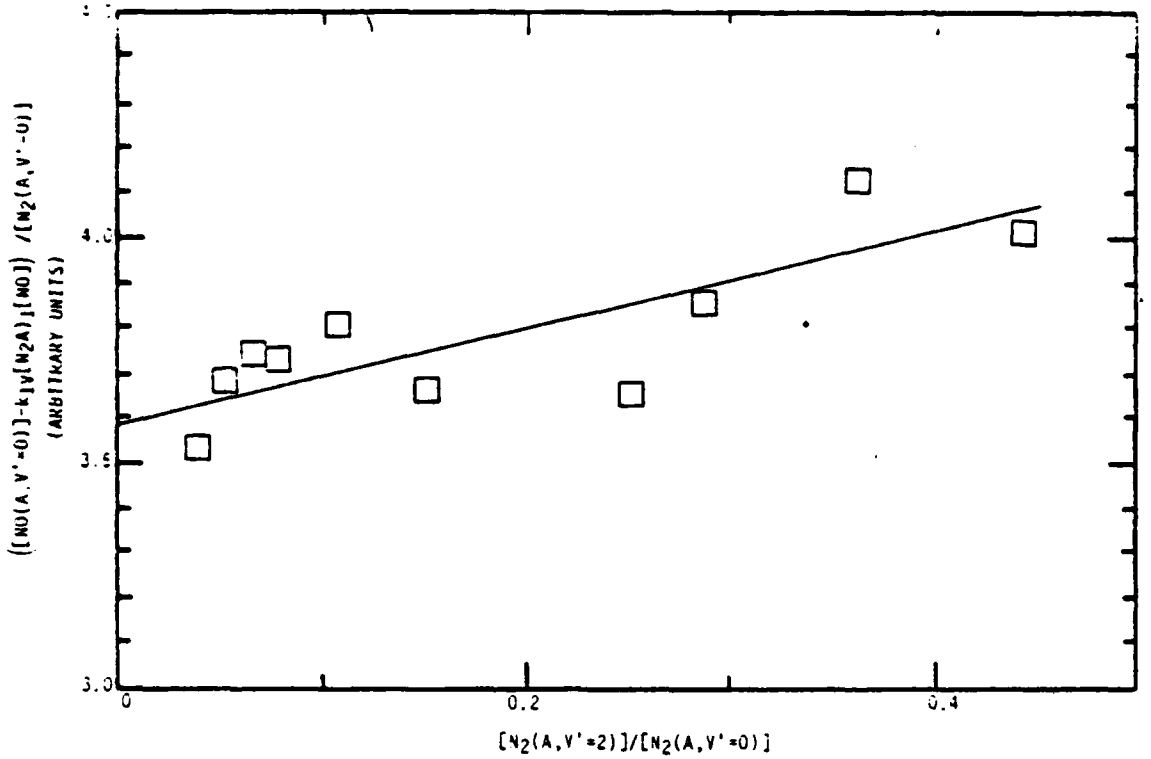

Figure 44. Excitation of NO(A, v' = 0) as a function of the ratio of N_2(A, v' = 2) to N_2(A, v' = 0).

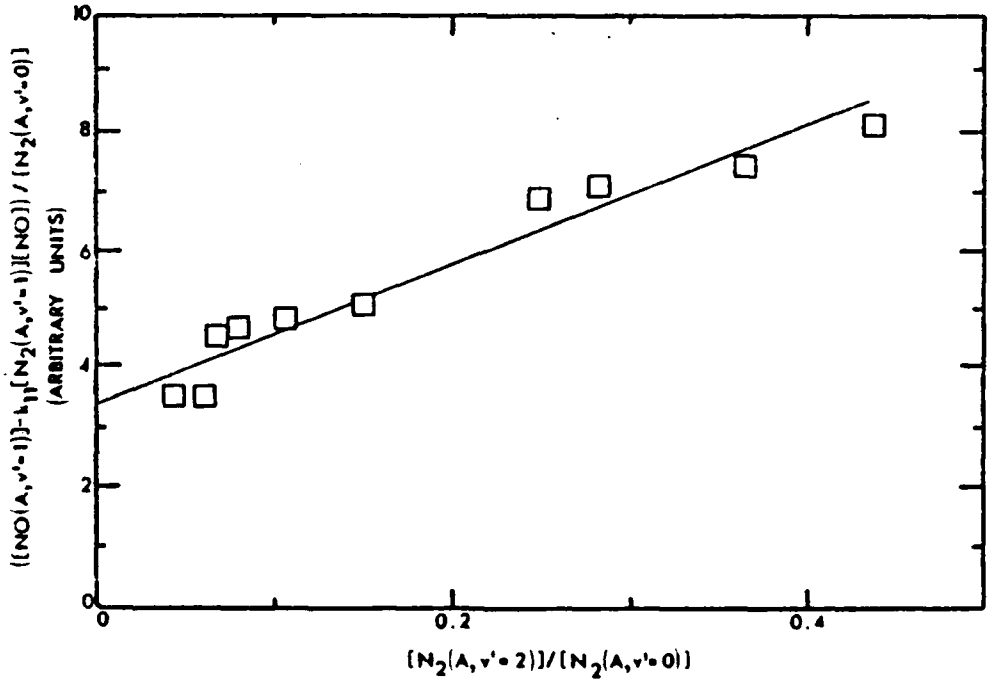

Figure 45. Variation in the excitation of NO(A, v' = 1) as a function of the ratio of N_2(A, v' = 2) to N_2(A, v' = 0).

TABLE 8. State-to-State Relative Excitation-Rate Coefficients.

$N_2(A)$ v'	NO(A) v' =	0	1	2	NO(B, v' = 0)
0		1*	0.094 ± 0.006	0.003	0.0032 ± 0.0007
1		1.11 ± 0.07	0.22 ± 0.03	0.024	0.033 ± 0.007
2		0.29 ± 0.07	0.32 ± 0.03		

*1 = 9.0×10^{-11} cm^3 $molecule^{-1}$ s^{-1}

3.1.4.4 Discussion--If the energy transfer between $N_2(A)$ and NO proceeds only through exit channels of radiating NO states, then the rate coefficients for $N_2(A, v' = 0)$ quenching by NO (6.6×10^{-11} cm^3 $molecule^{-1}$ s^{-1}) and for NO(A,B) excitation by $N_2(A,v' = 0)$ ($(10\pm3) \times 10^{-11}$ cm^3 $molecule^{-1}$ s^{-1}) ought to be the same. The lack of congruency between the two measurements is somewhat disturbing, even though they do overlap slightly at the extreme limits of their respective error bars. An attempt was made to cross check data carefully, and to vary the experimental conditions over a fairly wide range to find systematic trends which might explain the discrepancy. None were found. The conclusion, therefore, is that the Einstein coefficient for the $N_2(A-X)$ transition is in error by about 30 percent (it should be smaller).

The experimental determination of lifetimes on the order of 2s is extremely difficult and have manifold uncertainties. The accepted value of the Einstein coefficient for the $N_2(A-X)$ transition rests upon absorption measurements by Shemansky in the vacuum ultraviolet (Ref. 108) and his reanalysis (Ref. 109) of Carleton and Oldenberg's absorption measurements of $N_2(A)$ in a discharge (Ref. 110). His analysis requires a long extrapolation of the

transition-moment function with r-centroid from the region encompassed by his absorption measurements into the region of r-centroid sampled by the strong transitions from the v' = 0 level. He tied this extrapolation to the lifetime for the v' = 0 level derived from the Carleton and Oldenberg reanalysis. Carleton and Oldenberg (Ref. 110) attempted to measure simultaneously the absolute photon-emission rate of the 0,6 Vegard-Kaplan band and the absolute number density v' = 0 level of the A state via resonance absorption on the 1,0 transition of the first-positive system (N_2 B-A). Assuming that the experimental observations of Carleton and Oldenberg are accurate, and that Shemansky's re-analysis of their observations is correct, then their derived lifetime for N_2(A, v' = 0) depends directly upon the accuracy of the lifetime of the v' = 1 level of N_2(B). While the recent lifetime measurements of Eyler and Pipkin (Ref. 111) on the radiative lifetimes of N_2(B, v' = 5-12)indicate that the transition probabilities of the first-positive system given by Shemansky (Ref. 112) are essentially correct for $v' \gtrsim 3$, we do not feel confident that Shemansky's transition probabilities for the three lowest levels are necessarily accurate. The transition probabilities for these three levels depend predominantly upon an extrapolation of the electronic transition-moment function which Shemansky derived from relative intensity measurements of bands with r-centroid values between 1.35 and 1.6 Å out to r-centroid values as small as 1.0. This is generally a risky procedure. The recent ab initio calculations of the transition-moment function by Werner et al. (Ref. 113), Yeager and McKoy (Ref. 114), and Weiner and Öhrn (Ref. 115) all show a much slower increase in the transition moment to smaller r-centroid than is given by Shemansky's extrapolation (Fig. 46). The lifetimes Werner et al., calculate from their transition-moment function are consistently 16 percent larger than the lifetimes measured by Eyler and Pipkin (Ref. 111), but the relative variation of their calculated lifetimes with vibrational level matches that of Eyler and Pipkin quite well. They also match the relative variation in the lifetimes measured by Jeunehomme (Ref. 116), and by Carlson et al. (Ref. 117) and those calculated from Shemansky's transition probabilities for $v' > 4$. They deviate markedly from the experimental results, however, for the lowest vibrational levels, with the calculated lifetimes of Werner et al., being somewhat longer. If we reduce the calculated lifetimes of Werner et al. by

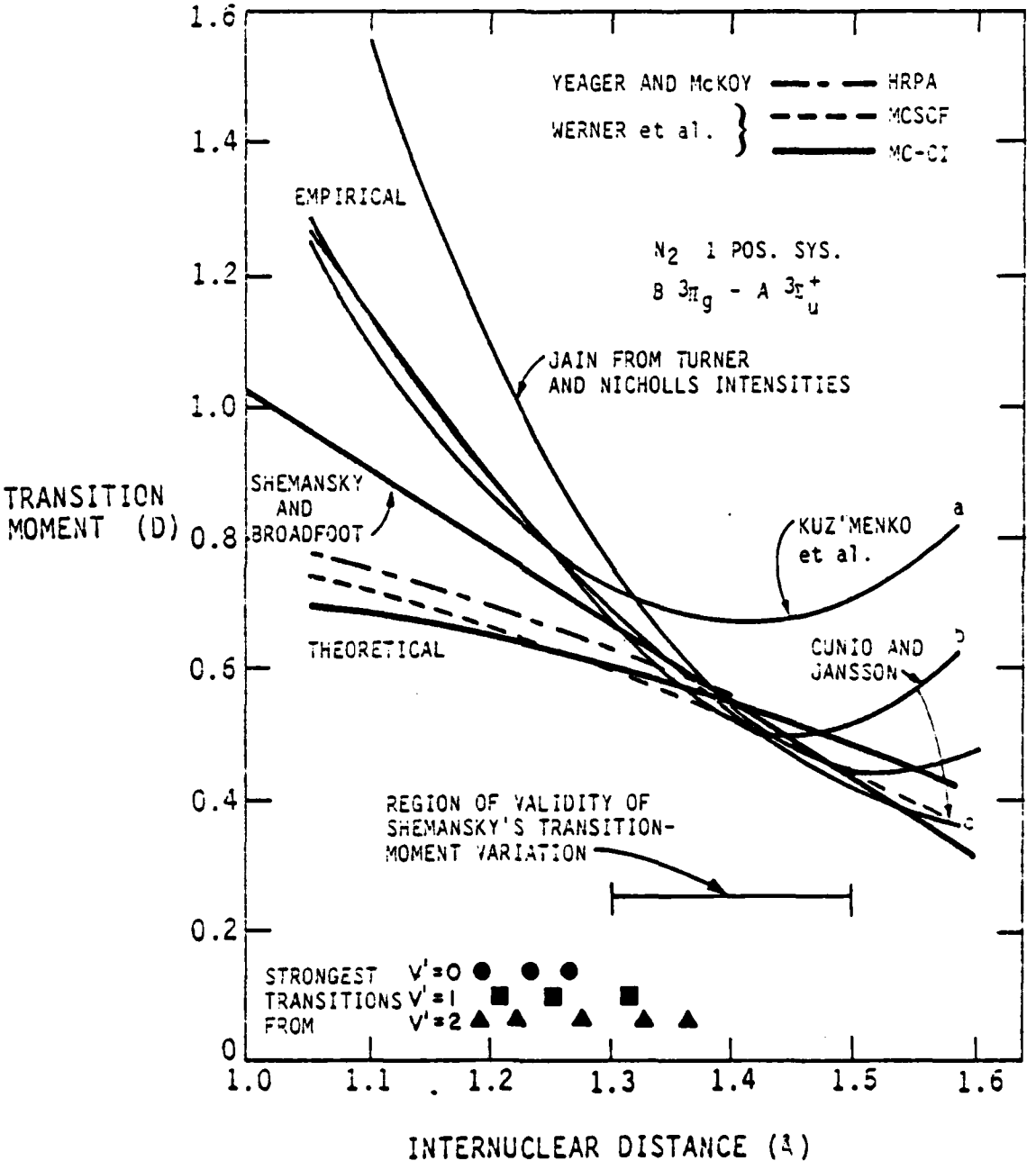

Figure 46. Electronic transition moments for $N_2(B^3\Pi_g - A^3\Sigma_u^+)$.

16 percent to make them coincide with Eyler and Pipkin's measurements for the high vibrational levels, a lifetime is obtained for v' = 1 of $N_2(B)$ of 9.5 μs in contrast to the value of 7.8 μs which results from Shemansky's transition probabilities. This large a change in the lifetime of the B state will reduce the transition probability for $N_2(A, v' = 0)$ from Carleton and Oldenberg's experiment by 20 percent. This reduction would then bring our quenching- and excitation-rate measurements into reasonable agreement. Taking the ab initio transition probabilities at face value would result in a Vegard-Kaplan transition probability about 40 percent smaller than the currently accepted values, and would bring the two measurements into almost perfect congruence. The other theoretical treatments agree with Werner et al.'s calculations. The lifetime of $N_2(B, v' = 0)$ measured by Heidner et al. (Ref. 118) via resonance fluorescence is also somewhat larger than given by Shemansky's extrapolation.

A reduction in the transition probability of $N_2(A,v'=0)$ state on the order of 20-30 percent would still give a variation in the absolute transition moment of the A--X transition fully consistent with the absolute measurements of Shemansky that sampled smaller values of the r-centroid, and the relative transition-moment measurements of Broadfoot and Maran (Ref. 119) which sampled larger r-centroid values, those sensitive to the Vegard-Kaplan transitions from v' = 0 (Fig. 47). We feel that good experimental measurements of the relative transition-moment variation of the first-positive system which sample smaller values of r-centroid are imperative to clear up this conflict. This will require relative intensity measurements extending out into the infrared to 1.5 μm.

The measurements on the vibrational-level dependence of NO excitation by $N_2(A)$ show that $N_2(A, v' = 1)$ excites NO(A,B) about 25 percent more efficiently than does $N_2(A, v'=0)$. $N_2(A, v'=2)$ however, is somewhat less efficient at exciting NO transitions. The reduction in observed intensity of NO(A,B) from excitation by $N_2(A, v' = 2)$ could result from one of three possibilities. First, the quenching efficiency could be smaller. Second, the more highly excited $N_2(A)$ can access higher lying levels of NO(A,B) which might be collisionally coupled into other states of NO which do not radiate or emit outside

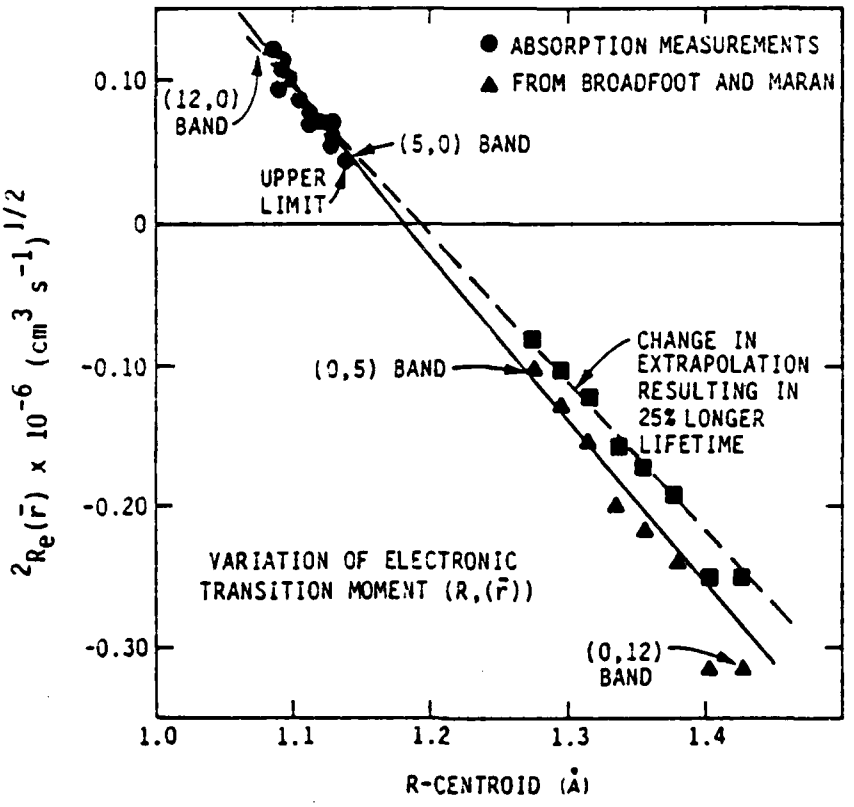

Figure 47. Variation of electronic transition moment for $N_2(A^3\Sigma_u^+ - X^1\Sigma_g^+)$.

the spectral bandpass, such as the $b^4\Sigma^-$ or $a^4\Pi$ states. The third possibility is that some of the encounters between $N_2(A, v' = 2)$ and NO end up dissociating the NO. Only vibrational levels of $N_2(A) \geq 2$ have sufficient energy to dissociate the NO. Atom production from this interaction has not been attempted, but such measurements would confirm this possibility.

The difference between the excitation rates of $N_2(A, v'=1)$ and $N_2(A, v' = 0)$ is not sufficiently great for us to observe significant changes in decay-rate measurements involving vibrationally excited and unexcited $N_2(A)$. Given a typical $v' = 1/v' = 0$ ratio of 0.6, we compute that the effective decay rate would increase by only 10 percent when both $N_2(A)$ vibrational levels were present. Within experiment error, this small enhancement is consistent with observations.

To investigate more completely the energy disposal in the reaction, we scanned the 0,6 and 1,7 bands of NO(A-X) under moderate resolution ($\Delta\lambda \approx 0.20$ nm) at pressures between 0.4 and 9 torr. This resolution was adequate to resolve partially the rotational structure. We then adjusted rotational temperatures in the fitting program until the observations could be monitored. At 0.4 torr, Boltzmann rotational temperatures of 1400 K and 800 K fit the emission from v' = 0 and 1, respectively. At higher pressures, however, the band contours were decidedly non-Boltzmann. Collisions with the Ar bath gas relaxed the lower rotational levels much more efficiently than they did the higher rotational levels. For examples, at 4.0 torr a rotational temperature of 600 K fit region around the heads of the 0,6 band quite well, while the high rotational levels which are prominent in the short-wavelength tail of the band followed an 1100 K Boltzmann distribution. Assuming a hard-sphere model with a 40 A^2 collision cross section, we calculate that an excited NO molecule will experience 1.5 collisions during a radiative lifetime at 1 torr. Thus, at 0.4 torr most of the NO(A) molecules will not experience a collision prior to radiation, whereas at 4 torr they will experience an average of six collisions. Thus, the rotational relaxation of NO(A) by Ar is a relatively efficient process, requiring only a few collisions to remove most of the rotational energy. The efficient rotational relaxation of low J levels of NO(A) by Ar and the correspondingly much smaller efficiency for high-J level relaxation has been studied in some detail by Ebata et al. (Ref. 120).

The efficient transfer of vibronic energy from $N_2(A)$ to NO may occur by a Franck-Condon type of mechanism. Deperasinska et al. (Ref. 121) have calculated Franck-Condon factors for the transitions relevant to the transfer of energy from $N_2(A, v' = 0)$ to NO. The Franck-Condon factors for producing NO(A) are three orders of magnitude greater than those for producing NO(B), which they claim is reflected in the much smaller efficiency for producing NO(B) relative to NO(A). Their calculated Franck-Condon factors, however, would predict roughly equal probabilities for producing vibrational levels v' = 0 and 1 of NO(A). In contrast, observations show that NO(A,v'=0) is produced ten times more efficiently than NO(A, v' = 1). They have not performed the relevant Franck-Condon calculations for $N_2(A, v' = 1, 2)$.

The kinetics of the $N_2(A)$ + NO energy transfer have been studied by several other investigators. Callear and Wood (Ref. 45) estimated rate coefficient ratios from thei work of k_{01}/k_{00} = 0.105 in reasonable agreement with the value of 0.094 ± 0.006 and k_{11}/k_{10} = 0.53 in disagreement with the value of 0.20 ± 0.03. Clark and Setser (Ref. 43) determined a population ratio for NO(A, v' = 0,1,2) of 1.0:0.15:0.014, respectively, from excitation by $N_2(A)$ with the ratio v' = 1/v' = 0 of 0.61. With the same $N_2(A)$ vibrational distribution, we calculate an NO(A) vibrational distribution from excitation rate coefficients of 1.0:0.14:0.011, respectively, in excellent agreement with Clark and Setser's observations. More recently Golde and Moyle (Ref. 122) have measured vibrational distributions of NO(A) from $N_2(A)$ excitation of 1.00:0.083:0.002 for excitation by $N_2(A,v'=0)$ and 1.00:0.17.0.025 for excitation by $N_2(A)$ with a vibrational distribution of 1.00:0.48:0.19:0.14 for v' = 0-3 respectively. Rate coefficients would predict an NO(A) vibrational distribution of 1.00:0.19:0.013 given the same initial $N_2(A)$ vibrational distribution. To make this comparison, it was assumed v' = 2 and v' = 3 had the same excitation rates. Golde and Moyle's data show a 7 percent decrease in total NO(A) intensity for the vibrationally excited case whereas our results would indicate that the intensities of the NO(A) produced from vibrationally excited and unexcited $N_2(A)$ would be within 2 percent of each other. Error limits encompass a range from a 6 percent decrease in intensity to a 3 percent increase with some additional uncertainty added by our having treated $N_2(A)$ vibrational levels 2 and 3 the same. They are therefore fully consistent with Golde and Moyle's result.

3.1.5 Summary--It has been shown that the transition-moment variation with r-centroid for the NO(A--X) transition is significant, especially for transitions with larger changes in v. The result of this variation is that the transition probabilities of the NO(A--X) transitions with $\Delta v < -3$ are substantially larger than had been believed previously. This means that the optical gain of some of the redder of the γ-band transitions will be larger than anticipated (Table 9), so that some of these transitions will probably have enough gain to support laser oscillation. The benefit of using these transitions with greater differences in vibrational level between the upper and lower states results both from reducing the probability of lower state

TABLE 9. Revised Optical Gain Predictions for NO(A-X) Transitions.

Transition v',v"	Wavelength (Å)	Normalized Optical Gain	
		Previous Prediction	Present Results
0,0	2269	0.73	0.66
0,1	2370	1.00	0.92
0,3	2479	0.78	0.77
0,2	2596	0.45	0.49
0,4	2722	0.22	0.27
0,5	2859	0.10	0.13
0,6	3009	0.04	0.06
0,7	3112	0.01	0.03

bottlenecking and from working in a region where optical difficulties are less severe.

The measurements on the quenching of $N_2(A)$ by NO show that NO(A) excitation is extremely efficient in this system, and that the system is scalable to moderate pressures, at which the $N_2(A)$ is predominantly vibrationally relaxed, without significant reduction in the excitation efficiency. Indeed, results show that some degree of vibrational relaxation is desirable since vibrational levels of $N_2(A)$ greater than or equal to two excite NO less efficiently than do the two lowest vibrational levels.

3.2 $N_2(A^3\Sigma_u^+)$ ENERGY POOLING

3.2.1 Introduction--Stedman and Setser (Ref. 123) first discovered energy pooling in triplet nitrogen when they observed that the intensity of nitrogen second-positive, $N_2(C^3\Pi_u - B^3\Pi_g)$ emission varied quadratically with the intensity of the Vegard-Kaplan emission in their reactor. They estimated the rate coefficient for energy pooling to form $N_2(C^3\Pi_u)$ to be 2.1×10^{-11} cm^3 molecule^{-1} s^{-1} In a series of investigations of time-resolved emissions in the afterglow of a pulsed nitrogen discharge, Hays et al. (Refs. 124-126) studied

$N_2(A)$ energy pooling and determined rate coefficients of 2.6×10^{-10} for formation of $N_2(C^3\Pi_u)$ (Ref. 126), 0.25×10^{-10} cm^3 $molecules^{-1}$ s^{-1} for the formation of $N_2(C'^3\Pi_u)$, and 1.1×10^{-9} cm^3 $molecule^{-1}$ s^{-1} for the formation of $N_2(B^3\Pi_g)$ (Ref. 125). In the case of the latter state, one would have to assume that their number was a lower bound, because their detection system could see only as far as $v' = 3$ of the B state. Thus, if significant energy from the pooling reaction flowed into $v' = 0$-2, the rate coefficient would be somewhat larger. Subsequent work by Clark and Setser (Ref. 43) confirmed a rate coefficient of about 2×10^{-10} cm^3 $molecule^{-1}$ s^{-1} for the production of $N_2(C^3\Pi_u)$ from $N_2(A^3\Sigma_u^+)$ energy pooling. They were unable, however, to see any evidence for formation of the $N_2(C'^3\Pi_u)$ state. Nadler et al. (Ref. 127) discovered in 1980 that the Herman Infrared (HIR) system was populated by $N_2(A)$ energy pooling, and showed that the distribution among the vibrational levels of that state depended strongly upon the vibrational distribution of the $N_2(A)$ state (Ref. 128). They estimated a lower limit for HIR formation of 2.5×10^{-11} cm^3 $molecule^{-1}$ s^{-1} which they have subsequently revised upwards to 7×10^{-11} cm^3 $molecule^{-1}$ s^{-1} (Ref. 128). They also showed that some production of the B state did indeed occur, but were unable to estimate the rate coefficient of B state formation because of that state's rapid quenching by nitrogen and argon. Nadler and Rosenwaks (Ref. 129) have also shown recently that the vibrational distribution of $N_2(C^3\Pi_u)$ formed by energy pooling also changes as a function of the $N_2(A)$ vibrational distribution, but that the total excitation rate of the C state appears to be independent of the vibrational distribution of $N_2(A)$.

Unpublished observations at PSI in the near infrared recorded the HIR system in $N_2(A)$ energy pooling, but failed to detect significant populations of $N_2(B)$ (Ref. 130). There is reason to be skeptical of the magnitude of the pooling rate coefficient which Hays and Oskam claimed made $N_2(B)$. The work of Nadler et al. also showed convincingly that HIR production had to be similar in magnitude to the production of $N_2(B)$. Thus, the present investigations were motivated in part by the desire to reconcile the conflict between Hays and Oskam's report, and the observations of Nadler et al. and our own. We

have investigated energy pooling in some detail and have been able to determine vibrational-level-specific rate coefficients for formation of $N_2(C^3\Pi_u$, v' = 0-4), $N_2(B^3\Pi_g$, v' = 1-12), and HIR v' = 2,3 by $N_2(A^3\Sigma_u^+$, v' = 0-2).

3.2.2 Experimental--Paragraph 3.1.2 describes apparatus and general operating procedures in some detail. Thus, only a brief summary will be given here. The studies all involved measuring spectra of the Vegard-Kaplan, first- and second-positive and HIR systems of molecular nitrogen in a flowing afterglow apparatus. The $N_2(A)$ is produced cleanly in the apparatus in the energy transfer reaction between argon and xenon metastables and molecular nitrogen (Refs. 61,62). A hollow-cathode discharge produces the rare gas metastables. The electrode has been fabricated from aluminum shim, but for some of the studies here, a 0.002-thick-tantalum shim was used as the electrode material. The tantalum electrodes gave about 30 percent more metastables and operated better at high pressures. The energy transfer reaction between metastable xenon and nitrogen produces $N_2(B^3\Pi_g$, v' $\leq$ 5 (Ref. 63). This eliminates the possibility of contamination of the results on $N_2(C)$ and the higher vibrational levels of $N_2(B)$ by scattered light from the rare-gas-metastable/nitrogen mixing region. The HIR system was studied at relatively high pressures ($\gtrsim$ 6 torr) with high partial pressures of nitrogen (1 to 2 torr) in the reactor. This procedure virtually eliminated overlapping of the HIR system by the first-positive system. The consequence of this procedure, however, was that the high partial pressures of nitrogen relaxed the $N_2(A)$ vibration to > 95 percent v' = 0,1, and thus the effects of higher vibrational levels could not be studied easily. The nitrogen B-state studies used a neon carrier gas to reduce electronic quenching (Refs. 131-133). Extrapolating measured populations to zero nitrogen pressure eliminated most significant quenching.

All spectra were fit by a least-squares computer program which determined the populations of all emitting states in the region of spectral coverage. This procedure eliminates the uncertainties introduced by overlapping spectral bands. Because the HIR system is unassigned, one cannot a priori generate a synthetic spectrum for this system. Therefore, experimental spectra (taken at high pressures for the basis sets in the synthetic fits) was used. Because

$N_2(A, v' = 0)$ energy pooling produces only $v' = 3$ of the HIR system, a basis set for that state could be generated cleanly. When only $v' = 0$ and 1 of $N_2(A)$ are present, only $v' = 3$ and 2 of the HIR system are produced. Thus, a fitting basis set was generated for $v' = 2$ of the HIR system by substracting out the previously determined $v' = 3$ components from a spectrum containing the two levels together. These basis sets were then used in analyzing the spectra containing $N_2(B)$ to eliminate confusion from HIR overlap. Energy pooling of higher vibrational levels of $N_2(A)$ do produce the two lowest vibrational levels of the HIR system. This only confuses the fitting of the $\Delta v = 2$ sequence of the first-positive system, and we were able to work around it.

The data analysis requires the measurement of absolute photon-emission rates in the reactor. Subsection 2.4.2 describes these calibration procedures in detail. In the case of the energy pooling reactions, the $N_2(A)$ and the $N_2(C,B, HIR)$ have radial density gradients which are different. The $N_2(A)$ radial density gradient follows the form of a Bessel function of first order,

$$[N_2(A)](r) = [N_2(A)]_o \, J_o(\lambda \frac{r}{r_o}) \tag{60}$$

where $[N_2(A)]_o$ is the centerline number density, r_o is the flow tube radius, and $\lambda = 2.405$, the first zero of $J_o(x)$. The field of view of the detector is essentially a rectangular parallel piped across the center of the tube with height, h, width, z, and length, $2r_o$ (Fig. 48). It was assumed that variations down the axis of the flow tube, across the field of view, could be neglected. The average number density of $N_2(A)$ observed in the field of view is then

$$\langle [N_2(A)] \rangle = \frac{[N_2(A)]_o \int_o^{r_o} J_o(\lambda \frac{r}{r_o}) \, r\Theta dr}{\int_o^{r_o} r\Theta dr} \tag{61}$$

where $[N_2(A)]_o$ is the $N_2(A)$ number density in the center of the flow tube. When r is less than or equal to h/2, Θ will equal π; but when r becomes greater than h/2, Θ will be given by $\sin^{-1}(h/2r)$. Thus, each integral in Eq. (61) becomes a sum of two integrals, one between the limits of 0 and h/2, the other running from h/2 to r_o. For the conditions of $r_o = 2.5$ cm and h = 1 cm, numerical integration gives

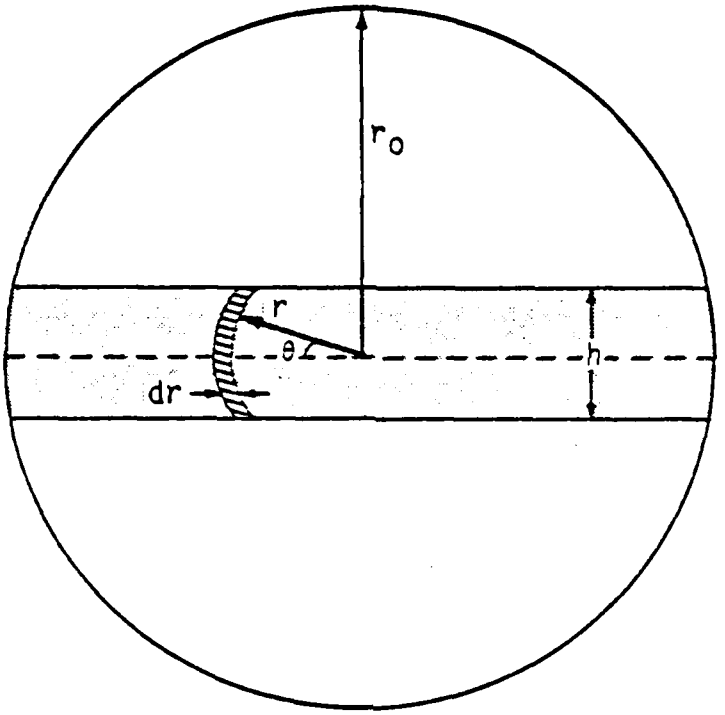

Figure 48. Cross-sectional view of flow tube illustrating the geometry germane to the radial number-density gradient problem. The shaded area approximates the monochromator's field of view.

$$\langle[N_2(A)]\rangle = 0.601\ [N_2(A)]_o \tag{62}$$

As shown below, the number density of $N_2(C,B,HIR)$ is proportional to the square of the $N_2(A)$ number density. Thus

$$\langle[N_2(C,B,HIR)]\rangle = k'[N_2(A)]^2 = \frac{k'[N_2A]_o^2 \int_o^{r_o} J_o^2(\lambda \frac{r}{r_o})\, r\partial dr}{\int_o^{r_o} r\partial dr} \tag{63}$$

where k' is the proportionality constant.

Integrating this expression in a similar manner to that given for $\langle[N_2A]\rangle$ gives

$$\langle[N_2(C,B,HIR)]\rangle = 0.458\ k'[N_2(A)]_o^2 \tag{64}$$

Finally, using Eq. (62) for $[N_2(A)]_o$, we find that

$$\langle[N_2(C,B,HIR)]\rangle = 1.267\ k'\langle[N_2(A)]\rangle^2 \qquad (65)$$

This correction must be made to the data on energy pooling to extract rate coefficients. This correction factor increases as the ratio h/r increases beyond unity, reacting a maximum value of 1.446 when h/r equals two (Fig. 49).

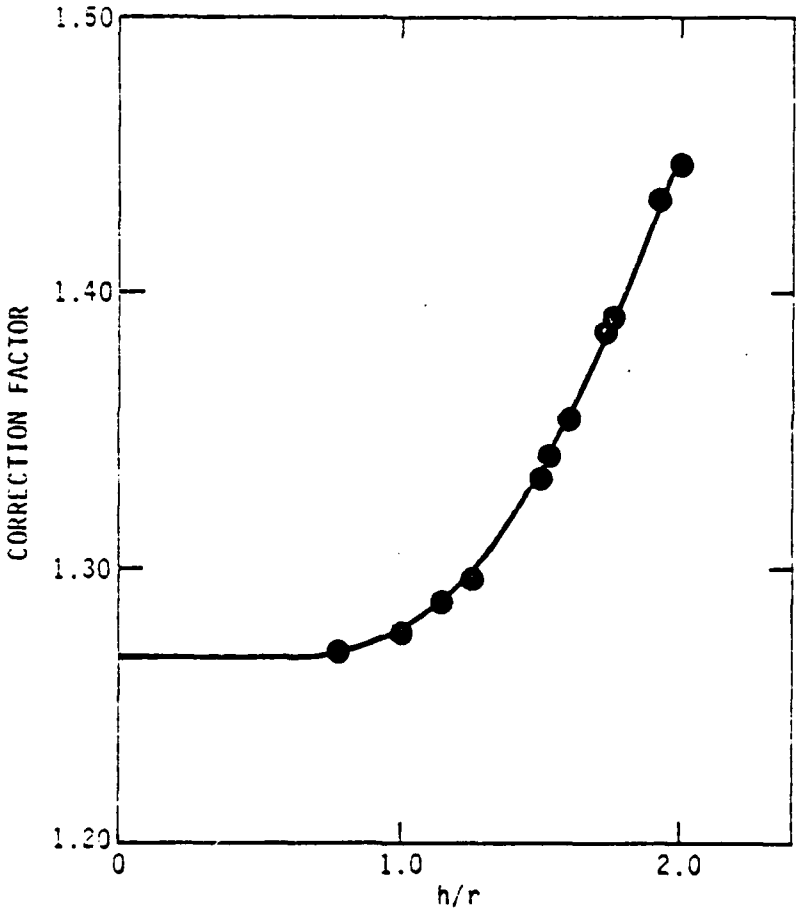

Figure 49. Variation in the correction factor for energy pooling measurements with the ratio h/r.

3.2.3 $N_2(C^3\Pi_u,\ v' = 0\text{-}4)$ formation in $N_2(A^3\Sigma_u^+,\ v' = 0\text{-}2)$ energy pooling--The processes controlling the formation and destruction of $N_2(C)$ in the energy pooling system are:

$$N_2(A,\ v') + N_2(A,\ v'') \xrightarrow{k^{C,v}_{v'v''}} N_2(C,v) + N_2(X,\ v''') \qquad (66a)$$

$$N_2(C,\ v) \xrightarrow{k^{C,v}_{rad}} N_2(B) + h\upsilon \qquad (66b)$$

where the superscript v denotes the vibrational level of the $N_2(C)$ product molecule, the subscript v's denote the vibrational levels of the $N_2(A)$ molecules, and k_{rad} is the radiative decay rate of $N_2(C)$. The lifetime of $N_2(C)$ is sufficiently short that electronic quenching of that state (Ref. 36) may be ignored. Because of its short radiative lifetime, $N_2(C)$ is in steady state in the reactor so that its formation and decay rates can be equated. Thus, we have

$$\frac{d[N_2(C,\ v)]}{dt} = 1.267 \sum_{v'} \sum_{v''} k^{C,v}_{v'v''} [N_2(A,\ v')]\ [N_2(A,\ v'')]$$

$$- k^{C,v}_{rad}\ [N_2(C,\ v)] = 0 \qquad (67)$$

$$[N_2(C,\ v)] = 1.267 \sum_{v''} \sum_{v'} \frac{k^{C,v}_{v'v''}}{k^{C,v}_{rad}} [N_2(A,\ v')][N_2(A,\ v'')] \qquad (68)$$

For the case of only one vibrational level of $N_2(A)$, Eq. (68) collapses to a single term for which the $N_2(C)$ number density varies linearly with the square of the $N_2(A)$ number density. The slope will equal the ratio of the energy-pooling rate coefficient to the radiative-decay rate of $N_2(C)$.

Figures 50 and 51 show representative spectra of the 220 to 400 nm region which encompasses most of the major emissions in the $N_2(A-X)$ and $N_2(C-B)$ systems. Comparison of the two figures shows how strongly the $N_2(C)$ intensity varies with the $N_2(A)$ intensity. Figures 52 through 56 show plots of the variation in the number density of $N_2(C,\ v'=0-4)$, respectively as a function

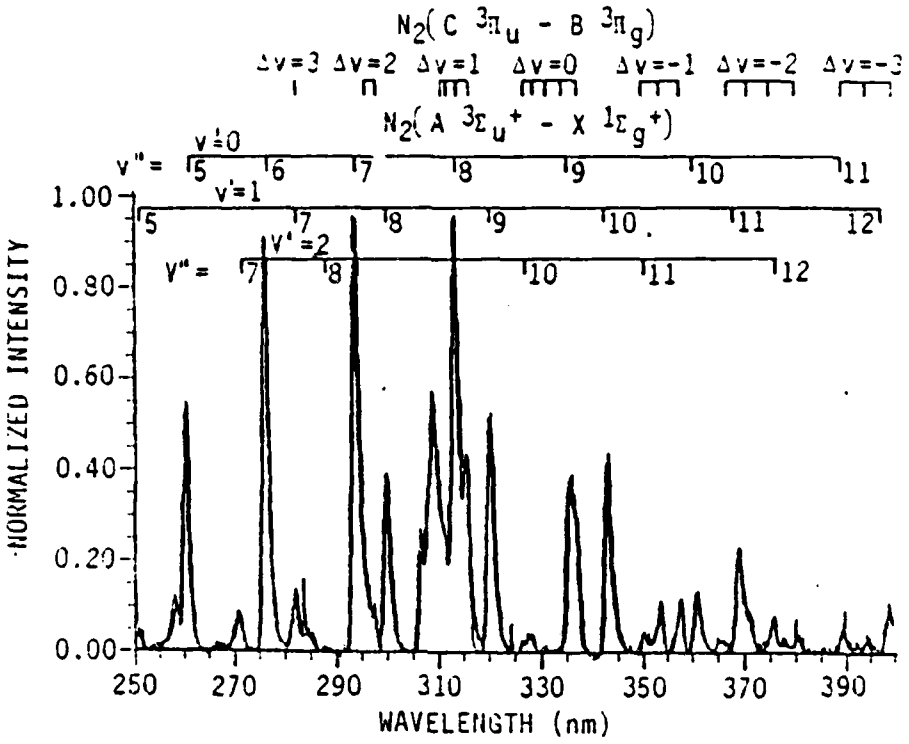

Figure 50. Observed (heavy line) and computed best fit (light line) to the spectral region between 250 and 400 nm. Resolution 1.0 nm.

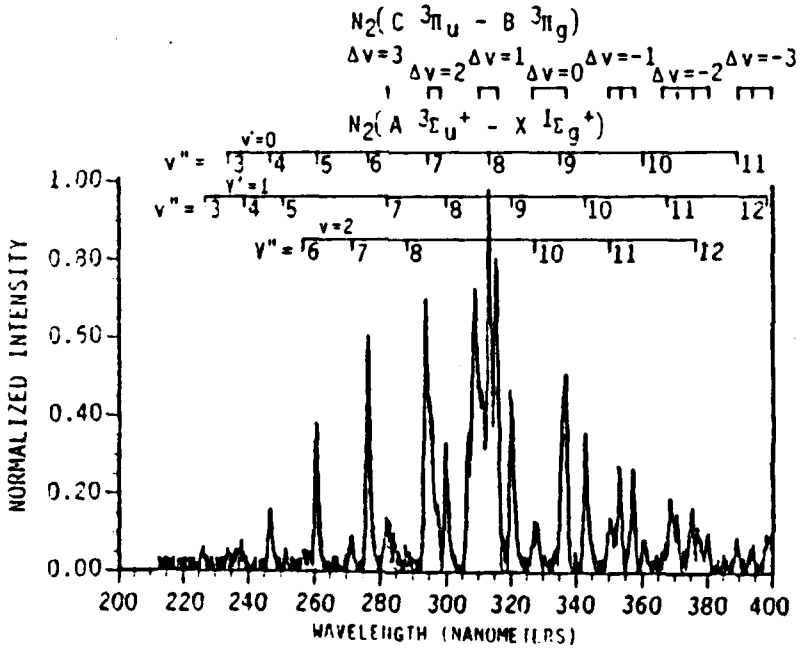

Figure 51. Observed (heavy line) and computed best fit (light line) to the spectral region between 220 and 400 nm. Note that the second-positive emissions are much stronger in this spectrum relative to the Vegard-Kaplan emissions than is the case in Figure 50. Resolution 1.0 nm.

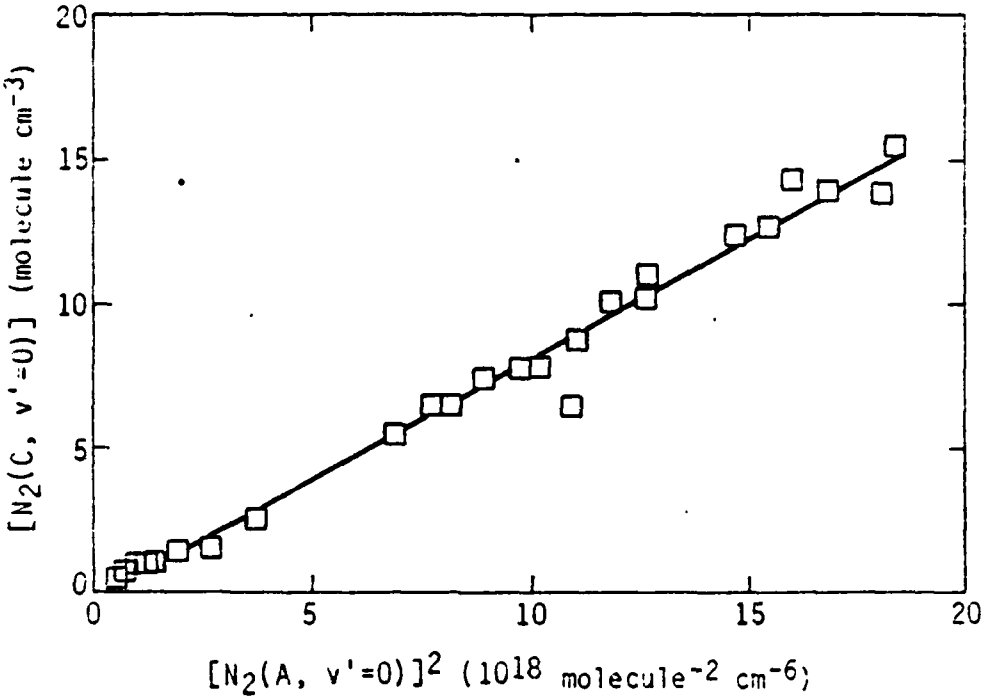

Figure 52. Variation in the number density of $N_2(C, v' = 0)$ as a function of the square of the number density of $N_2(A, v' = 0)$.

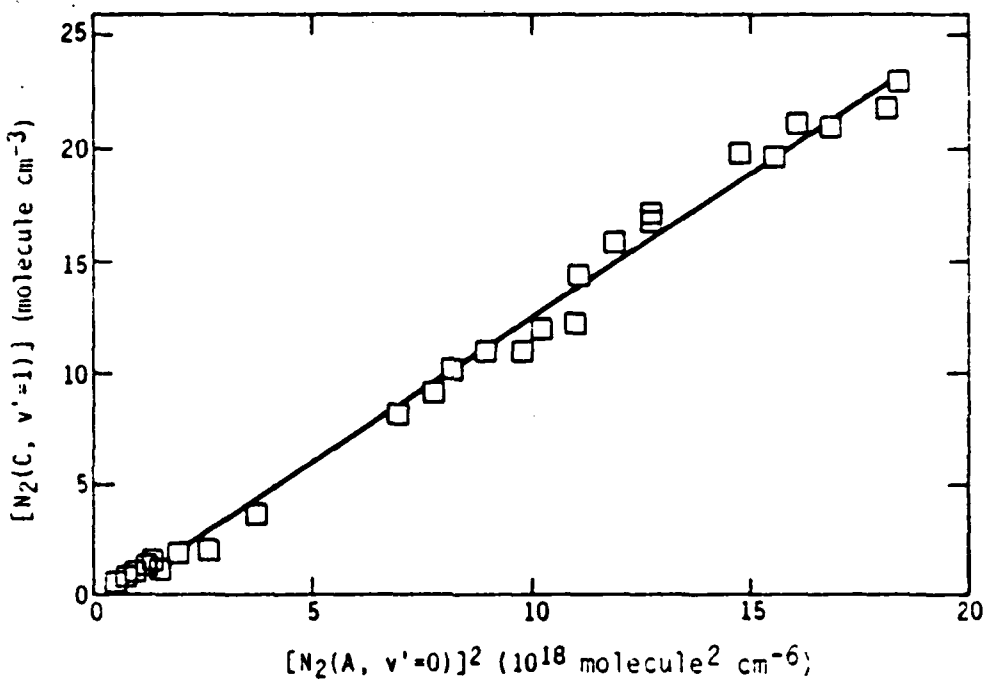

Figure 53. Variation in the number density of $N_2(C, v' = 1)$ as a function of the square of the number density of $N_2(A, v' = 0)$.

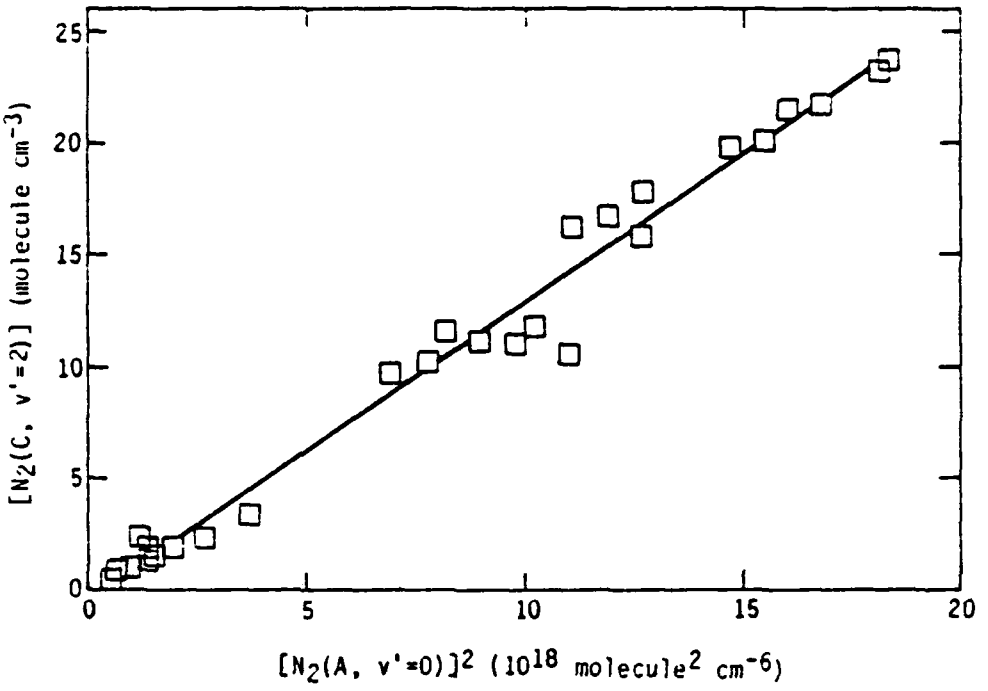

Figure 54. Variation in the number density of $N_2(C, v' = 2)$ as a function of the square of the number density of $N_2(A, v' = 0)$.

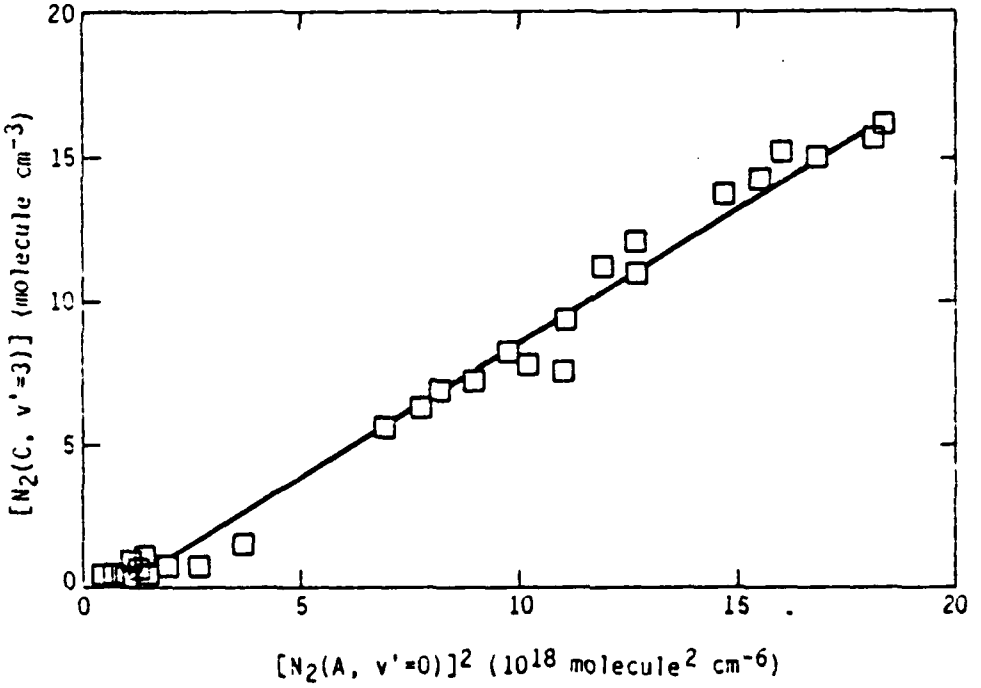

Figure 55. Variation in the number density of $N_2(C, v' = 3)$ as a function of the square of the number density of $N_2(A, v' = 0)$.

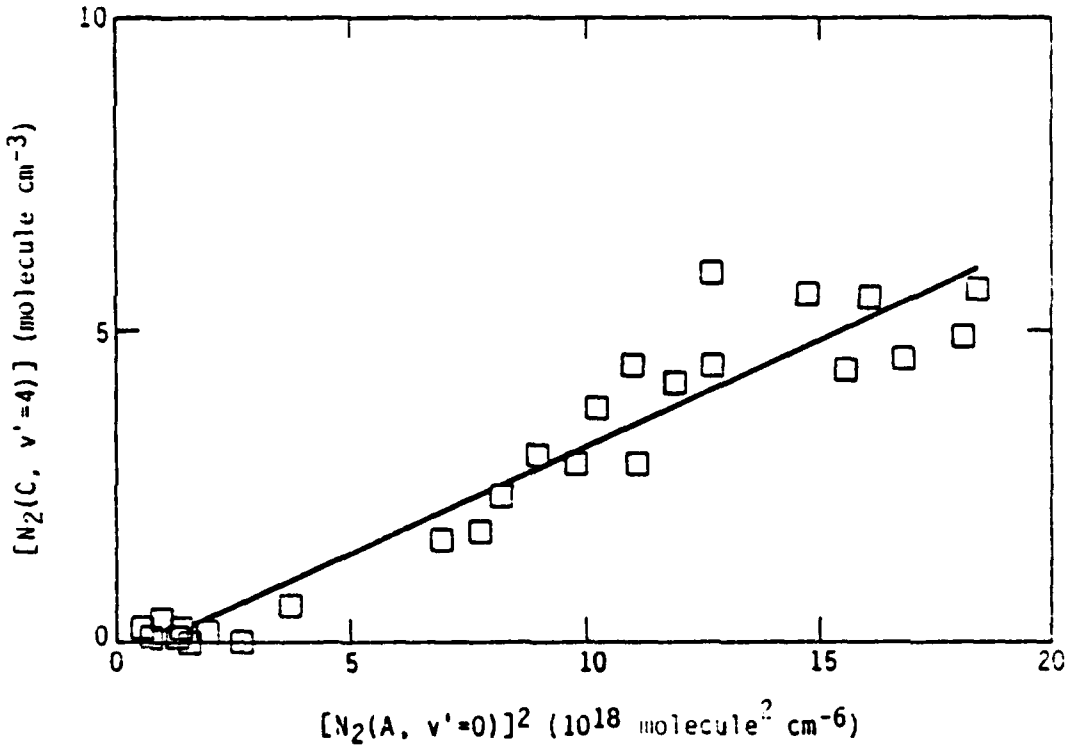

Figure 56. Variation in the number density of $N_2(C, v' = 4)$ as a function of the square of the number density of $N_2(A, v' = 0)$.

of the square of the $N_2(A)$ number density under conditions where only $v' = 0$ of the A state was in the reactor.

If only vibrational levels of 0 and 1 of $N_2(A)$ are present, Eq. (68) becomes

$$[N_2(C, V)] = 1.267 \frac{k_{00}^{C,v}}{k_{rad}^{C,v}} [N_2(A, v' = 0)]^2 + 2.534 \frac{k_{01}^{C,v}}{k_{rad}^{C,v}} [N_2(A, v' = 0)][N_2(A, v' = 1)] + 1.267 \frac{k_{11}^{C,v}}{k_{rad}^{C,v}} [N_2(A, v' = 1)]^2 \quad (69)$$

Dividing this equation through by $[N_2(A, v' = 0)]^2$ gives a quadratic equation in the parameter $[N_2(A, v' = 1)]/[N_2(A, v' = 0)]$:

$$\frac{[N_2(C, v)]}{[N_2(A, v'=0)]^2} = 1.267 \frac{k_{00}^{C,v}}{k_{rad}^{C,v}} + 2.534 \frac{k_{01}^{C,v}}{k_{rad}^{C,v}} \frac{[N_2(A, v'=1)]}{[N_2(A, v'=0)]} + 1.267 \frac{k_{11}^{C,v}}{k_{rad}^{C,v}} \left\{ \frac{[N_2(A, v'=1)]}{[N_2(A, v'=0)]} \right\}^2 \quad (70)$$

Figures 57 through 61 show data plotted in this fashion for each of the $N_2(C)$ vibrational levels excited in the energy-pooling reaction. The most interesting thing these plots show is the absence of a significant quadratic term. The intercepts of the plots, of course, give rate coefficients that agree to within 20 percent with those previously determined from studying just v'=0 pooling. Table 10 shows the results of $N_2(C)$ energy-pooling studies. Our value for the total pooling into all vibrational levels of $N_2(C)$ is about 70 percent lower for v'=0 pooling than previous studies.[43,124,126] Part of this difference results from the 27 to 45 percent correction for radial density effects which have not been included in other flowing afterglow studies. Applying our measured rate coefficients to Clark and Setser's 0.61/1 v'=1/v'=0 A state distribution gives an overall rate coefficient of 1.28×10^{-10} cm^3 molecule^{-1} s^{-1}. This is about half of what they reported. Our results indicate that their measurements may have been contaminated by scattered light, and therefore too large because they observed roughly equal populations in $N_2(C)$ v'=0 and 1 whereas for the same $N_2(A)$ vibrational distribution as they had, we observe a ratio of v'=0/v'=1 of 0.76. If scattered light contamination is a problem, then it will enhance $N_2(C,v'=0)$ more than the other vibrational levels.

3.2.4 HIR formation from $N_2(A)$ energy pooling--The HIR system was first observed 30 years ago by R. Herman.[134] Subsequent spectroscopic work on the system has failed to identify either the upper or lower states in the

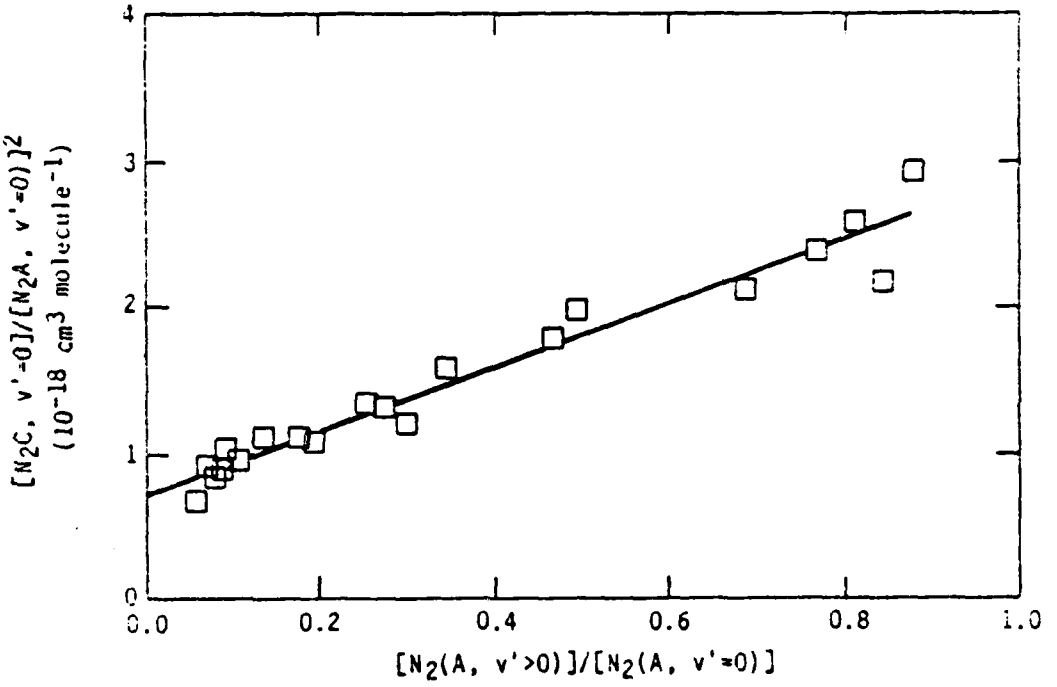

Figure 57. Variation in the ratio of the number density of $N_2(C, v' = 0)$ to the square of the number density of $N_2(A, v' = 0)$ as a function of the ratio of the number densities of vibrationally excited to unexcited $N_2(A)$.

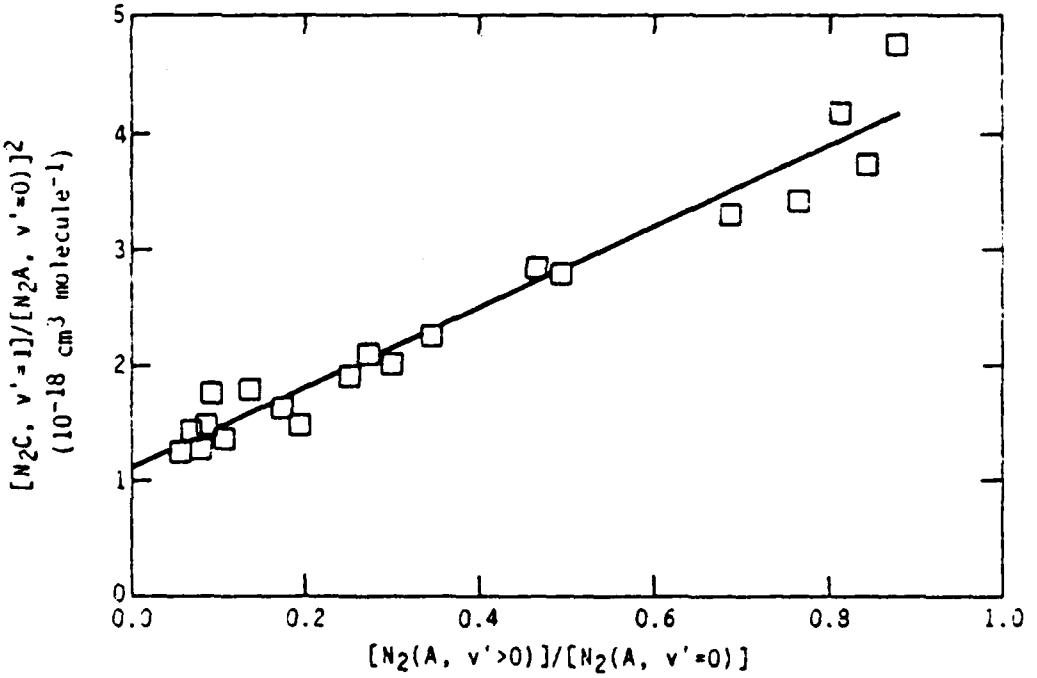

Figure 58. Variation in the ratio of the number density of $N_2(C, v' = 1)$ to the square of the number density of $N_2(A, v' = 0)$ as a function of the ratio of the number densities of vibrationally excited to unexcited $N_2(A)$.

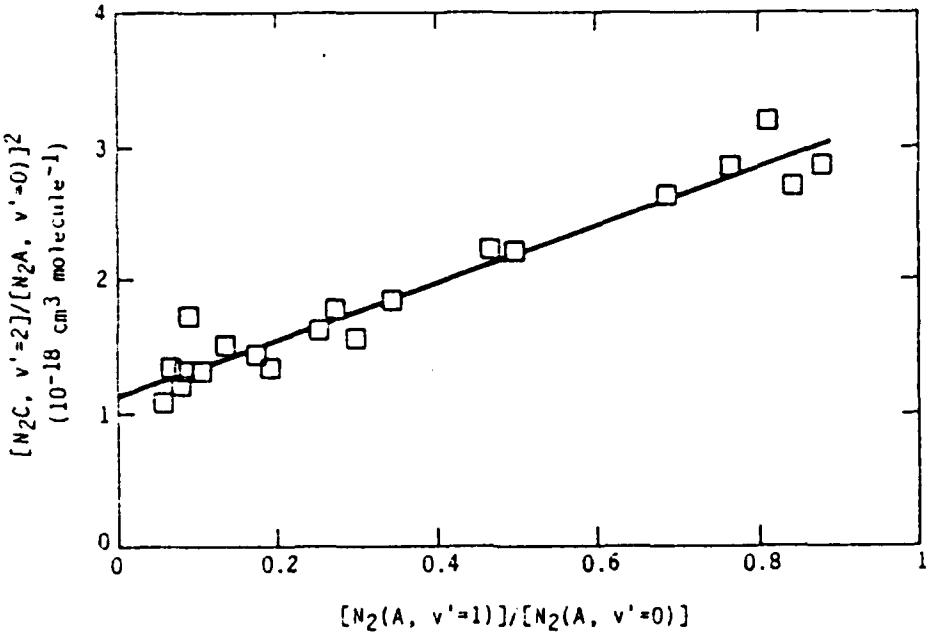

Figure 59. Variation in the ratio of the number density of $N_2(C, v' = 2)$ to the square of the number density of $N_2(A, v' = 0)$ as a function of the ratio of the number densities of vibrationally excited to unexcited $N_2(A)$.

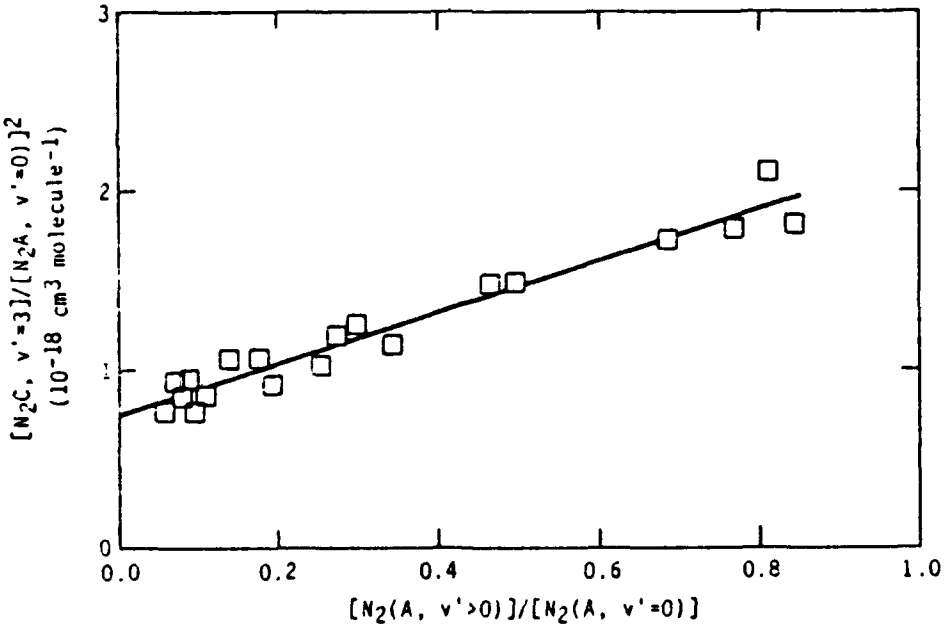

Figure 60. Variation in the ratio of the number density of $N_2(C, v' = 3)$ to the square of the number density of $N_2(A, v' = 0)$ as a function of the ratio of the number densities of vibrationally excited to unexcited $N_2(A)$.

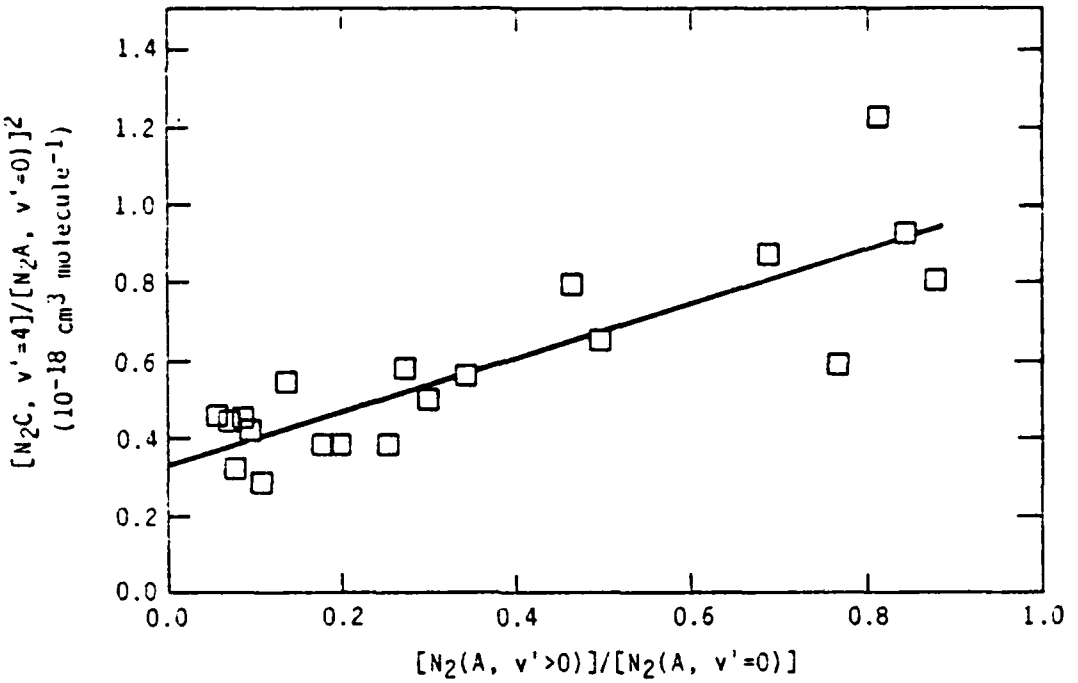

Figure 61. Variation in the ratio of the number density of $N_2(C, v' = 4)$ to the square of the number density of $N_2(A, v' = 0)$ as a function of the ratio of the number densities of vibrationally excited to unexcited $N_2(A)$.

TABLE 10. Rate Coefficients for $N_2(C^3\Pi_u)$ Formation from $N_2(A^3\Sigma_u^+)$ Energy Pooling.

$N_2(C, v')$	$k_{00}^{C, v'}$	$k_{01}^{C, v'}$	$k_{11}^{C, v'}$
0	2.6 ± 0.1	3.4 ± 0.7	< 1.0
1	4.1 ± 0.2	5.4 ± 1.2	< 2.0
2	4.1 ± 0.2	3.3 ± 0.8	< 1.0
3	2.8 ± 0.2	2.2 ± 0.5	< 0.7
4	1.0 ± 0.1	1.0 ± 0.6	< 0.6
Total $N_2(C)$	14.6 ± 0.8	15.3 ± 3.8	< 5.3

Rate coefficients are in units of 10^{-11} cm^3 molecules^{-1} s^{-1}.
Error bars represent 2σ statistical uncertainties.

transition,[135-137] although Nadler and Rosenwaks[129] have been able to establish an upper limit to the upper state term energy of 12.02 eV. Nadler and Rosenwaks have discussed the identification of the two states and concluded lower state might be the $G^3\Delta_g$, the lower state of the Gaydon-Herman Green system, and that the upper state was a $^3\Pi_u$ state which is known only through Michaels' calculations (Ref. 138). Gilmore disputes these identifications, however, and suggests $C''^5\Pi_u$ and $A'^5\Sigma_g^+$ as the upper and lower states, respectively (Ref. 139).

Figures 62 and 63 show the HIR system excited in energy pooling of $N_2(A,\ v' = 0)$ and $N_2(A,\ v' = 0,1)$ respectively. The spectra were taken at 7.5 Torr total pressure with a nitrogen partial pressure of 1.5 torr. Thus, nitrogen first-positive emission is virtually absent from the spectrum. The ratio of the HIR intensity to the square of the $N_2(A)$ number density does not vary with pressure (Ref. 127). Thus the state is not quenched electronically under our conditions, and a steady-state analysis similar to that given above for the $N_2(C)$ state applies here. We write

$$I_{HIR} = 1.267\ k_{rad}^{HIR,3}\ [HIR,\ v' = 3] = 1.267\ k_{00}^{HIR,3}\ [N_2(A,\ v' = 0)]^2 \quad (71)$$

Figure 64 shows data for $v' = 3$ of the HIR system plotted this way. For these studies, CF_4 or CH_4 was added to the reactor to relax the $N_2(A)$ vibrational energy to $v' = 0$. From the slope of the plot, we find that the rate coefficient for producing $v'=3$ of the HIR system in the energy pooling of two $N_2(A,\ v' = 0)$ molecules is 8.1×10^{-11} cm^3 molecule^{-1} s^{-1}. Strictly speaking, this figure is a lower limit, because other transitions of the HIR system from $v' = 3$ might appear outside the bandpass of the detection system. The relative intensities observed of the four bands, however, indicate that both sides of the Condon parabola have been sampled. Thus in all probability, the major emissions from $v' = 3$ have been observed. When the $N_2(A)$ was vibrationally excited, the ratio of the HIR $v' = 3$ intensity to the square of the $N_2(A,\ v' = 0)$ number density remains constant. Thus, vibrationally excited $N_2(A)$ appears not to play any role in exciting $v' = 3$ from energy pooling.

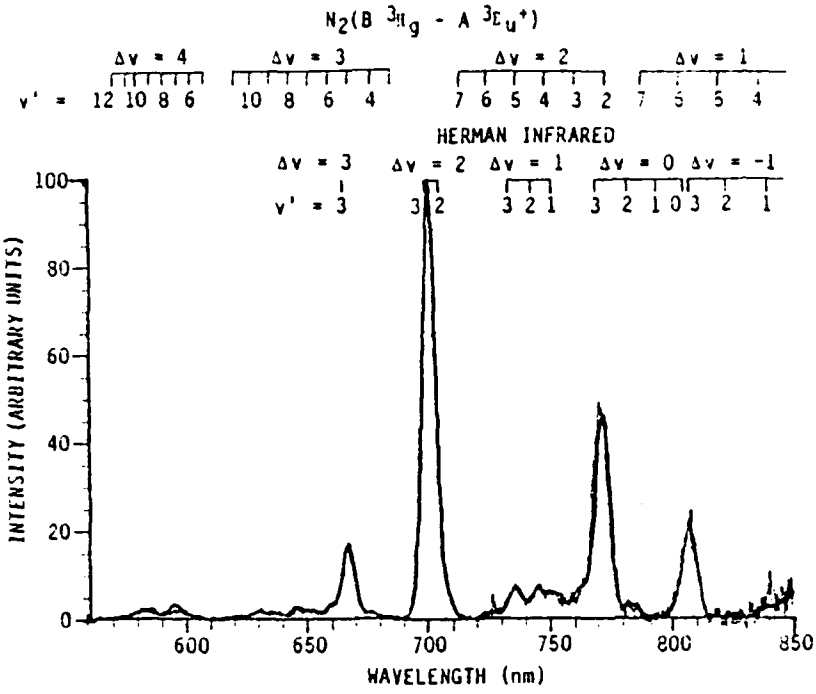

Figure 62. Spectrum of the Herman infrared v'=3 system excited in the energy pooling of N_2(A, v'=0). P_{total} = 7.5 torr, X_{N_2} = 0.20.

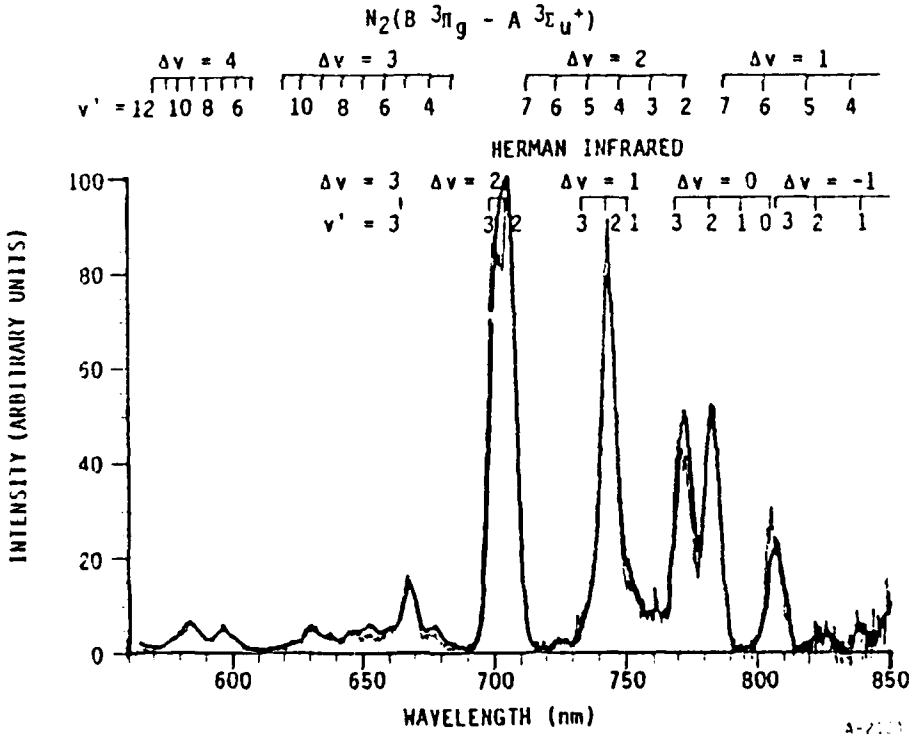

Figure 63. Spectrum of the Herman infrared v'=2,3 systems excited in the energy pooling of N_2(A, v'=0,1). P_{total} = 7.5 torr, X_{N_2} = 0.20.

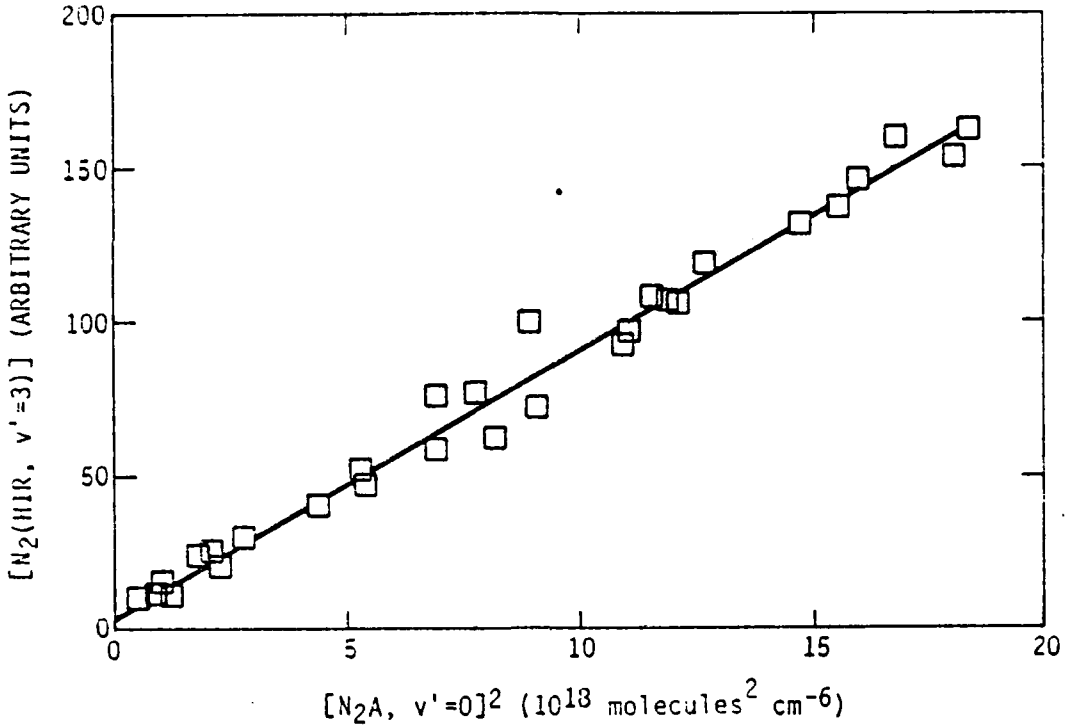

Figure 64. Variation in the number density of N_2(HIR, v'=3) as a function of the square of the number density of N_2(A, v'=0).

Under conditions where only v' = 0 and 1 of the N_2(A) are present emission from v' = 2 of the HIR system is seen. The lower two vibrational levels of the HIR system appear only when the number densities of v' = 2 and 3 of the N_2(A) become important. The HIR v' = 2 data can be analyzed in a similar fashion to our analysis for vibrational effects in N_2(C) production, but since it is already known that two v' = 0 molecules do not pool to make an HIR v' = 2 molecule, the first term in the equation can be eliminated. Thus,

$$I^{HIR,2} = 2.534\, k_{01}^{HIR,2} [N_2(A, v' = 0)][N_2(A, v' = 1)] + 1.267\, k_{11}^{HIR} [N_2(A, v' = 1)]^2 \quad (72)$$

$$\frac{I^{HIR,2}}{[N_2(A, v' = 0)][N_2(A, v' = 1)]} = 2.534\, k_{01}^{HIR,2} + 1.267\, k_{11}^{HIR,2} \frac{[N_2(A, v' = 1)]}{[N_2(A, v' = 0)]} \quad (73)$$

Figure 65 shows the data for the HIR v'=2 system. The intercept of the plot, after application of the appropriate corrections, gives the value for the mixed v' = 0/v' = 1 pooling rate coefficient, 9.9 x 10^{-11} cm^3 $molecule^{-1}$ s^{-1}. Within statistical uncertainty, the linear term is not significant, again implying that energy pooling by two v'=1 molecules is negligible. Table 11 summarizes our results on the Herman infrared system. Data further show that HIR v' = 2 is not formed by pooling of vibrational levels of $N_2(A)$ higher than v' = 1. Adequate data has yet to be collected on the formation of HIR v' = 0,1 which is formed in pooling of $N_2(A, v' > 2)$.

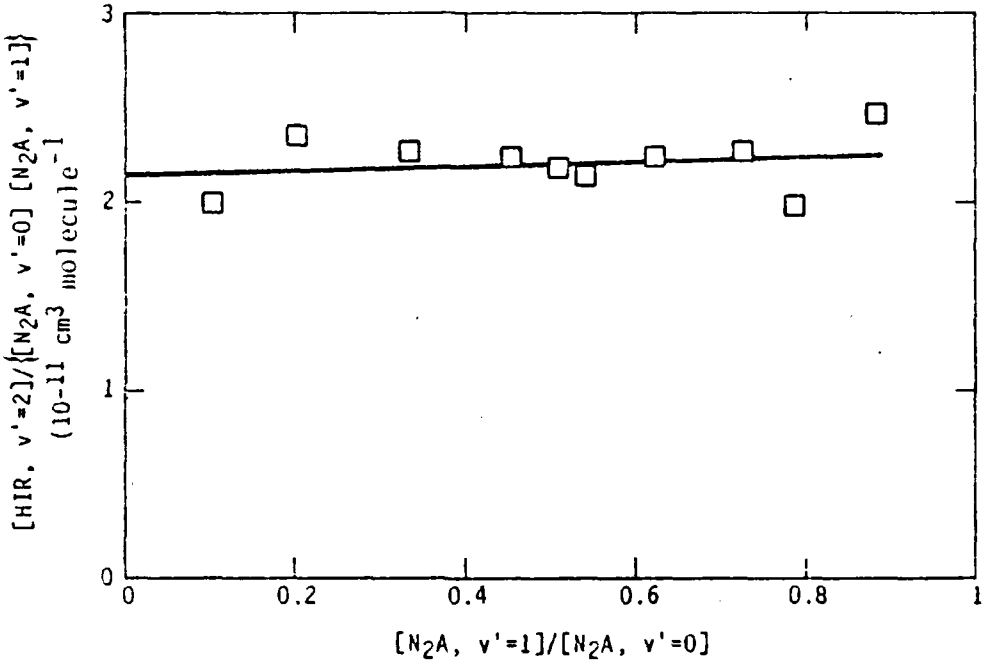

Figure 65. Variation in the ratio of the N_2(HIR, v'=2) number density to the product of the number densities of $N_2(A)$ v'=0 and v'=1 as a function of the ratio of the number densities of $N_2(A)$ v'=1 to v'=0.

TABLE 11. Rate Coefficients for Herman Infrared Formation from $N_2(A)$ Energy Pooling.

HIR, v'	k_{00}	k_{01}	k_{11}
3	>8.1 ± 0.4	-	-
2	-	>9.9 ± 1.0	-

Rate coefficients are in units of 10^{-11} cm^3 $molecule^{-1}$ s^{-1}. Error bars represent 2σ statistical uncertainty.

3.2.6 Formation of $N_2(B^3\Pi_g, v' = 1\text{-}12)$ in $N_2(A)$ energy pooling--The formation of $N_2(B)$ from the energy pooling of $N_2(A)$ in a neon buffer has been studied. Neon is a weak quencher of $N_2(B)$, so that under conditions where the number densities of argon, xenon, and nitrogen are minimized, the observed B state populations are fairly representative of nascent distributions. The best yields of $N_2(A)$ resulted when both argon and xenon were discharged along with the neon. The nitrogen was added down stream from the discharge as usual. Fairly modest argon flow rates ($\approx$150 μmol s^{-1} in a total flow of 3500 μmol s^{-1}) gave adequate $N_2(A)$ production, so that the number density of argon was well below that which would produce noticeable quenching effects. Nitrogen was still a significant quencher, so its quenching effects were experimentally determined by repeatedly scanning at successively lower nitrogen flow rates. Modifying Eq. (68) to reflect B state formation by $N_2(A, v' = 0)$ only and quenching of the B state by molecular nitrogen gives:

$$[N_2(B, v)] = 1.267 \frac{k_{00}^{B,v}}{k_{rad}^{B,v}} [N_2(A, v' = 0)]^2 \left\{1 + \frac{k_Q^{B,v}}{k_{rad}^{B,v}} [N_2]\right\}^{-1} \quad (74)$$

Rearranging this equation shows that the ratio of the square of the A state number density to the B state number density will vary linearly with the number density of the added nitrogen:

$$\frac{[N_2(A, v'=0)]^2}{[N_2(B, v)]} = 0.789 \frac{k_{rad}^{B,v}}{k_{00}^{B,v}} + 0.789 \frac{k_Q^{B,v}}{k_{00}^{B,v}} [N_2] \quad (75)$$

Figures 66 and 67 show spectra of the region between 500 and 850 nm with nitrogen partial pressures of 0.46 and 0.027 torr, respectively. Clearly, the first-positive bands increase strongly with the reduced nitrogen partial pressures. Figures 68 through 71 show data on the formation of the B state from the pooling of $N_2(A, v' = 0)$ plotted according to Eq. (75). From these plots and similar ones for the other vibrational levels studied, we obtained both rate coefficients for B state formation from energy pooling and rate coefficients for quenching $N_2(B)$ by molecular nitrogen. The bulk of the experiments

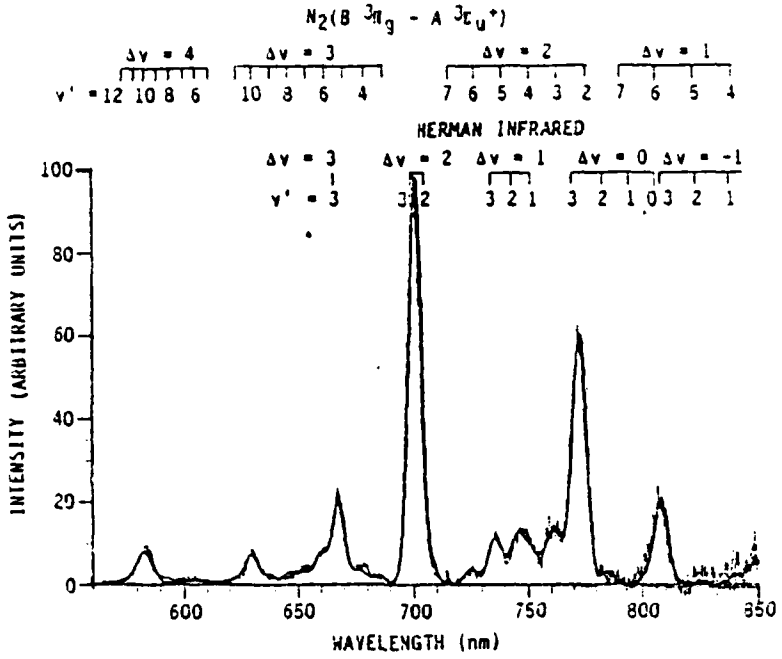

Figure 66. Spectrum of the nitrogen Herman infrared v' = 3 and first-positive systems excited in the energy pooling of $N_2(A, v' = 0)$ for a nitrogen partial pressure of 0.46 torr. The experimental spectrum is the light line while the heavy line shows the synthetic best fit to the spectrum.

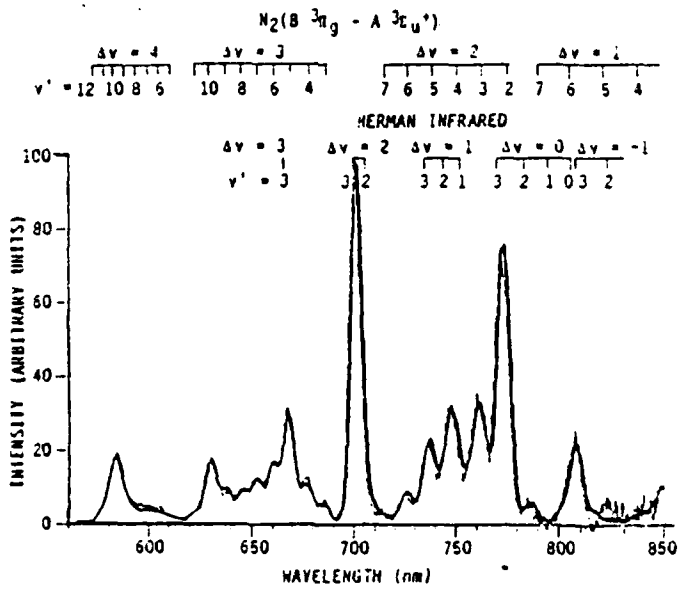

Figure 67. Spectrum of the nitrogen Herman infrared v' = 3 and first-positive systems excited in the energy pooling of $N_2(A, v' = 0)$ for a nitrogen partial pressure of 0.027 torr. The experimental spectrum is the light line while the heavy line shows the synthetic best fit to the spectrum.

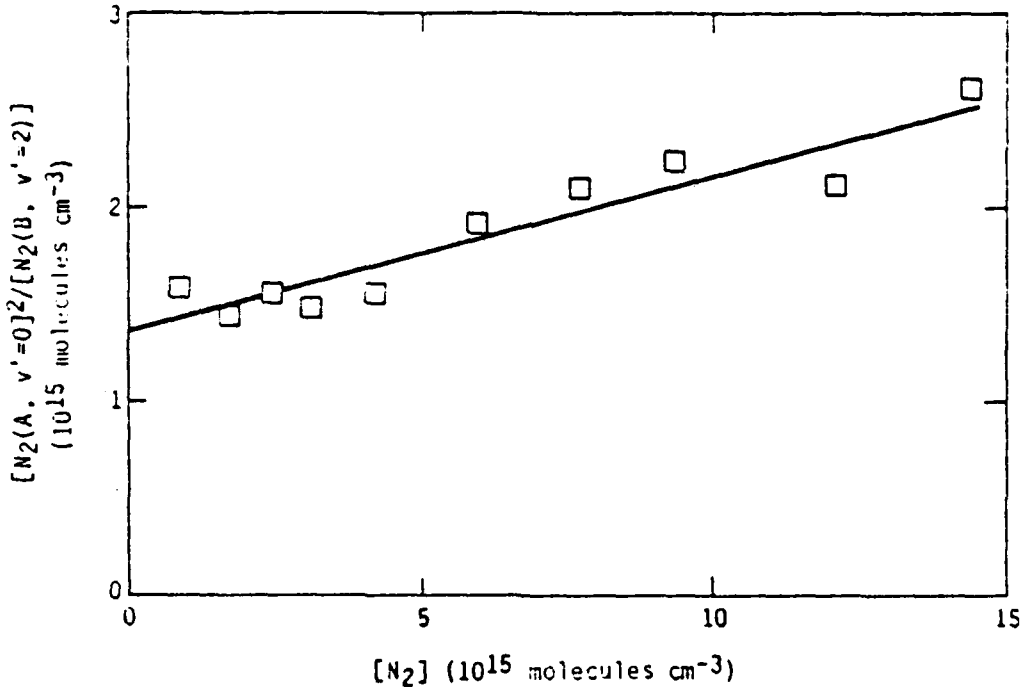

Figure 68. Variation in the ratio of the square of the number density of $N_2(A, v' = 0)$ to that for $N_2(B, v' = 2)$ as a function of the molecular nitrogen number density.

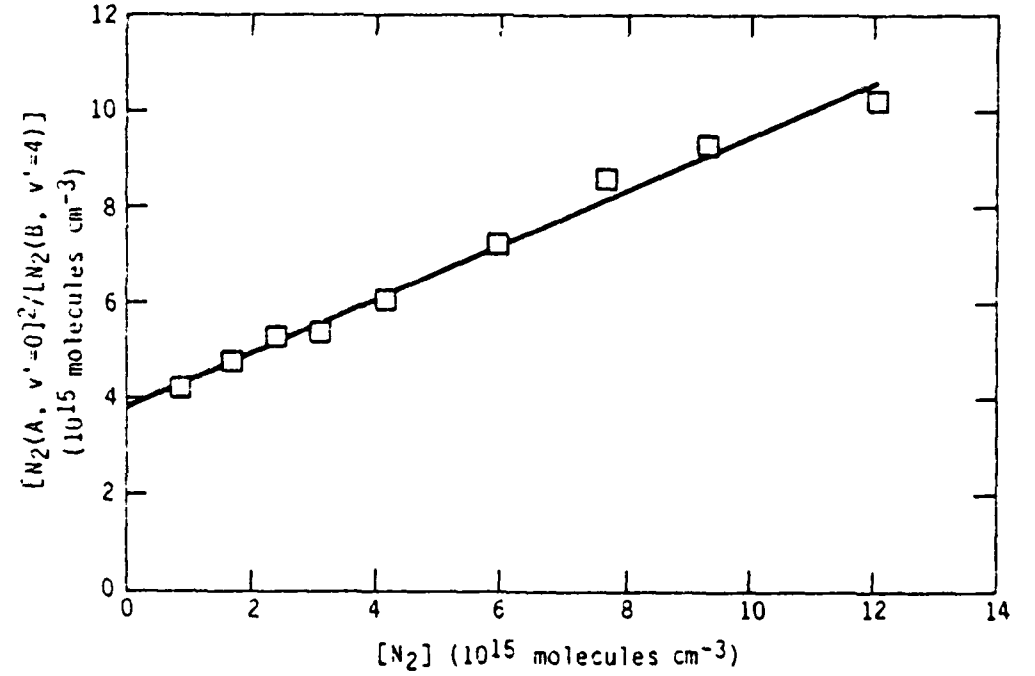

Figure 69. Variation in the ratio of the square of the number density of $N_2(A, v' = 0)$ to that for $N_2(B, v' = 4)$ as a function of the molecular nitrogen number density.

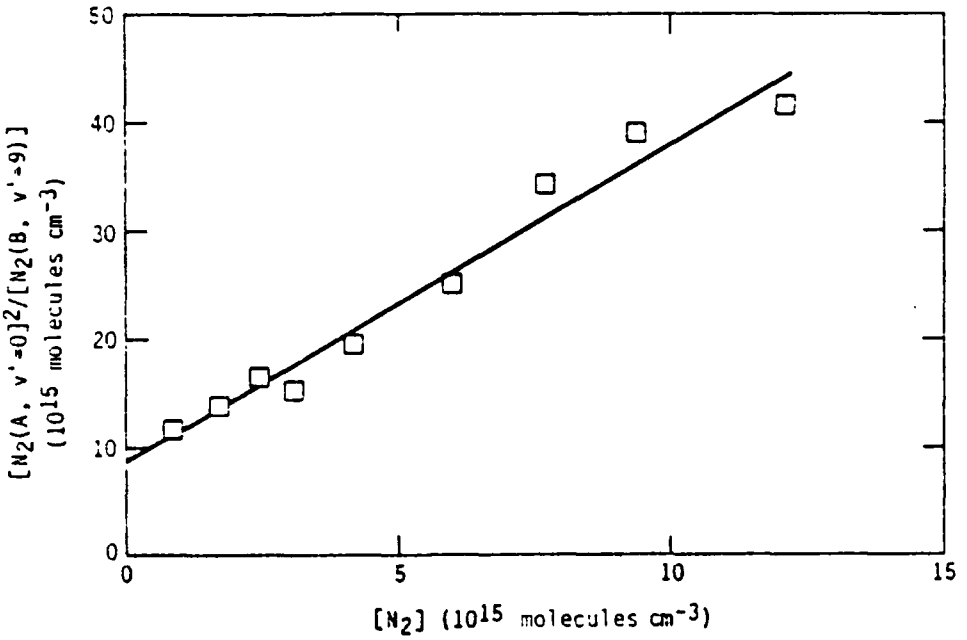

Figure 70. Variation in the ratio of the square of the number density of $N_2(A, v' = 0)$ to that for $N_2(B, v' = 9)$ as a function of the molecular nitrogen number density.

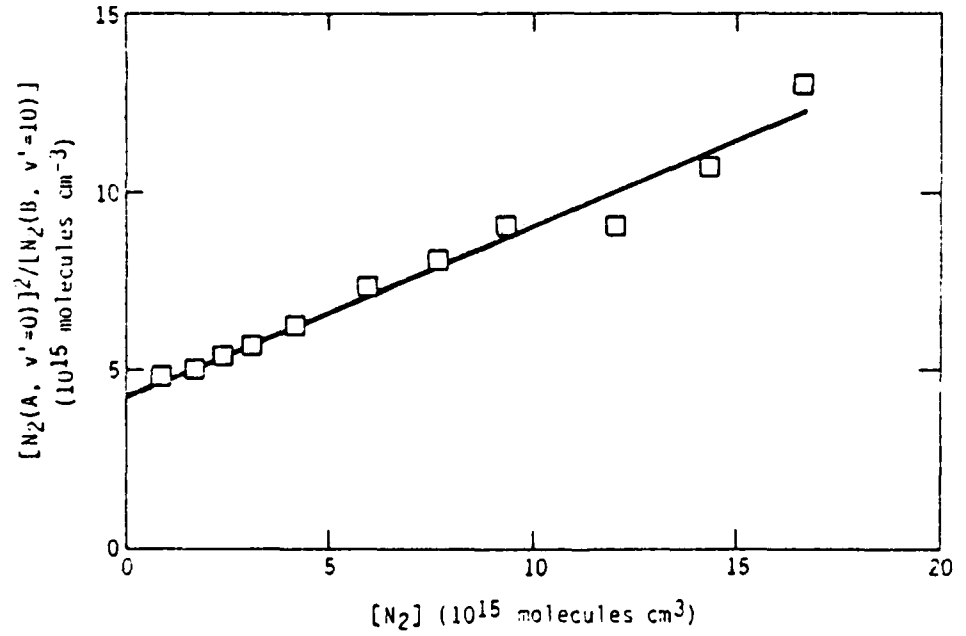

Figure 71. Variation in the ratio of the square of the number density of $N_2(A, v' = 0)$ to that for $N_2(B, v' = 10)$ as a function of the molecular nitrogen number density.

were at 3.0 torr total pressure, but scans at 1.5 and 6 torr gave similar vibrational distributions, and similar ratios of B state number density to the square of the A state number density as the data just discussed (Fig. 72). Thus, at the lowest nitrogen partial pressures studied, $N_2(B)$ quenching by the neon, argon, xenon, and CH_4 in the reactor did not appear to be significant. Therefore, a study was made of the variations in B state formation from the energy pooling of vibrationally excited $N_2(A)$ under conditions comparable to those producing the minimum B state quenching observed in the $N_2(A, v' = 0)$ studies.

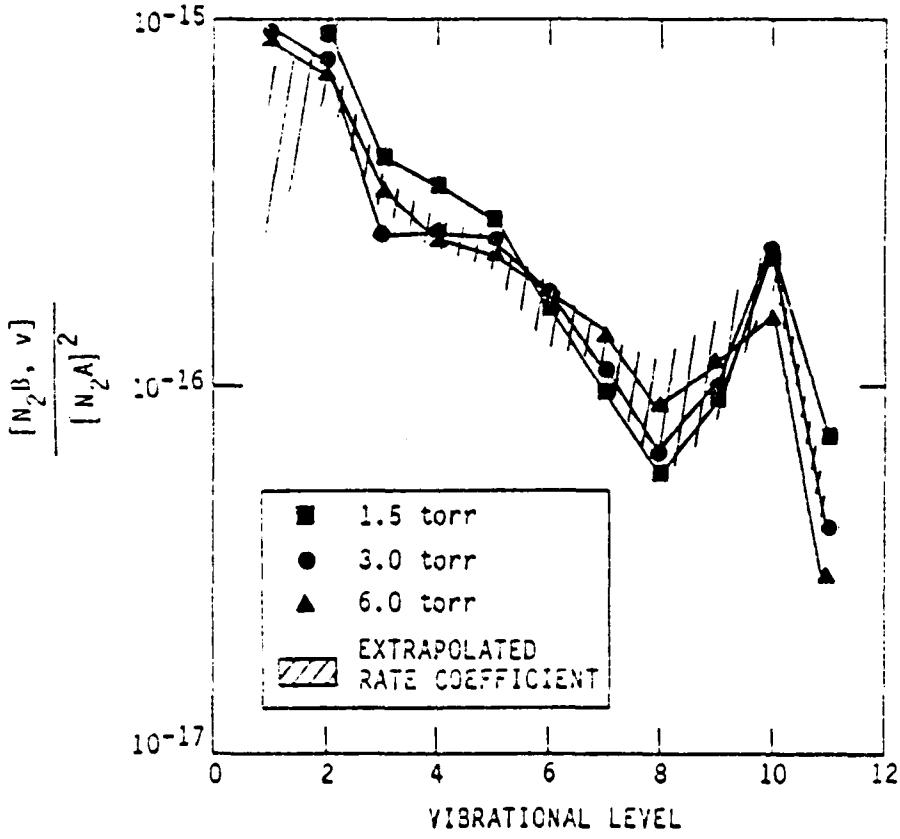

Figure 72. Variation in $N_2(B, v)$ excited from energy pooling of $N_2(A, v'=0)$ with neon pressure.

For these studies, the system was considered to be essentially two vibrational levels of $N_2(A)$, i.e., $v' = 0$ and $v' > 0$. An analysis similar to that given above for the $N_2(C)$ state gives

$$\frac{[N_2(B,\ v')]\left\{1 + \frac{k_2^{B,v}}{k_{rad}^{B,v}}[N_2]\right\}}{[N_2(A,\ v'=0)]^2} = 1.267\,\frac{k_{00}^{B,v}}{k_{rad}^{B,v}} + 2.534\,\frac{k_{0v}^{B,v}}{k_{rad}^{B,v}}\,\frac{[N_2(A,\ v'>0)]}{[N_2(A,\ v'=0)]}$$

$$+ 1.267\,\frac{k_{vv}^{B,v}}{k_{rad}^{B,v}}\left\{\frac{[N_2(A,\ v'>0)]}{[N_2(A,\ v'=0)]}\right\}^2 \qquad (76)$$

where we have corrected only for molecular-nitrogen quenching (~ 10 percent effect). Quenching-rate coefficients determined in the $N_2(A,\ v'=0)$ studies were used. Figures 73 through 75 show how the spectrum between 550 and 720 nm changes as the degree of vibrational excitation in the $N_2(A)$ changes. Figures 76 through 78 show several different B state vibrational levels plotted according to Eq. (76). The intercepts of these plots gave results within 10 percent of these $v' = 0$ results. These results also show that the pooling between a $v' = 0$ and a $v' > 0$ is somewhat faster than the pooling between two $v' = 0$ molecules or between two $v' > 0$ molecules. Table 12 summarizes the rate coefficients measured.

3.2.6 Discussion of energy-pooling results--Examination of the data shows several interesting results. Close to half of the B state formation arises as a result of radiative cascade out of $N_2(C)$. Furthermore, summing up the rate coefficients for energy pooling into all three observed electronic states gives a value of 3.0 and 4.7 x 10^{-10} cm^3 $molecule^{-1}$ s^{-1} for energy pooling of two $N_2(A,\ v' = 0)$ and of $N_2(A,\ v' = 0) + N_2(A,\ v' = 1)$, respectively. These numbers represent a lower limit to the total energy pooling rate coefficient, because dark states might be involved, and also because we have not been able to evaluate the contributions of $N_2(B,\ v' = 0)$ formation. Since vibrational levels 1 through 8 are all formed at least 50 percent by radiative cascade from the C state, we would expect $N_2(B,\ v' = 0)$ to follow suit. This would raise the total pooling rate coefficient by less than 10 percent. The formation of dark states cannot readily be assessed. A

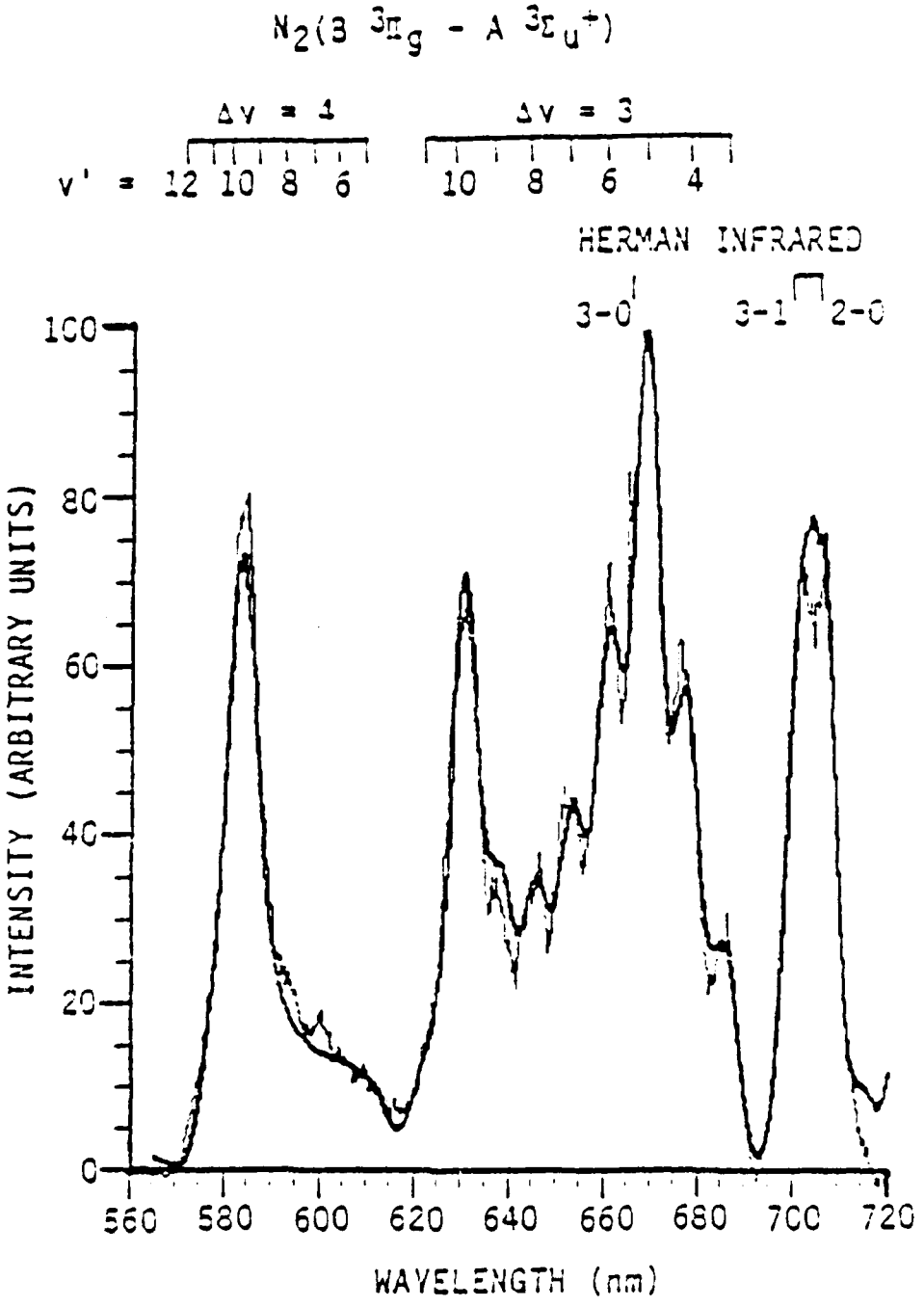

Figure 73. Variation in $N_2(B,A)$ spectrum produced in $N_2(A)$ energy pooling with changes in nitrogen and argon partial pressures.

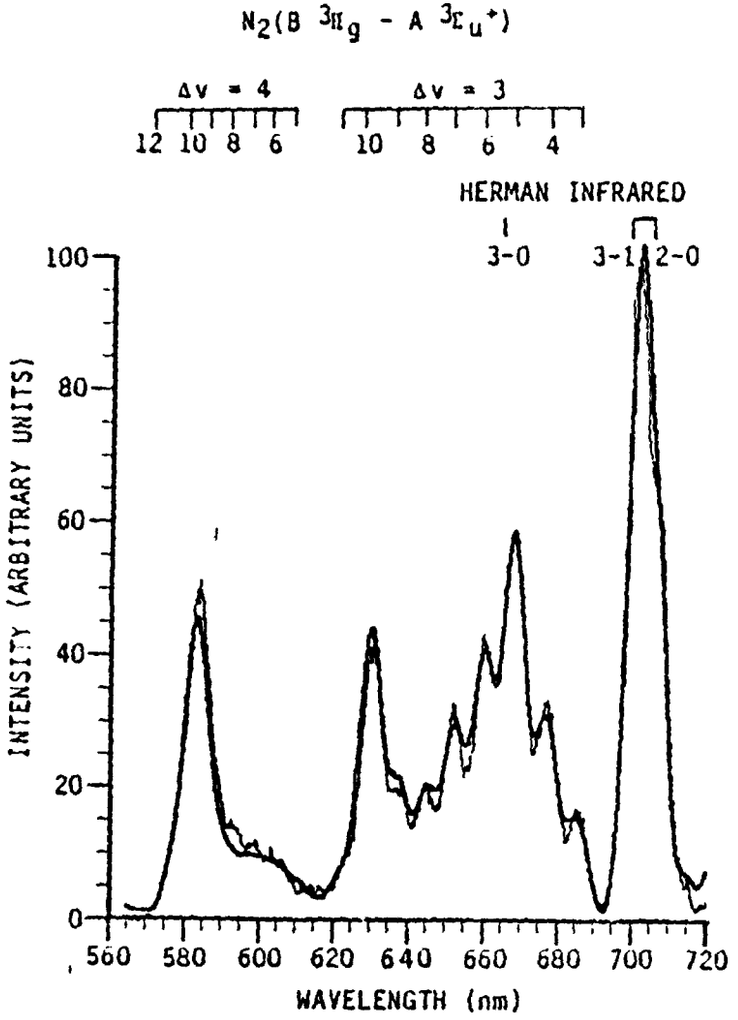

Figure 74. Spectrum of the nitrogen Herman infrared v' = 2,3 and first-positive systems excited in the energy pooling of $N_2(A,v' = 0,1)$ for a nitrogen partial pressure of 38 mtorr and a methane partial pressure of 1.4 mtorr.

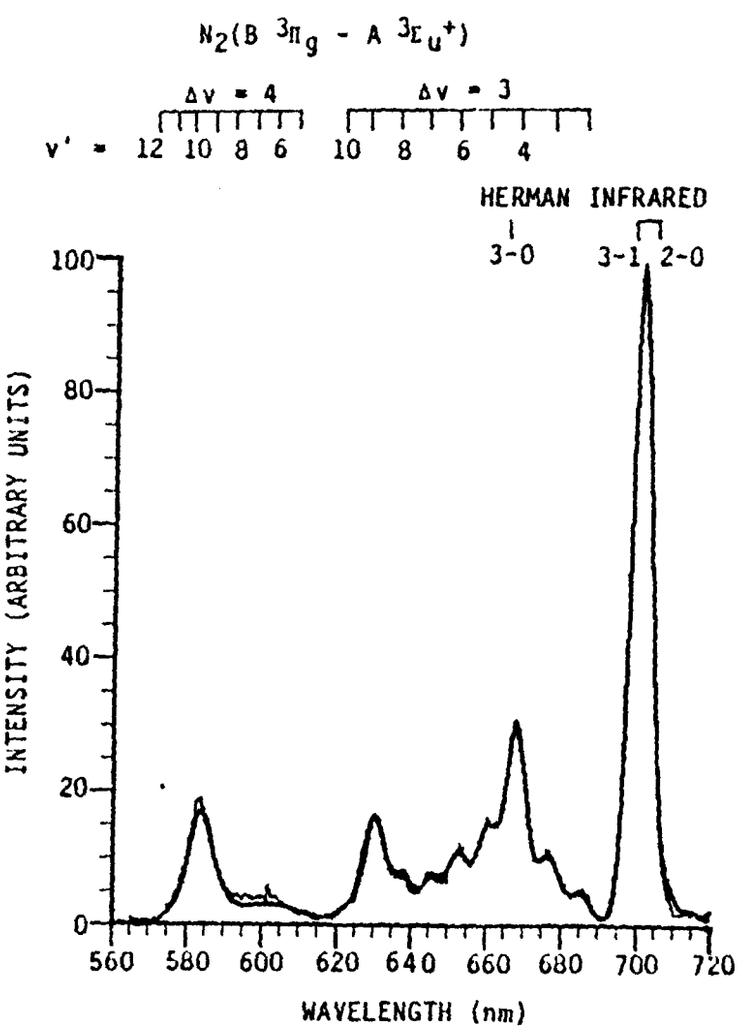

Figure 75. Spectrum of the nitrogen Herman infrared v' = 2,3 and first-positive systems excited in the energy pooling of $N_2(A,v' = 0,1)$ for a nitrogen partial pressure of 38 mtorr and a methane partial pressure of 4.9 mtorr.

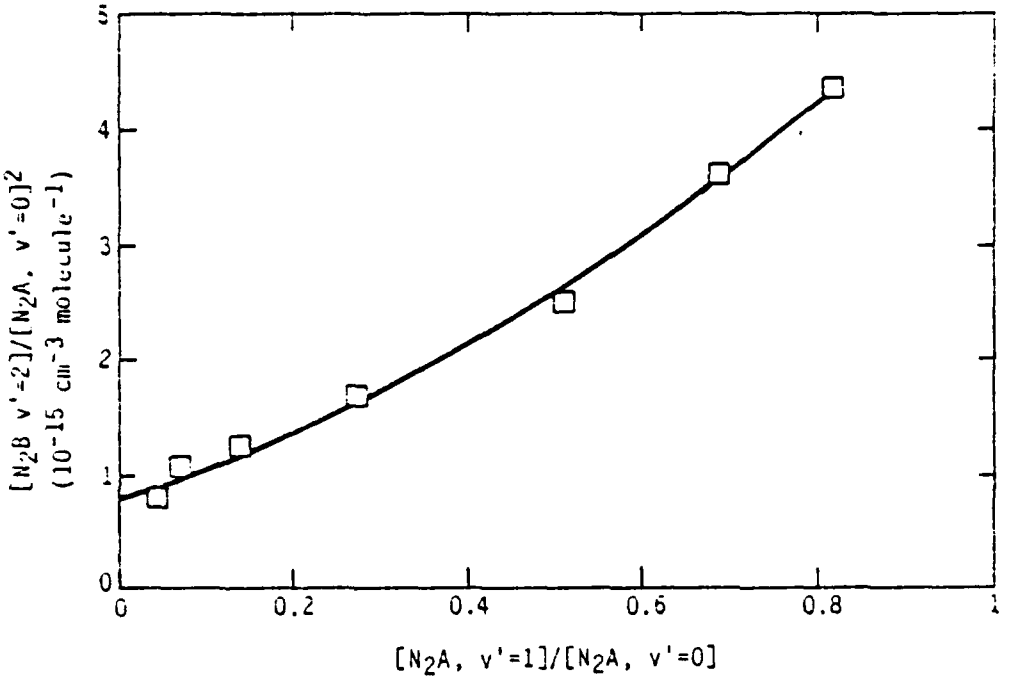

Figure 76. Variation in the ratio of the number density of $N_2(B,\ v' = 2)$ to the square of the number density of $N_2(A,\ v' = 0)$ as a function of the ratio of $N_2(A)$ $v' = 1$ to $v' = 0$.

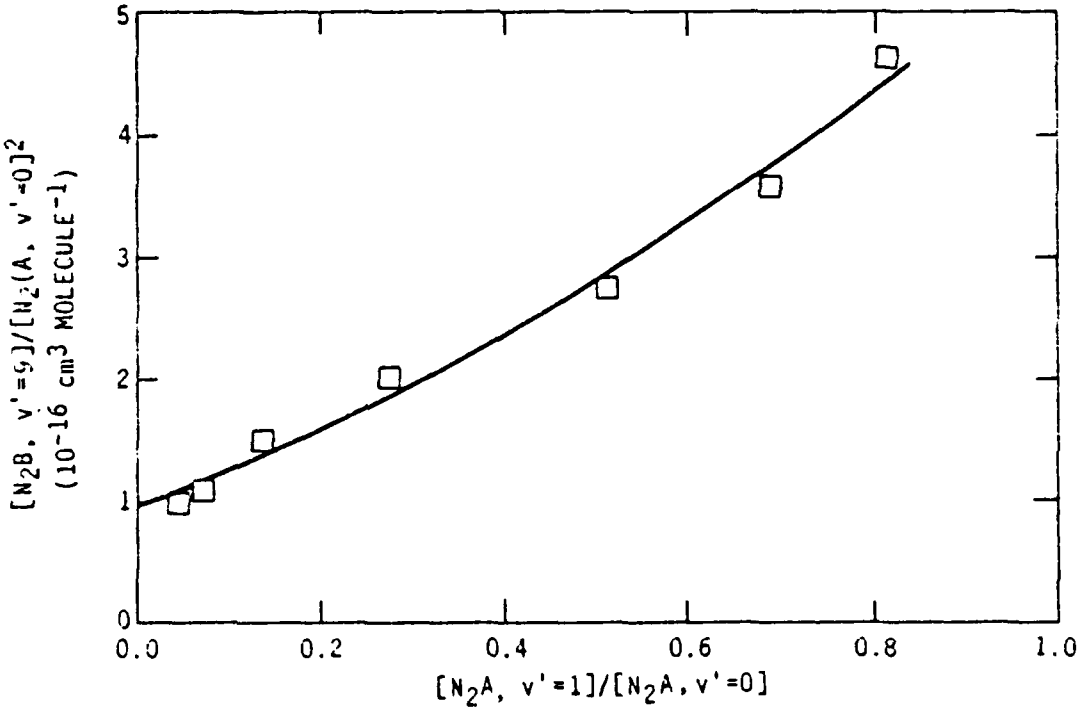

Figure 77. Variation in the ratio of the number density of $N_2(B,\ v' = 9)$ to the square of the number density of $N_2(A,\ v' = 0)$ as a function of the ratio of $N_2(A)$ $v' = 1$ to $v' = 0$.

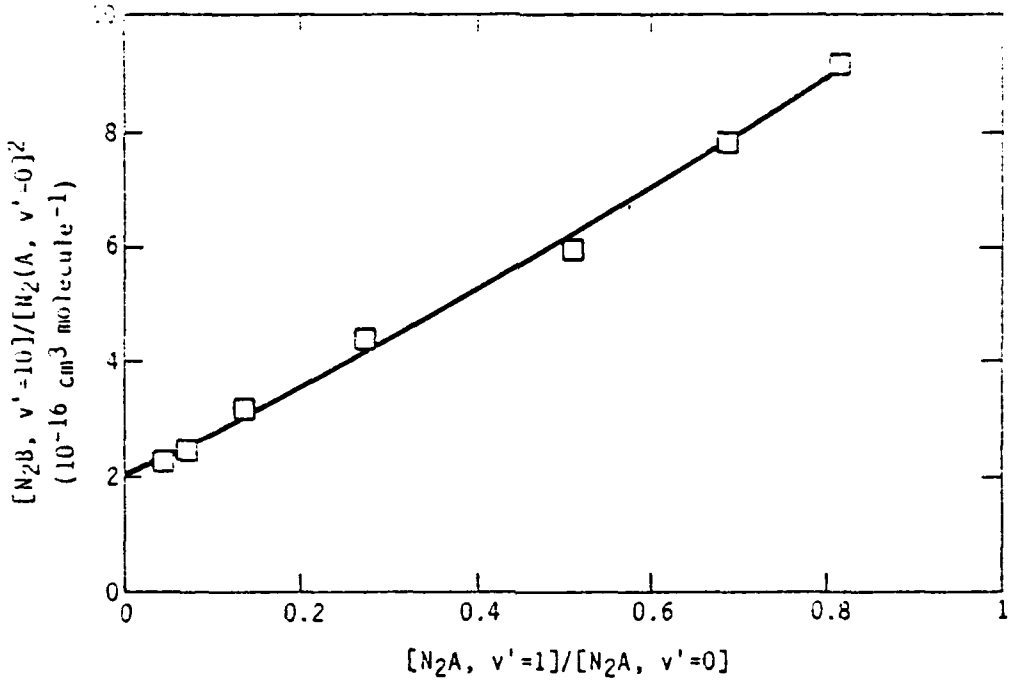

Figure 78. Variation in the ratio of the number density of $N_2(B, v' = 10)$ to the square of the number density of $N_2(A, v' = 0)$ as a function of the ratio of $N_2(A)$ $v' = 1$ to $v' = 0$.

TABLE 12. Rate Coefficients for $N_2(B^3\Pi_g)$ Formation from $N_2(A^3\Sigma_u^+)$ Energy Pooling

	$k_{00}^{B,v}$			$k_{01}^{B,v}$			$k_{11}^{B,v}$		
$N_2(B,v')$	OBSERVED	CASCADE	DIRECT	OBSERVED	CASCADE	DIRECT	OBSERVED	CASCADE	DIRECT
1	2.4 ± 0.6	3.6	---	6.6 ± 1.0	3.3	3.3 ± 1.0	---		
2	3.9 ± 0.2	2.3	1.6 ± 0.2	5.6 ± 1.8	2.6	3.0 ± 1.8	14.7 ± 4.3		
3	1.9 ± 0.1	1.5	0.4 ± 0.1	5.8 ± 0.3	1.6	4.2 ± 0.3	---		
4	1.6 ± 0.1	1.1	0.5 ± 0.1	2.7 ± 1.0	1.1	1.6 ± 1.0	3.8 ± 2.5		
5	1.5 ± 0.1	0.8	0.7 ± 0.1	2.2 ± 0.6	0.6	1.6 ± 0.6	4.5 ± 1.3		
6	1.1 ± 0.1	0.5	0.6 ± 0.1	1.7 ± 0.2	0.4	1.3 ± 0.2	1.5 ± 0.5		
7	0.9 ± 0.1	0.3	0.6 ± 0.1	1.6 ± 0.1	0.3	1.3 ± 0.1	---		
8	0.6 ± 0.1	0.2	0.4 ± 0.1	1.3 ± 0.1	0.2	1.1 ± 0.1	---		
9	0.9 ± 0.1	0.1	0.8 ± 0.1	1.0 ± 0.4	0.1	0.9 ± 0.4	1.6 ± 1.0		
10	1.8 ± 0.1		1.8 ± 0.1	2.8 ± 0.5		2.8 ± 0.5	1.3 ± 1.1		
11	0.3_2 ± 0.0[illegible]		0.3_2 ± 0.0[illegible]	0.4 ± 0.2		0.4 ± 0.2	1.0 ± 0.5		
$N_2(B)$ TOTAL			7.7 ± 1.0			21.5 ± 6.2	28 ± 11		

RATE COEFFICIENTS ARE IN UNITS OF 10^{-11} cm^3 MOLECULE^{-1} s^{-1}

available, most notably the $W^3\Delta_u$ and $B'\ ^3\Sigma_u^-$ states. We do see the 5-1 band of the B'-B system at 825 nm. In addition, a small amount of emission has been seen in the 140 to 180 nm region which is probably from the Lyman-Birge-Hopfield system, but the intensities are much too weak to resolve for an adequate identification. The singlet states would not be expected to form a significant exit channel even though their radiative lifetime is long, which will in itself diminish the observed intensities of an otherwise strong exit channel.

Clearly, the Hays and Oskam result for the formation of $N_2(B)$ is incorrect. Their studies were performed in the afterglow of a pulsed discharge of nitrogen. A number of metastable species in addition to $N_2(A)$ will persist in the afterglow of a nitrogen discharge, and we expect that one of these other metastables is responsible for Hays and Oskam's observations. This hypothesis was tested briefly by diverting the nitrogen flow in our reactor to mix with the main argon flow upstream from the discharge. Figure 79 shows the result

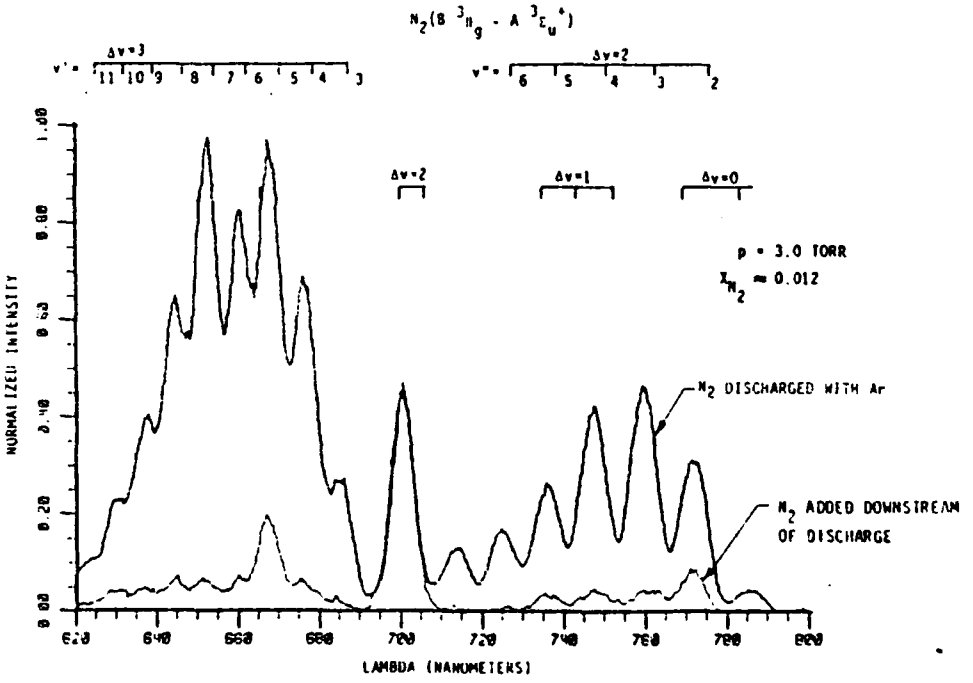

Figure 79. Spectra of HIR $v' = 3$ and N_2 first-positive systems when the $N_2(A)$ is formed by direct discharge of the N_2 with the argon and when it is formed in the conventional manner by adding the N_2 downstream from the discharge.

graphically. While discharging the nitrogen with the argon increased the $N_2(A)$ number density in the observation region by about a factor of 3, the populations of the $N_2(B)$ vibrational levels grew by a factor of 70. The HIR 3,1 band which is relatively free from first-positive overlap, and which is a good monitor of the increase in A state pooling, grew by only a factor of 9 as would be expected. Metastable $N_2(a'^1\Sigma_u^-)$ molecules are formed in the discharge (Refs. 65,140), and do have enough energy to excite $N_2(B)$, but they were not responsible for $N_2(B)$ formation. Adding H_2 downstream from the discharge, but upstream from the observation region, completely eliminated $N_2(a')$ emission at 171 nm but reduced the B state emission by less than 15 percent. Other alternatives are being considered to the precursor of the enhanced B state emission.

Table 13 lists the rate coefficients for electronic quenching of $N_2(B,v')$ determined in this study along with several other sets of values in the literature. Agreement with the measurements of Mitchell (Ref. 141) and of Shemansky (Ref. 142), both of whom excited $N_2(B,v)$ by electron impact, is fair as is agreement with Gartner and Thrush's (Refs. 143,144) measurements in a recombining N-atom afterglow. Agreement with Becker et al.'s (Ref. 145) afterglow observations and the kinetic absorption spectroscopy determination of Dreyer and Perner (Ref. 146) following excitation of nitrogen by reletivistic electrons is not good. These numbers are effective two-body quenching rate coefficients. The actual processes involved are much more complex. The $B^3\Pi_g$ state of nitrogen is coupled collisionally into a number of other nested electronic states including the $A^3\Sigma_u^+$, $B'^3\Sigma_u^-$, $W^3\Delta_u$, and perhaps various states of the singlet manifold including $X^1\Sigma_g^+$ (Refs. 131-133,143,147,148). Thus the quenching is actually a complex process which involves transferring energy back and forth between the various states involved. Sadeghi and Setser (Refs. 131, 132) and Rotem et al. (Refs. 133,147,148) have demonstrated this coupling between the states unequivocally. These groups have excited specific vibrational levels of the $B^3\Pi_g$ state by laser pumping $A^3\Sigma_u^+$-state molecules. Subsequent to the laser pumping they observe emission from $B'^3\Sigma_u^-$-state levels, and lower vibrational levels of the $B^3\Pi_g$ state, as well as pressure-dependent, multiexponential decays of the fluorescence from the initially populated

TABLE 13. Rate Coefficients[a] for $N_2(B)$ Quenching by N_2.

N_2B,v	This Work	Mitchell	Shemansky	Becker et al.	Rotem[b] and Rosenwaks	Gartner and Thrush	Dreyer and Perner
1	1.0±0.8	0.8	~1		1.2	>0.77	0.22±0.02
2	0.8±0.1	1.2	1.9±0.2		3.6	>0.89	0.32±0.02
3	3.0±0.2	2.1	1.7±0.2		9.0		
4	2.4±0.1	1.9	1.8±0.2		4.3		
5	2.6±0.1	1.8	2.3±0.2		6.8		
6	2.1±0.3	1.8	4.1±0.4		-		
7	6.4±0.3	2.4	6.6±0.4		-		
8	8.0±2.4		7.2±0.4		7.5		
9	7.0±1.2		9.8±1.0	0.9	2.8		
10	2.3±0.2		6.3±0.8	2.8	5.3	4.4±0.9	
11	2.8±0.2		2.0±0.3	7.2	-		

a. Units 10^{-11} cm^3 $molecule^{-1}$ s^{-1}.
b. Based on two-state coupling model.

level. In most cases the fluorescence decays can be separated into two pressure dependent components, one fairly fast, and the other quite slow. The rapidly decaying component represents coupling into a reservoir state which is in equilibrium with the initially pumped level. Generally the $W^3\Delta_u$ state is identified as the primary reservoir state.

Sadeghi and Setser (Ref. 132) and Rotem et al. (Refs. 133,147,148) tried to describe their observations using the two-state coupling model given by Yardley (Ref. 149). An attempt has been made to derive a steady-state expression consistent with this model so that our observations could be compared with those of Rotem and Rosenwaks (Ref. 133).

The following reactions describe the model:

$$N_2(A) + N_2(A) \xrightarrow{k_{ep}} N_2(B) + N_2(X) \tag{77}$$

$$N_2(B) + N_2(X) \underset{k_{WB}}{\overset{k_{BW}}{\rightleftharpoons}} N_2(W) + N_2(X) \tag{78}$$

$$N_2(B) + N_2(X) \xrightarrow{k_Q^B} 2N_2(X) \tag{79}$$

$$N_2(B) \xrightarrow{k_r^B} N_2(X) + h\nu \tag{80}$$

$$N_2(W) + N_2(X) \xrightarrow{k_Q^W} 2N_2(X) \tag{81}$$

$$N_2(W) \xrightarrow{k_r^W} N_2(B) + h\nu \tag{82}$$

where we have assumed W as the reservoir state. This set of equations defines the following rates:

$$R_f = k_{ep}[N_2(A)]^2 \tag{83}$$

$$R_1 = k_r^B + k_Q^B[N_2] \tag{84}$$

$$R_2 = k_{BW}[N_2] \tag{85}$$

$$R_{-2} = k_{WB}[N_2] \tag{86}$$

$$R_3 = k_r^W + k_Q^W[N_2] \tag{87}$$

The rate of formation of state W is

$$\frac{d[W]}{dt} = R_2[B] - (R_{-2} + R_3)[W] \tag{88}$$

Under steady-state conditions we obtain

$$[W] = \frac{R_2[B]}{R_{-2} + R_3} \tag{89}$$

The rate of formation of state B is

$$\frac{d[B]}{dt} = R_f - (R_1 + R_2)[B] + R_{-2}[W] \tag{90}$$

Under steady-state conditions, with the inclusion of Eq. (89), Eq. (90) becomes

$$\frac{R_f}{[B]} = \frac{(R_1 + R_2)(R_{-2} + R_3) - R_2R_{-2}}{R_{-2} + R_3} \tag{91}$$

The two-state coupling model of Yardley explains bi-exponential decay of state B as

$$\frac{[B](t)}{[B](t=0)} = A_1e^{-\lambda_1 P} + A_2e^{-\lambda_2 P} \tag{92}$$

Under conditions such that $\lambda_1 >> \lambda_2$ the following expressions apply:

$$\lambda_1 = R_2 + R_{-2} = k_{BW}P(1+\chi) \tag{93}$$

$$\lambda_2 = \frac{(R_1 + R_2)(R_{-2} + R_3) - R_2R_{-2}}{R_2 + R_{-2}} \tag{94}$$

$$= \frac{k_r^B\chi + k_r^W}{1 + \chi} + \frac{k_2^B\chi - k_2^W}{1 + \chi} P \tag{95}$$

$$\chi = K_{eq}^{-1} = \frac{k_{WB}}{k_{BW}} = \frac{A_2}{A_1} \tag{96}$$

Combining Eqs. (91) and (94) gives

$$\frac{R_f}{[B]} = \lambda_2\left(\frac{R_2 + R_{-2}}{R_{-2} + R_3}\right) = \lambda_2\left(\frac{1 + \chi}{\chi + \frac{R_3}{R_2}}\right) \tag{97}$$

Applying expression (95) for λ_2 gives

$$\frac{R_f}{[B]} = \frac{k_r^B\chi + k_r^W}{\chi + \frac{R_3}{R_2}} + \frac{k_Q^B\chi + k_Q^W}{\chi + \frac{R_3}{R_2}} P \tag{98}$$

This expression has a form similar to Eq. (75) which describes the quenching of $N_2(B)$. The product of the ratio of the factor multiplied by P to the constant term in Eq. (97) times k_r^B gives the effective rate coefficient for quenching, based upon rates determined experimentally from the laser-pumping experiments, i.e.,

$$k_Q^{eff} = \frac{k_Q^B\chi + k_Q^W}{k_r^B\chi + k^W} k_r^B \tag{99}$$

Rotem and Rosenwaks (Ref. 133) studied vibrational-level dependent decays as a function of nitrogen pressure. The effective rate coefficient of their slowly decaying component is

$$k_s = \frac{d\lambda_2}{dp} = \frac{k_Q^B\chi + k_Q^W}{1 + \chi} \tag{100}$$

This expression combines with Eq. (98) to give

$$k_2^{eff} = \frac{k_s(1+\chi)}{k_r^B\chi + k_r^W} k_r^B \tag{101}$$

We list values of k_2^{eff} based upon their measurements of k_s and χ in Table 13. We used the radiative lifetimes of $N_2(B)$ and $N_2(W)$ (calculated by Werner et al. (Ref. 113)) were used to derive the k_2^{eff} values listed. The calculation

assumes that the coupling is with the vibrational level of the $W^3\Delta_u$ state which is closest in energy resonance to the vibrational level of $B^3\Pi_g$ considered. Clearly this approximation is somewhat simplistic and may account for the rather mediocre agreement between the measured, effective quenching rate coefficients, and those we calculate based upon the two-state coupling model and Rotem and Rosenwaks' experimental results. Under the circumstances, perhaps a factor of 2 to 3 agreement is acceptable. The coupling is probably too complex to be explained either by an effective quenching rate coefficient, or by only a two state model.

The microscopic details of the quenching processes strongly depend upon the quenching partner. Nitrogen appears to quench electronic energy out of all levels at roughly comparable rates (Ref. 150). Argon, on the other hand, is much less efficient than nitrogen at quenching $B^3\Pi_g$ manifold electronically, but it rather efficiently alters the vibrational distribution. Figure 80 demonstrates this point dramatically. The spectrum in Fig. 80a, for which the nitrogen partial pressure is 0.21 torr, shows fairly strong first-positive band attenuation relative to the unquenched HIR band at 703 nm. The vibrational distribution, however, is quite similar to that in Fig. 73 which was taken under conditions of sufficiently low nitrogen partial pressure that electronic quenching is minimal. Figure 80b shows that reducing the nitrogen partial pressure so as to eliminate N_2 quenching effects results in a much stronger first-positive system intensity. In argon, however, the vibrational-level distribution is drastically altered. Raising the argon pressure further, as shown in Figs. 80c and d, does result in some reduction in the first-positive system intensity, but more noticeable is the continual shifting of the vibrational distribution. Especially interesting in Fig. 80d, which is in 10 torr of argon, is that the vibrational distribution appears to hang up in $v' = 8$. The apparent electronic quenching by argon in Fig. 80c and d compared to Fig. 80b might result only from shifting the $B^3\Pi_g$ population into vibrational levels $v' = 0$-2 which do not emit in the spectral region observed. The observations would have to be extended into the infrared to clarify this point. Clearly $N_2(B^3\Pi_g)$ quenching is an extremely complex process, and simple models such as implied by Eq. (75) or even Eq. (98) are not completely adequate.

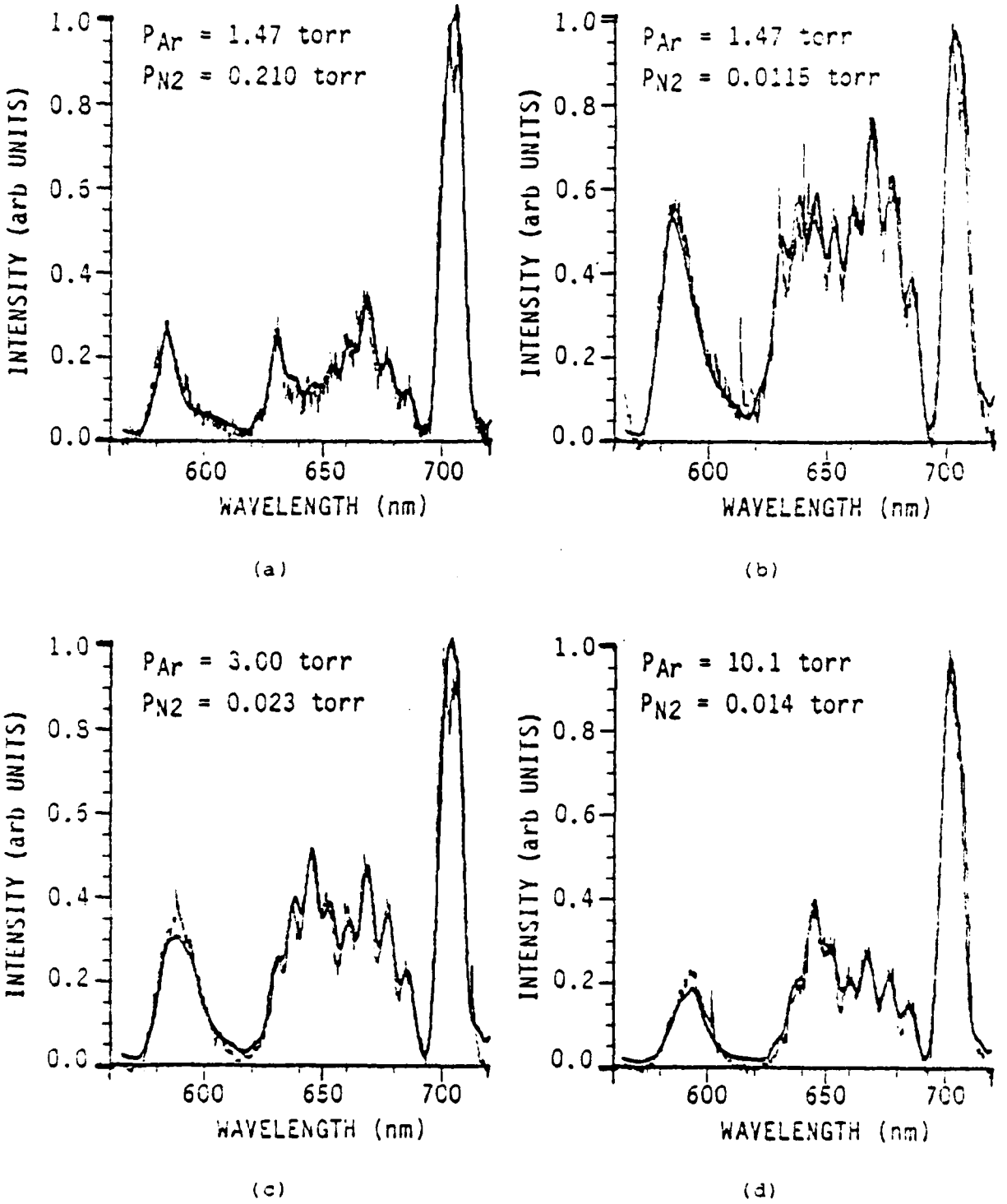

Figure 80. Variation in $N_2(B,A)$ spectrum produced in $N_2(A)$ energy pooling with changes in nitrogen and argon partial pressures.

3.3 ACTIVE NITROGEN EXCITATION OF IF

3.3.1 Introduction--Two years ago it was observed that adding iodine monofluoride to a stream of active nitrogen resulted in strong excitation of $IF(B^3\Pi_0^+)$ (Ref. 6). The effective excitation rate of the IF(B) appeared to correlate with the number density of $N_2(B^3\Pi_g)$ in the observation zone. The $N_2(B)$ could be ruled out as the precursor of the IF(B) excitation, however, because an excitation rate coefficient several orders of magnitude greater than gas kinetic would have been required to explain the magnitude of the IF(B) fluorescence observed. The $N_2(B)$ appeared to act as a tracer of a dark species which itself was responsible for the excitation. The excitation-rate measurements indicated that the product of the excitation-rate coefficient and the number density of the exciting species was approximately 1 s^{-1}. This implies that the number density of the exciting species is at least 10^{10} molecule cm^{-3}, given that the maximum expected excitation rate coefficient is roughly 10^{-10} cm^3 $molecule^{-1}$ s^{-1}. Various arguments indicated that most of the common metastables in the active nitrogen flow, such as $N(^2D,^2P)$, $N_2(a^1\Pi_g)$, $N_2(a'^1\Sigma_u^-)$, $N_2(A^3\Sigma_u^+)$, and $N_2(W^3\Delta_u)$, were all present in too low a concentration to be responsible for the excitation, or else varied in number density with changes in conditions in a fashion incompatible with the observed changes in IF(B) excitation rate. It was concluded, therefore, that the most likely species in the reactor responsible for the excitation was ground-electronic-state, molecular nitrogen in relatively high vibrational levels. Observations would, therefore, be classified as observations of vibrational-to-electronic (V-E) energy transfer. Several cases of this phenomenon exist in the literature (Refs. 151-153).

The observations of fairly large number densities of $N_2(B)$ were interesting in that the the vibrational distribution and intensity of the observed first positive bands were incompatible with formation from N-atom recombination. One indication of this is that adding molecules like O_2, CO, and CO_2 drastically reduced the first-positive intensity, by more than an order of magnitude. Under the conditions of our experiments, however, none of these molecules reacts at any significant rate with atomic nitrogen. Thus the

reduction in intensity was not a result of N-atom removal. Furthermore, the residual first-positive intensities did begin to show the spectral distribution characteristic of the N-atom-recombination-produced, Lewis-Rayleigh afterglow. Since these measurements were all made 10 to 20 ms downstream from the exciting discharge, some species in the active nitrogen, with a lifetime against quenching and radiation in excess of tens of milliseconds, must be collisionally coupled to the $N_2(B)$ (and upon addition of IF, the IF(B)) in the observation volume. The contention again was that this collisional coupling is effected through high vibrational levels of the ground-electronic state of molecular nitrogen. The kinetics of these coupling processes are discussed in some detail in Refs. 154,155.

The purpose of this task was to try to quantify our observations more carefully than in the past, and to try to provide some additional support for the contention that $N_2(v)$ was the energetic species responsible for the IF excitation. Some time was spent: trying to develop a relatively clean source of $N_2(v)$ which would have reduced number densities of nitrogen atoms and various atomic and molecular metastables; trying to implement and characterize a diagnostic for vibrationally excited nitrogen in the flow reactor, and additionally to study more fully the transfer of energy between active nitrogen and IF.

3.3.2 Development of $N_2(v)$ source and diagnostic

3.3.2.1 Introduction--A source of vibrationally excited, ground-state nitrogen that was free from atoms or atomic and molecular metastables would prove invaluable in these studies. Morgan and Schiff showed that vibrationally excited nitrogen, which was created in a microwave discharge through nitrogen, was easily removed with only a slight reduction in the number density of nitrogen atoms when a glass wool plug was placed in the flow reactor somewhere downstream from the discharge (Ref. 156). This technique developed from their observation that the vibrationally excited nitrogen was more efficiently removed from their flow reactor by wall collisions than were the nitrogen atoms. If one could reverse the order of wall-recombination

efficiencies, then one could envision removing the nitrogen atoms -- or at least drastically reducing them -- while retaining the vibrationally excited nitrogen. Because wall collisions remove electronic metastable species with almost unit efficiency, one would then be left with a flow that was vibrationally excited, ground-electronic-state nitrogen. Wire screens were added to the flow tube downstream from the discharge, hoping that they would remove the atoms efficiently, while leaving the vibrationally excited nitrogen largely unaffected. This idea stems largely from the work of Reeves and coworkers (Refs. 157,158), and Kenner and Ogryzlo (Ref. 159), who have observed electronic excitation following catalytic recombination of atoms on various wire screens. Most of the work used screens made from nickel wire.

The first idea for developing a diagnostic for vibrationally excited nitrogen was to extend the pioneering work of Schmeltekopf et al. (Ref. 160) and Young and Horn (Refs. 161,162). They relied on the vertical nature of Penning-ionization transitions from ground-electronic-state, neutral nitrogen to produce $N_2^+(B^2\Sigma_u^+,v)$ distribution characteristic of the ground-state distributions. Mixing metastable helium atoms with a flow of molecular nitrogen results in strong emission of the nitrogen first-negative system, $N_2^+(B\ ^2\Sigma_u^+ - X^2\Sigma_g^+)$. Since the Penning-ionization process follows a Franck-Condon excitation pathway, the vibrational distribution in the neutral, ground state will determine the distribution observed in the upper, ionic state. One problem with this approach is that care must be taken not to have any He^+ or He_2^+ in the flow of metastable helium. Both of those species also excite $N_2^+(B)$ quite strongly in charge-transfer reactions, but with an $N_2^+(B)$ vibrational distribution that is decidedly non-Franck-Condon (Ref. 163). The major problem in applying this diagnostic to our studies of energy transfer to IF is that the diagnostic is most sensitive to vibrational excitation of the first few vibrational levels in the ground state. The excitation of IF(B), and $N_2(B)$, on the other hand, requires vibrational excitation of about 10 and 30 vibrational quanta respectively to effect the excitation. We had hoped to be able to estimate the overall vibrational distribution of the ground-state nitrogen by combining our experimental determination of the vibrational distribution in the first few levels with modeling calculations on the temporal development of the fully coupled vibrational-state manifold (Refs. 164,165).

3.3.2.2 Experimental--The apparatus used in these experiments has been described in most respects in Subparagraphs 3.1.2 and 3.2.2. This paragraph describes the modifications required for the measurements related to $N_2(v)$. Figure 81 shows the configuration of the flow reactor. A microwave discharge at the upstream end of the flow reactor, through a flow of helium and nitrogen, created the active nitrogen. The active nitrogen entered a section of 2-in-diameter Pyrex® containing three side arms. Small amounts of SF_6 flowed through the first side arm to attach electrons created in the Penning-ionization reactions. A rod, to which the metal screens were attached, extended through the second side arm. This allowed the screen to be rotated either parallel to, or normal to, the gas flow so as to vary the effective diffusion length between the gas species and the wire surfaces on the screen. Thus, the efficiency could be varied with which the screen scavenged active species from the flow. The metastable helium atoms entered through the third side arm. A second length of 2-in flow tube separated the $N_2(v)$ preparation and characterization section from the stainless steel viewing region. This

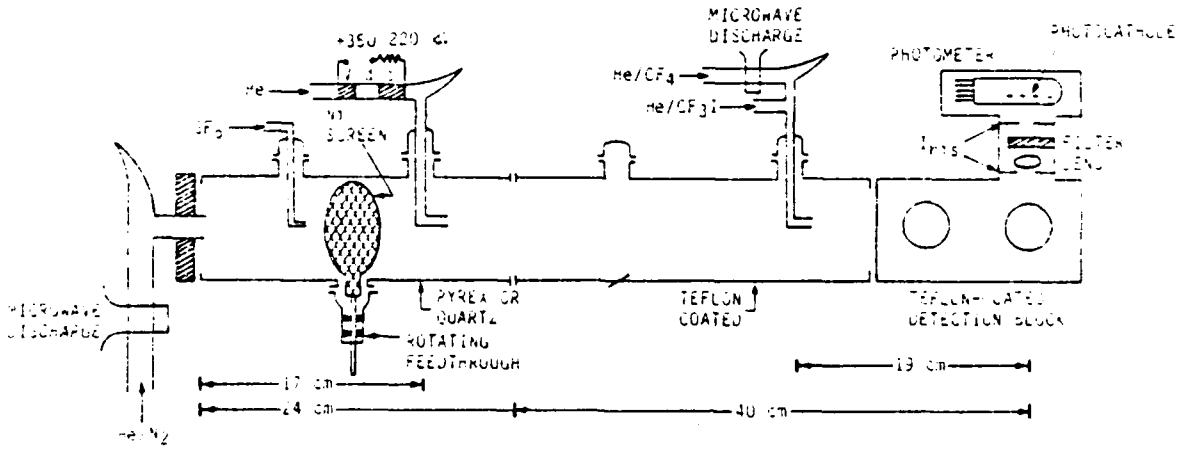

Figure 81. Flow reactor for studies on the vibrational energy content of active nitrogen and of IF excitation by active nitrogen.

section was Teflon coated and contained an injector for IF. We have discussed and characterized the IF source previously (Ref. 6). The 0.5-m monochromator is mounted on rails so that it could be moved toward the upstream end of the reactor to observe the fluorescence created in the Penning-ionization reaction, or back to the stainless steel viewing region to observe the interaction of active nitrogen with IF. A photomultiplier/interference filter combination (580 ± 5 nm) provided photometric measurements of the intensity of the nitrogen first-positive bands in the viewing region.

A hollow-cathode, dc discharge through a flow of purified helium created the metastable helium atoms. Flowing the gas through a molecular-sieve trap at liquid nitrogen temperature upstream from the discharge removed most of the impurities in the helium, including nitrogen and oxygen, with the exception of some residual neon. The small amounts of neon (≤10 ppm) have no effect on observations. A number of years ago, it was shown that operating the hollow-cathode discharge at high voltage and high current tended to produce significant number densities of atomic and molecular helium ions (Ref. 163). These ions are an anathema to the Penning-ionization measurements because they produce highly non-Franck-Condon distributions in the $N_2^+(B)$. Thus one would be led to false conclusions regarding the extent of ground-state vibrational excitation. The discharge was operated at 350 V with a current, limited by a 200 kΩ resistor, below a milliamp. The absence of significant ionic number densities was confirmed by failing to observe $N_2^+(B, v' > 2)$ when the active-nitrogen discharge was off.

3.3.2.3 Theory behind the Penning-ionization measurements--The Penning-ionization between metastable helium atoms and molecular nitrogen is a vertical process. One can calculate the vibrational distribution in the final state, therefore, knowing only the vibrational distribution in the lower state and the Franck-Condon factors that couple the two states together. Thus

$$N_{v'} = \sum_{v''} N_{v''} f_{v'v''} \qquad (102)$$

where v' and v" represent the vibrational levels of the upper and lower states, respectively, and $f_{v'v''}$ is the Franck-Condon factor coupling them. In theory, if one measured the vibrational distribution in the upper state, it could be determined in the lower state by simply inverting the Franck-Condon matrix, and multiplying this inverse matrix on both sides of Eq. (102). This procedure does not work in practice because the measurements of the upper-state populations have some uncertainty associated with them, and the uncertainties become greatly magnified by the matrix multiplication. Jolly et al. (Ref. 166) apparently did use this approach to analyze $N_2(v)$ distributions created in a glow discharge. We do not understand their success in light of our lack of it. Our spectral fitting approach for determining $N_2^+(B)$ number densities ought to be more accurate than their graphical integration of one branch from each band. Our data was analyzed using a model to describe the $N_2(X)$ vibrational distributions to predict $N_2^+(B)$ vibrational distributions and then comparing these predictions with the observations.

A set of Franck-Condon factors was calculated over the range of ground-electronic-state vibrational levels of 0-18, and $N_2^+(B)$-state vibrational levels of 0-9. The calculational procedure was previously discussed for determining Franck-Condon factors (Ref. 167). Table 14 shows the results of these calculations. Given the Franck-Condon factors in Table 14, the expected $N_2^+(B)$-state vibrational populations were calculated relative to that in $N_2^+(B, v' = 0)$ for a number of values of vibrational temperature of ground-state nitrogen between 300 and 30,000 K, assuming a Boltzmann distribution among the levels. Figure 82 shows the results of these calculations. If the ground-state vibrational level populations follow a Boltzmann distribution, one can use experimentally derived ratios of the populations of the various vibrational levels of $N_2^+(B)$ relative to that for $N_2^+(B, v' = 0)$ and Figure 82 to find the vibrational temperatures of ground-state nitrogen which corresponds to those excited-state population ratios. The excited-state population ratios, of course, result from analyzing the $N_2^+(B-X)$ spectrum excited in the Penning-ionization reaction.

TABLE 14. Franck-Condon Factors of $N_2^+(B^2\Sigma_u^+, v') - N_2(X^1\Sigma_g^+, v'')$.

v' \ v''	0	1	2	3	4	5	6	7	8	9	10	11	12	13	14	15
0	0.8836	0.1034	0.0117	0.0012												
1	0.1141	0.6917	0.1611	0.0285	0.0039											
2	0.0023	0.2030	0.5573	0.1854	0.0458	0.0076	0.0012									
3		0.0048	0.2630	0.4694	0.1964	0.0611	0.0122	0.0023								
4			0.0060	0.2087	0.4192	0.1711	0.0726	0.0165	0.0037							
5			0.0006	0.0049	0.3382	0.4008	0.1444	0.0841	0.0199	0.0054	0.0012					
6				0.0018	0.0019	0.3506	0.4098	0.1099	0.0940	0.0217	0.0075	0.0016				
7					0.0043	-	0.3405	0.4422	0.0711	0.1065	0.0211	0.0100	0.0025			
8						0.0079	0.0056	0.2994	0.4904	0.0339	0.1256	0.0171	0.0138	0.0049	0.0017	
9							0.0113	0.0300	0.2198	0.5355	0.0072	0.1560	0.0094	0.0206	0.0027	0.0013

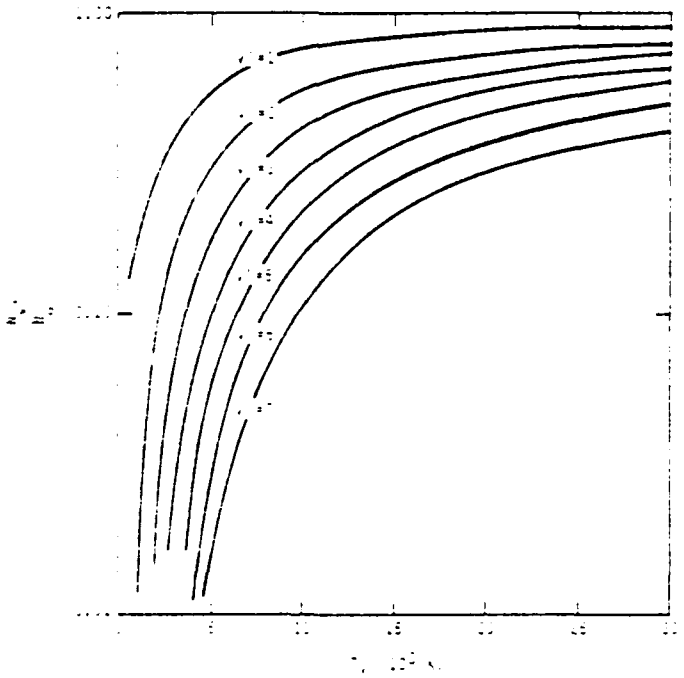

Figure 82. Ratio of the populations of $N_2^+(B, v')$ to $N_2^+(B, v' = 0)$ created in He^* Penning-ionization of $N_2(X, v'')$ as a function of the vibrational temperature of the ground-state nitrogen.

If the ground-electronic-state vibrational levels do not follow a Boltzmann distribution, one can still compute expected excited state populations from Eq. (101), if the ground-state distribution is known. Effluents from nitrogen discharges are known to have nonequilibrium vibrational distributions, with the higher vibrational levels generally more strongly populated than would be predicted on the basis of a Boltzmann distribution. Capitelli and Dilonardo (Ref. 168) provided an analytical approximation which is reasonably accurate for ground-state vibrational levels below about v" = 10. For vibrational levels below the Treanor minimum, v^*, the distribution is that given by Treanor et al. (Ref. 169):

$$\frac{N_{v"}}{N_{v"=0}} = \exp\left[- v" \left(\frac{1.4388(\omega_e - 2\omega_e x_e)}{\theta_1} - (v"-1) \frac{1.4388\ \omega_e x_e}{T} \right) \right] \qquad (103)$$

where θ_1 is the Boltzmann vibrational temperature referenced to v" = 1, T is the ambient gas temperature, and ω_e and $\omega_e x_e$ are spectroscopic constants in units of cm^{-1}. The Boltzmann vibrational temperature is given by

$$\theta_1 = \frac{\omega_e - 2\omega_e x_e}{\kappa \ln(N_{v"=1}/N_{v"=0})} \qquad (104)$$

For vibrational levels above the Treanor minimum, we have

$$\frac{N_{v"}}{N_{v"=0}} = \frac{v^*+1}{v+1} \left[\exp - (v^*)^2 \frac{\omega_e x_e}{T} - 0.5 \right] \qquad (105)$$

where v^* is

$$v^* = \frac{T\ \omega_e x_e}{2(\omega_e - 2\omega_e x_e)\ \theta_1} + 0.5 \qquad (106)$$

The Penning-ionization spectrum calculated from a ground-state distribution based upon Eqs. (102), (103), and (104) is significantly different from what one would calculate from a Boltzmann ground-state distribution. The Penning-ionization technique, therefore ought to differentiate between the two ground-state distributions rather easily.

3.3.2.4 Results of the Penning-ionization measurements--Figures 83 and 84 show a portion of the nitrogen first-negative spectrum with the active-nitrogen discharge off and on, respectively. Clearly, the vibrational development of the emission is greatly enhanced by discharging the gas. We determined vibrational populations in the upper state by fitting the spectrum in the manner already described in Subparagraph 3.1.2. Early in this measurement program, it was discovered that moving the monochromator slightly downstream from the injector, through which the He^* entered the reactor, resulted in a much different vibrational distribution in the upper state. There appeared to be no reason why the vibrational distribution in the active nitrogen should change over short distances. A diffuse emission could be seen extending somewhat downstream from the well-defined flame created by the Penning-ionization. Several centimeters downstream from the injector, the Penning-ionization flame disappeared, and only the diffuse emission remained. Figure 85 shows this spectrum. On the assumption that the emission was caused by energetic electrons exciting $N_2^+(X)$, a trace of SF_6 was added to act as a scavenger for the electrons. This addition eliminated the diffuse flame, and also resulted in $N_2^+(B)$ vibrational distributions which did not change with the location of the monochromator relative to the He^* injector. Presumably, the electrons created in the Penning-ionization reaction pick up some extra kinetic energy either from stray microwave fields which have penetrated downstream, or else from collisions with energetic species in the active nitrogen. The amount of energy must be fairly considerable, because exciting $N_2^+(B)$ from $N_2^+(X)$ requires more than 3 eV. All the results given in the following paragraph were obtained in the presence of small traces of SF_6.

The first-negative spectra were fit to obtain populations for levels 0-8, although, for the most part, only vibrational levels 0-7 contributed any significant intensity to the spectra. A number of different and conflicting sets of Einstein coefficients for the $N_2^+(B^2\Sigma_u^+ - X^2\Sigma_g^+)$ fill the literature (Refs. 38,112,170,171). In particular, the constancy of the electronic transition moment with r-centroid is unsettled (Refs. 172,173). For the analysis of data taken for this report, a set of Einstein coefficients have been calculated based upon the relative electronic transition moment variation given by Brown and Landshoff (Refs. 172,174,175), the Franck-Condon factors of

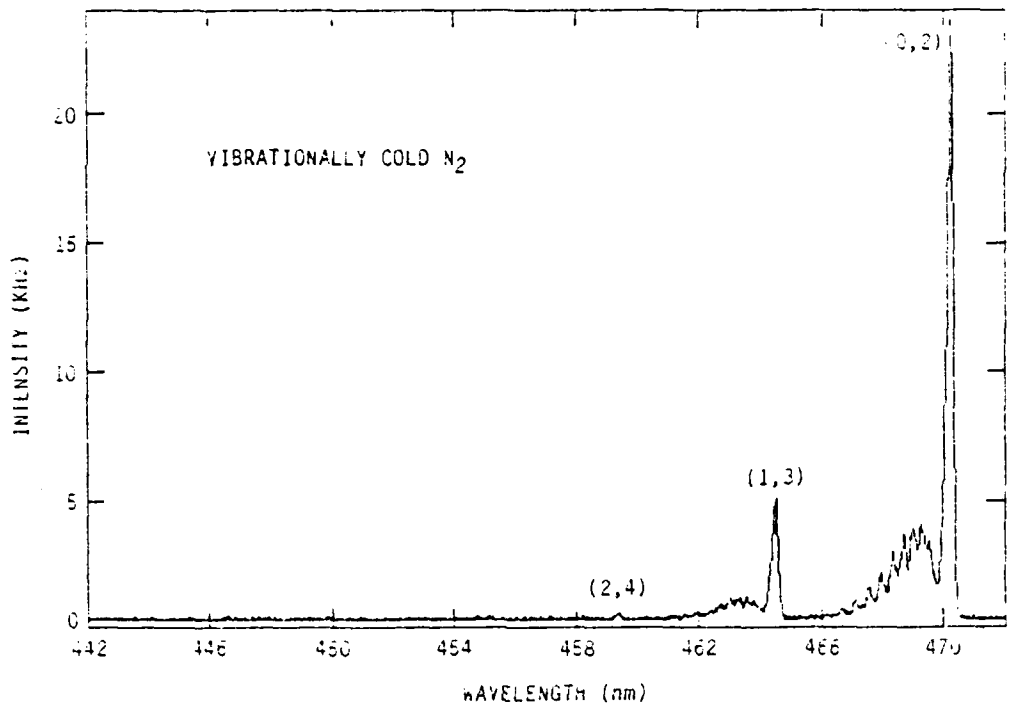

Figure 33. Spectrum of the $\Delta v = -2$ sequence of the $N_2^+(B^2\Sigma_u^+ - X^2\Sigma_g^+)$ system excited in the Penning-ionization of nitrogen by $He^*(2\ ^3S)$.

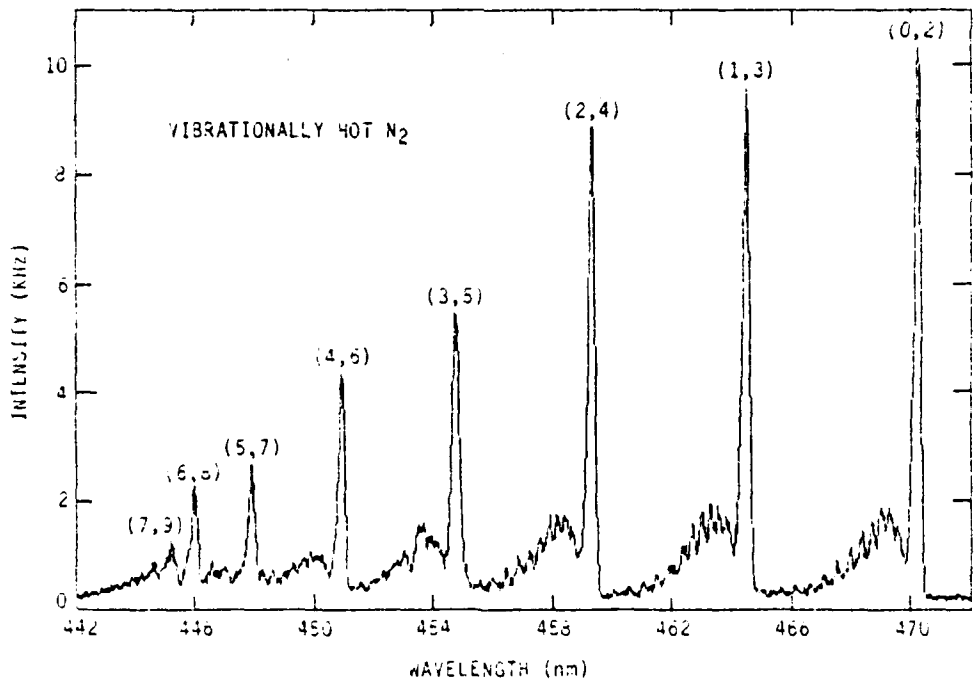

Figure 34. Spectrum of the $\Delta v = -2$ sequence of the $N_2^+(B\ ^2\Sigma_u^+ - X^2\Sigma_g^+)$ system excited in the Penning-ionization of active nitrogen by $He^*(2\ ^3S)$

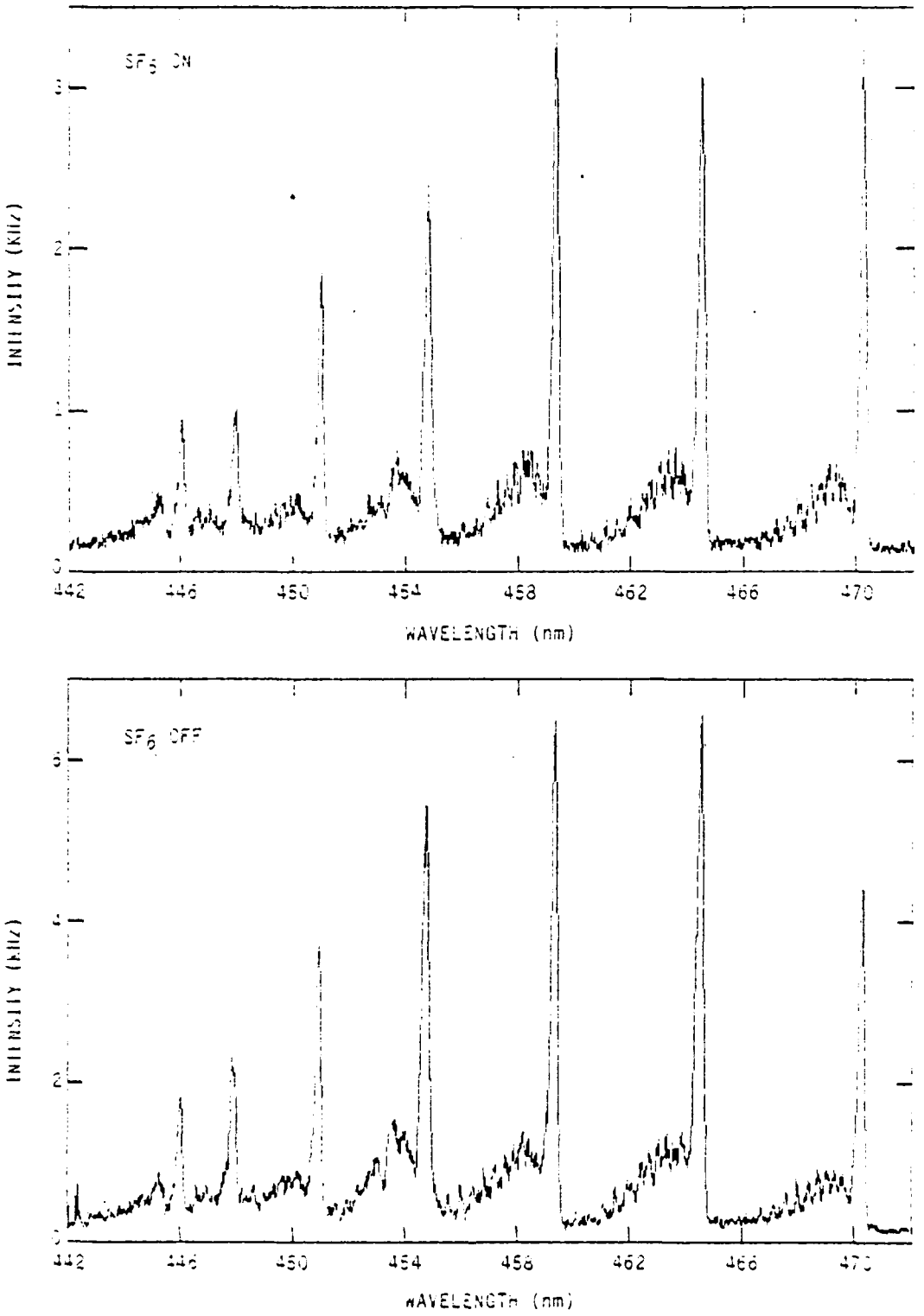

Figure 35. Spectra of the $\Delta v = -2$ sequence of the $N_2^+(B^2\Sigma_u^+ - X^2\Sigma_g^+)$ system excited in the Penning-ionization of active nitrogen by $He^*(2\,^3S)$ in the presence and absence of SF_6.

Albritton et al. (Ref. 83) and a radiative lifetime of $N_2^+(B,v'=0)$ of 62.5 ns (Ref. 38). Table 15 lists the calculated Einstein coefficients. This issue of transition-moment variation is being investigated further. The intermolecular potential constants given in Lofthus and Krupenie (Ref. 38) were found to be inadequate for predicting band positions accurately. The fitting program uses the recent potential constants of Gottscho et al. (Ref. 176).

TABLE 15. Einstein Coefficients for $N_2^+(B^2\Sigma_u^+ - X^2\Sigma_g^+)$.[a]

v' \ v"=	0	1	2	3	4	5	6	7	8	9	10
0	11.1	3.87	0.886	0.154	0.026						
1	5.87	3.75	4.34	1.71	0.454	0.097	0.018				
2	0.991	7.82	0.817	3.50	2.20	0.789	0.214	0.049			
3	0.053	2.29	7.92	0.038	2.33	2.29	1.08	0.361	0.098	0.023	
4		0.154	3.54	7.29	0.086	1.34	2.09	1.26	0.506	0.161	
5			0.253	4.32	6.59	0.327	0.662	1.74	1.31	0.622	0.227
6				0.319	5.21	6.17	0.452	0.284	1.38	1.26	0.690
7				0.010	0.261	5.46	6.19	0.345	0.075	1.08	1.15
8					0.066	0.128	6.32	8.32	0.174	0.008	0.957

a. Units of 10^6 s^{-1}

Analyzing the $N_2^+(B,v')$ vibrational distributions with the help of Figure 82 gave different ground-state vibrational temperatures depending upon which upper-state vibrational level was considered. The data fell into three groups. The temperature determined from v' = 1 was only 63 percent of that determined from v' = 2 and 3, which were themselves reasonably consistent. Vibrational temperatures determined from v' = 4-7 also were reasonably consistent with each other, but were 30 percent larger than temperatures determined from vibrational levels 2 and 3. Clearly, a Boltzmann model for the ground-state vibrational distribution is inadequate.

Fitting our distributions to the analytical model given by Capitelli and Dilonardo was more successful. Figures 86 and 87 show two examples. Clearly, the nonequilibrium model does a reasonable job of fitting observations out through v' = 6. The sudden discrepency at v'=7 is not clearly understood. The distribution is shown which would be predicted were the ground-state to be determined by a Boltzmann distribution. This shows graphically the inadequacy of that model for the ground-state levels. We hope to use an improved model to predict the population distribution up to higher vibrational levels.

Observations show that effective vibrational temperatures, θ_1, as determined from fits of the data to Eqs. (103) and (105) rather than what one would calculate from Eq. (104), tended to be smaller with larger nitrogen mole fractions flowing through the discharge (Figure 88) and also at higher total pressures. Placing a nickel screen in the reactor, downstream from the discharge, only slightly reduced the effective vibrational temperature of the nitrogen (about 5 percent). The Penning-ionization technique appears to provide a reasonably accurate monitor of the vibrational distribution of ground-electronic-state nitrogen, at least for the lower vibrational levels. Extending the model to include higher vibrational levels would need experimental confirmation. An $N_2(v)$ diagnostic is being developed which should prove sensitive to higher vibrational levels under another contract.

It was uncertain as to how well the populations of the more energetic vibrational levels of $N_2(v)$ could be determined using the technique just described coupled with model calculations, we sought a diagnostic for $N_2(v)$ containing energies of several eV. These are the levels which would be responsible for the observed excitation of IF(B) and $N_2(B)$. One possibility is to search for tail bands of the first-negative system. The tail bands are bands from high lying levels of $N_2^+(B)$; e.g., v' = 12-16, which are red degraded and which appear to the red of the normal, blue degraded sequences of the first-negative system. Levels up through v' = 18 are energetically accessible from v" = 0 of $N_2(X)$, but vertical transitions to these levels would most likely occur from v" = 15-20 which lie 4 to 5 eV above v" = 0.

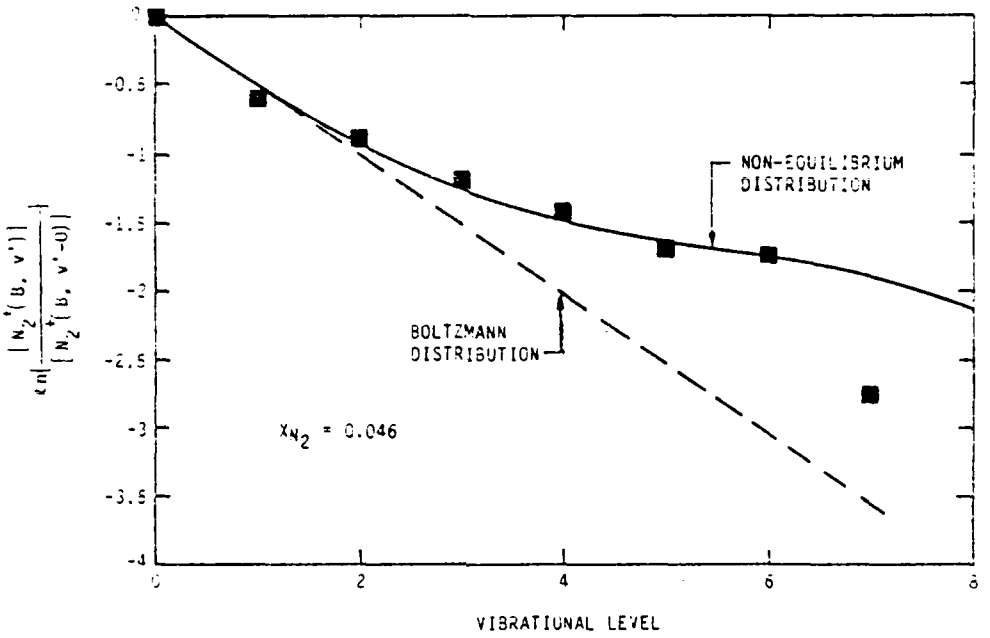

Figure 36. Comparison between experimental and calculated vibrational distributions of $N_2^+(B)$ created in the Penning-ionization of active nitrogen by metastable helium atoms for a nitrogen mole fraction of 0.011 (p = 1.5 torr, transit time from discharge = 11 ms).

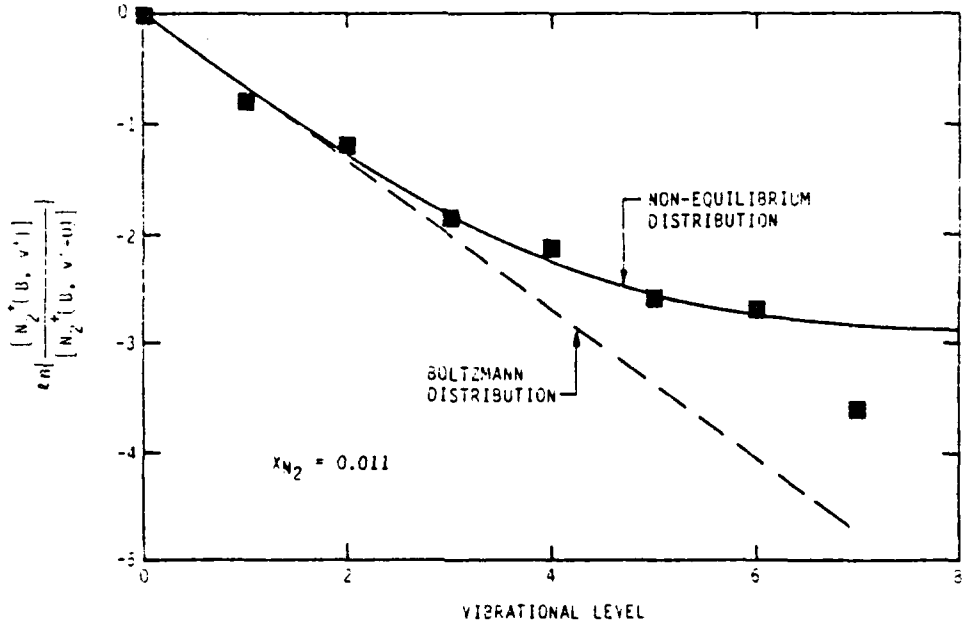

Figure 37. Comparison between experimental and calculated vibrational distributions of $N_2^+(B)$ created in the Penning-ionization of active nitrogen by metastable helium atoms for a nitrogen mole fraction of 0.046 (p = 1.5 torr, transit time from discharge = 11 ms).

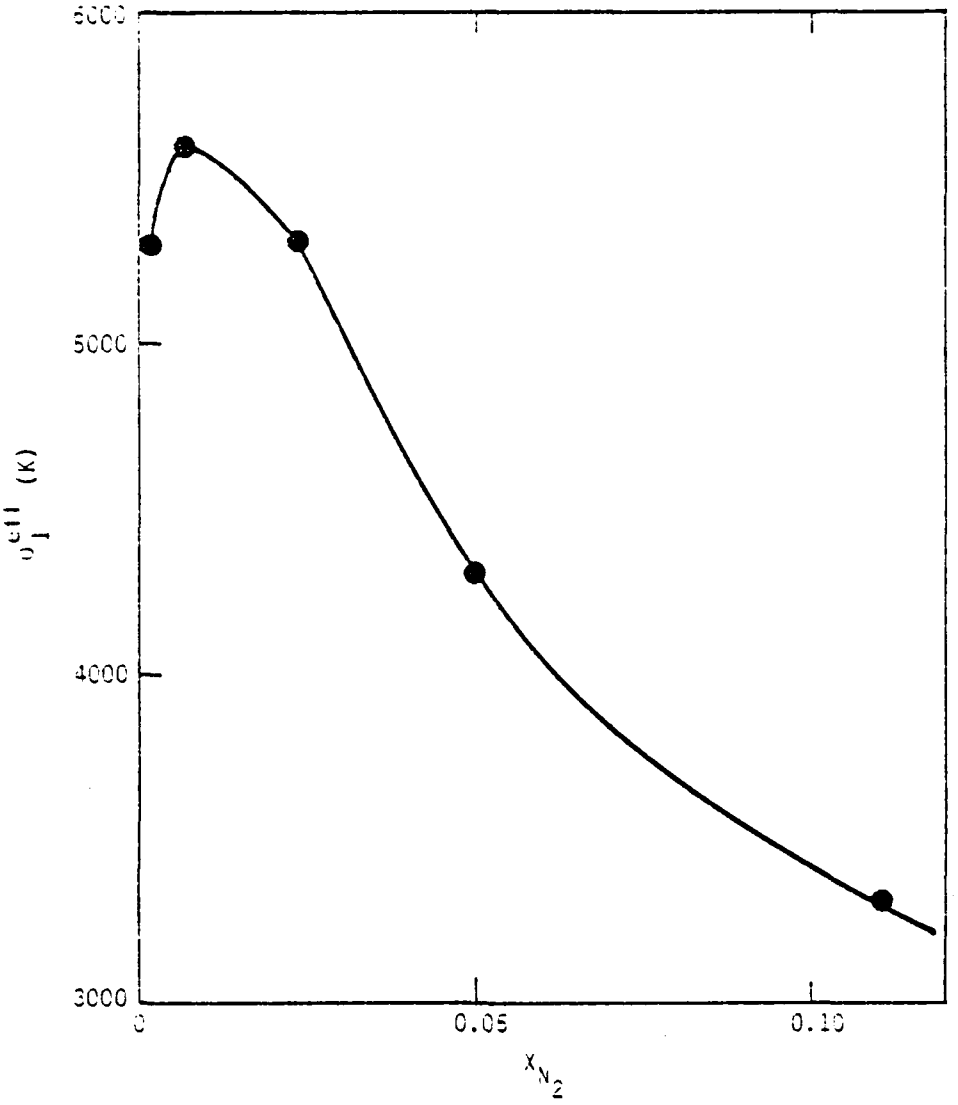

Figure 88. Effective vibrational temperature from the nonequilibrium model versus nitrogen mole fraction through the discharge.

Another possibility is to excite the nitrogen second-negative system, $N_2^+(C^2\Sigma_u^+ - X^2\Sigma_g^+)$. This system can be excited by collisions between metastable helium and molecular nitrogen only if the nitrogen has at least 3.8 eV of internal energy. Because the $N_2^+(C)$ potential curve is somewhat offset from that of $N_2(X)$, vertical transitions connecting the two states would arise from ground-state levels around v" = 10. Observing the second-negative system, therefore, would provide unequivocal evidence of highly excited ground-state nitrogen in the reactor.

A quartz piece was built for the flow reactor so that a search could be made for the second-negative system in the ultraviolet between 185 and 200 nm. Figure 89 shows the spectral region between 188 and 208 nm with the metastable helium off and on. In both cases, the active-nitrogen discharge is on. The two features appearing at 191 and 199 nm are the $\Delta v = -6$ and -7 sequences, respectively, of the nitrogen second-negative system. The $\Delta v = -8$ sequence at 206 nm is masked by the 2,0 band of the $NO(A^2\Sigma^+ - X^2\Pi)$ system. This system is excited by interactions between $N_2(A^3\Sigma_u^+)$ created in the active-nitrogen discharge, and some impurity NO also created in the discharge (Ref. 177). Scans with the active-nitrogen discharge off, but the metastable-helium discharge on resulted in no observed emissions. This latter observation is important because it establishes that He^+ is absent from the metastable helium flow. Charge-transfer between He^+ and $N_2(X)$ is a well-known source of the second-negative system (Refs. 163,178).

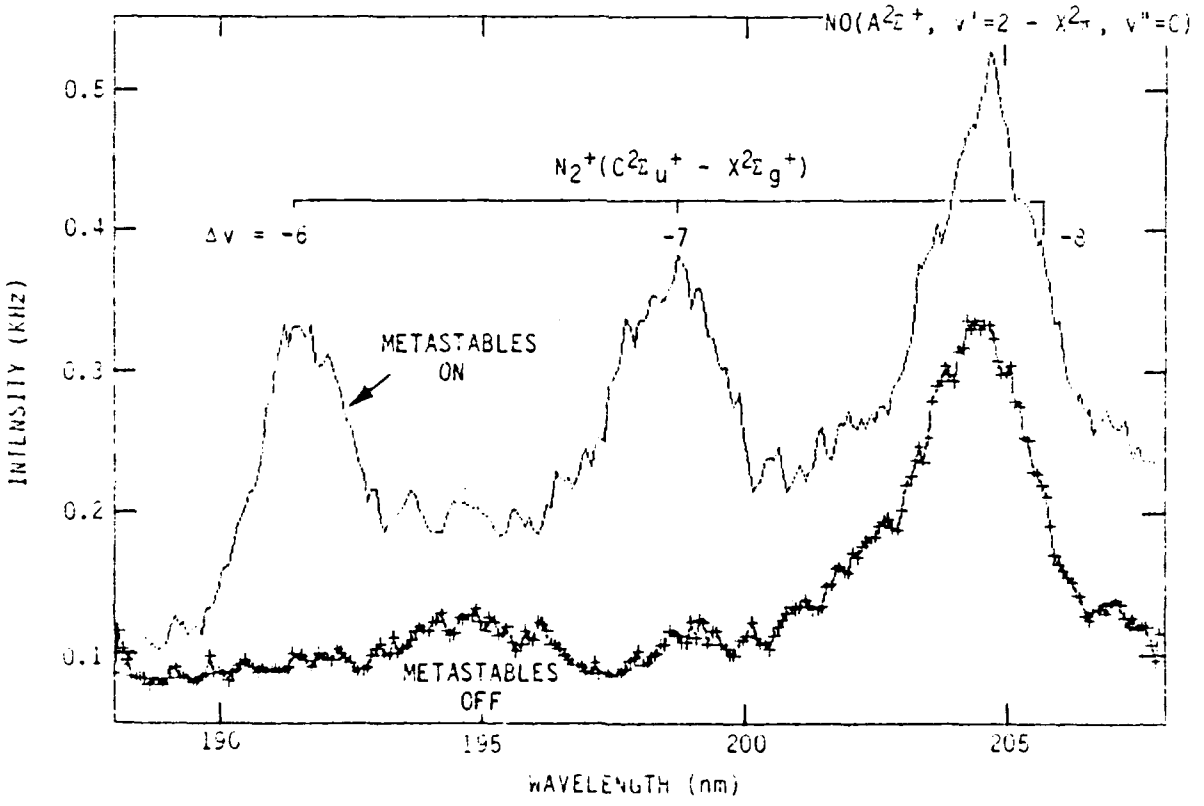

Figure 89. Spectra from active nitrogen between 184 and 208 nm in the absence and presence of metastable helium atoms.

Observing the nitrogen second-negative system from the interaction between metastable helium atoms and active nitrogen establishes the presence in the afterglow of metastable nitrogen containing at least 3.8 eV. One possibility for these metastables might be $N_2(A^3\Sigma_u^+)$ or $N_2(a'^1\Sigma_u^-)$ both of which have been observed in active nitrogen afterglows. Clean sources have been made of these two metastables, therefore, and observed the resulting spectra when they were mixed with helium metastables. The $N_2(A^3\Sigma_u^+)$ is produced cleanly by adding N_2 downstream from a hollow-cathode, d.c. discharge through a mixture of helium and argon. Scans of the Vegard-Kaplan bands between 220 and 400 nm established that the $N_2(A)$ number densities from this source were of comparable magnitude to those obtained from the active-nitrogen discharge. Turning the metastable nitrogen on and off in the presence of metastable helium had no effect on the emissions in the region between 185 and 200 nm. $N_2(a')$ is made along with slightly enhanced number densities of $N_2(A)$ - about a factor of 3 - when the molecular nitrogen flows through the dc discharge with the He/Ar mixture. Again, turning the metastable nitrogen on and off had no effect on the emissions between 185 and 200 nm. It was concluded that interactions between metastable helium and $N_2(A)$ and $N_2(a')$ do not produce $N_2^+(C)$. The appearance of $N_2^+(C)$ from the interaction between metastable helium and active nitrogen, therefore, appears to be the result of Penning-ionization of ground-electronic-state nitrogen containing at least 3.8 eV of vibrational energy.

The first-negative bands in the presence and absence of the molecular nitrogen metastables were monitored, to see if the hollow-cathode sources produced any significant levels of vibrationally excited nitrogen in lower vibrational levels. The ratio of the populations of $v' = 1$ to $v' = 0$ of $N_2^+(B)$ remained unchanged in the presence or absence of $N_2(A)$ or $N_2(a')$, and we saw no evidence of any higher levels of $N_2^+(B)$ except for the trace of $v' = 2$ which accounts for 0.2 percent of the Penning-ionization of 300 K N_2. We conclude that the vibrational temperature produced in the hollow-cathode discharges is below 1000 K and that this discharge produces no significant levels of vibrationally excited nitrogen, i.e., > 96 percent $v' = 0$.

In summary, Penning-ionization of $N_2(v)$ by metastable helium atoms excites $N_2^+(B)$ up to at least $v' = 8$. Analysis indicates the ground-state nitrogen vibrational distribution is highly non-Boltzmann, with effective vibrational temperatures of up to 6,000 K at times up to 30 ms downstream from the active-nitrogen discharge. The diagnostic is complicated by the presence of free electrons created in the Penning-ionization. These free electrons absorb energy from the active-nitrogen medium and produce further excitation of $N_2^+(B)$. Adding traces of SF_6 removes the free electrons from the reactor, and thereby, eliminates their interfering effects. Observing emission from $N_2^+(B)$, from Penning-ionization reactions in the afterglow, demonstrates the presence of $N_2(v)$ containing at least 3.8 eV internal energy.

3.3.2.6 Observations of nitrogen first-positive emission--
Another possible diagnostic for the presence of $N_2(v)$ with relatively large amounts of internal energy is to monitor the emission of the nitrogen first-positive bands, $N_2(B^3\Pi_g - A^3\Sigma_u^+)$. These bands emit strongly in the afterglow many tens of milliseconds downstream from the discharge (Figure 90). Some of the observed emission, of course, is just normal Lewis-Rayleigh afterglow which is excited from the recombination of atomic nitrogen. Such emission, however, has a very characteristic vibrational-level distribution, peaking strongly in vibrational levels 10-12 at low pressures in nitrogen or helium bath gas (Figure 91). In addition, for the N-atom number densities present in the reactor and the total pressures in the system, such emission is relatively weak. The primary emission observed has a vibrational distribution which peaks at low vibrational levels, is relatively strong at low pressures, and quenches readily upon the addition of molecular species such as O_2, CO, and CO_2. The quenching is much too efficient to be either electronic quenching of the first-positive emission itself, or to result from reactions of the molecules themselves with atomic nitrogen. Thus, a long-lived metastable state of nitrogen travels down the flow reactor many milliseconds, and then is coupled collisionally into the $B^3\Pi_g$ state in the field of view. In this way, the nitrogen first-positive emission can act as a tracer of this metastable species.

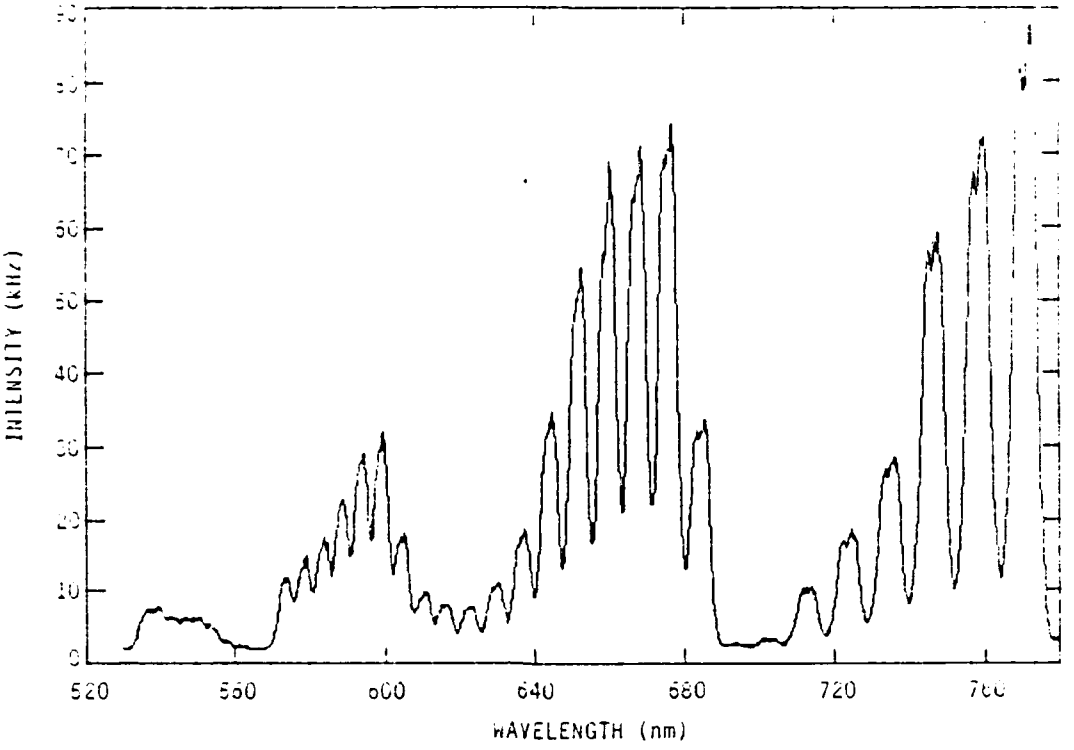

Figure 90. First-positive spectrum, $N_2(B^3\Pi_g - A^3\Sigma_u^+)$, from active nitrogen in helium (p = 1.5 torr, X_{N_2} = 0.011).

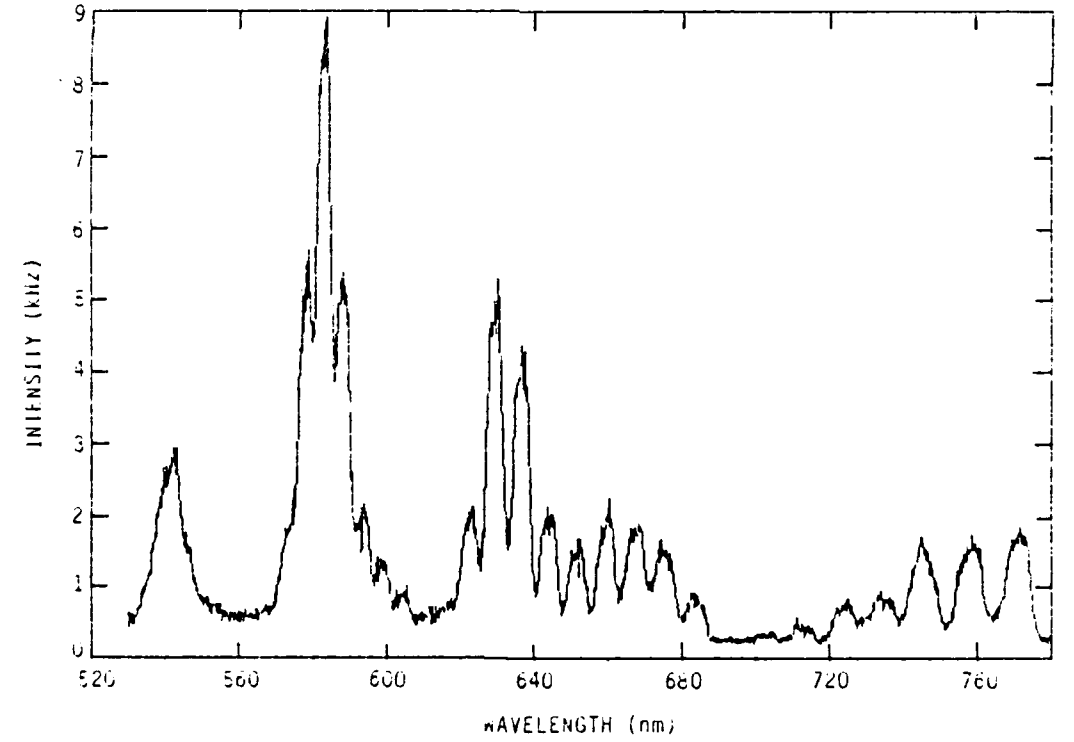

Figure 91. First-positive spectrum resulting from N-atom recombination in helium.

The only three known electronically excited nitrogen metastables with sufficiently long lifetimes to travel tens of milliseconds down the flow reactor are $N_2(A^3\Sigma_u^+)$, $N_2(a^1\Sigma_u^-$, v' = 0), and $N_2(W^3\Delta_u$, v' = 0). Energy-pooling reactions of $N_2(A)$ are, indeed, a source of $N_2(B)$ excitation. Measurements in Paragraph 3.3, however, have demonstrated that energy pooling of $N_2(A)$ at number densities of 10^9 to 10^{10} molecules cm^{-3} produce $N_2(B)$ number densities of only 10^3 to 10^4 molecules cm^{-3}. The active-nitrogen source of $N_2(B)$, on the other hand, generates number densities three to four orders of magnitude greater than this. Molecular hydrogen readily quenches $N_2(a')$ (Ref. 140). Adding small traces of molecular hydrogen to the active nitrogen afterglow, however, has little effect the first-positive intensities at number densities sufficient to remove all the the $N_2(a')$. The $N_2(W, v'=0)$ state lies 73.8 cm^{-1} above $N_2(B, v' = 0)$ (Ref. 179). Several workers have shown that the B- and W-states are coupled quite efficiently (Ref. 132,133,147). Collisions with the helium bath gas would couple the $N_2(W, v' = 0)$ to $N_2(B, v' = 0)$ where it would decay radiatively on the time scale of tens of microseconds. It is concluded, therefore, that high vibrational levels of the ground-electronic state of nitrogen couple with $N_2(B)$ in the reactor.

Placing the Ni screen in the reactor does attenuate the $N_2(B)$ intensities, but does not change the observed vibrational distribution (Figure 90). By rotating the screen either normal to or parallel to the gas flow, we could vary the first-positive intensity by up to a factor of 30. Similar changes in screen position reduced effective nitrogen vibrational temperatures by only only 5 to 10 percent. The $N_2(B)$ number density does vary linearly with the number density of $N_2(X, v > 5)$, as determined from vibrational temperature measurements (Fig. 93), but placing a Ni screen in the flow reduces the $N_2(B)$ number density drastically but has only a small effect on the $N_2(X, v > 5)$ number density. Thus, the correlation is only qualitative, and no quantitative relationships result from it. The measurements should be repeated using $N_2^+(C)$ as the $N_2(v)$ diagnostic.

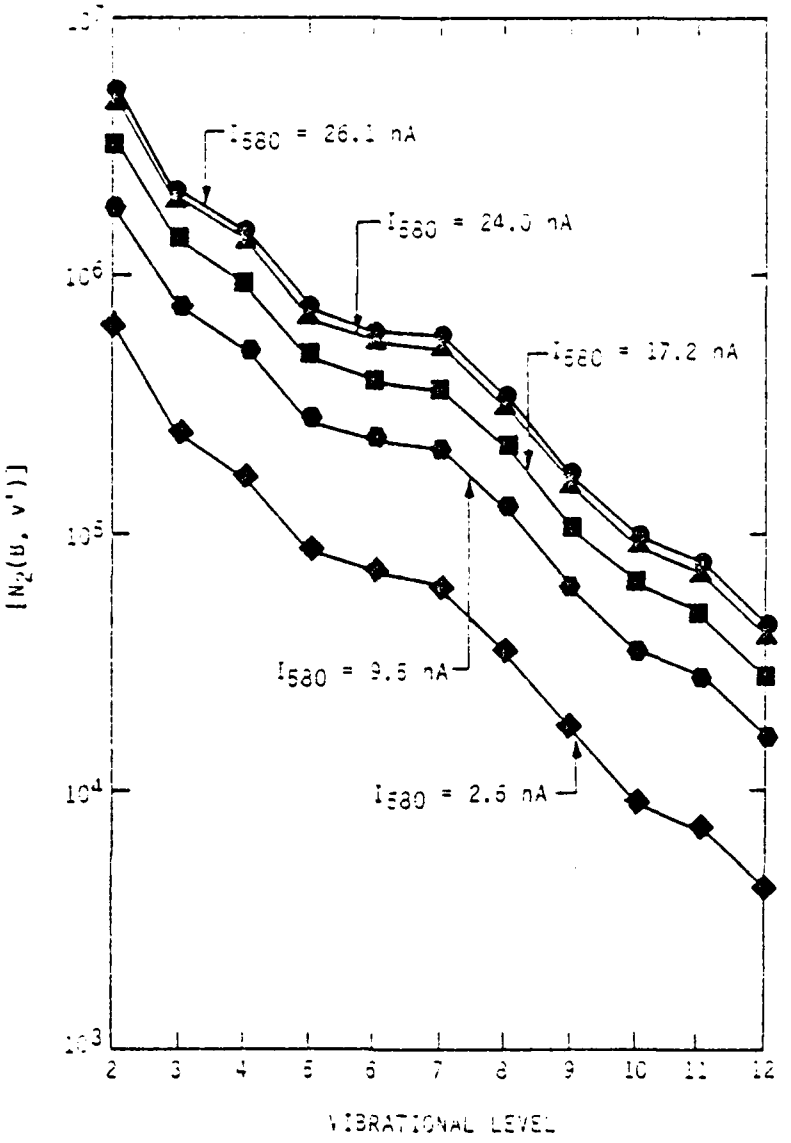

Figure 92. Vibrational distribution of $N_2(B^3\Pi_g)$ in active nitrogen for various attenuations by a Ni screen downstream from the discharge, but upstream from the observation region.

For a number of the measurements to be discussed in the next paragraph, a photometer centered at 580 nm was used to measure relative $N_2(B)$ number densities. Care must be taken in using this diagnostic that the relative vibrational distribution of the $N_2(B)$ remains constant. If the vibrational distribution does not change, Fig. 94 shows that the photometer does give an accurate determination of the $N_2(B)$ number density.

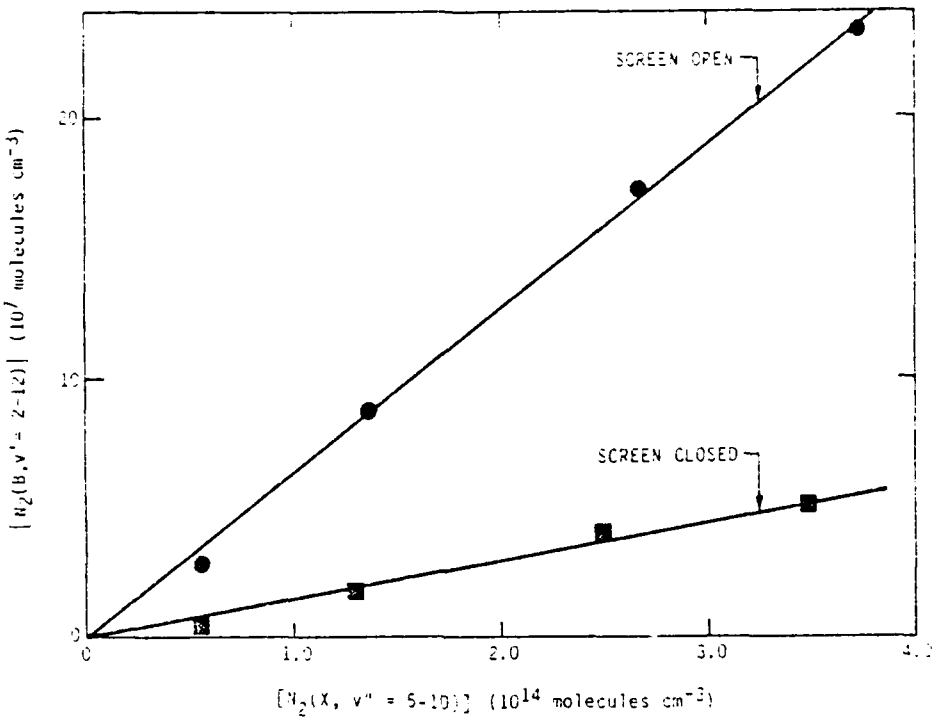

Figure 93. Variation in $N_2(B)$ number density with number density of vibrationally-excited, ground-electronic-state nitrogen.

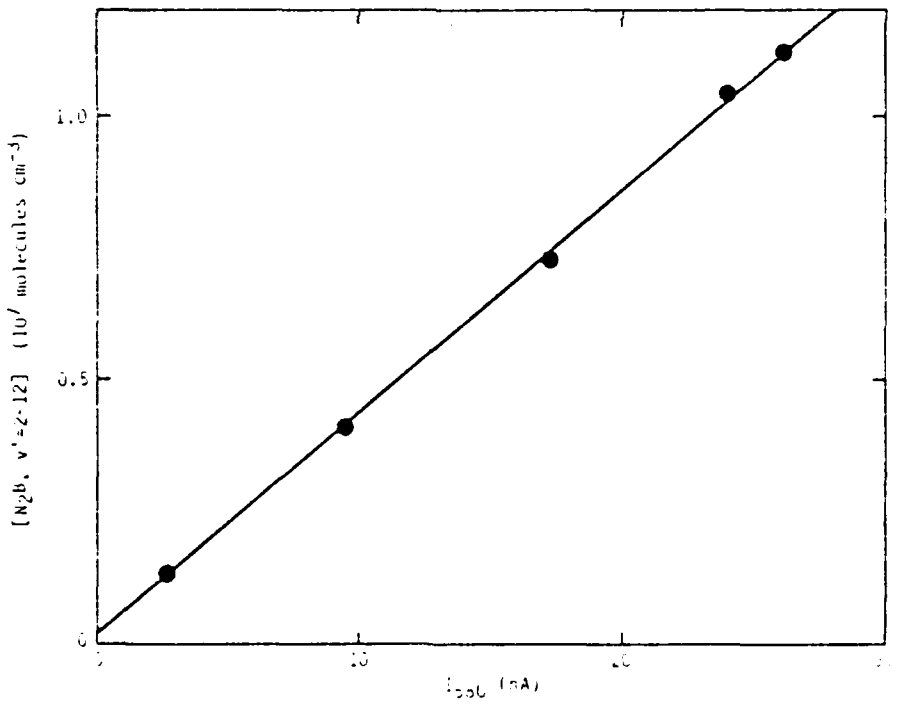

Figure 94. Variation in $N_2(B)$ number density with the signal from a photometer centered at 380 nm.

3.3.3 The excitation of IF by active nitrogen

3.3.3.1 Spectroscopy of active N_2 plus IF--Figure 95 shows the spectrum of active nitrogen between 480 and 780 nm in the absence and presence of added IF. To characterize the spectrum better, we normalized the two spectra to the 2,0 through 4,2 first-positive bands between 740 and 780 nm, and then subtracted the active nitrogen spectrum from that with active nitrogen plus IF. Figure 96 shows the result. While some of the features in the spectrum are the IF($B^3\Pi_0^+$--$X^1\Sigma^+$), a number of the spectral features belong to bands have not been identified as being known bands of IF or similar molecules. Two such systems have been identified which are labeled 1 and 2 in Fig. 96. Figures 97 and 98 show plots of the transition energies for systems 1 and 2, respectively, plotted against the number of the peak as it appears on the spectrum. Assuming that the two observed sequences result either from transitions from a common upper-state vibrational level to a number of different lower-state vibrational levels, or else transitions from a number of different upper-state vibrational levels to a common lower-state vibrational level, the slopes of these plots give ω_e for the state of varying quantum number. The resulting slopes give ω_e values of 667 ± 3 and 587 ± 10 cm^{-1} for systems 1 and 2, respectively. Table 16 shows the ω_e values for the known electronic states of IF and similar molecules which might possibly be in the active nitrogen flow. System 2 is not too greatly different from the ω_e values for the ground-electronic states of IF and IN. In that case, however, the observed system would be a new one since the observed bands do not line up with any of the known transitions in IF and IN which terminate on the ground-electronic state. The ω_e value for system 1 corresponds more closely with that for the ground-electronic state of IO, but here again, the observed spectrum does not match with known transitions of IO. It was concluded that two new band systems of IF or a similar molecule had been discovered. We hope to obtain better spectra in the future to aid spectral identification.

Some of the observed spectral features are from the well known IF($B^3\Pi_0^+$--$X^1\Sigma^+$) system. Because the identity of the new systems is unknown, the

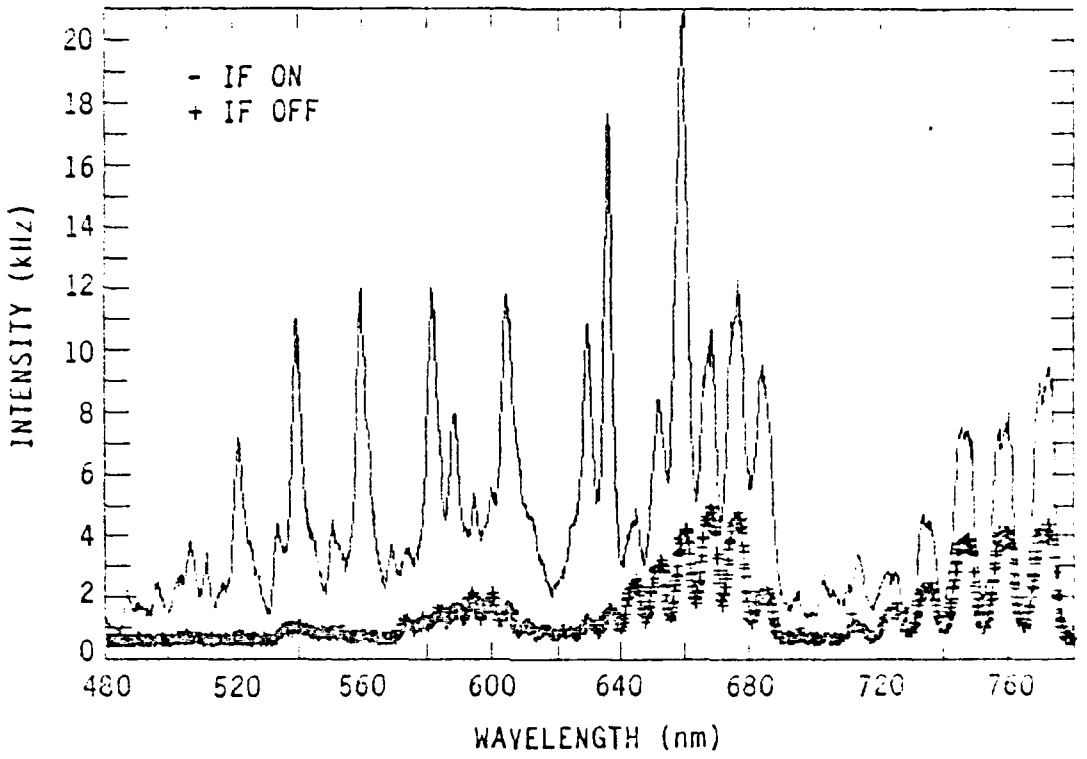

Figure 95. Spectrum of active nitrogen between 480 and 780 nm in the absence and presence of IF.

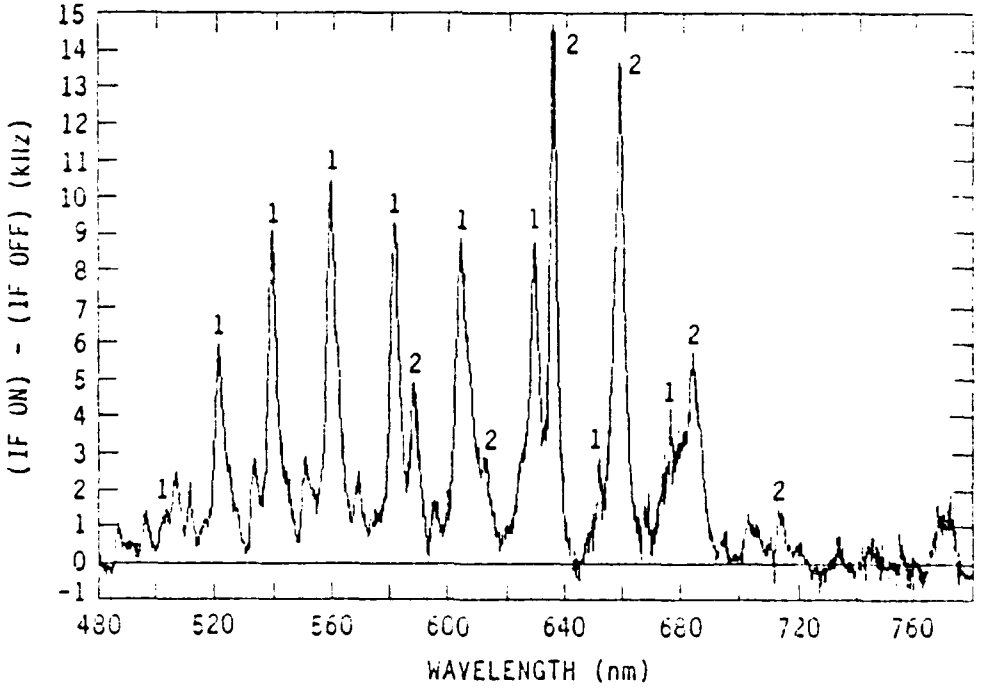

Figure 96. Spectrum between 480 and 680 nm from active nitrogen plus IF with the $N_2(B)$ spectral features subtracted out.

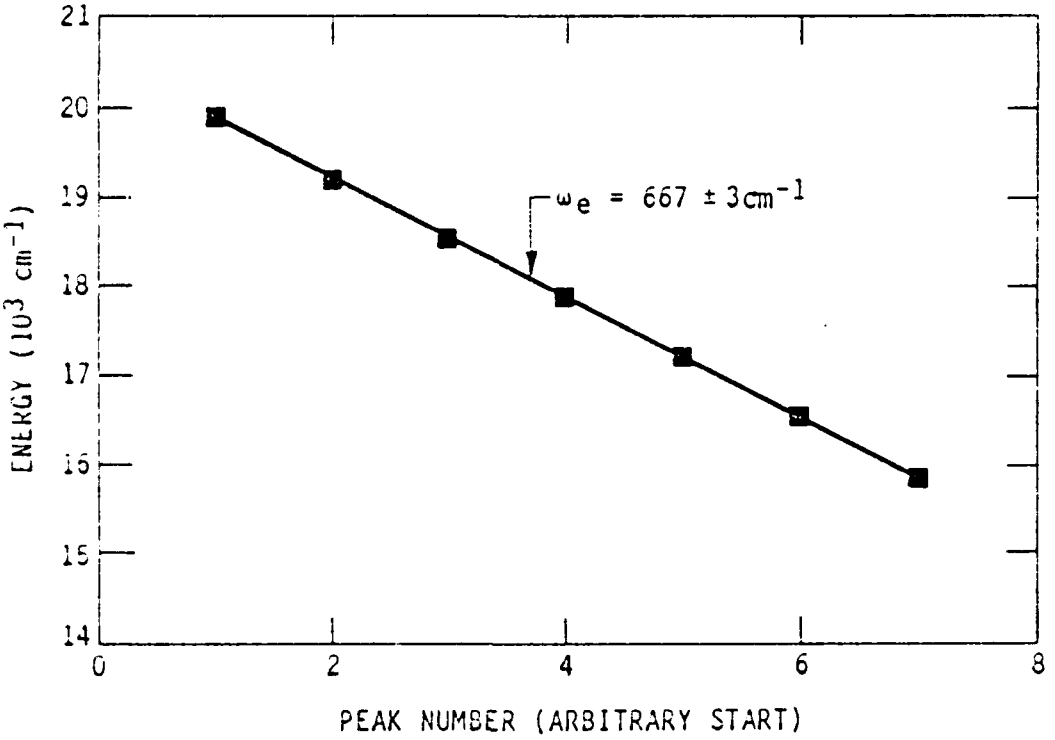

Figure 97. ω_e plot for IF system 1.

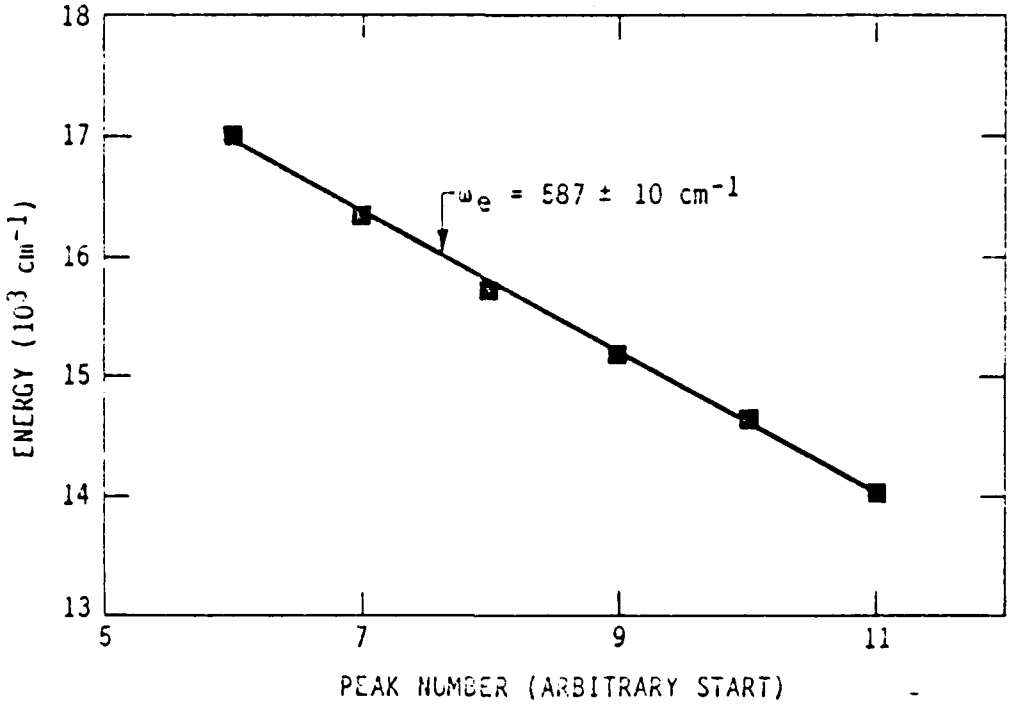

Figure 98. ω_e plot for IF system 2.

TABLE 16. Spectroscopic Parameters of IF and Similar Molecules.

Molecule	State	$\omega_e(cm^{-1})$	$T_o(cm^{-1})$
IF	D'	307	
	D'	411	19256
	A'	~250	
	A	381	15896
	X	610	305
IO	A	514.6	21815
	X	681.5	341
IN	$b^1\Sigma^+$	704	13726
	X	603	301
System 1		667±3	
System 2		587±10	

observed spectrum cannot fit by the normal least-squares approach. We have determined the contributions to the spectrum from IF(B) by fitting individual IF(B) basis functions by trial and error until an adequate agreement is obtained with the obvious IF(B) features. Figures 99 through 101 illustrate this procedure over three different wavelength regions. The observed spectra already have had the N_2 first-positive contributions subtracted out of them. The spectral region between 450 and 500 nm contains mostly bands of IF(B) from vibrational levels v' = 3-8. The populations of these vibrational levels, therefore, can be determined fairly cleanly in this spectral region. The contributions of these levels to the spectrum at longer wavelengths then will be reasonably well determined. Over the wavelength region between 500 and 600 nm, the major vibrational levels of IF(B) contributing to the spectrum are v' = 0-2. Fairly isolated bands at 533, 551, and 568 nm determine the v' = 1 population reasonably well. In the spectrum shown, the v' = 0 and 2 populations can be determined only by fitting shoulders of bands. Certain conditions in the reactor favor the IF(B) over systems 1 and 2, so that some spectral fits give quite good populations for v' = 0. Figure 102 summarizes the

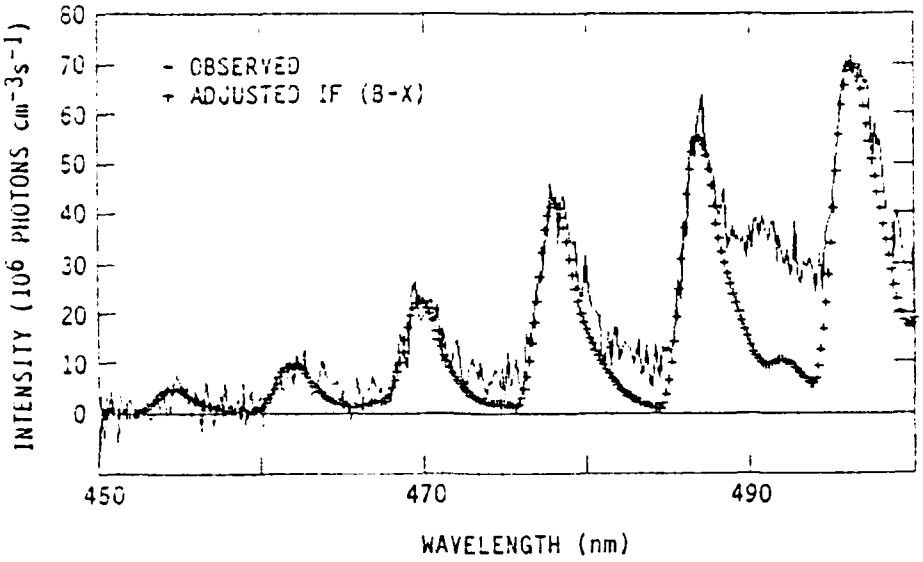

Figure 99. Fitting of the IF($B^3\Pi_0^+$--$X^1\Sigma^+$) bands between 450 and 500 nm to the spectrum excited by adding IF to active nitrogen.

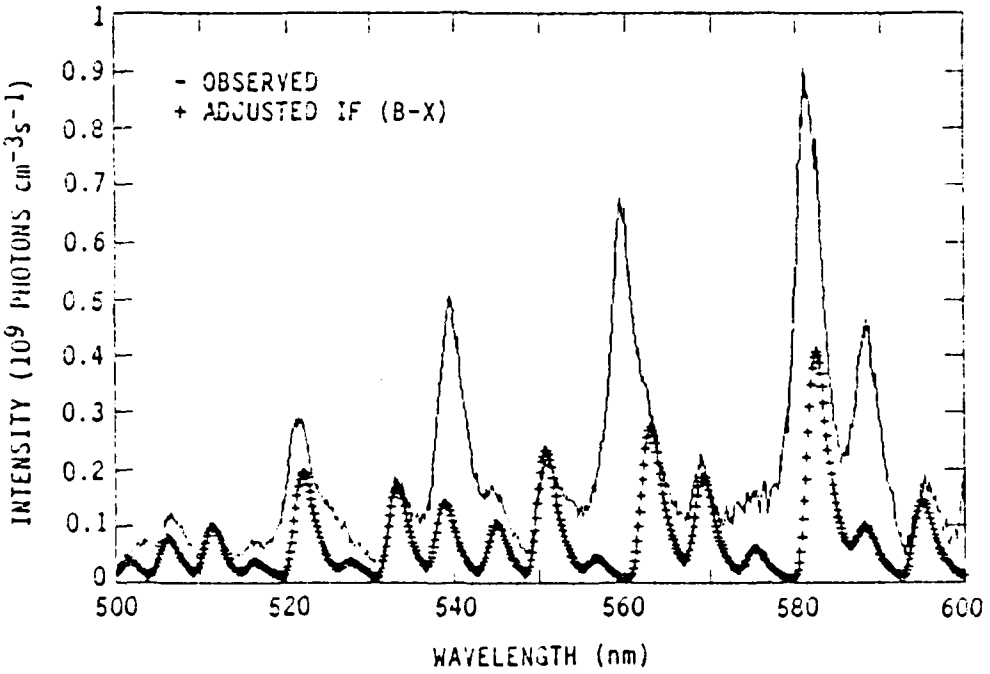

Figure 100. Fitting of the IF($B^3\Pi_0^+$--$X^1\Sigma^+$) bands between 500 and 600 nm to the spectrum excited by adding IF to active nitrogen.

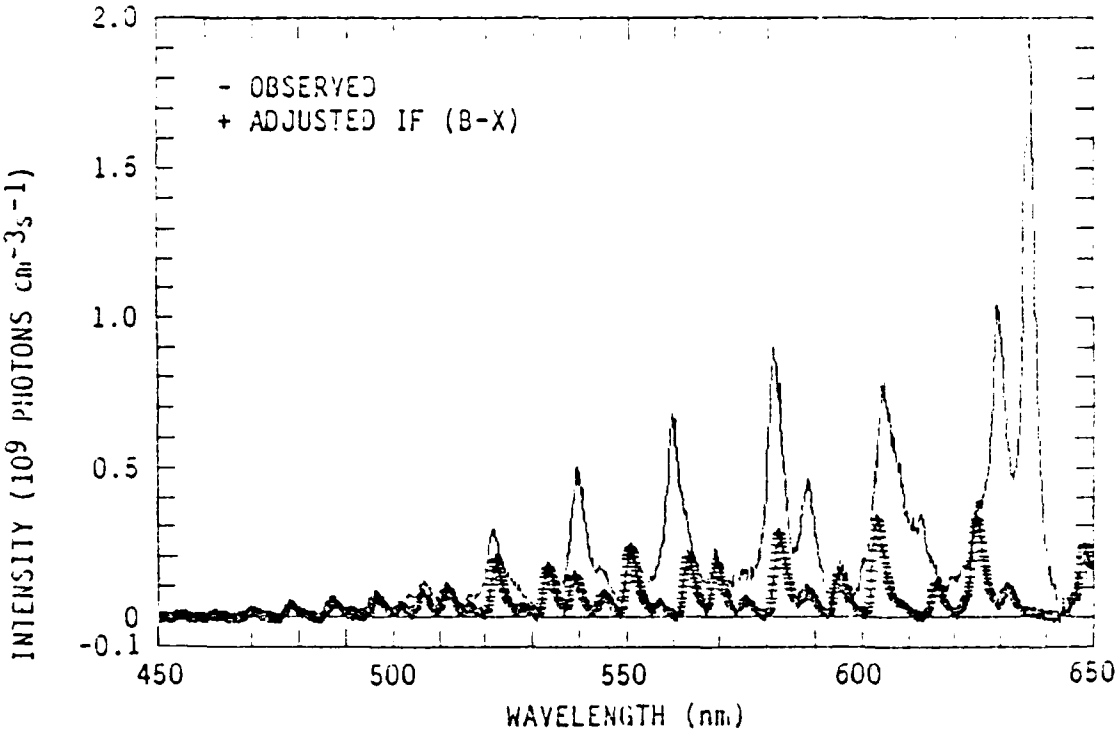

Figure 101. Fitting of the IF($B^3\Pi_0^+$--$X^1\Sigma^+$) bands between 450 and 650 nm to the spectrum excited by adding IF to active nitrogen.

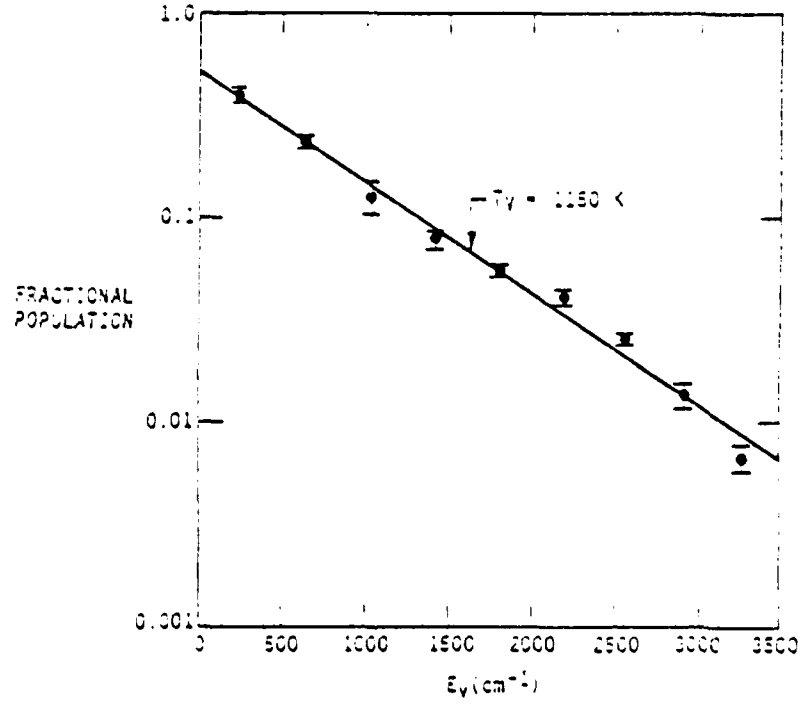

Figure 102. Vibrational distribution of IF($B^3\Pi_0^+$) excited by active nitrogen.

population distributions determined from fits to several spectra. The vibrational distribution fits quite well to that given by an 1150 K Boltzmann vibrational temperature. The significance of a Boltzmann distribution in terms of the dynamics of the energy transfer is unclear. In addition, such distributions are somewhat dependent on the conditions of the measurement since IF(B) vibrational relaxation by He, Ar, and N_2 is efficient (Refs. 6,7). Figure 103 shows the residual spectrum of the two new band systems when both the active nitrogen and the IF(B) contributions have been subtracted out. Figures 104 and 105 show spectra between 450 and 650 nm taken under conditions to enhance system 1 and IF(B) features, respectively, relative to the other two systems.

3.3.3.2 IF* Excitation Rates in Active N_2--To characterize the energy transfer between active nitrogen and IF, some IF* excitation rates have been measured. The IF* will be in steady state in the observation volume so that its formation and destruction rates can be equated. Neglecting IF* quenching gives

$$I_{IF^*} = k_{rad}[IF^*] = k_{ex}[N_2^*][IF] \qquad (107)$$

where k_{ex} is the excitation rate coefficient for IF* excitation by active N_2, and k_{rad} is the IF* radiative-decay rate. Equation (107) shows that without knowing the identity of the precursor for the IF* excitation, the product of the excitation-rate coefficient and the number density of the precursor species can be determined.

Figure 106 shows the variation in the intensity of the 5,0 band of IF(B) as a function of number density of added IF for a number of different initial $N_2(B)$ number densities in the reactor. The $N_2(B)$ number density was varied by changing the angle of rotation of a Ni screen in the flow, and was monitored with the 580 nm photometer. Figure 107 shows that the excitation rates determined from the slopes of the lines in Fig. 106, corrected for absolute photon emission rates and for the fraction of total IF(B) emission appearing in the 5,0 band, vary linearly with the measured $N_2(B)$ number densities. If $N_2(B)$ were the species responsible for the IF(B) excitation, the slope in Fig. 107

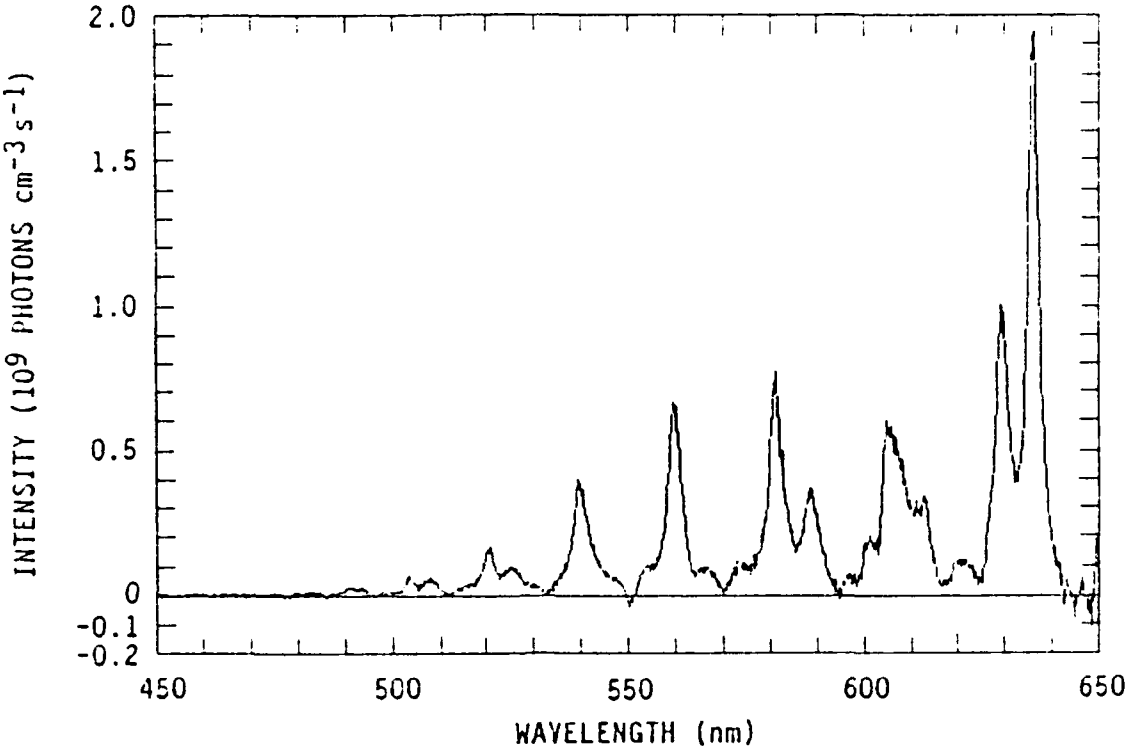

Figure 103. Residual spectrum of active nitrogen plus IF after spectral features belonging to the nitrogen first-positive and IF($B^3\Pi_0^+$--$X^1\Sigma^+$) systems have been subtracted out.

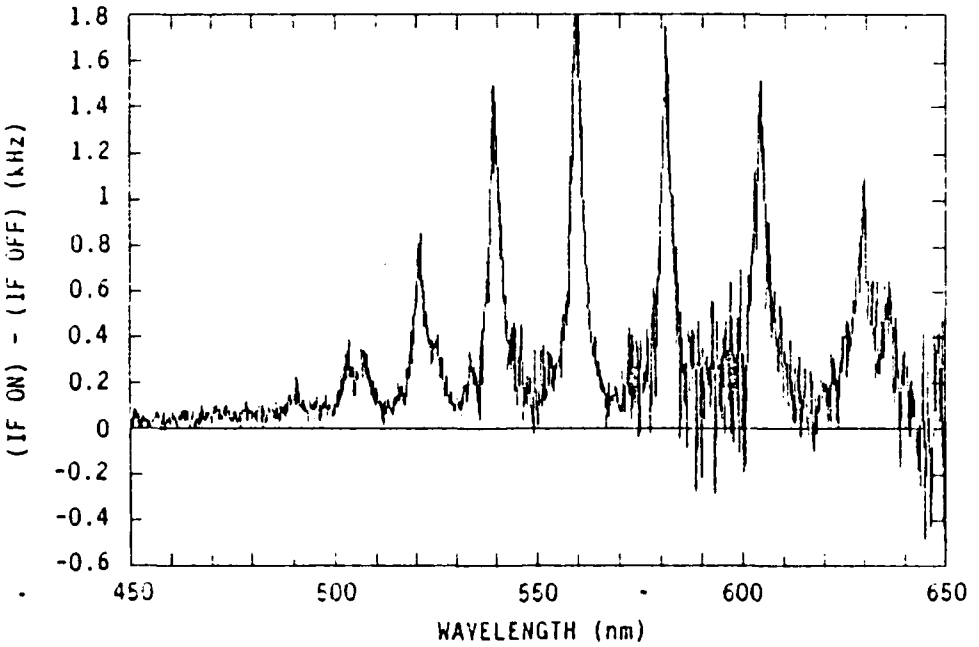

Figure 104. Spectrum of active nitrogen plus IF with the nitrogen first-positive features subtracted out taken under conditions which enhance IF system 1 relative to other IF spectral features.

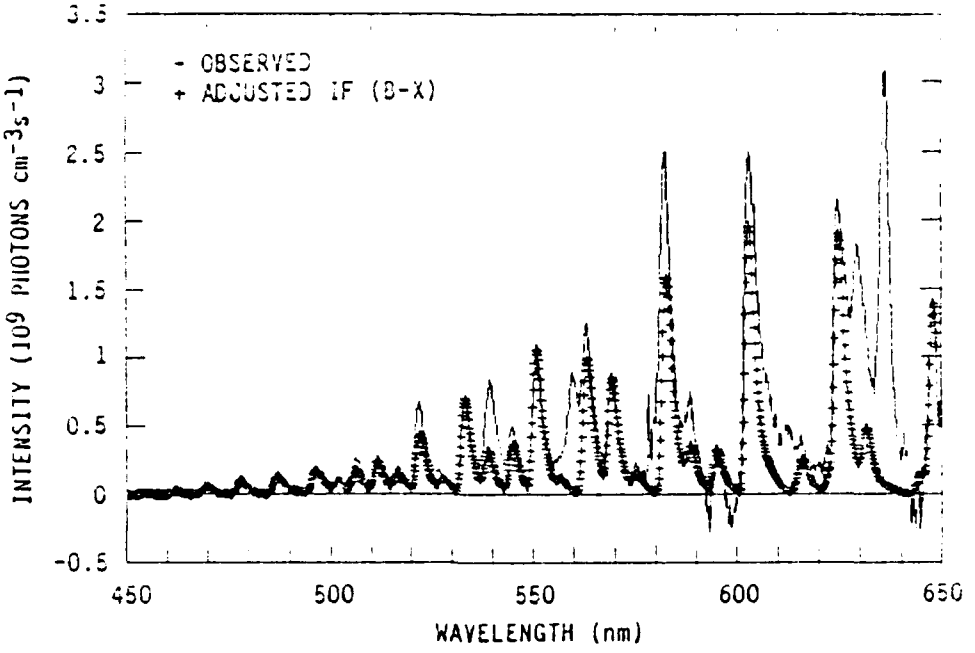

Figure 105. Spectrum of active nitrogen plus IF with the nitrogen first-positive features subtracted out taken under conditions which enhance the IF(B-X) system relative to other IF spectral features.

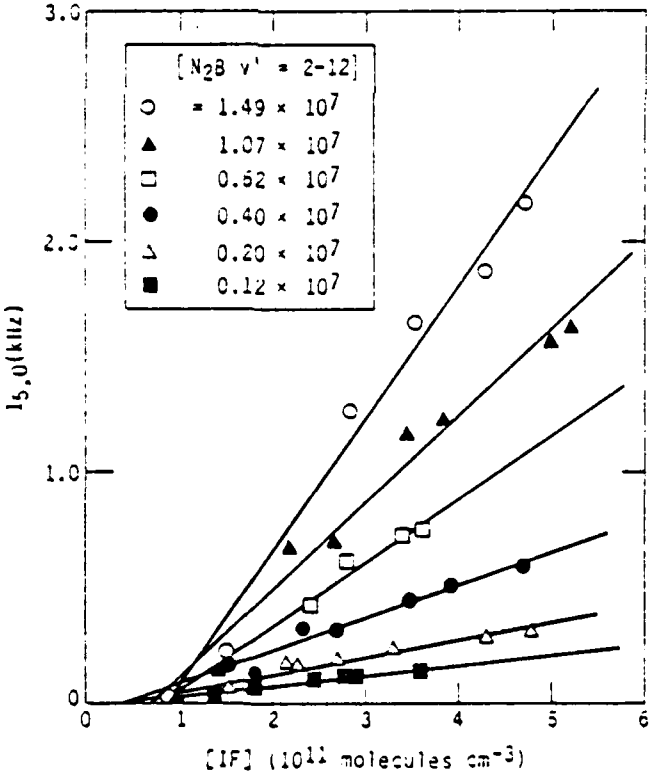

Figure 106. Variation in the intensity of the IF(B, 5,0) band as a function of added IF number density for various number densities of $N_2(B)$ in the flow reactor.

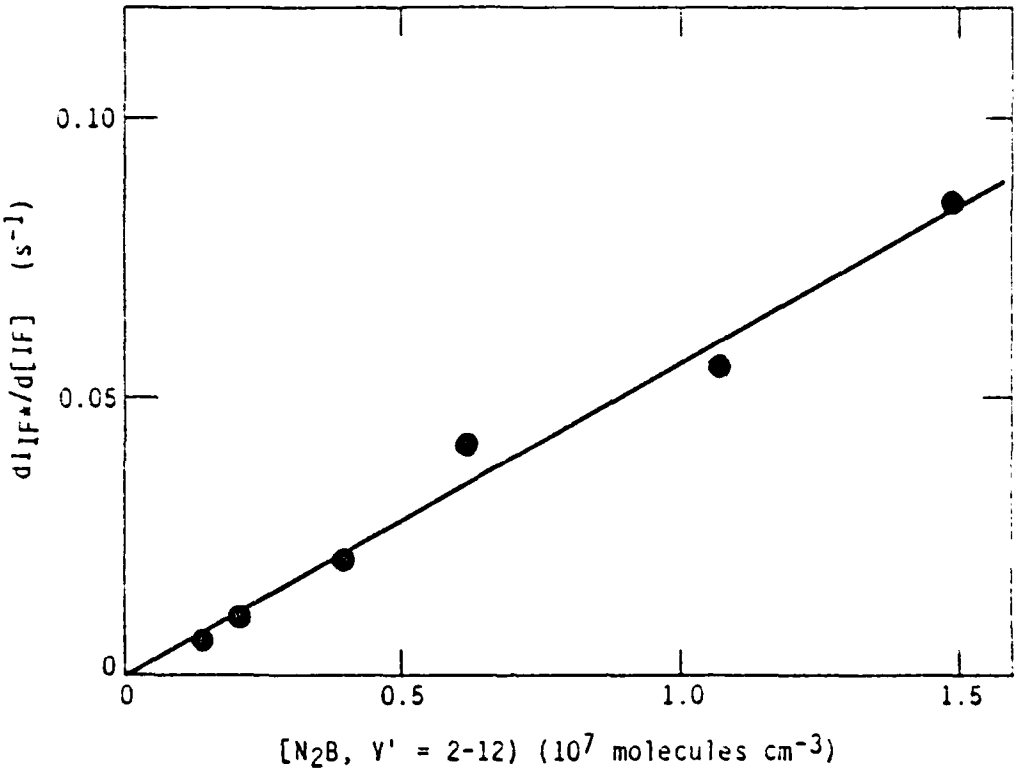

Figure 107. Excitation rates of IF(B) versus $N_2(B)$ number density.

would give the excitation rate coefficient. The value derived, however, is $(5.6 \pm 0.4) \times 10^{-3}$ cm^{-3} $molecule^{-1}$ s^{-1}, more than an order of magnitude greater than gas kinetic, meaning that $N_2(B)$ cannot be the excitation partner. The data show quite clearly that the excitation rates do vary with $N_2(B)$ number density. A previous study indicated this was probably true (Ref. 6), but scatter in that data prevented unequivocal confirmation of this correlation. Figure 108 shows that the intensity of the series 2 band at 636 nm varies linearly with added IF, and Fig. 109 shows that the series 1 and 2 band intensities also vary linearly with the $N_2(B)$ number density in the flow reactor when the IF number density is held constant. We wish to stress that the $N_2(B)$ does not appear to be the actual precursor itself, rather the metastable which excites the IF^* emissions apparently also is coupled collisionally to the $N_2(B)$ state.

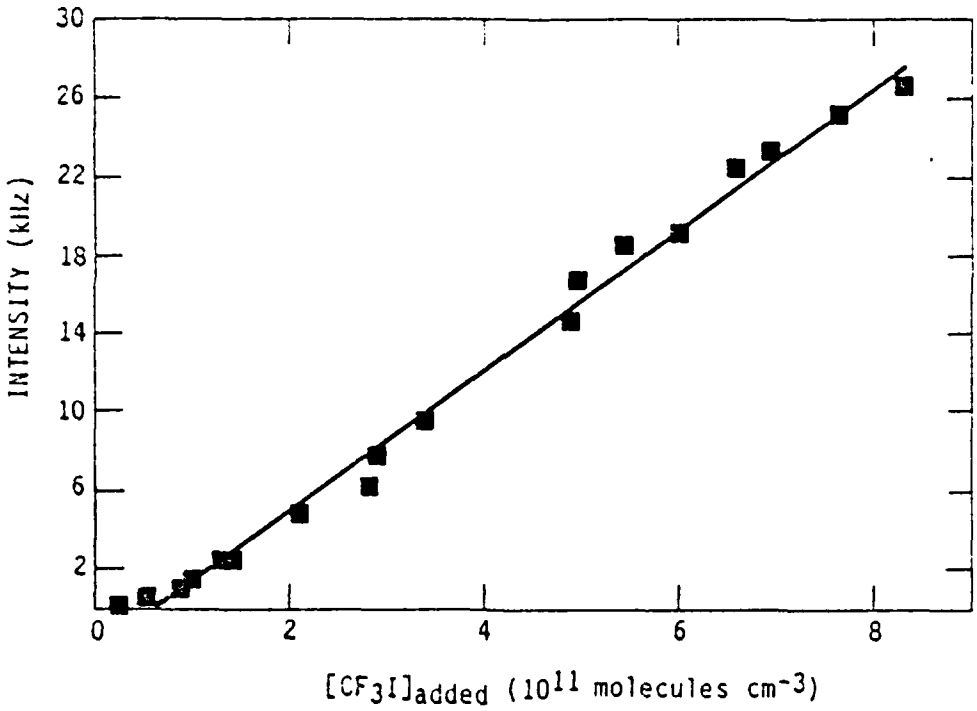

Figure 108. Intensities of the IF series 2 band at 636 nm as a function of added IF number density.

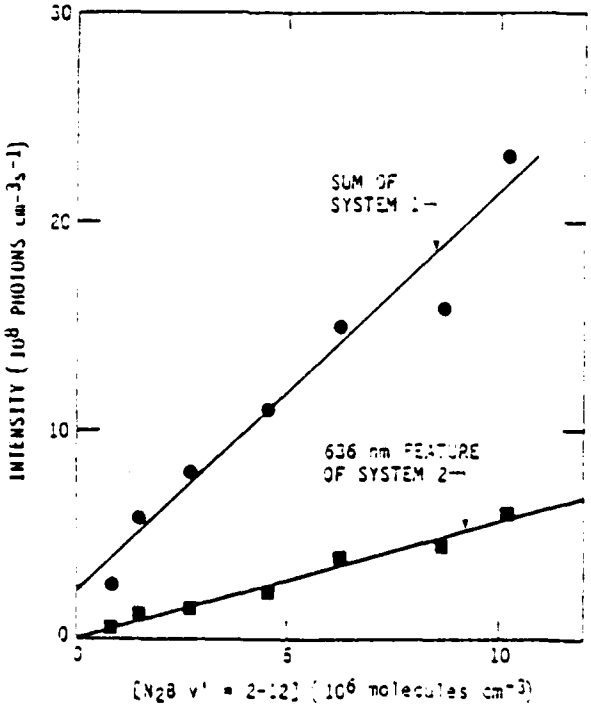

Figure 109. Intensities of IF series 1 and series 2 emissions as a function of $N_2(B)$ number density for constant IF number density.

In the previous study, the excitation rates of IF(B) were chosen to be either too large to be caused by the known long-lived metastables in the reactor, or else they varied in a way which was incompatible with expected variations in the number densities of other metastables in the reactor. This point still remains to be proven unequivocally. In particular, simultaneous determination of IF^* excitation rates and number densities of the atomic nitrogen metastables, $N(^2D, ^2P)$ remains to be done. In addition, the $N_2(A^3\Sigma_u^+)$ number density in the active nitrogen has not been pinned down, although the observed IF(B) vibrational distribution is incompatible with excitation primarily by $N_2(A)$, and the previous studies demonstrated clearly that systems 1 and 2 are not products of the interaction of $N_2(A)$ with IF (Ref. 7). The IF(B) excitation rates measured in this study are somewhat smaller than those determined previously, but transit times between the discharge and the observation region were somewhat shorter, so presumably the number density of the active species has been quenched somewhat more extensively in the present work.

REFERENCES

1. Cheah, C.T., Clyne, M.A.A., and Whitefield, P.D., "Reactions Forming Electronically-Excited Free Radicals, I. Ground State Reactions Involving NF_2 and NF Radicals," J.C.S. Faraday II 76, 711 (1980).

2. Cheah, C.T. and Clyne, M.A.A., "Reactions Forming Electronically-Excited Free Radicals. II. Formation of $N(^4S)$, $N(^2D)$, and $N(^2P)$ Atoms in the $H+NF_2$ Reaction, and N Atom Reactions," J.C.S. Faraday II 76, 1543 (1980).

3. Cheah, C.T. and Clyne, M.A.A., "Reactions Forming Electronically-Excited Free Radicals. III. Formation of Excited Molecular States in the $H-NF_2$ Reaction," J. Photo Chem. 15, 21 (1981).

4. Piper, L.G. and Taylor, R.L., "Investigation of Induced Unimolecular Decomposition for Development of Visible Chemical Lasers," PSI TR-96, prepared for the Department of Energy under Contract #EY-76-C-02-2960, *000 (1977).

5. Piper, L.G., Krech, R.H. and Taylor, R.L., "Generation of N_3 in the Thermal Decomposition of NaN_3," J. Chem. Phys. 71, 2099 (1979).

6. Piper, L.G., Marinelli, W.J., Green, B.D., Rawlins, W.T., Murphy, H.C., Donahue, M.E., and Lewis, P.F., "Kinetics of Iodine Monofluoride Excitation by Energetic Nitrogen," Final Report prepared for Air Force Contract No. F29601-80-C-0051, Physical Sciences Inc. Technical Report No. TR-460 (1985).

7. Piper, L.G., Marinelli, W.J., Rawlins, W.T., and Green, B.D., "The Excitation of $IF(B^3\Pi_{0^+})$ by $N_2(A^3\Sigma_u^+)$," J. Chem. Phys. 83, 5602 (1985).

8. Clyne, M.A.A. and White, I.F., Chem. Phys. Lett. 6, 465 (1970).

9. Herbelin, J.M. and Cohen, N., "The Chemical Production of Electronically Excited States in the H/NF_2 System," Chem. Phys. Lett. 20, 605 (1973).

10. Clyne, M.A.A. and Stedman, D.H., "Reactions of Atomic Hydrogen with Hydrogen Chloride and Nitrosyl Chloride," Trans. Faraday Soc. 62, 2164 (1966).

11. Clyne, M.A.A. and Thrush, B.A., "Mechanism of Chemiluminescent Reactions Involving Nitric Oxide -The H+NO Reaction," Discuss. Faraday Soc. 33, 139 (1962).

12. Ding, A., Karlaw, J., and Weiss, J., "Production of H-Atom and O-Atom Beams by a Cooled Microwave Discharge Source," Rev. Sci. Instrum. 48, 1002 (1977).

13. Kwok, M.A., Herbelin, J.M., and Cohen, N., "Collisional Quenching and Radiation Decay Studies of NF($a^1\Delta$) and NF($b^1\Sigma$)," Electronic Transition Lasers, MIT Press (1976).

14. Fontijn, A., Meyer, C.B., and Schiff, H.I., "Absolute Quantum Yield Measurements of the NO-O Reaction and Its Use a Standard for Chemiluminescent Reactions," J. Chem. Phys. 40, 64 (1964).

15. Vanpee, M., Hill, K.D., and Kineyko, W.R., "Absolute Rate Constant Measurements for the Radiative Combination of Atomic Oxygen with Nitric Oxide," AIAA J. 9, 135 (1971).

16. Golde, M.F., Roche, A.E., and Kaufman, F., "Absolute Rate Constant for the O+NO Chemiluminescence in the Near Infrared," J. Chem. Phys. 59, 3953 (1973).

17. Golomb, D. and Brown, J.H., "The Temperature Dependence of the NO-O Chemiluminous Recombination. The RMC Mechanism," J. Chem. Phys. 63, 5246 (1975).

18. Woolsey, G.A., Lee, P.H., and Slafer, W.D., "Measurement of the Rate Constant for NO-O Chemiluminescence Using a Calibrated Piston Source of Light," J. Chem. Phys. 67, 1220 (1977).

19. Sutoh, M., Morioka, Y., and Nakamura, M., "Absolute Rate Constant for the Chemiluminescent Reaction of Atomic Oxygen with Nitric Oxide," J. Chem. Phys. 72, 20 (1980).

20. Pravilov, a.M. and Smirnova, L.G., "Spectral Distribution of the Chemiluminescence Rate Constant in the O+CO(+M) and O+NO(+He) Reactions," Kinet. and Catal. 19, 202 (1978).

21. Kaufman, F., "The Air Afterglow and Its Use in the Study of Some Reactions of Atomic Oxygen," Proc. Roy. Soc. (London) A 247, 123 (1958).

22. Kaufman, F., "The Air Afterglow Revisited," Chemiluminescence and Biluminescence, M.J. Cormier, D.M. Hercules, and J. Lee, eds., pp. 63-100 (1973).

23. Husain, D. and Slater, N.K.H., "Kinetic Study of Ground State Atomic Nitrogen, N($2^4S_{3/2}$) by Time-Resolved Atomic Resonance Fluorescence," J.C.S. Faraday II 76, 606 (1980).

24. Lee, J.H., Michael, J.V., Payne, W.A., and Stief, L.J., "Absolute Rate of the Reaction of N(^4S) with NO from 196-400 K with DF-RF and FP-RF Techniques," J. Chem. Phys. 69, 3069 (1978).

25. Clyne, M.A.A. and McDermid, I.S., "Mass Spectrometric Determinations of the Rates of Elementary Reactions of NO and NO_2 with Ground State N(^4S) Atoms," J.C.S. Faraday I, 71, 2189 (1975).

26. Slanger, T.G., "Generation of $O_2(c^1\Sigma_u^-, C^3\Delta_u, A^3\Sigma_u^+)$ from Oxygen Atom Recombination," J. Chem. Phys. 63, 4779 (1978).

27. L.G. Piper, unpublished results (1978).

28. Baulch, D.L., Drysdale, D.D., Horne, D.G., and Lloyd, A.C., Evaluated Kinetic Data for High Temperature Reactions. II. Homogeneous Gas Phase Reactions of the H_2-N_2-O_2 Systems. (Butterworths, London, 1973).

29. Piper, L.G., Murphy, H.C., and Rawlins, W.T., "Development of Cochise UV Absorption System," AFGL-TR-81-0318 (1981).

30. Mitchell, A.C.G. and Zemansky, M.W., "Resonance Radiation and Excited Atoms," Cambridge University Press, London U.K. (1971).

31. Rawlins, W.T. and Kaufman, F., "Characteristics of O(I) and N(I) Resonance Line Broadening in Low Pressure Helium Discharge Lamps," J. Quant. Spectrosc. Radiat. Transfer 18, 561 (1977).

32. Kaufman, F., and Parkes, D.A., "Sources of Error in Using Resonance Light Absorption to Measure Atomic Concentrations," Trans. Faraday Soc. 66, 1579 (1970).

33. Tellinghuisen, J. and Clyne, M.A.A., "Role of Hyperfine Structure in Atomic Absorption: Oscillator Strengths in Br and I," J.C.S. Faraday II 72, 783 (1976).

34. Clyne, M.A.A. and Piper, L.G., "Kinetic Spectroscopy in the Far Vacuum Ultraviolet, Parts 3. Oscillator Strengths for the 3S, 4S, and 5S ^3S-$2p^4$ $^3P_2$ Transitions in Atomic Oxygen," J.C.S. Faraday II 72, 2178 (1976).

35. a. Clyne, M.A.A. and Monkhouse, P.B., "Energy Transfer in Collisions of $Ar(^3P_{0,2})$ Metastable Atoms with $H(^2S)$ Atoms. I. Total Rate Constant and Mechanism," Chem. Phys. 28, 447 (1978).

b. Clyne, M.A.A., Heaven, M.C., Bayes, K.D., and Monkhouse, P.B., "Energy Transfer in Collisions of Excited $Ar(^3P_{0,2})$ Metastable Atoms with $H(^2S)$ Atoms. II. Lyman-α Emission Profile," Chem. Phys. 47, 179 (1980).

c. Piper, L.G. and Clyne, M.A.A., "Determination of the Translational Energy of $O(3s^3S)$ Excited by the Dissociative Excitation of O_2 and NO by $He^*(2^3S)$," Chem. Phys. 63, 77 (1981).

36. Donahue, T.M., Anderson, J.G., Rawlins, W.T., Kaufman, F., and Hudson, R.D., "Apollo-Suyuz $O(^3P)$ and $N(^4S)$ Density Measurement by UV Spectroscopy," Geophys. Res. Lett. 4, 79 (1977).

37. Malins, R.J. and Setser, D.W., "Rate Constants, Branching Ratios, and Energy Disposal for $NF(b,a,X)$ and $HF(v)$ Formation for the $H+NF_2$ Reaction," J. Phys. Chem. 85, 1342 (1981).

38. Lofthus, A., and Krupenie, P.H., "The Spectrum of Molecular Nitrogen," J. Phys. Chem. Ref. Data 6, 287 (1977).

39. Piper, L.G., Donahue, M.E., and Rawlins, W.T., "Rate Coefficients for $N(^2D)$ Reactions," J. Phys. Chem., submitted (1986).

40. Koffend, J.B., Gardner, C.E., and Heidner, R.F., "Kinetics of the H_2-NF_2 System," Aerospace Report SD-TR-85-55 (1985).

41. Burrows, M.D., Baughcum, S.L., and Oldenborg, R.C., "Optically Pumped $NO(A^2\Sigma^+ \rightarrow X^2\Pi)$ Ultraviolet Laser," Appl. Phys. Lett. 46, 22 (1985).

42. Hill, R.M., Gutcheck, R.A., Huestis, D.L., Mukherjee, D. and Lorents, D.C., "Studies of E-beam Pumped Molecular Lasers," SRI Report No. MP74-39 under ARPA Contract No. N00014-72-C-0478 (1974).

43. Clark, W.G. and Setser, D.W., "Energy Transfer Reactions of $N_2(A\ ^3\Sigma_u^+)$ V: Quenching by Hydrogen Halides, Methyl Halides, and Related Molecules," J. Phys. Chem. 84, 2225 (1980).

44. Young, R.A. and St. John, G.A., "Experiments on $N_2(A^3\Sigma_u^+)$. II. Excitation of NO," J. Chem. Phys. 48, 898 (1971).

45. Callear, A.B. and Wood, P.M., "Rates of Energy Transfer From $N_2(A^3\Sigma_u^+)$ to Various Molecules. Initial and Final Quantum States in the Transfer to NO $X^2\Pi$ and H_2 (6^1S_0) and Vibrational Relaxation of N_2 $(A^3\Sigma_u^+)$ $(v = 1)$ in in Helium," Trans. Faraday Soc. 67, 272 (1971).

46. Mandel, A. and Ewing, J.J., "Quenching of $N_2(A^3\Sigma_u^+)$ by I_2," J. Chem. Phys. 67, 3490 (1977).

47. Dreyer, J.W., Perner, D. and Roy, C.R., "Rate Constants for the Quenching of $N_2(A^3\Sigma_u^+, v_A = 0\text{-}8)$ by CO, CO_2, NH_3, NO and O_2," J. Chem. Phys. 61, 3164 (1974).

49. Rawlins, W.T., Piper, L.G., Caledonia, G.E. and Green, B.D., "COCHISE Research," Physical Sciences Inc. Technical Report TR-298 (1981).

50. Piper, L.G., Caledonia, G.E. and Kennealy, J.P., "Rate Constants for Deactivation of $N_2(A\ ^3\Sigma_u^+\ v'=0,1)$ by O_2," J. Chem. Phys. 74, 2888 (1981).

51. Piper, L.G., Caledonia, G.E. and Kennaly, J.P., "Rate Constants for Deactivation of $N_2(A\ ^3\Sigma_u^+\ v'=0,1)$ by O," J. Chem. Phys. 75, 2847 (1981).

52. Piper, L.G., "The Excitation of $O(^1S)$ in the Electronic Energy Transfer Between $N_2(A\ ^3\Sigma_u^+)$ and O," J. Chem. Phys. 77, 2373 (1982).

53. Piper, L.G., Murphy, H.C. and Rawlins, W.T., "Development of COCHISE UV Absorption System: Final Report," TR-292 (November 1981), AFGL-TR-81-0318, Air Force Geophysics Laboratory Report (1981).

54. Rawlins, W.T. and Piper, L.G., "Effect of Excitation Mechanism on Linewidth Parameters of Conventional VUV Discharge Line Sources," Proc. Soc. Photo. Opt. Instr. Eng. 279, 58 (1981). Also presented at the Technical symposium East '81 of the Society of Photo-Optical Instrumentation Engineers, Washington, D.C. (April, 1981).

55. Krech, R.H., Diebold, G.J. and McFadden, D.L., "Kinetics of the O + F_2 Reaction: A Case of Low Reactivity of Elemental Fluorine," J. Am. Chem. Soc. 99, 4605 (1977).

56. Krech, R.H., "ESR Discharge - Flow Kinetics: The O + F_2 Reaction," Masters dissertation, Dept. of Chem., Boston College, 1976.

57. Pak, S.J., Krech, R.H., McFadden, D.L. and MacLean, D.I., "EPR Discharge-Flow Kinetics: The H - ClF_3 Reaction," J. Chem. Phys. 62, 3419 (1975).

58. Kaufman, M. and Kolb, C.E., "Molecular Beam Analysis of the Reaction Between Atomic Fluorine and Carbon Tetrachloride," NR 092-531, 6 (1971).

59. Berg, H.C. and Kleppner, D., "Storage Technique for Atomic Hydrogen," Rev. Sci. Instrum. 33, 248 (1962).

60. Lewis, P.F. and Green, B.D., "Computation of Electronic Spectra of Diatomic Molecules," PSI TR-413 (1984).

61. Setser, D.W., Stedman, D.H., and Coxon, J.A., "Chemical Applications of Metastable Argon Atoms. IV. Excitation and Relaxation of Triplet States of N_2," J. Chem. Phys. 53, 1004 (1970).

62. Stedman, D.H. and Setser, D.W., "Chemical Applications of Metastable Argon Atoms II. A Clean System for the Formation of $N_2(A\ ^3\Sigma_u^+)$," Chem. Phys. Lett. 2, 542 (1968).

63. Sadeghi, N. and Setser, D.W., "Primary $N_2(B)$ Vibrational Distributions from Excitation-Transfer Reactions Between $Kr(^3P_2)$ or $Xe(^3P_2)$ Atoms and N_2," Chem. Phys. Lett. 82, 44 (1981).

64. Thomas, J.M. and Kaufman, F., "Production and Kinetics of $N_2(A\ ^3\Sigma_u^-$, $v<3)$," Photochemistry Symposium, Harvard University, August (1984).

65. Golde, M.F., "Vacuum UV Emission by Electronically Excited N_2: The Collisional-Induced $N_2(a\ ^1\Pi_g\ v=0) \rightarrow N_2(a'\ ^1\Sigma_u^-, v'=0)$ Transition," Chem. Phys. Lett. 31, 348 (1975).

66. Thomas, J.M., Jeffries, J.B. and Kaufman, F., "Vibrational Relaxation of $N_2(A\ ^3\Sigma_u^+, v'=1,2,3)$ by CH_4 and CF_4," Chem. Phys. Lett. 102, 50 (1983).

67. Robinson, D. and Nicholls, R.W., "Intensity Measurements on the O_2^+ Second Negative, CO Angstrom and Third Positive an NO γ and β Molecular Band Systems," Proceedings of the Physical Society LXXI, 957 (1958).

68. Keck, J.C., Allen, R.A. and Taylor, R.L., "Electronic Transition Moments for Air Molecules," J. Quant. Spectrosc. Radiat. Transfer 3, 335 (1963).

69. Callear, A.B., Pilling, M.J. and Smith, I.W.M., Trans. Faraday Soc. 62, 2997 (1966).

70. Bubert, H., "Population and Predissociation of Vibronic States of Nitric Oxide," J. Chem. Phys. 56, 1113 (1972).

71. Brzozowski, J., Erman, P. and Lyyra, M., "Predissociation Rates and Perturbations of the A, B, B', C, D and F States in NO Studied Using Time Resolved Spectroscopy," Physica Scripta 14, 290 (1976).

72. Kuz'menko, N.E., Kuznetsova, L.A., Monyakin, A.P. and Kuzyakov, Yu. Ya., "Probabilities for Electronic Transitions of Molecular Systems of High-Temperature Air Components--II. The γ and β Systems of NO and the (4+) System of CO," J. Quant. Spectrosc. Radiat. Transfer 24, 219 (1980).

73. Poland, H.M. and Broida, H.P., "Fluorescence of the γ, ε and β Systems of Nitric Oxide; Polarization and Use of Calculated Intensities for Spectrometer Calibration," J. Quant. Spectrosc. Radiat. Transfer 11, 1863 (1971).

74. Jeunehomme, M., "Transition-Moment Variation in the γ System of NO", J. Chem. Phys. 45, 4433 (1966).

75. Mumma, M.J., "Molecular Branching-Ratio Method for Intensity Calibration of Optical Systems in the Vacuum Ultraviolet," J. Opt. Soc. Amer. 62, 1459 (1972).

76. Mohlmann, G.R., Van Sprang, H.A., Bloemen, E. and De Heer, F.J., "Experimental Determination of the Electronic Transition Moment for the NO($A\ ^2\Sigma^+ - X\ ^2\Pi$) System. Lifetimes of the NO($A\ ^2\Sigma$, v'=0,1,2) Levels," Chem. Phys. 32, 239 (1978).

77. McGee, T.J., Miller, G.E., Burris, J., Jr. and McIlrath, T.J., "Fluorescence Branching Ratios from the $A\ ^2\Sigma^+$(v'=0) State of NO," J. Quant. Spectrosc. Radiat. Transfer 29, 333 (1983).

78. Navati, B.S. and Korwar, V.M., "Electronic Transition Moment Variation for the $A\ ^2\Sigma - X\ ^2\Pi$ Transition of the NO Molecule," Physica 124C, 421 (1984).

79. Witt, G., Dye, J. and Wilhelm, N. and "Rocket-borne Measurements of Scattered Sunlight in the Mesosphere," J. Atmos. Terr. Phys. 38, 223 (1976).

80. Slanger, T.G., Bischel, W.K., Dyer, M.J., "Nascent NO Vibrational Distribution from 2485 Å NO_2 Photodissociation," J. Chem. Phys 79, 2231 (1983).

81. Herm, R.R., Sullivan, B.J. and Whitson, M.E., "Nitric Oxide Vibrational Excitation from the $N(^4S) + O_2$ Reaction," J. Chem. Phys. 79, 2221 (1983).

82. Nicholls, R.W., "Franck-Condon Factors to High Vibrational Quantum Numbers IV: NO Band Systems," J. Res. NBS 68A, 535 (1964).

83. Albritton, D.L., Schmeltekopf, A.L. and Zare, R.N., "Diatomic Intensity Factors," private communication via D.W. Setser (1985).

84. Zacharias, H., Halpern, J.B. and Welge, K.H., "Two-Photon Excitation of NO($A\ ^2\Sigma^+$; v'=0,1,2,) and Radiation Lifetime and Quenching Measurements," Chem. Phys. Let. 43, 41 (1976).

85. Smith, A.J. and Read, F.H., "Measured Lifetimes of the $A\ ^2\Sigma^+$, $D\ ^2\Sigma^+$ and $C\ ^2\Pi$ States of NO," J. Phys. B: Atom. Molec. Phys. 11, 3263 (1978).

86. McDermid, I.S. and Laudenslager, J.B., "Radiative Lifetimes and Electronic Quenching Rate Constants for Single-Photon Excited Rotational Levels of NO ($A\ ^2\Sigma^+$, v'=0)," J. Quant. Spectrosc. Radiat. Transfer 27, 483 (1982).

87. Crosley, D.R., Zare, R.N., J. Chem. Phys. 49, 4231 (1968).

88. Brozozowski, J., Elander, N. and Erman, P., Phys. Scr. 9, 99 (1974).

89. Benoist D'Azy, O., Lopez-Delgado, R. and Tramer, A., Chem. Phys. 9, 327 (1975).

90. Hesser, J., J. Chem. Phys. 48, 2518 (1968).

91. Bubert, H. and Froben, F.W., Chem. Phys. Lett. 8, 242 (1971).

92. German, K.R., Zare. R.N. and Crosley, D.R., J. Chem. Phys. 54, 4039 (1971).

93. Weinstock, E.M. and Zare, R.N., "Lifetime Determination of the NO $A\ ^2\Sigma^+$ State," J. Chem. Phys. 56, 3456-3462 (1972).

94. Hasson, V., Farmer, A.J.D., Nicholls, R.W. and Anketell, J., "Application of Dispersion Techniques to Molecular Band Intensity Measurements II. Oscillator Strength of the (0,0) Band of NO-γ($A\ ^2\Sigma - X\ ^2\Pi$) System," J. Phys. B: Atom. Molec. Phys. 5, 1248 (1972).

95. Farmer, A.J.D., Hasson, V. and Nicholls, R.W., "Absolute Oscillator Strength Measurements of the (v"=0, v'=0-3) Bands of the ($A\,^2\Sigma - X\,^2\Pi$) γ-System of Nitric Oxide," J. Quant. Spectrosc. Radiat. Transfer 12, 627 (1972).

96. Pery-Thorne, A. and Banfield, F.P., J. Phys. B: Atom. Molec. Phys. 3, 1011 (1970).

97. Weber, D. and Penner S.S., "Absolute Intensities for the Ultraviolet γ-Bands of NO", J. Chem. Phys. 26 860 (1957).

98. Bethke, G.W. "Oscillator Strengths in the Far Ultraviolet. I. Nitric Oxide", J. Chem. Phys. 31, 662 (1959).

99. Ferguson, E.E., Fehsenfeld, F.C., and Schmeltekopf, A.L., "Flowing Afterglow Measurements of Ion-Neutral Reactions," Advances in Atomic and Molecular Physics V, edited by D. R. Bates, New York, Academic Press, (1970).

100. Bolden, R.C., Hemsworth, R.S., Shaw, M.J., and Twiddy, N.D., "Measurements of Thermal-Energy Ion-Neutral Reaction Rate Coefficients for Rare-Gas Ions," J. Phys. B 3, 45 (1970).

101. Farragher, A.L., "Ion-Molecule Reaction Rate Studies in a Flowing Afterglow System," Trans. Faraday Soc. 66, 1411 (1970).

102. Huggins, R.W. and Cahn, J.H., "Metastable Measurements in Flowing Helium Afterglow," J. Appl. Phys. 38, 180 (1967).

103. Walker, R.E., "Chemical Reaction and Diffusion in a Catalytic Tubular Reactor," Phys. Fluids 4, 1211 (1961).

104. Poirier, R.V. and Carr, R.W., "The Use of Tubular Flow Reactors for Kinetic Studies Over Extended Pressure Ranges," J. Phys. Chem. 75, 1593 (1971).

105. Cher, M. and Hollingsworth, C.S., "Chemiluminescent Reactions of Excited Helium with Nitrogen and Oxygen," Adv. Chem. Ser. 80, 118 (1969).

106. Kolts, J.H. and Setser, D.W., "Decay Rates of Ar(4s, $^3P_2$), Ar(4s, $^3P_0$) Kr(4s, $^3P_2$), and Xe(6s, $^3P_2$) Atoms in Argon," J. Chem. Phys. 68, 4848 (1978).

107. Shibuya, K., Imajo, T., Obi, K and Tanka, I., "Formation and quenching of Metastable $N_2A\,^3\Sigma_u^+$ in the Electronic Relaxation of NO $C^2\Pi$ and $D^2\Sigma^+$ in an NO/N_2 Mixture, J. Phys. Chem. 88, 1457 (1984).

108. Shemansky, D.E., "N_2 Vegard-Kaplan System in Absorption," J. Chem. Phys. 51, 689 (1969).

109. Shemansky, D.E., and Carleton, N.P., "Lifetime of the N_2 Vegard-Kaplan System", J. Chem. Phys. 51, 682 (1969).

110. Carleton, K.P. and Oldenberg, O., "Lifetime of the Lowest Excited Level of N_2," J. Chem. Phys. 36, 3460 (1967).

111. Eyler, E.E. and Pipkin, F.M., "Lifetime Measurements of the B $^3\Pi_g$ State of N_2 Using Laser Excitation," J. Chem. Phys. 79, 3654 (1983).

112. Shemansky, D.E. and Broadfoot, A.L., "Excitation of N_2 and N_2^+ Systems by Electrons-I Absolute Transition Probabilities," J. Quant. Spectrosc. Radiat. Transfer 11, 1385 (1971).

113. Werner, H.J., Kalcher, J. and Reinsch, E.A., "Accurate ab initio Calculations of Radiative Transition Probabilities Between the A $^3\Sigma_u^+$, B $^3\Pi_g$, W $^3\Delta_u$, B'$^3\Sigma_u^-$, and C $^3\Pi_u$ States of N_2," J. Chem. Phys. 81, 2420 (1984).

114. Yeager, D.L. and McKoy, V., "Transition Moments Between Excited Electronic States of N_2^*," Chem. Phys. 67, 2473 (1977).

115. Weiner, B. and Öhrn, Y., "A Note on the Radiative Lifetimes of the $B^3\Pi_g$ State of N_2," J. Chem. Phys. 80, 5866 (1984).

116. Jeunehomme, M., "Transition Moment of the First Positive Band System of Nitrogen," J. Chem. Phys. 45, 1805 (1966).

117. Carlson, T.A., Duric. N., Erman, P. and Larsson, M., "Collisional Transfer to the B State in N_2," Physica Scripta 19, 25 (1979).

118. Heidner, R.F., III, Sutton, D.G., and Suchard, S.N., "Kinetic Study of $N_2(B^3\Pi_g,v)$ Quenching by Laser-Induced Fluorescence," Chem. Phys. Lett. 37, 243 (1976).

119. Broadfoot, A.L. and Maran, S.P., "Electronic Transition Moment for the N_2 Vegard-Kaplan Bands," J. Chem. Phys. 51, 678 (1969).

120. Ebata, T., Anezaki, Y., Fujii, M., Mikami, N., and Ito, M., "Rotational Energy Transfer in NO($A_2\Sigma^+$, v=0 and 1) Studied by Two-Color Double-Resonance Spectroscopy," Chem. Phys. 84, 151 (1984).

121. Deperasinska, I., Beswick, J.A. and Tramer, A., "A Distorted Wave Calculation for Electronic Energy Transfer in Molecular Collisions. Application to $N_2(A\ ^3\Sigma_u^+) + CO(X\ ^1\Sigma^+) \rightarrow N_2(X\ ^1\Sigma_g^+) + CO(a\ ^3\Pi)$ System," J. Chem. Phys. 71, 2477 (1979).

122. Golde, M.F. and Moyle, A.M., "Study of the Products of the Reactions of $N_2(A^3\Sigma_u^+)$: The Effect of Vibrational Energy in $N_2(A)$," Chem. Phys. Lett. 117, 375 (1985).

123. Stedman, D.H. and Setser, D.W., "Energy Pooling by Triplet Nitrogen ($A^3\Sigma_u^+$) Molecules," J. Chem. Phys. 50, 2256 (1969).

124. Hays, G.N., Tracy, C.J., Demonchy, A.R., and Oskam, H.J., "Production of $N_2(C^3\Pi_u)$ and $N_2(C'^3\Sigma_u)$ by Mutual Collisions of $N_2(A^3\Sigma_u^+)$ Metastable Molecules," Chem. Phys. Lett. 14, 352 (1972).

125. Hays, G.N. and Oskam, H.J., "Population of N_2 ($B\ ^3\Pi_g$) by N_2 ($A\ ^3\Sigma_u^+$) During the Nitrogen Afterglow," J. Chem. Phys. 59, 1507 (1973).

126. Hays, G.N. and Oskam, H.J., "Reaction Rate Constant for $2N_2(A^3\Sigma_u^+) \rightarrow N_2(C\ ^3\Pi_u) + N_2(X\ ^1\Sigma_g^+, v' > 0)$," J. Chem. Phys. 59, 6088 (1973).

127. Nadler, I., Setser, D.W., and Rosenwaks, S., "Production of the N_2 Herman Infrared System by the Energy Pooling Reaction of $N_2(A^3\Sigma_u^+)$ Metastable Nitrogen Molecules," Chem. Phys. Lett. 72, 536 (1980).

128. Nadler, I., Rotem, A., and Rosenwaks, S., "Observation of New Bands in the N_2 Herman Infrared System and Kinetic Study of its Formation in a Pulsed-Discharge Apparatus," Chem. Phys. 69, 375 (1982).

129. Nadler, I. and Rosenwaks, S., "Studies of Energy Transfer Processes in Triplet States of N_2. I. Energy Pooling by Vibrationally selected $N_2(A^3\Sigma_u^+, v)$ Molecules," J. Chem. Phys. 83, 3932 (1985).

130. Piper, L.G., unpublished results (1980).

131. Sadeghi, N. and Setser, D.W., "Collisional Coupling of $N_2(B^3\Pi_g$ and $N_2(W^3\Delta_u)$ States Studied by Laser-Induced Fluorescence," Chem. Phys. Lett. 77, 304 (1981).

132. Sadeghi, N. and Setser, D.W., "Collisional Coupling and Relaxation of $N_2(B^3\Pi_g)$ and $N_2(W^3\Delta_u)$ Vibrational Levels in Ar and Ne," J. Chem. Phys. 79, 2710 (1983).

133. Rotem, A. and Rosenwaks, S., "Laser-Induced Fluorescence Studies of Molecular Nitrogen," Optical Engineering, 22, 564 (1983).

134. Herman, R. "Nonvelle Transition Interdite de la Molecule N_2," C. R. Acad. Sci. (Paris) 233, 738 (1951).

135. Carroll, P.K. and Sayers, N.D., "The Band Spectrum of Nitrogen: New Studies of the Triplet Systems," Proc. Phys. Soc. (London) 64, 1133 (1953).

136. Pleiter, D., "Spectral Observations on a Radio-Frequency Excited Nitrogen Jet," Can. J. Phys. 41, 1245 (1963).

137. Mahon-Smith, D. and Carroll, P.K., "Isotope Shifts and the Vibrational Structure in Some Weaker Systems of N_2," J. Chem. Phys. 41, 1377 (1964).

138. a. Michaels, H.H., in The Excited State in Chemical Physics, J.W. McGowan, ed., New York: Wiley, Vol. II, Ch. 3 (1981).

b. Michaels, H.H., private communication to S. Rosenwaks (1985). Cited in Ref. 129.

139. Gilmore, F.R., private communication (1986).

140. Piper, L.G. and DeFaccio, M.A., "Quenching Rate Coefficients for $N_2(a'^1\Sigma_u^-)$," J. Chem. Phys. submitted (1986).

141. Mitchell, K.B., "Fluorescence Efficiencies and Collisional Deactivation Rates for N_2 and N_2^+ Bands Excited by Soft X Rays," J. Chem. Phys. 53, 1795 (1970).

142. Shemansky, D.E., "$A^3\Sigma_u^+$ Molecules in the N_2 Afterglow," J. Chem. Phys. 64, 565 (1976).

143. Gartner, E.M. and Thrush, B.A., "Infrared Emission by Active Nitrogen. I. The Kinetic Behaviour of $N_2(B'^3\Sigma_u^-)$," Proc. R. Soc. Lond. A. 346, 103 (1975).

144. Gartner, E.M. and Thrush, B.A., "Infrared Emission by Active Nitrogen. II. The Kinetic Behaviour of $N_2(B'^3\Sigma_g)$," Proc. R. Soc. Lond. A. 346, 121 (1975).

145. Becker, K.H., Fink, E.H., Groth, W., Jud, W., and Kley, D., "N_2 Formation in the Lewis-Rayleigh Afterglow," Discuss. Faraday Soc. 53, 35 (1972).

146. Dreyer, J.W. and Perner, D., "The Deactivation of $N_2B^3\Pi_g$, v=0-2 and $N_2a'^1\Sigma_u^-$, v=0 by Nitrogen," Chem. Phys. Lett. 16, 169 (1972).

147. Rotem, A., Nadler, I., and Rosenwaks, S., "Direct Observation of Collision Induced Transitions from $N_2(B^3\Pi_g)$ to $N_2(B'^3\Sigma_u^-)$," J. Chem. Phys. 76, 2109 (1982).

148. Rotem, A., Nadler, I., and Rosenwaks, S., "Laser-Induced Fluorescence Studies of Collisional Coupling of $N_2(B^3\Pi_g)$ with $N_2(W^3\Delta_u)$ and $N_2(A^3\Sigma_u^+)$," Chem. Phys. Lett. 83, 281 (1981).

149. Yardley, J.T., Introduction to Molecular Energy Transfer, Academic Press, New York, 1980.

150. Marinelli, W.J., Green, B.D., Piper, L.G., and Blumberg, W.A.M., "Nitrogen First-Positive Excitation and Quenching," Manuscript in preparation.

151. Krause, H.F., Fricke, J., and Fite, W.L., "Excitation of Na D-Line in Collisions of Sodium Atoms with Internally Excited H_2, D_2, and N_2," J. Chem. Phys. 56, 4593 (1972).

152. Rich, J.W., Bergman, R.C., and Raymonda, J.W., "Vibration-Vibration Pumping of Carbon Monoxide Initiated by an Optical Source," Appl. Phys. Lett. 27, 363 (1975).

153. Starr, W., "Excitation of Electronic Levels of Sodium by Vibrationally Excited Nitrogen," J. Chem. Phys. 43, 73 (1965).

154. Piper, L.G. and Caledonia, G.E., "Long-Lived States in Nitrogen Afterglows", 38th Annual Gaseous Electronics Conference, Monterey, California(1985). Bull. Am. Phys. Soc. 26, xxx(1986).

155. Caledonia, G.E., Davis, S.J., Green, B.D., Piper, L.G., Rawlins, W.T., Simons, G.A., and Weyl, G.M., "Analysis of Metastable State Production and Energy Transfer," Physical Sciences Inc. Final Technical Report TR-576, Prepared for AFWAL under Contract No. F33615-85-C-2568 (1986).

156. Morgan, J.E. and Schiff, H.I., "The Study of Vibrationally-Excited N_2 Molecules with the Aid of an Isothermal Calorimeter," Can. J. Chem. 41, 903 (1963).

157. Harteck, P. and Reeves, R.R., Jr., "Formation and Reactions of the Excited $O_2(A^3\Sigma_u^+)$ Molecules," Discuss Faraday Soc. 37, 82 (1964).

158. Chu, A.L., Reeves, R.R., and Halstead, J.A., "Surface-Catalyzed Formation of Electronically Excited Nitrogen Dioxide and Oxygen," J. Phys. Chem. 90, 466 (1986).

159. Kenner, R.D. and Ogryzlo, E.A., "Quenching of $O_2(c^1\Sigma_u^-)$ v=0 by $O(^3P)$, $O_2(a^1\Delta_g)$, and Other Gases," Can. J. Chem. 61, 921 (1983).

160. Schmeltekoff, A.L., Ferguson, E.F., and Fensenfeld, F.C., "Afterglow Studies of the Reactions He^+ $He(2^2S)$, and O^+ with Vibrationally-Excited N_2," J. Chem. Phys. 48 (1968).

161. Young, S.J. and Horn, K.P., "Measurement of Temperatures of Vibrationally-Excited N_2," Chem. Phys. 57, 4835 (1972).

162. Young, S.J., "Measurement of Vibrational Temperature of CO and N_2 Using the $He(2^3S)$ Penning-Ionization Technique," J. Chem. Phys. 38, 1603 (1973).

163. Piper, L.G., Gundel, L., Velazco, J.E., and Setser, D.W., "Excitation of Nitrogen and Carbon Monoxide Ionic Emissions by $He(2^3S)$, He^+, and He_2^+," J. Chem. Phys. 62, 3883 (1975).

164. Caledonia, G.E. and Center, R.E., "Vibrational Distribution Functions in Anharmonic Oscillators," J. Chem. Phys. 55, 552 (1971).

165. Center, R.E. and Caledonia, G.E., "Anharmonic Effects in the Vibrational Relaxation of Diatomic Molecules in Expanding Flows," Appl. Opt. 10, 1795 (1971).

166. Jolly, J., Touzeau, M., and Ricard, A., "Determination of Non-Boltzmann Vibrational Level Populations of Excited Nitrogen Using the Penning-Ionization Technique," J. Phys. B 14, 473 (1981).

167. Marinelli, W.J. and Piper, L.G., "Franck-Condon Factors and Absolute Transition Probabilities for the IF ($B^3\Pi_{0^+}$-$X^1\Sigma^+$) Transition," J. Quant. Spectrosc. Radiat. Transfer 34, 321 (1985).

168. Dilonardo, M. and Capitelli, M., "Non-Equilibrium Dissociation of Nitrogen," Rev. Phys. Appl. 13, 115 (1978).

169. Treanor, C.E., Rich, J.W., and Rehn, R.G., "Vibrational Relaxation of Anharmonic Oscillators with Exchange-Dominated Collisions," J. Chem. Phys. 43, 1798 (1968).

170. Nichols, R.W., "Einstein A Coefficients, Oscillator Strengths and Absolute Band Strengths for the N_2 Second Positive and N_2^+ First Negative Systems," J. Atmos. Terrest. Phys. 25, 218 (1963).

171. Broadfoot, A.L., "Resonance Scattering by N_2^{+*}," Planet. Space Sci. 15, 1801, (1967).

172. Brown, W.A. and Landshoff, R.K., "The Electronic Transition Moment of the N_2^+ First Negative System," J. Quant. Spectrosc. Radiat. Transfer 11, 1143 (1971).

173. Lee, L.C. and Judge, D.L., "The Electronic Transition Moment of the N_2^+ ($B^2\Sigma_u^+$-$X^2\Sigma_g^+$) System," J. Phys. B: 6, L121 (1973).

174. Comes, E.J. and Speier, F., "The Optical Formation and the Collisional Deactivation of the First Negative System of Nitrogen," Chem. Phys. Lett. 4, 13 (1969).

175. Chang, R.S.F., Setser, D.W., and Taylor, G.W., "Assignment of Rate Constants to Exit Channels from Quenching of He(2^3S) Metastable Atoms," Chem. Phys. 25, 201 (1978).

176. Gottscho, R.A., Field, R.W., Dick, K.A., and Benesch, W., "Deperturbation of the N_2^+ First Negative Group $B^2\Sigma_u^+$-$X^2\Sigma_g^+$," J. Mol. Spec. XX, 435 (1979).

177. Piper, L.G., Cowles, L.M., and Rawlins, W.T., "State-to-State Excitation of NO($A^2\Sigma^+$, v'=0,1,2) by N_2($A^3\Sigma_u^+$, v'=0,1,2)," J. Chem. Phys. 85, 3369 (1986).

178. Inn, E.C.Y., "Charge Transfer Between He^+ and N_2," Planet. Space Sci., 15, 19 (1967).

END

DATE

FILMED

DTIC

6-88